



University
of Glasgow

Ghouri, Iffath Ayesha (2011) *A study of mitochondrial redox state in cardiac muscle*. PhD thesis.

<http://theses.gla.ac.uk/2367/>

Copyright and moral rights for this thesis are retained by the author

A copy can be downloaded for personal non-commercial research or study, without prior permission or charge

This thesis cannot be reproduced or quoted extensively from without first obtaining permission in writing from the Author

The content must not be changed in any way or sold commercially in any format or medium without the formal permission of the Author

When referring to this work, full bibliographic details including the author, title, awarding institution and date of the thesis must be given

A Study of Mitochondrial Redox State in Cardiac Muscle

Iffath Ayesha Ghouri, B.Sc (Hons)

Submitted in fulfilment of the degree of

Doctor of Philosophy

To

Institute of Cardiovascular and Medical Sciences

College of Medical, Veterinary and Life Sciences

University of Glasgow

February 2011

Abstract

This thesis describes the use of intrinsic fluorescence measurements as a means for examining mitochondrial function in different cardiac preparations and phenotypes.

Cardiac myocytes are intrinsically fluorescent and spectroscopic analysis of rabbit ventricular myocytes indicated that the majority of this fluorescence arises from the metabolic coenzymes nicotinamide adenine dinucleotide in the reduced state (NADH) and flavin adenine dinucleotide (FAD) in the oxidised state. Calibration of the NADH and FAD fluorescence signal with the mitochondrial inhibitors sodium cyanide (NaCN) and carbonyl cyanide *p*-(trifluoromethoxy) phenylhydrazone (FCCP) enabled calculation of mitochondrial redox states. Redox measurements reflect the balance between reduced and oxidised forms of the NAD and FAD pools and provide an index for assessing mitochondrial function in cells and tissue. The major advantage of this technique is that the intrinsically fluorescent nature of these metabolites obviates the need for exogenous indicators of mitochondrial function, which can themselves influence mitochondrial behaviour.

Mitochondrial redox state was established using a variety of fluorescence techniques. Values for $\text{NAD}_{\text{state}}$ represent the proportion of the NADH/NAD⁺ redox couple in the reduced state. Calculation of $\text{NAD}_{\text{state}}$ using single photon, two photon and wide-field epifluorescence microscopy revealed very similar values ranging from 0.57 ± 0.18 to 0.59 ± 0.17 (mean \pm SD). FAD fluorescence measurements were used to establish $\text{FAD}_{\text{state}}$ (the proportion of the FADH₂/FAD redox couple in the oxidised state). However, FAD fluorescence could only be detected by epifluorescence and single photon excitation fluorescence microscopy. Once again, comparable values of 0.17 ± 0.10 and 0.18 ± 0.07 respectively were obtained, thus demonstrating the reproducibility of the technique. Attempts were made to perform these measurements in intact cardiac tissue preparations. However, difficulties encountered with the delivery of mitochondrial inhibitor to specific areas of tissue and problems with inner filter effects complicating the interpretation of fluorescence recordings meant that this was not possible.

Measurements of intrinsic fluorescence were utilised in order to assess the mitochondrial redox response of cardiac cells to increased energy demand. Isolated rabbit ventricular myocytes were field stimulated and fractional shortening was simultaneously recorded with epifluorescence measurements of NADH and FAD. Cells were paced at 0.5Hz and the stimulation frequency step increased to 1Hz, 2Hz and 3Hz in order to increase work intensity and energy demand. Step increasing stimulation frequency resulted in a decrease in NADH fluorescence and an increase in FAD fluorescence before reaching an essentially steady state. This indicated oxidation of the cell environment, suggesting a transient mismatch between metabolite supply and demand. The magnitude of this response was related to stimulation frequency, with the biggest responses taking place at the highest work intensity. Reducing work intensity back to 0.5Hz pacing resulted in immediate recovery of metabolite fluorescence.

Investigation into the redox response to increased work intensity in the stroke prone spontaneously hypertensive rat (SHRSP) model of cardiac hypertrophy found that energy supply and demand matching was in fact improved in these cardiomyocytes compared to Wistar Kyoto (WKY) control myocytes. Work intensity was increased from 1Hz to 2, 4 and 6Hz pacing and the oxidative response to increased workload was found to be significantly less in SHRSP cardiomyocytes compared to WKY myocytes ($p < 0.01$). This was despite similar levels of contractile work being performed by the two groups and may be related to the young age of the animals (16 weeks). At this age, hypertrophy of the SHRSP hearts is likely to still be in the compensated state and mitochondrial function may indeed be improved rather than detrimentally affected at this stage.

Table of Contents

Abstract	2
Table of Contents	4
List of Tables.....	12
List of Figures.....	13
Acknowledgements.....	17
Author's Declaration	18
Abbreviations	19
1 Introduction.....	25
1.1 Excitation-contraction coupling in cardiac muscle	26
1.2 Cellular respiration in the heart.....	27
1.2.1 Glycolysis	28
1.2.2 Tricarboxylic acid cycle	28
1.2.3 Oxidative phosphorylation	30
1.2.3.1 Redox potential	31
1.2.4 Regulation of ATP synthesis by mitochondrial Ca^{2+}	33
1.2.4.1 Mitochondrial Ca^{2+} influx and efflux pathways	33
1.3 Assessing mitochondrial redox state	34
1.3.1 Intrinsic fluorescence in cells	34
1.3.2 Mitochondrial redox state values reported in the literature	37
1.3.3 Other methods for assessing redox state	38
1.4 Confocal laser scanning microscopy	39
1.4.1 Single photon excitation fluorescence microscopy.....	40
1.4.1.1 Problems associated with 1P excitation CLSM.....	40
1.4.2 Two photon excitation fluorescence microscopy.....	41
1.5 Applications for real time monitoring of mitochondrial redox state....	43
1.5.1 O_2 availability in intact tissue preparations.....	43
1.5.2 Mitochondrial metabolite supply and demand matching	44
1.6 Importance of maintaining redox potential.....	45
1.6.1 ROS	45
1.6.2 Role of NADH in antioxidant control mechanisms	46
1.7 Energy metabolism in failing hearts	47
1.7.1 Altered substrate utilisation	47
1.7.2 Impaired oxidative phosphorylation	49

1.7.3	Derangement of energy transfer systems.....	49
1.7.4	Effects of metabolic changes on contractile function	50
1.8	Investigating energy supply and demand matching in animal models of cardiac hypertrophy	52
1.8.1	The SHRSP model.....	52
1.8.2	Energy supply and demand matching in pressure overload- induced models of LV hypertrophy	53
1.9	Aims of the project.....	55
2	Methods.....	57
	Solutions used	58
2.1.1	Extracellular solutions.....	58
2.1.2	Mitochondrial inhibitors	58
2.2	Cell isolation	59
2.2.1	Cell isolation procedure for rabbit ventricular myocytes	59
2.2.2	Cell isolation procedure for rat ventricular myocytes.....	60
2.3	Left ventricular wedge preparation.....	60
2.4	Langendorff-perfused whole heart preparation.....	61
2.5	Fluorescence spectroscopy.....	63
2.5.1	Determination of excitation spectra	63
2.5.2	Determination of emission spectra	64
2.6	Fluorescence microscopy	64
2.6.1	1P excitation CLSM.....	64
2.6.2	2P laser scanning fluorescence microscopy	66
2.6.3	Wide-field epifluorescence microscopy.....	68
2.7	Measurements of mitochondrial redox state	69
2.7.1	Mitochondrial redox state measurements using fluorescence spectroscopy.....	70
2.7.2	Perfusion system for isolated cardiomyocytes	70
2.7.2.1	Perfusion protocol for isolated cardiomyocytes.....	72
2.7.3	Delivering mitochondrial inhibitor to tissue preparations.....	73
2.7.3.1	Perfusion protocol for tissue preparations.....	74
2.7.4	Calculation of mitochondrial redox state.....	74
2.8	Electrical stimulation of isolated cardiomyocytes	75
2.8.1	Pacing protocol for metabolic challenge in isolated cardiomyocytes	76

2.9	Statistical analysis.....	77
3	Characterisation of intrinsic fluorescence in ventricular myocytes	79
3.1	Introduction	80
3.2	Methods	80
3.2.1	Fluorescence spectroscopy	80
3.2.1.1	Preparation of pure metabolites and determination of spectra	80
3.2.1.2	Spectral measurements of intrinsic fluorescence from isolated ventricular myocytes	81
3.2.2	Excitation and emission fingerprinting.....	81
3.2.2.1	Emission fingerprinting using 1P-excitation CLSM.....	81
3.2.2.2	2P-excitation fingerprinting.....	82
3.3	Results.....	82
3.3.1	Pure NADH and FAD spectra	82
3.3.2	Pure NADH and FAD 2P excitation spectra	83
3.3.2.1	Effect of oxidising agent on NADH fluorescence	84
3.3.2.2	Effect of reducing agent on FAD fluorescence	85
3.3.3	Fluorescent properties of NADH-FAD solution mixture	85
3.3.4	Comparison of intrinsic fluorescence in cells with pure NADH and FAD fluorescence.....	87
3.3.4.1	Spectrophotometer measurements	87
3.3.4.2	Emission fingerprinting using 1P confocal methods.....	89
3.3.4.3	Excitation fingerprinting using 2P-excitation methods.....	90
3.4	Discussion	91
4	Establishing mitochondrial redox state in isolated rabbit ventricular myocytes.....	94
4.1	Introduction	95
4.1.1	Intrinsic fluorescence arising from cellular flavins.....	95
4.1.2	Intrinsic fluorescence measurements as an indicator of mitochondrial function.....	96
4.1.3	Mechanism of action of mitochondrial inhibitors.....	97
4.1.3.1	FCCP	97
4.1.3.2	NaCN.....	98
4.1.4	Aims of the chapter.....	98
4.2	Methods	99

4.2.1	Fluorescence spectroscopy	99
4.2.1.1	Cell counting	99
4.2.1.2	Calculating mitochondrial redox state from spectral measurements	99
4.2.2	Fluorescence microscopy.....	100
4.2.2.1	Excitation and emission settings in relation to NADH and FAD spectra	100
4.2.2.1.1	1P-excitation CLSM	100
4.2.2.1.2	2P-excitation fluorescence microscopy.....	100
4.2.2.1.3	Wide-field epifluorescence microscopy	101
4.2.2.2	Calculating mitochondrial redox state in single cells	102
4.3	Results.....	103
4.3.1	Mitochondrial redox state of cell aggregates assessed by fluorescence spectrometry	103
4.3.2	Mitochondrial redox state of single cells assessed by fluorescence microscopy	105
4.3.2.1	1P-excitation CLSM	105
4.3.2.2	2P-excitation fluorescence microscopy.....	107
4.3.2.3	Wide-field epifluorescence microscopy	108
4.3.3	Summary of mitochondrial redox state values assessed by intrinsic fluorescence methods	109
4.4	Discussion	109
4.4.1	Reproducibility of technique	109
4.4.2	Comparison with redox state values in the literature	110
4.4.3	Possible sources of residual fluorescence	111
4.4.4	Relationship between NAD and FAD states	113
5	Establishing mitochondrial redox state in intact ventricular tissue preparations.....	114
5.1	Introduction	115
5.1.1	LV wedge preparation	115
5.1.2	Horizontal Langendorff preparation.....	116
5.1.3	Inhibitors of contraction	116
5.1.3.1	2,3-Butanedione monoxime	117
5.1.3.2	Blebbistatin.....	117

5.1.3.3	Low Ca ²⁺ solution	118
5.1.4	Inner filter effect on NADH fluorescence transmission	119
5.1.5	Aims of the chapter	119
5.2	Methods	120
5.2.1	Preparation and imaging of tissue	120
5.2.1.1	Arterially perfused LV wedge preparation	120
5.2.1.2	Horizontal Langendorff preparation	120
5.2.2	Delivery of mitochondrial inhibitors.....	121
5.2.3	Normalisation of fluorescence	121
5.2.4	Assessing perfusion through the coronary vessels	121
5.2.5	Assessing the effects of mitochondrial inhibitors on light transmission through the tissue.....	122
5.2.6	FAD absorption measurements	123
5.2.7	Mb absorption measurements	124
5.3	Results.....	124
5.3.1	Mitochondrial inhibitor responses in the LV wedge preparation ..	124
5.3.2	Confirmation of coronary artery perfusion in the horizontal Langendorff preparation	126
5.3.3	Mitochondrial inhibitor responses in the horizontal Langendorff preparation	129
5.3.4	Transmission of emission light through the tissue.....	133
5.3.5	FAD absorption properties	135
5.3.6	Mb absorption spectra	136
5.4	Discussion	137
5.4.1	Movement of the preparation	137
5.4.1.1	Viability of the preparation	137
5.4.2	Measurements in the LV wedge preparation	138
5.4.3	NADH responses to FCCP in intact tissue preparations	139
5.4.4	NADH responses to CN in intact tissue preparations	139
5.4.5	Examining the influence of inner filter effects on NADH fluorescence measurements.....	140
5.4.5.1	Mb transmission properties.....	141
5.4.5.2	Sources contributing to inner filter effects arising from the mitochondria.....	143
5.4.5.3	Influence of light scattering.....	144

5.4.5.4	Overall effect on transmission of NADH specific wavelengths	145
5.4.6	Effects of absorption on NADH fluorescence changes in response to CN	146
5.4.7	Conclusions	147
6	Mitochondrial redox response to increased work intensity in rabbit ventricular myocytes	149
6.1	Introduction	150
6.1.1	Advantages of simultaneously measuring NADH and FAD fluorescence	151
6.1.2	PCr as an energy buffer	151
6.1.3	Aim of the chapter	151
6.2	Methods	151
6.2.1	Stimulation protocol for metabolic challenge	152
6.2.2	Analysis of rate of oxidative change and work performed by the cell	153
6.2.3	Verifying the mitochondrial origin of the intrinsic fluorescence response	153
6.2.4	Verifying contractile work to be the source of metabolic demand	154
6.2.5	Assessing possible role of PCr in energy supply and demand matching	155
6.3	Results	156
6.3.1	Intrinsic fluorescence response to metabolic challenge	156
6.3.2	Relationship between work and mitochondrial oxidative response	159
6.3.3	Mitochondrial origin of fluorescence changes	163
6.3.4	Contractile work as source of increased metabolic demand	164
6.3.5	Interpreting the cause of the delayed oxidative response to increased work intensity	166
6.4	Discussion	170
6.4.1	Energy supply and demand matching in rabbit ventricular myocytes	170
6.4.1.1	Regulation of oxidative phosphorylation	174
6.4.1.2	Comparison of results with previous studies	175

6.4.2	Analysing the kinetics of oxidative responses upon transitions in work intensity	177
6.4.2.1	Problems associated with the protocol	177
6.4.3	Confirming the cause of increased metabolic demand and source of fluorescence changes.....	178
6.4.4	Investigating the delayed oxidative response following workload transitions.....	179
6.4.5	Conclusions.....	180
7	Mitochondrial redox response to increased work intensity in a rat model of cardiac hypertrophy.....	181
7.1	Introduction	182
7.1.1	SHRSP model of cardiac hypertrophy.....	182
7.1.2	Effects of cardiac hypertrophy on mitochondrial function.....	182
7.1.3	Aim of the chapter	183
7.2	Methods	184
7.2.1	Cell sizing.....	184
7.2.2	Stimulation protocol for metabolic challenge	184
7.2.3	Statistical analysis	184
7.3	Results.....	185
7.3.1	Measurements of cell size.....	185
7.3.2	Redox response to increased work intensity	185
7.3.3	Comparison of work performed by WKY and SHRSP cardiomyocytes	187
7.3.4	Analysis of rate of fluorescence change in response to transitions in workload.....	188
7.4	Discussion	190
7.4.1	Comparison with guinea pig model of cardiac hypertrophy.....	191
7.4.2	Comparison with rat model of cardiac hypertrophy induced by aortic banding	192
7.4.3	Comparison of intrinsic fluorescence responses to increased workload in rat and rabbit cardiac myocytes	193
7.4.3.1	Differences in magnitude of oxidative response	193
7.4.3.2	Delay in oxidative response following increase in work intensity	195
7.4.4	Problems encountered.....	196

7.4.5	Conclusions	196
7.4.6	Future Studies	197
8	General Discussion	198
8.1	Establishing mitochondrial redox state in isolated rabbit ventricular myocytes	199
8.2	Establishing mitochondrial redox state in intact tissue preparations from rabbit heart.....	200
8.3	Mitochondrial redox responses to increased work intensity in isolated rabbit ventricular myocytes.....	201
8.4	Mitochondrial redox responses to increased work intensity in cardiac myocytes from the SHRSP model of cardiac hypertrophy compared to WKY controls.....	202
8.5	Further work	203
8.6	Summary of conclusions	204
	References.....	205

List of Tables

Table 1-1 Standard reduction potentials of selected reactions	32
Table 4-1 Summary of mitochondrial redox state values obtained using each fluorescence technique.....	109

List of Figures

Figure 1-1 E-C coupling in the cardiomyocyte	27
Figure 1-2 The TCA cycle	29
Figure 1-3 Oxidative phosphorylation	31
Figure 1-4 Mitochondrial Ca^{2+} signalling pathways	34
Figure 1-5 Redox equilibrium of NAD^+/NADH	35
Figure 1-6 Redox equilibrium of FAD/FADH_2	36
Figure 1-7 Meaning of $\text{NAD}_{\text{state}}$ and $\text{FAD}_{\text{state}}$ values	38
Figure 1-8 Confocal Laser Scanning Microscopy	39
Figure 1-9 Jablonski diagram illustrating principle of 1P fluorescence excitation	40
Figure 1-10 Jablonski diagram illustrating principle of 2P fluorescence excitation	42
Figure 1-11 Fluorescence emission by fluorescein following 1P and 2P excitation	43
Figure 1-12 Changes in cardiac energy metabolism in HF	51
Figure 1-13 NADH fluorescence changes in guinea pig ventricular myocytes in response to increased work intensity.....	54
Figure 1-14 NADH fluorescence changes in rat isolated trabeculae in response to increased work intensity	55
Figure 2-1 Position and orientation of Langendorff-perfused heart for 2P imaging	62
Figure 2-2 LS 55 fluorescence spectrometer setup	63
Figure 2-3 Emission fingerprinting using META detector	65
Figure 2-4 Optical settings for 1P CLSM	66
Figure 2-5 Optical settings for 2P excitation fluorescence microscopy	67
Figure 2-6 Optical settings for epifluorescence microscopy	69
Figure 2-7 Apparatus for perfusion of isolated cardiomyocytes	71
Figure 2-8 Mitochondrial inhibitor delivery system for tissue preparations	73
Figure 2-9 Calculation for $\text{NAD}_{\text{state}}$	75
Figure 2-10 Calculation for $\text{FAD}_{\text{state}}$	75
Figure 2-11 Metabolic challenge stimulation protocol in rabbit cells	77
Figure 2-12 Metabolic challenge stimulation protocol in rat cells	77
Figure 3-1 Excitation and emission spectra of pure NADH and FAD in solution ..	83

Figure 3-2 2P-excitation spectra of pure NADH and FAD in solution (predicted and measured)	83
Figure 3-3 NADH emission spectra before and after oxidation	84
Figure 3-4 FAD emission spectra before and after reduction	85
Figure 3-5 Excitation and emission spectra of pure NADH and FAD solution mixture.....	86
Figure 3-6 Spectrophotometric comparison of cellular intrinsic fluorescence with pure NADH and FAD	88
Figure 3-7 Comparison of cellular intrinsic fluorescence with pure NADH and FAD emission characteristics using the META detector.....	89
Figure 3-8 Comparison of cellular intrinsic fluorescence with pure NADH and FAD 2P-excitation characteristics	91
Figure 4-1 Mechanism of FCCP action on the respiratory chain	97
Figure 4-2 Mechanism of CN ⁻ action on the respiratory chain	98
Figure 4-3 Excitation wavelengths used and emission wavelengths detected with 1P CLSM in relation to NADH and FAD spectra	100
Figure 4-4 Excitation wavelengths used and emission wavelengths detected with 2P excitation fluorescence microscopy	101
Figure 4-5 Excitation wavelengths used and emission wavelengths detected with wide-field epifluorescence methods in relation to NADH and FAD spectra.....	102
Figure 4-6 Effect of FCCP and CN on NADH emission spectrum	104
Figure 4-7 Effect of FCCP and CN on intrinsic fluorescence measured by 1P CLSM	106
Figure 4-8 Effect of FCCP and CN on NADH fluorescence measured by 2P-excitation fluorescence microscopy	107
Figure 4-9 Effect of FCCP and CN on intrinsic fluorescence measured by wide-field epifluorescence microscopy	108
Figure 5-1 Spectral properties of blebbistatin	118
Figure 5-2 Positioning of LEDs in the LV of the horizontal Langendorff preparation.....	123
Figure 5-3 NADH fluorescence localisation in intact tissue	124
Figure 5-4 NADH fluorescence response to CN in LV wedge preparation.....	126
Figure 5-5 Perfusion of the coronary vessels imaged with 5(6)-carboxyfluorescein	127

Figure 5-6 5(6)-Carboxyfluorescein uptake and washout in presence and absence of mitochondrial inhibitors.....	128
Figure 5-7 NADH fluorescence response to FCCP in the horizontal Langendorff preparation.....	130
Figure 5-8 NADH fluorescence response to CN in the horizontal Langendorff preparation.....	131
Figure 5-9 NADH fluorescence response to control in the horizontal Langendorff preparation.....	132
Figure 5-10 Mean effects of CN on transmission of blue emission light through LV and RV tissue.....	133
Figure 5-11 Alternative transmission responses to CN treatment in the RV.....	134
Figure 5-12 Mean effects of CN on transmission of green emission light through the left and right ventricular tissue.....	134
Figure 5-13 FAD absorption spectra in the oxidised and reduced state.....	135
Figure 5-14 Mb absorption spectra in the presence and absence of CN.....	136
Figure 5-15 Transmission profile of Mb compared with LED emission profiles ..	142
Figure 5-16 Effect of Mb absorption in the LV and RV on light transmission through the tissue.....	146
Figure 5-17 Effect of Mb absorption on light transmission at distances relevant to tissue and isolated cell measurements.....	148
Figure 6-1 Pacing protocol to establish mitochondrial origin of intrinsic fluorescence response to increased work intensity.....	154
Figure 6-2 Pacing protocol to establish contractile work as source of metabolic demand.....	154
Figure 6-3 Representative trace showing effects of metabolic challenge on intrinsic fluorescence.....	157
Figure 6-4 Mean effect of step increasing stimulation frequency on intrinsic fluorescence levels.....	158
Figure 6-5 Time course of fluorescence change and work performed upon increase in work intensity to 2Hz and 3Hz pacing.....	159
Figure 6-6 Time course of fluorescence change and work performed upon decrease in work intensity from 2Hz and 3Hz pacing to 0.5Hz pacing.....	161
Figure 6-7 Rate of fluorescence change following increased and decreased workload.....	162

Figure 6-8 Fluorescence responses to 3Hz stimulation in control conditions and in the presence of mitochondrial inhibitors	163
Figure 6-9 Example and mean fluorescence responses to 3Hz stimulation in control conditions and with contractile function inhibited with cyto D.....	165
Figure 6-10 Effect of iodoacetamide on fluorescence responses to 3Hz stimulation	167
Figure 6-11 Effect of switching between control solutions on fluorescence response to 3Hz stimulation	168
Figure 6-12 Effect of cyclocreatine on fluorescence responses to 3Hz stimulation	169
Figure 6-13 Summary of postulated sequence of metabolic events that take place upon increases in work intensity	173
Figure 7-1 Mean cardiac myocyte size isolated from WKY and SHRSP hearts ...	185
Figure 7-2 Mean effect of step increasing stimulation frequency on intrinsic fluorescence levels in cardiomyocytes isolated from WKY and SHRSP hearts ...	186
Figure 7-3 Comparison of work performed by cardiomyocytes isolated from WKY and SHRSP hearts.....	187
Figure 7-4 Mean time course of fluorescence changes following workload transitions in WKY and SHRSP cardiomyocytes.....	189
Figure 7-5 Mean rate of fluorescence changes in WKY and SHRSP cardiomyocytes following workload transitions	190
Figure 7-6 Comparison of time course of intrinsic fluorescence response to increased workload in rabbit and rat cardiomyocytes	195

Acknowledgements

In the name of God, the most merciful, the most kind.

I would like to start by expressing my gratitude to my supervisors Prof. Godfrey Smith and Dr Ole Kemi, who initially gave me the opportunity to undertake this research and have encouraged me and advised me throughout. Godfrey's enthusiasm, dedication and knowledge of seemingly everything related to physiology are quite amazing and an inspiration to every student that has passed through the Smith lab. Ole's careful and thorough approach has set a great example for an aspiring scientist. He has particularly encouraged me to attend meetings, submit papers and apply for grants that I would never have considered otherwise, and this has stood me in good stead for the future. Funding for this Ph.D was provided by the BBSRC, and I would like to thank them for providing financial support.

The importance of the technical support provided by Mrs Aileen Rankin, Mrs June Irvine and Mr Michael Dunne cannot be overemphasised. In particular, I would like to thank Aileen for her help with the 2P whole heart experiments. Many a long day was spent in a dark, windowless room and her patience and chat made these (often unsuccessful) experiments bearable. The Smith lab has always been a great place to work, and this is down to the fantastic colleagues and friends who work here. No one is ever too busy to help, no matter what the problem is.

I have been blessed with an incredibly supportive family who have encouraged me throughout my life. My parents have instilled in me an ethos of hard work and high achievement from an early age, but have always encouraged me to follow my own aspirations. For this I am very grateful. To my brothers Nazim and Asim, thank you providing the light relief and the odd lift home after a late stay in the lab.

Finally, the ability and motivation required to complete this thesis are a gift from God, and for that I will always be thankful.

Author's Declaration

Rabbit cardiac myocyte isolations were performed by Mrs Aileen Rankin, Mrs June Irvine and Mr Michael Dunne. The rabbit ventricular wedge preparations were produced by Dr Rachel Myles and Dr Soontaree Petchdee. All of the experimental work presented in this thesis was carried out by myself and has not been submitted for the fulfilment of any other degree.

Some of the results obtained during the period of research have been published in abstract form and are detailed below:

IA Ghouri, OJ Kemi, GL Smith: Spectroscopic, Confocal and 2-Photon Characterisation of Intrinsic Fluorescence in Isolated Heart Cells for Metabolic Studies. Abstract - Biophysical Society annual meeting, Long Beach, USA. *Biophysical Journal* 2008; **94(2)**, 493-501

IA Ghouri, OJ Kemi, GL Smith: Mitochondrial Redox Responses to Increased Work Intensity in Rabbit Ventricular Myocytes. Abstract - Biophysical Society annual meeting, Boston, USA. *Biophysical Journal* 2009; **96(3)**, 242a-243a

IA Ghouri, OJ Kemi, GL Smith: Mitochondrial Oxidative Responses to Increased Work Intensity in Rabbit Ventricular Myocytes Assessed by Intrinsic Fluorescence Methods. Abstract - Physiological Society main meeting, Dublin, Ireland. *Proceedings of the Physiological Society* 2009; **15**, PC102

Abbreviations

1P	Single photon
2P	Two photon
ADP	Adenosine diphosphate
ANOVA	Analysis of variance
ATP	Adenosine triphosphate
a.u.	Arbitrary units
BDM	2,3-Butanedione monoxime
BSA	Bovine serum albumin
Ca ²⁺	Calcium ion
CaCl ₂	Calcium chloride
[Ca ²⁺] _i	Intracellular calcium concentration
[Ca ²⁺] _m	Mitochondrial calcium concentration
CaUP	Calcium uniporter
CC	Cyclocreatine
CCD	Charge coupled device
CK	Creatine kinase
CLSM	Confocal laser scanning microscopy
CN	Cyanide

CO ₂	Carbon dioxide
CoA	Coenzyme A
Cr	Creatine
Cyto D	Cytochalasin D
DMBQ	Dimethoxy-1,4-benzoquinone
E-C	Excitation-contraction
EF	Ejection fraction
EGTA	Ethylene glycol bis(2-aminoethyl ether)-N,N,N',N'-tetraacetic acid
ETC	Electron transport chain
ETF	Electron transferring flavoprotein
F	Fluorescence
FAD	Flavin adenine dinucleotide (oxidised)
FADH ₂	Flavin adenine dinucleotide (reduced)
FAD _{state}	Proportion of the FADH ₂ /FAD redox couple in the oxidised state
FCCP	Carbonyl cyanide <i>p</i> -(trifluoromethoxy) phenylhydrazone
FMN	Flavin mononucleotide
GSH	Glutathione (reduced)
GSSG	Glutathione (oxidised)

H ⁺	Hydrogen ion (proton)
H ₂	Hydrogen
HEPES	4-(2-hydroxyethyl)-1-piperazine-1-ethanesulfonic acid
HF	Heart failure
H ₂ O ₂	Hydrogen peroxide
Hz	Hertz
IR	Infrared
KCl	Potassium chloride
LED	Light emitting diode
LipDH	Lipoamide dehydrogenase
LV	Left ventricle
LVH	Left ventricular hypertrophy
Mb	Myoglobin
Mg ²⁺	Magnesium ion
MgCl ₂	Magnesium chloride
MgSO ₄	Magnesium sulphate
mM	Millimolar concentration
mPTP	mitochondrial permeability transition pore
NA	Numerical aperture

Na^+	Sodium ion
NaCl	Sodium chloride
NaCN	Sodium cyanide
NAD^+	Nicotinamide adenine dinucleotide (oxidised)
NADH	Nicotinamide adenine dinucleotide (reduced)
Na-dithionite	Sodium dithionite
NADP^+	Nicotinamide adenine dinucleotide phosphate (oxidised)
NADPH	Nicotinamide adenine dinucleotide phosphate (reduced)
NAD(P)H	Nicotinamide adenine dinucleotide and nicotinamide adenine dinucleotide phosphate (reduced)
$\text{NAD}_{\text{state}}$	Proportion of the NADH/NAD^+ redox couple in the reduced state
NaHCO_3	Sodium hydrogen carbonate
NaH_2PO_4	Sodium dihydrogen orthophosphate
$[\text{Na}^+]_i$	Intracellular sodium concentration
NCX	Sodium/calcium exchanger
NIR	Near infrared
nm	Nanometre
O_2	Oxygen
$\text{O}_2^{\cdot-}$	Superoxide anion

PCr	Phosphocreatine
P _i	Inorganic phosphate
PMT	Photomultiplier tube
Q	Ubiquinone
QH ₂	Ubiquinol
Redox	Reduction/oxidation
ROI	Region of interest
ROS	Reactive oxygen species
RV	Right ventricle
RyR	Ryanodine receptor
SD	Standard deviation
SEM	Standard error of the mean
SERCA	Sarco/endoplasmic reticulum calcium adenosine triphosphatase
SHR	Spontaneously hypertensive rat
SHRSP	Stroke prone spontaneously hypertensive rat
SR	Sarcoplasmic reticulum
TCA	Tricarboxylic acid
UV	Ultraviolet
VDAC	Voltage dependent anion channel

WKY	Wistar Kyoto rat
$\Delta\psi_m$	Mitochondrial membrane potential
λ	Wavelength
μM	Micromolar concentration

1 Introduction

The heart is a highly metabolic organ that requires a continuous supply of energy in order to function. Within the cell, energy is transduced mainly in the form of the high energy compound adenosine triphosphate (ATP). The phosphate groups of ATP are attached by phosphodiesterase bonds, the resonance structure of these bonds is such that their hydrolysis yields a large negative change in free energy. The standard free energy change (ΔG°) for the hydrolysis of ATP to adenosine diphosphate (ADP) and inorganic phosphate (P_i) is 30.5 kJ mol^{-1} . The energy released can be utilised by the cell to power metabolically demanding processes such as contraction of the heart muscle.

In the presence of oxygen (O_2), the majority of ATP is produced by the mitochondria, the "powerhouses" of the cell. These organelles have a double membrane structure consisting of an outer membrane and a folded inner membrane which forms finger-like projections called cristae. Enclosed within the inner membrane is the mitochondrial matrix, which contains the respiratory enzymes. Mitochondria are particularly abundant in metabolically active cells with high energy requirements, such as cardiac myocytes. Mitochondrial volume density quantified by ultrastructure morphometry has been reported to be between 22% and 37% of left ventricular myocyte volume (depending on species) (Barth *et al.*, 1992).

1.1 Excitation-contraction coupling in cardiac muscle

Contraction and relaxation of the heart muscle takes place by the process of excitation-contraction (E-C) coupling (Figure 1-1). Contraction of a cardiac myocyte is initiated by the arrival of an action potential down the transverse tubule (T-tubule), depolarising the cell and opening voltage sensitive calcium (Ca^{2+}) channels in the membrane (L-Type Ca^{2+} channels). The subsequent rise in intracellular $[Ca^{2+}]$ ($[Ca^{2+}]_i$) activates nearby ryanodine receptors (RyRs) present in the membrane of the sarcoplasmic reticulum (SR), leading to the release of Ca^{2+} from SR Ca^{2+} stores through the RyR channels. The resulting rise in $[Ca^{2+}]_i$ activates contractile proteins, leading to crossbridge formation and cycling and cardiac muscle contraction. Ca^{2+} ions return to the SR via the Sarco/Endoplasmic Reticulum Ca^{2+} -ATPase (SERCA) pump and are removed from the cell via the sodium (Na^+)/ Ca^{2+} exchanger (NCX) and sarcolemmal Ca^{2+} -ATPase. The fall in

$[Ca^{2+}]_i$ results in the dissociation of Ca^{2+} from the myofilaments and subsequent relaxation of the cardiomyocyte, allowing the cycle to begin again (Bers, 2002). The process of E-C coupling is energy demanding and requires a continuous supply of ATP to power contractile proteins and ion pumps. Around 60–70% of ATP is used to fuel contractile shortening, and the remaining 30–40% is primarily used to power SERCA and other ion pumps (Stanley *et al.*, 2005).

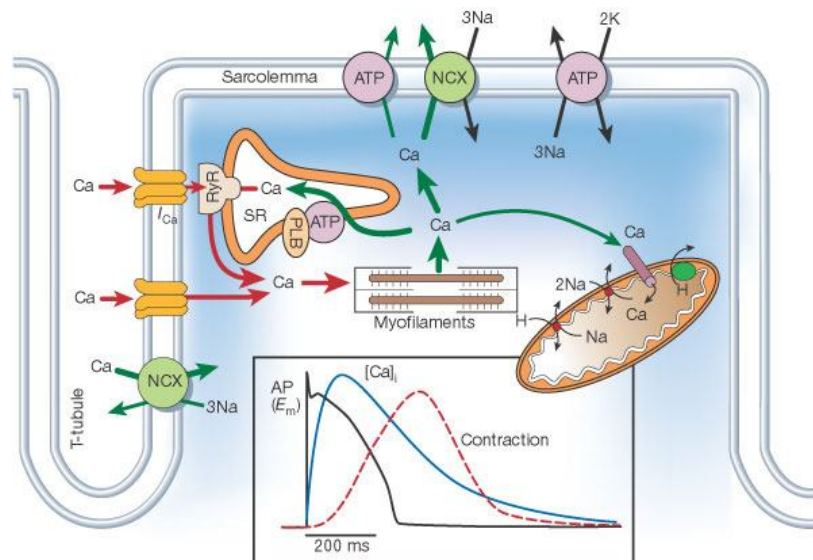


Figure 1-1 E-C coupling in the cardiomyocyte

The Ca^{2+} signalling events which occur during E-C coupling. Also shown is the time course of the action potential, Ca^{2+} transient and contraction during one cycle measured in a rabbit ventricular myocyte at 37°C. Reprinted by permission from MacMillan Publishers Ltd: [Nature] (Bers, D. M. (2002). Cardiac excitation-contraction coupling. *Nature* 415, 198-205), copyright (2002)

1.2 Cellular respiration in the heart

ATP is produced by the cell through the process of cellular respiration. This consists of a series of reactions that transduce biochemical energy from nutrients such as glucose, fatty acids and lactate into ATP. In the presence of O_2 (aerobic conditions), the majority of ATP is produced by the mitochondria. However, the initial steps of glucose metabolism are the same in aerobic and anaerobic (O_2 absent) conditions.

1.2.1 Glycolysis

Glycolysis is an anaerobic process that takes place in the cytoplasm of the cell. It involves the breakdown of 6 carbon glucose to 2 molecules of 3 carbon pyruvate through a series of reactions. The process leads to the net gain of 2 ATP molecules and is an example of substrate-level phosphorylation, as the phosphate group is transferred directly to ADP to form ATP, without a coupled oxidation reaction. Glycolysis also results in the reduction of 2 molecules of the electron carrier nicotinamide adenine dinucleotide (NAD^+) to form reduced nicotinamide adenine dinucleotide (NADH).

When O_2 is limited in the cell, pyruvate is converted to lactate in a reaction catalysed by the enzyme lactate dehydrogenase. NADH acts as the reducing agent and is oxidised to reform NAD^+ , resulting in the formation of 2 more molecules of ATP. In the presence of O_2 , pyruvate is transferred to the next stage of aerobic respiration (Stryer, 1988).

1.2.2 Tricarboxylic acid cycle

Pyruvate enters the mitochondrial matrix where it is oxidised and decarboxylated to form acetyl coenzyme A (CoA). This results in the reduction of 1 molecule of NAD^+ to form NADH, and the removal of 1 carbon atom, which is released in the form of carbon dioxide (CO_2). The 2-carbon acetyl group then combines with oxaloacetate to form tricarboxylic acid (citrate). The breakdown of citrate to eventually regenerate oxaloacetate by a series of enzymatic steps is known as the tricarboxylic acid (TCA) or citric acid cycle, also known as the Krebs cycle (Figure 1-2), which was identified by Hans Krebs in the 1930s (Krebs *et al.*, 1938).

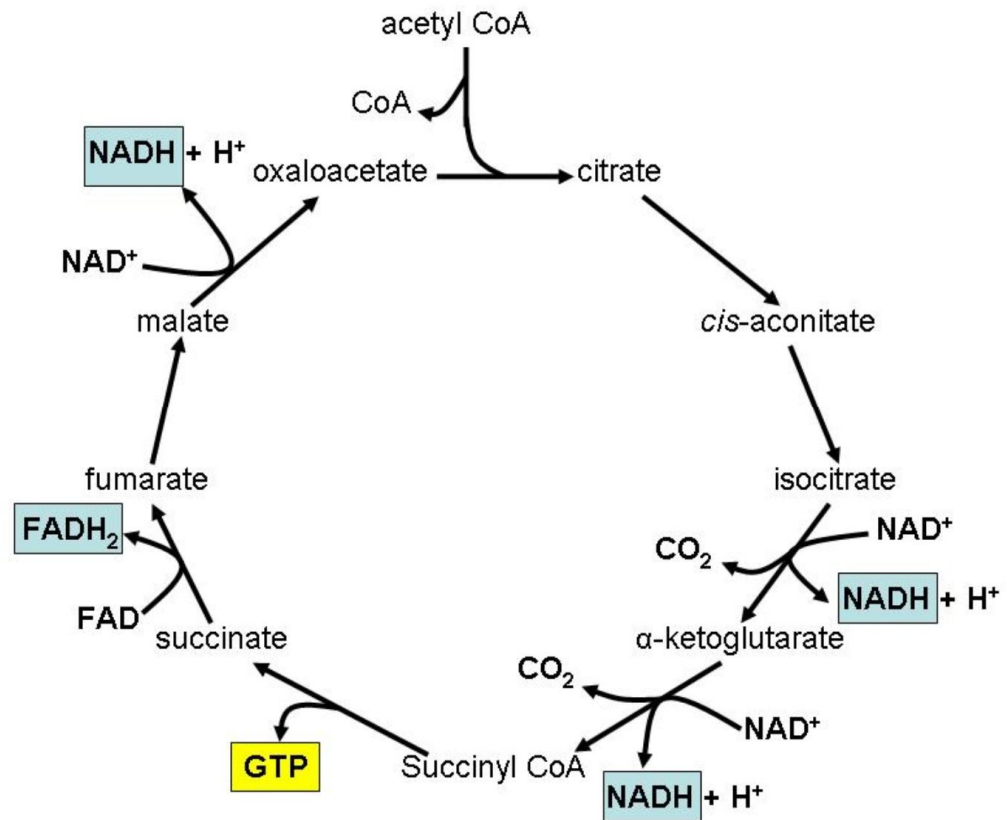


Figure 1-2 The TCA cycle

4-carbon oxaloacetate condenses with a 2-carbon acetyl unit to form 6-carbon citrate. Citrate is broken down through a series of enzymatic reactions to regenerate oxaloacetate. In the process, 2 carbon atoms are removed in the form of CO₂ and 4 hydrogen molecules (8 pairs of electrons) are transferred to NAD⁺ and FAD to form 3 molecules of NADH and one molecule of FADH₂ (highlighted in blue). One molecule of GTP (highlighted in yellow) is also formed through substrate-level phosphorylation. This can be readily converted to ATP. Direct formation of ATP has also been demonstrated in some tissues (Weitzman *et al.*, 1986).

Flavin adenine dinucleotide (FAD) and NAD⁺ act as hydrogen acceptors (and thus electron carriers) and are reduced to FADH₂ and NADH respectively. These reduced coenzymes have the potential to produce more ATP through the process of oxidative phosphorylation.

As well as glucose, cells can also metabolise other substrates including fatty acids and lactate. In fact, the majority of ATP production in the well-perfused heart *in vivo* is due to the oxidation of fatty acids (Stanley *et al.*, 2005). Before entering the mitochondria, fatty acids must first be activated in the cytosol to form acyl CoA, which is then shuttled (bound to carnitine) into the mitochondrial matrix. Here, the long chain fatty acids are split and acyl CoA is converted to

acetyl CoA by the process of β -oxidation, which can combine with oxaloacetate to enter the TCA cycle. Each cycle of β -oxidation also produces one molecule of NADH and one molecule of FADH_2

1.2.3 Oxidative phosphorylation

Oxidative phosphorylation takes place at the electron transport chain (ETC), also known as the respiratory chain, located in the inner mitochondrial membrane. Oxidative phosphorylation is the process by which ATP is formed as electrons are transferred from NADH or FADH_2 through a series of electron carriers to the final electron acceptor, O_2 (Figure 1-3). Unlike with substrate-level phosphorylation, oxidative phosphorylation couples oxidation with phosphorylation to produce ATP.

The ETC consists of complexes of integral proteins. Here, hydrogen (H) atoms are released by NADH and FADH_2 (which are oxidised back to NAD^+ and FAD) and split into their constituent protons (H^+) and electrons. The electrons are transferred from one complex of the chain to the next, shuttled by the electron carriers ubiquinone (Q) and cytochrome c, through a series of coupled reduction and oxidation (redox) reactions. The final electron acceptor is O_2 , which is reduced to form water at complex IV (cytochrome c oxidase, COX). The stepwise transfer of electrons generates energy, which is used to pump protons across the inner mitochondrial membrane to the intermembrane space. The inner mitochondrial membrane is impermeable to protons and an electrochemical gradient composed of both the pH gradient and electrical gradient forms, the mitochondrial membrane potential ($\Delta\psi_m$) being some 150-200mV negative to the cytosol. This generates a proton-motive force, which is harnessed as protons flow back across the inner membrane through the F_1F_0 -ATP synthase complex, driving the synthesis of ATP. This chemiosmotic process powering oxidative phosphorylation was first elucidated by Peter Mitchell in the 1960s (Mitchell, 1961).

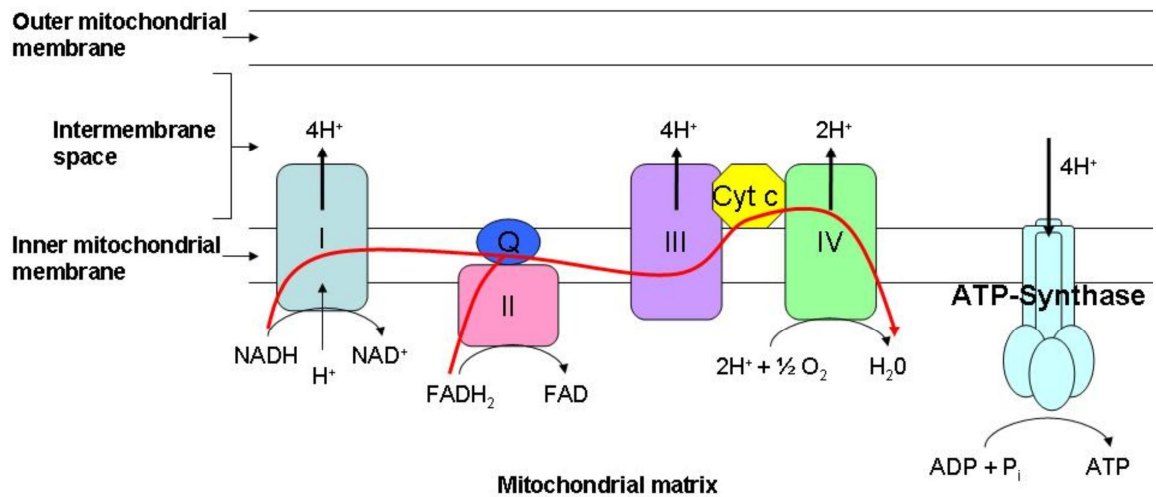


Figure 1-3 Oxidative phosphorylation

Electrons are transferred from NADH or FADH₂ along the electron transport chain from one complex to the next (red arrow indicates electron path). The final electron acceptor is O₂, which is reduced to form water. Electron transfer along the chain generates energy, which is used to pump protons across the inner mitochondrial membrane. The generated proton-motive force drives the formation of ATP as protons flow back across the membrane via the ATP-synthase complex.

Oxidation of NADH has the potential to produce 2.5 ATP, whereas oxidation of FADH₂ can potentially yield 1.5 ATP. Electrons from NADH enter the ETC at complex I (NADH dehydrogenase) and pass through complex III (cytochrome bc₁ complex) and complex IV. Electrons from FADH₂ enter at complex II (succinate Q reductase complex) and are transferred via an iron-sulphur cluster to Q, reducing it to ubiquinol (QH₂). FADH₂ cannot pump protons across the membrane at complex II and thus this electron transfer does not contribute to the proton gradient. This is the reason why FADH₂ yields less ATP than NADH. QH₂ transfers electrons to complex III, which then follow the same route as electrons released from NADH.

1.2.3.1 Redox potential

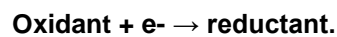
The driving force for oxidative phosphorylation is the electron transfer potential, or redox potential, of NADH and FADH₂ relative to O₂. The redox potential of a redox couple (a pair of molecules where one acts as the reductant and the other acts as the oxidant) describes the affinity for electrons of the redox couple relative to the H₂/H⁺ redox couple. The reduction potentials of selected redox couples are shown in Table 1-1. NADH and FADH₂ are strong reducing agents (i.e.

electron donors), with negative redox potentials and a low affinity for electrons. O_2 is a strong oxidizing agent with a positive redox potential and high affinity for electrons (i.e. electron acceptor). The direction of electron transfer is thus from NADH and $FADH_2$ towards O_2 . The rate of NADH and $FADH_2$ supply from the TCA cycle must match the rate of electron flux through the ETC in order to maintain the redox potential and allow oxidative phosphorylation to proceed. The redox potential can be expressed in terms of the redox state of the cell i.e. the NADH/ NAD^+ and $FADH_2$ / FAD ratios.

Oxidant	Reductant	<i>N</i>	E'_0 (V)
NAD^+	$NADH + H^+$	2	-0.32
FAD	$FADH_2$	2	-0.22
$\frac{1}{2} O_2 + 2H^+$	H_2O	2	+0.82

Table 1-1 Standard reduction potentials of selected reactions

The standard reduction potential (E'_0) is measured at pH 7 and 25°C. *N* is the number of electrons transferred. E'_0 refers to the partial reaction written as:



The standard oxidation potential is the negative of the reduction potential (E'_0 values taken from (Berg *et al.*, 2006))

It is thought that the mitochondrial redox state plays an important role in the control of oxidative phosphorylation (Balaban, 1990). Increasing the redox potential by increasing the supply of the reducing equivalents to the ETC increases $\Delta\psi_m$. As $\Delta\psi_m$ is the driving force for proton influx through ATP-synthase, $\Delta\psi_m$ must be maintained in order to support ATP production at high rates. Measurements of mitochondrial redox state, particularly the NADH/ NAD^+ ratio (NAD_{state}), thus provide a useful tool for evaluating mitochondrial energetics in both *in vitro* and *in vivo* studies (Mayevsky & Barbiro-Michaely, 2009; Esumi *et al.*, 1991; Eng *et al.*, 1989; Chance *et al.*, 1962; Chance & Schoener, 1962).

1.2.4 Regulation of ATP synthesis by mitochondrial Ca^{2+}

Work by Denton *et al.* in the 1970s led to the discovery that a number of rate limiting dehydrogenases (pyruvate dehydrogenase, 2-oxoglutarate dehydrogenase and NAD^+ isocitrate dehydrogenase), critical elements of substrate metabolism, are regulated by mitochondrial Ca^{2+} (McCormack & Denton, 1979; Denton *et al.*, 1978; Denton *et al.*, 1972). Mitochondria have Ca^{2+} influx and efflux pathways, and an increase in intramitochondrial Ca^{2+} concentration could therefore stimulate mitochondrial dehydrogenase activity, increasing mitochondrial $[\text{NADH}]$ and $[\text{FADH}_2]$, and subsequently increase the rate of ATP production. Mitochondrial Ca^{2+} is also thought to activate F_1F_0 -ATP synthase, and thus stimulate ATP synthesis directly (Territo *et al.*, 2000; Das & Harris, 1990). Taken together, this suggests that Ca^{2+} also plays an important role in regulating ATP production, for example in response to increasing workload, in addition to regulation by ADP and P_i through feedback control.

1.2.4.1 Mitochondrial Ca^{2+} influx and efflux pathways

It has been recognised for a number of decades now that mitochondria have Ca^{2+} signalling capabilities and possess the ability to sequester Ca^{2+} (Dhalla, 1969; Deluca & Engstrom, 1961). Mitochondrial Ca^{2+} signalling pathways are summarised in Figure 1-4. The influx of Ca^{2+} ions into mitochondria is driven by the negative $\Delta\psi_m$. The outer mitochondrial membrane is freely permeable to Ca^{2+} due to the presence of voltage-dependent anion channels (VDAC), which have a cation selective conductance state (Pavlov *et al.*, 2005). However, the inner membrane is not freely permeable to Ca^{2+} and ion uptake must therefore be via the mitochondrial Ca^{2+} uniporter (CaUP). Influx of Ca^{2+} causes depolarisation of $\Delta\psi_m$, and it has been reported that in the absence of $\Delta\psi_m$, Ca^{2+} uptake by the uniporter could not occur, even in the presence of an 8 fold external to internal concentration gradient (Kapus *et al.*, 1991). Mitochondria must therefore also possess Ca^{2+} efflux systems in order to maintain $\Delta\psi_m$.

Ca^{2+} efflux from the mitochondria is against a concentration gradient and thus requires either ATP hydrolysis or energetically favourable exchange with an extra-mitochondrial ion travelling down an electrochemical gradient. In the heart, brain and skeletal muscle, the NCX predominates (Gunter *et al.*, 1994).

However, the stoichiometry of this exchange is still controversial and it is unclear if this exchange is $\text{Ca}^{2+}/2\text{Na}^{+}$ or $\text{Ca}^{2+}/3\text{Na}^{+}$. A Na^{+} independent efflux pathway also exists, involving a $\text{Ca}^{2+}/2\text{H}^{+}$ exchanger and this system dominates in the mitochondria of the liver and kidney. Mitochondria possess a third mechanism for Ca^{2+} efflux - the Cyclosporin A inhibitable mitochondrial permeability transition pore (mPTP). The opening of this pore is triggered by Ca^{2+} overload of the mitochondrial matrix and oxidative stress and results in rapid equilibration of ion gradients. Irreversible opening of the mPTP pore results in cell death, but a physiological role for transient mPTP opening is still controversial. It has recently been shown that mice lacking the cyclophilin D gene, an important modulator of mPTP opening, demonstrated elevated mitochondrial matrix Ca^{2+} levels which limited the metabolic flexibility of the heart. Thus, the mPTP may play a physiological role in homeostatic control of mitochondrial Ca^{2+} levels to enable metabolism to be matched with alterations in myocardial workload (Elrod *et al.*, 2010).

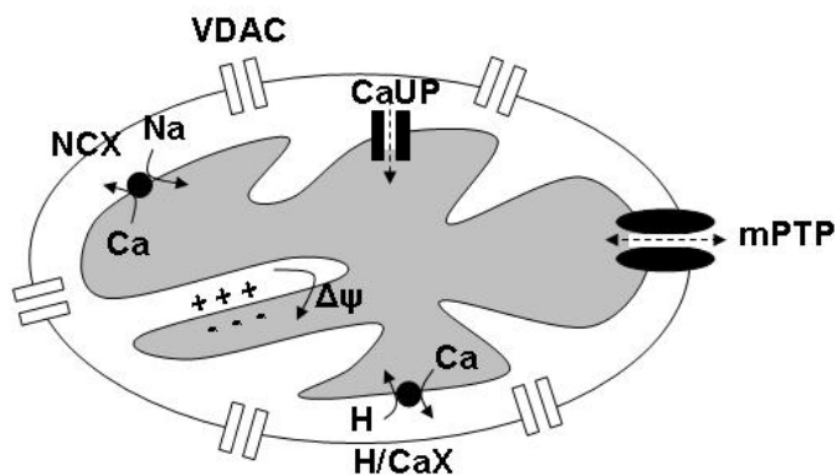


Figure 1-4 Mitochondrial Ca^{2+} signalling pathways

The mechanisms by which Ca^{2+} enters and exits the mitochondria.

1.3 Assessing mitochondrial redox state

1.3.1 Intrinsic fluorescence in cells

The mitochondrial redox state of the cell or tissue can be studied using fluorescence techniques. This is because NADH (in the reduced state) and FAD (in the oxidised state) are intrinsically fluorescent (autofluorescent) when

excited at particular wavelengths. Cells consequently have endogenous fluorescence without the artificial introduction of fluorescence indicators.

Both NADH and reduced nicotinamide adenine dinucleotide phosphate (NADPH) absorb light in the ultraviolet (UV) region and emit blue fluorescence. However, NADH concentrations predominate over NADPH within cardiac mitochondria and the NADH fluorescence yield is as much as 4-fold greater than NADPH (Estabrook, 1962). NADH is present in both cytosolic and mitochondrial compartments, but the fluorescence signal is primarily mitochondrial in origin (Nuutinen, 1984). This is mainly due to the fact that mitochondrial NADH binding causes fluorescence to be enhanced ~10 fold (Jöbsis & Duffield, 1967; Avi-Dor *et al.*, 1962; Estabrook, 1962). In the cytosol NADH strongly binds to glyceraldehyde phosphate dehydrogenase, which diminishes NADH fluorescence (Chapman, 1972). Taking these factors into account, around 80% of the UV-excited blue fluorescence arises from mitochondrial NADH (Eng *et al.*, 1989).

The molecular changes that take place when NAD^+ is reduced to NADH are shown in Figure 1-5.

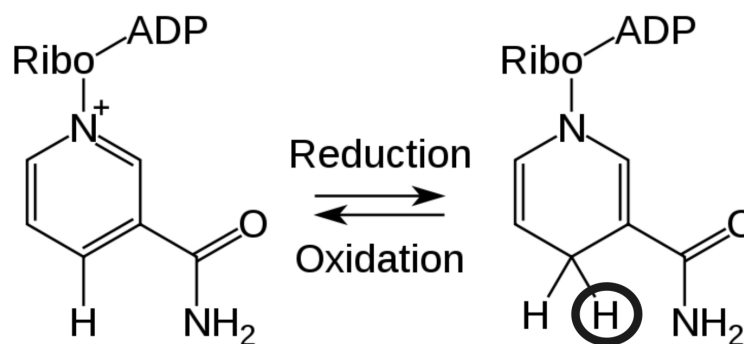


Figure 1-5 Redox equilibrium of NAD^+/NADH

Uptake of hydrogen at position 4 of the pyridine ring (circled) results in the appearance of a new absorption band. The fluorescence yield of pyridine nucleotides in the oxidised state (NAD^+ , NADP^+) is some 1000 fold less than in the reduced state at excitation wavelengths longer than 300nm (Koenig & Schneckenburger, 1994). Thus, a shift in the mitochondrial NADH/NAD^+ balance

towards the reduced state results in an **increase** in UV-excited blue autofluorescence.

FAD is derived from riboflavin (vitamin B₂). Any protein with a flavin, FAD or flavin mononucleotide (FMN) moiety attached is described as a flavoprotein. The molecular changes that take place when FAD is reduced to FADH₂ are shown in Figure 1-6.

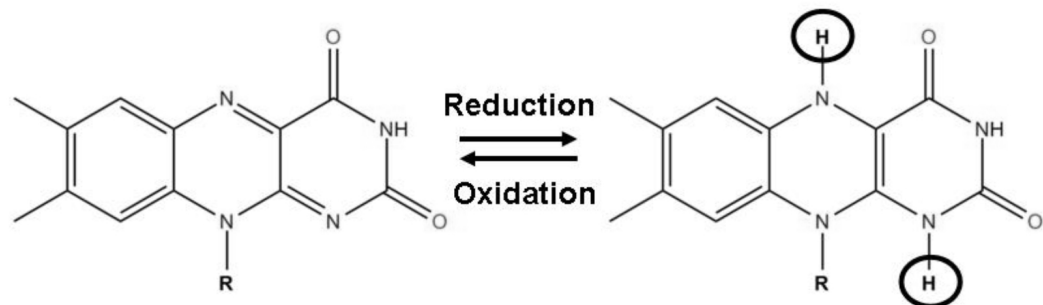


Figure 1-6 Redox equilibrium of FAD/FADH₂

FAD in the oxidised state is excited by blue light and fluoresces in the green. Reduction of FAD to FADH₂ (positions of H uptake are circled) causes the molecular structure to change from a planar into a “butterfly” configuration. This results in a decrease in absorption and subsequently a decrease in fluorescence emission (Koenig & Schneckenburger, 1994). Thus, a shift in the mitochondrial FADH₂/FAD balance towards the reduced state results in a **decrease** in green autofluorescence.

As NADH is fluorescent in the reduced state and FAD is fluorescent in the oxidised state, simultaneous measurement of both fluorescent species provides an indication of the balance between reduced and oxidised forms of these electron carriers in the mitochondria (Chance *et al.*, 1979; Chance *et al.*, 1972; Scholz *et al.*, 1969). Fluorometry based on this endogenous fluorescence is therefore a valuable tool for assessing the metabolic status of cells and tissue.

1.3.2 Mitochondrial redox state values reported in the literature

A range of values for resting $\text{NAD}_{\text{state}}$ have been described in the literature. Examination of NADH/NAD^+ in different cells found some variation between cell types (Duchen & Biscoe, 1992). In rat and mouse chromaffin cells isolated from the adrenal medulla, $\text{NAD}_{\text{state}}$ was found to be 0.45, a similar value to that found in freshly isolated mouse dorsal root ganglion neurons (0.53). However, type 1 cells from rabbit carotid body were found to be in a more oxidised state, with average $\text{NAD}_{\text{state}}$ measured as 0.27. This was attributed to higher O_2 consumption in these cells. FAD fluorescence measurements were also made in these experiments, but the signal-to-noise ratio was found to be too low to obtain values for $\text{FAD}_{\text{state}}$. In resting isolated rat cardiac myocytes, $\text{NAD}_{\text{state}}$ was found to be 0.44 (Eng *et al.*, 1989) and 0.27 (White & Wittenberg, 1993), whereas the $\text{NAD}_{\text{state}}$ in isolated guinea pig ventricular myocytes was 0.31 in the resting state (Minezaki *et al.*, 1994) and around 0.2 when paced at 0.1Hz (Jo *et al.*, 2006). These values suggest that in isolated cells, 25-50% of the NAD^+ pool is in the reduced state. The more oxidised $\text{NAD}_{\text{state}}$ reported in guinea pig cardiomyocytes, particularly by Jo *et al.*, points towards substrate limited respiration, and may suggest that ATP production by the mitochondria was compromised in these experiments. In a rat cardiac trabeculae preparation paced at 1Hz, the mitochondria were found to be in a slightly more reduced state, with the $\text{NAD}_{\text{state}}$ quoted as 0.63 (Brandes & Bers, 1996). The same value was reported in isolated rat cardiomyocytes stimulated to contract at 1Hz (Esumi *et al.*, 1991).

Although FAD fluorescence measurements have been used to assess mitochondrial redox state in isolated cardiac cells (Chorvat *et al.*, 2004; Romashko *et al.*, 1998), no values for $\text{FAD}_{\text{state}}$ have been quoted in the literature for this cell type. However in both these studies, the FAD pool was shown to be mainly in the reduced state.

This thesis employs a number of different fluorescence techniques in order to simultaneously measure NADH and FAD fluorescence and consequently establish both $\text{NAD}_{\text{state}}$ and $\text{FAD}_{\text{state}}$ in the same cell. Figure 1-7 summarises the significance of the $\text{NAD}_{\text{state}}$ and $\text{FAD}_{\text{state}}$ values.

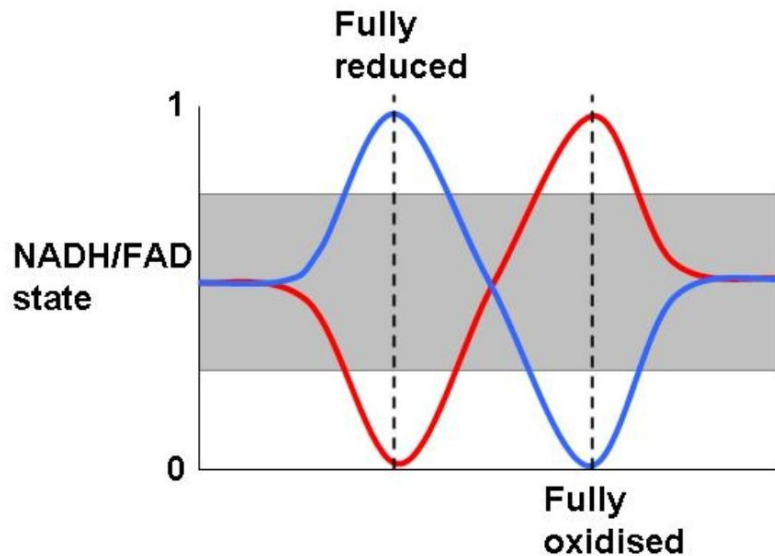


Figure 1-7 Meaning of NAD_{state} and FAD_{state} values

Range of NADH and FAD fluorescence changes and the corresponding metabolic states they represent (following calculations described in Figures 2-9 and 2-10). Blue trace represents NADH fluorescence and red trace represents FAD fluorescence. When the mitochondria are in the fully reduced state, NADH fluorescence is maximal and $NADH_{state}=1$. Conversely, FAD fluorescence is minimal and $FAD_{state}=0$. In the fully oxidised state, NADH fluorescence is minimal and $NADH_{state}=0$, whereas FAD fluorescence is maximal and $FAD_{state}=1$. Grey shaded area gives a rough indication of expected $NADH_{state}$ and FAD_{state} values in the normoxic, actively respiring cell.

1.3.3 Other methods for assessing redox state

The redox state of the cell can also be determined indirectly by measuring the concentrations of metabolite couples in NAD-linked enzyme reactions. In the cytosol, the pyruvate/lactate couple can be assayed, whereas measurements of the β -hydroxybutyrate/acetoacetate couple reflects the mitochondrial NAD redox state (Williamson *et al.*, 1967). These ratios reflect the $NADH/NAD^+$ state exclusively in the cytosolic or mitochondrial compartments and distinguish between $NADH/NAD^+$ and $NADPH/NADP^+$ redox states. However, real time monitoring of redox state is not possible by this method and measurements are not sensitive to rapid changes. In addition, in order for this method for assessing mitochondrial redox state to be valid, the rate of reaction must be high enough to be in equilibrium. The β -hydroxybutyrate dehydrogenase reaction is at equilibrium in liver mitochondria, but there is evidence that this is not the case in the heart (Nuutinen *et al.*, 1981; Opie & Owen, 1975).

1.4 Confocal laser scanning microscopy

Confocal microscopy was pioneered by Marvin Minsky in 1955 (Minsky, 1988) and allows the creation of sharp, high resolution images of a specimen. This is made possible by point-by-point illumination of the specimen and use of a pinhole aperture to prevent out of focus light reaching the detector. In fluorescence confocal microscopy, lasers are used as the light source to excite fluorescence in a specimen. Fluorescence confocal microscopy is therefore described as confocal laser scanning microscopy (CLSM) and is illustrated in Figure 1-8. A dichroic mirror or beam-splitter separates excitation and emission light and emission light is directed to the photomultiplier tube (PMT) detector by dichroic mirrors. The pinhole aperture improves optical sectioning and ensures that detected light is from a thin focal plane. As a result, a sharper, better resolved fluorescent image of the focal plane is produced in comparison to wide-field microscopy.

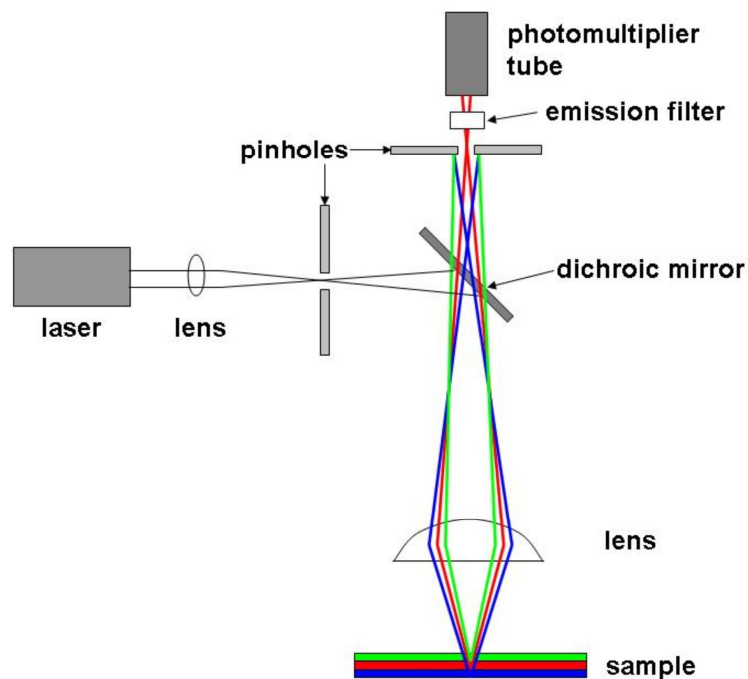


Figure 1-8 Confocal Laser Scanning Microscopy

The sample is excited by a laser beam and fluorescence emission from the fluorophore is directed to the PMT by dichroic mirrors. Only light from the focal plane (red) is directed through the pinhole aperture. Out of focus light from above (green) and below (blue) the focal plane is rejected.

1.4.1 Single photon excitation fluorescence microscopy

In CLSM, the fluorophore in the sample is excited by a laser emitting photons of a particular wavelength. The photon is absorbed by the fluorophore molecule and it enters a higher energy state (the excited state). Some of the energy is lost and the fluorophore enters a semi-stable state. When the fluorophore returns to the ground state, it emits a photon of light (fluorescence) of lower energy, and consequently longer wavelength (Figure 1-9). If a single high energy photon is sufficient to excite the fluorophore molecule, this is known as single photon (1P) excitation.

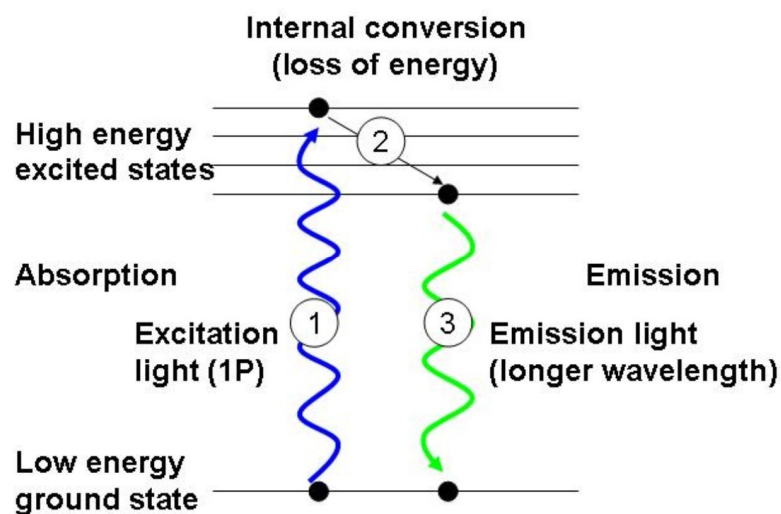


Figure 1-9 Jablonski diagram illustrating principle of 1P fluorescence excitation

(1) A single photon of light of a particular wavelength is absorbed by the fluorophore molecule and an electron enters a higher energy (excited) state. (2) Some loss of energy occurs in the vibration state through internal conversion and the electron enters a semi-stable state. (3) When the electron returns to the ground state, a photon of light of lower energy (and thus longer wavelength) is emitted (fluorescence).

1.4.1.1 Problems associated with 1P excitation CLSM

There are a number of problems associated with CLSM. The use of high intensity lasers, particularly when using short wavelengths, can cause severe photodamage in living cells by the formation of reactive oxygen species (ROS). Laser excitation of chemical structures such as aromatic porphyrins, which are a component of haemoproteins including haemoglobin, myoglobin and the cytochromes, can lead to the formation of ROS (König, 2006). These ROS can cause deoxyribonucleic acid (DNA) damage and oxidation of lipid and protein structures within the cell, as well as playing an important role in triggering cell

death by apoptosis (König, 2000; Cunningham *et al.*, 1985) Excitation light can also cause fluorophores to fade irreversibly, a process known as photobleaching. The problems of photodamage and photobleaching can be minimised by reducing the laser power used for excitation, but this will limit the intensity of fluorescence produced.

The presence of the detector pinhole means that the number of photons reaching the detector is limited and the signal-to-noise ratio may be low. This can be improved by increasing the intensity of laser excitation, but this increases the likelihood of photodamage and photobleaching occurring. Alternatively, the pinhole diameter may be increased in size, but this leads to loss of x, y and z resolutions. Another problem with 1P-excitation CLSM is that the penetration depth is limited to a maximum of 40-50 μm (Centonze & White, 1998).

1.4.2 Two photon excitation fluorescence microscopy

Many of the problems associated with 1P excitation CLSM can be minimised by using two photon (2P) excitation fluorescence microscopy. This method requires the simultaneous absorption of two lower energy photons in order to excite the fluorophore molecule and allows the use of infrared (IR) or near infrared (NIR) light (Figure 1-10). As the probability of absorption is proportional to the square of the instantaneous light intensity, lasers that generate ultra-short but intense pulses are used. Pulses are $\sim 10^{-13}\text{s}$ long and occur at repetition rates of $\sim 100\text{MHz}$ (Denk *et al.*, 2006). The instantaneous light intensity is extremely high, but the average power reaching the sample is not excessive (Centonze & White, 1998).

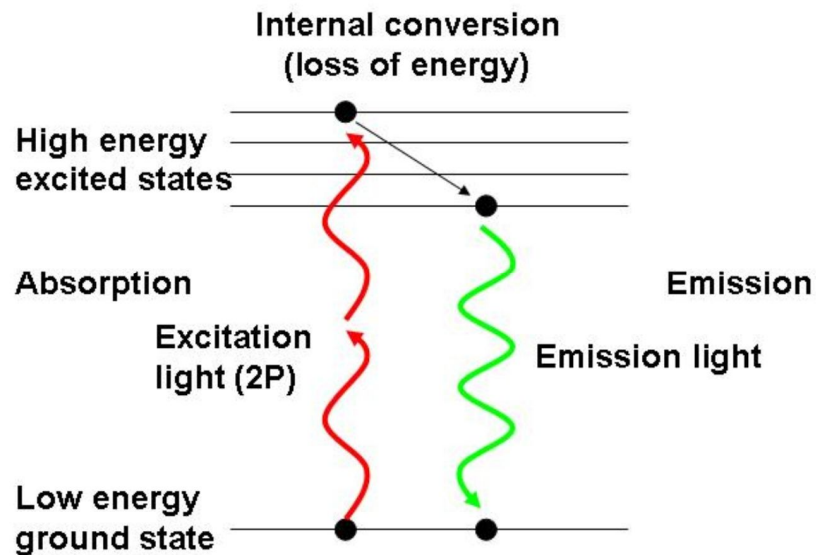


Figure 1-10 Jablonski diagram illustrating principle of 2P fluorescence excitation

2P fluorescence excitation requires the simultaneous absorption of 2 longer wavelength (lower energy) photons of light by the fluorophore in order for fluorescence to be emitted.

As the probability of two photons being absorbed at the same time is much lower than if a single photon was absorbed, fluorescence emission is limited to the focal volume of the objective where the intensity is highest (Figure 1-11). The lower average power and limited excitation thus restricts photodamage and photobleaching to the focal volume of the objective. In addition, IR and NIR light is less damaging than shorter wavelengths of light, especially from the UV region. In 1P excitation CLSM, fluorescence is emitted from above and below the focal plane, but the detector pinhole ensures that only in-focus light is directed to the PMT. Because 2P-excitation does not generate out-of-focus fluorescence, optical sectioning can be achieved without a detector pinhole, resulting in greater fluorescence collection efficiency. This, along with the fact that NIR light scatters much less than shorter wavelengths, means that 2P-excitation fluorescence microscopy allows for greater imaging penetration depth, around 10 times deeper or more (Rubart, 2004; Huang *et al.*, 2002; Centonze & White, 1998; Denk *et al.*, 1990). 2P-excitation fluorescence microscopy can therefore be performed on thicker specimens, such as intact tissue, whereas 1P excitation CLSM is largely limited to use on single cells.

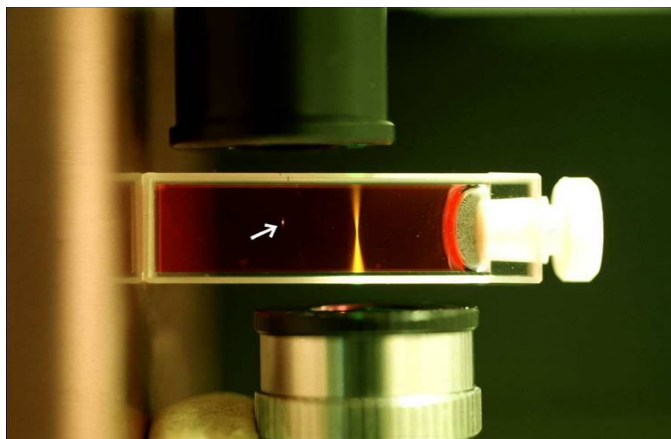


Figure 1-11 Fluorescence emission by fluorescein following 1P and 2P excitation

A cuvette of fluorescein excited by 1P excitation (right line) and 2P excitation (localised spot of fluorescence indicated by arrow) illustrating that 2P excitation is confined to the focus of the excitation beam (Amos, 2000).

1.5 Applications for real time monitoring of mitochondrial redox state

1.5.1 O₂ availability in intact tissue preparations

Measurements of NADH fluorescence have been widely used to investigate O₂ availability in whole tissue preparations. Areas of low perfusion and thus low O₂ supply can be identified by increased NADH fluorescence. This is because the presence of O₂ is required for oxidative phosphorylation to proceed. When the O₂ supply is limited, ETC activity is inhibited and reducing equivalents accumulate, resulting in an increase in NADH fluorescence and a decrease in FAD fluorescence.

Early work in a Langendorff-perfused rat heart preparation used the UV-component of a xenon flash to excite NADH fluorescence and photographs were taken of surface fluorescence emission (Barlow & Chance, 1976). This provided a 2-dimensional recording of NADH levels on the surface of the heart and demonstrated heterogeneity of O₂ delivery to the tissue at low perfusion pressures. When the coronary artery was ligated to produce local ischaemia, the area of tissue in the apex of the left ventricle (LV) where perfusion had been blocked could be identified by the strong NADH fluorescence signal in that area.

NADH fluorescence measurements have since been used in numerous studies to identify areas of ischaemia and hypoxia/anoxia in different tissue types (summarised by (Mayevsky & Rogatsky, 2007)). The degree of ischaemia and boundaries between well perfused and poorly perfused areas can be identified by levels of NADH fluorescence. This information can be utilised to study the effect of ischaemia on factors such as electrical activity and Ca^{2+} signalling in the heart (Kay *et al.*, 2008; Swift *et al.*, 2008). Recently, Aldakkak *et al.* have simultaneously measured NADH and FAD fluorescence to monitor mitochondrial bioenergetics in isolated perfused guinea pig hearts during ischaemia and reperfusion (Aldakkak *et al.*, 2009; Aldakkak *et al.*, 2008).

1.5.2 Mitochondrial metabolite supply and demand matching

Real time monitoring of mitochondrial redox state also gives an indication of how well cells and tissue are able to match metabolite supply with demand in response to increased workload. Contraction of the cell requires energy, so work intensity is usually increased by increasing the frequency of contraction (and/or afterload in whole heart preparations). When the rate of ATP synthesis is increased, there must be a proportional increase in the rate of reducing equivalent supply from the TCA cycle. If an increase in work intensity results in oxidation of the mitochondrial environment, this suggests that the rate of delivery of reducing equivalents is not increasing to the same extent as the rate of oxidative phosphorylation is increased to maintain ATP supply. If the mitochondrial redox state becomes more reduced, this would indicate an increased rate of reducing equivalent supply in excess of the increased rate of oxidative phosphorylation. However, in intact tissue preparations, it could also indicate a limited O_2 supply inhibiting oxidative phosphorylation and ATP production. If the redox state does not change, this would suggest that metabolite supply and demand are well matched.

Previous studies in the heart, using measurements of NADH fluorescence alone, have demonstrated different oxidative responses to changes in work intensity. Some studies have shown no change in the NADH fluorescence upon increased stimulation frequency in isolated rat and guinea pig myocytes (Griffiths *et al.*, 1998) and in a whole rabbit heart preparation (Heineman & Balaban, 1993).

Other studies in rat demonstrate a decrease in NADH fluorescence, indicating oxidation of the isolated ventricular myocyte (Heinzel *et al.*, 2006; White & Wittenberg, 2000; White & Wittenberg, 1993) and whole heart preparation (Ashruf *et al.*, 1995) in response to increased workload. A similar response was reported in isolated papillary muscle from the rabbit (Chapman, 1972). It has also been shown in the guinea pig that NADH fluorescence falls in conditions of high intracellular Na^+ concentration ($[\text{Na}^+]_i$), such as in cells from failing hearts, in response to increased work intensity, whereas control myocytes with normal $[\text{Na}^+]_i$ show no significant change (Liu & O'Rourke, 2008; Maack *et al.*, 2006).

In contrast, an increase in NADH fluorescence has been reported in response to increased pacing frequency in glucose perfused rat hearts (Katz *et al.*, 1987) and isolated rat cardiomyocytes (Griffiths *et al.*, 1997). Finally, in a series of studies performed on isolated trabeculae from rat heart, Brandes *et al.* demonstrated that the initial response to increased work was a fall in NADH/NAD⁺ ratio, followed by a mitochondrial Ca^{2+} dependent increase in NADH during fast pacing (Brandes & Bers, 2002; Brandes & Bers, 1999; Brandes *et al.*, 1998; Brandes & Bers, 1997; Brandes & Bers, 1996). These findings were supported by experiments performed on isolated guinea pig myocytes (Jo *et al.*, 2006).

To my knowledge, no study has used FAD measurements, or a combination of NADH and FAD measurements, to assess changes in redox state in response to changes in workload.

1.6 Importance of maintaining redox potential

As well as being the driving force for oxidative phosphorylation and supplying the electrons required to produce ATP, maintenance of the redox potential is also important in order to control oxidative stress within the mitochondria.

1.6.1 ROS

The electron transfer process of oxidative phosphorylation represents the major intracellular source of ROS within the cell (Turrens, 2003). The respiratory complexes of the ETC can leak electrons to O_2 , mainly producing the superoxide

anion ($O_2^{\cdot-}$), which is a mediator of oxidative chain reactions and the precursor for most other ROS. Low concentrations of ROS are thought to play a role as signalling molecules in some cell signalling pathways (D'Autreaux & Toledano, 2007) and they have been shown to be involved in the signalling mechanisms leading to the cardioprotective effects of ischaemic pre and postconditioning (Penna *et al.*, 2009). However, their highly reactive nature can have damaging effects on the cell. In oxidative stress conditions, high levels of ROS are associated with deleterious effects on DNA, lipids and proteins. To protect against this and keep ROS levels low, a number of antioxidant control mechanisms exist within the mitochondrial compartment. These include the superoxide dismutase, glutathione peroxidase and glutathione reductase systems (Sies, 1993).

1.6.2 Role of NADH in antioxidant control mechanisms

ROS scavenging mechanisms within the cell are ultimately linked to the mitochondrial redox balance (Liu & O'Rourke, 2009). In the reduced state, antioxidants can donate electrons to unstable molecules, such as ROS, thereby detoxifying them. Glutathione in the reduced state (GSH) is an antioxidant involved in the clearance of hydrogen peroxide (H_2O_2). Two molecules of GSH are oxidised to reduce one molecule of H_2O_2 to two molecules of water in a reaction catalysed by glutathione peroxidase. Oxidised glutathione (GSSG) can be reduced back to GSH in a reaction catalysed by glutathione reductase, which requires NADPH as an electron donor. NADPH is oxidised in the process to $NADP^+$, and in order for glutathione to be kept in the reduced state and for the redox chain to be maintained, NADPH supply must be preserved.

There are three main reactions which regenerate NADPH and keep glutathione in the reduced state: $NADP^+$ -dependent isocitrate dehydrogenase, malic enzyme and nicotinamide nucleotide transhydrogenase (Vogel *et al.*, 1999). The $NADP^+$ -dependent isocitrate dehydrogenase and malic enzyme reactions depend on the levels of TCA cycle intermediates. However, the nicotinamide nucleotide transhydrogenase reaction requires NADH to reduce $NADP^+$ and production of NADPH is strongly favoured in the presence of an electrochemical proton gradient. Thus, maintenance of $NADH/NAD^+$ plays a role in the mitochondria's

defences against oxidative stress. The role of NADH and NADPH (NAD(P)H) as indirect antioxidants is well established. However, there is also some evidence to suggest that NAD(P)H may have direct antioxidant actions in the cell (Petrat *et al.*, 2003; Kirsch & de Groot, 2001)

The importance of NADH as an indirect or direct antioxidant has recently been shown experimentally. In guinea pig cardiomyocytes, a transient fall in NADH fluorescence levels was accompanied by an increase in H₂O₂ levels detected using the H₂O₂-sensitive dye 5-(and-6)-chloromethyl-2',7'-dichlorodihydrofluorescein diacetate, acetyl ester (CM-DCF) (Kohlhaas *et al.*, 2010; Knopp *et al.*, 2009). H₂O₂ levels returned to baseline when NADH levels recovered. In addition, in rat cardiomyocytes, oxidation of NADH in response to increased work intensity resulted in an increase in ROS, an effect which was attenuated by the antioxidant *N*-acetylcysteine (NAC) (Heinzel *et al.*, 2006).

1.7 Energy metabolism in failing hearts

Heart failure (HF) is a syndrome resulting from the inability of the heart to pump blood at a rate sufficient to meet the body's metabolic demands. Causes of HF include past myocardial infarction, hypertension, cardiomyopathy and congenital heart disease. Metabolic changes occur in HF which are likely to contribute to impaired contractile function of the heart muscle. The failing heart has a reduced capacity to transduce the energy from substrates into ATP (Ingwall & Weiss, 2004; van Bilsen *et al.*, 2004) and has thus been described as "An engine out of fuel" (Neubauer, 2007).

1.7.1 Altered substrate utilisation

In the well-perfused healthy heart, over 95% of ATP is produced by oxidative phosphorylation and ~60-90% of this is derived from metabolism of fatty acids (Stanley *et al.*, 2005). There are conflicting reports of changes in substrate utilisation in heart failure. Studies using animal models of cardiac hypertrophy and HF performed in the dog (Lei *et al.*, 2004; Osorio *et al.*, 2002; Recchia *et al.*, 1998) and rat (Christe & Rodgers, 1994) have shown a switch from fatty acid to glucose metabolism. This is often described as a switch to the "foetal

phenotype" and has shown to be associated with a down-regulation of genes involved in fatty acid β -oxidation (Bugger *et al.*, 2010; Akki *et al.*, 2008; Barger & Kelly, 2000; Sack *et al.*, 1996). However, studies of substrate utilisation in human HF patients have produced varied results. Some reports reproduce the changes seen in animal studies (las Fuentes *et al.*, 2003; Davila-Roman *et al.*, 2002), some report no change (Funada *et al.*, 2009), while others still report an increase in fatty acid uptake in HF patients (Taylor *et al.*, 2001; Paolisso *et al.*, 1994). The conflicting reports in human studies may be due to differences in the severity of HF in the participating patients, or may be due to the influence of co-morbidities such as obesity, insulin resistance or Type 2 diabetes (van Bilsen *et al.*, 2009). In the advanced stages of HF, glucose uptake is also thought to decline due to the development of myocardial insulin resistance (Neubauer, 2007).

Recent work by Elrod *et al.* (2010) using cyclophilin D knock-out mice has shown that the increased activity of Ca^{2+} dependant dehydrogenases, (particularly pyruvate dehydrogenase) due to higher mitochondrial matrix Ca^{2+} levels resulted in increased glucose oxidation relative to fatty acids under normal conditions. This limited the metabolic flexibility of the heart which is necessary for compensation during stress (for example during exercise or in pressure overload). As a result, cardiac structure and function was more severely affected following pressure overload induced hypertrophy in these animal compared to wild type controls.

It remains unclear whether this switch towards a dependence on glucose utilisation is beneficial or detrimental to the heart. Oxidation of glucose is more efficient than oxidation of fatty acids. However, the ATP yield of fatty acids such as palmitate is much greater than for glucose (~129 ATP compared to ~36 ATP). Thus many more glucose molecules need to be oxidised to produce the ATP produced by oxidation of one molecule of palmitate (van Bilsen *et al.*, 2009). Ultimately, the increase in glucose oxidation does not fully compensate for the decrease in fatty acid oxidation. Therefore, the hypertrophied and failing heart remains energy compromised.

1.7.2 Impaired oxidative phosphorylation

Impaired oxidative phosphorylation by the mitochondria also appears to be a factor leading to reduced respiratory function in HF. It has been demonstrated that mitochondrial protein content and the activity of ETC complexes and ATP-synthase is reduced in animal models of HF (Bugger *et al.*, 2010; Lin *et al.*, 2007; Garnier *et al.*, 2003; Liu *et al.*, 2001; Marin-Garcia *et al.*, 2001). Reduced complex IV activity has also been reported in human patients with idiopathic dilated cardiomyopathy (Quigley *et al.*, 2000). The efficiency of ATP synthesis also appears to be reduced in HF, with reports of increased levels of cardiac uncoupling proteins in blood samples from HF patients (Murray *et al.*, 2004), and impaired state 3 respiration by isolated mitochondria to a similar extent as in the presence of an uncoupling agent (Bugger *et al.*, 2010). When respiration is uncoupled, ETC activity is not linked to phosphorylation of ADP, and consequently the mitochondria produce heat instead of ATP.

1.7.3 Derangement of energy transfer systems

ATP is rapidly transferred out of the mitochondria into the cytosol for utilisation by myofibrillar proteins and ion pumps via the creatine kinase phosphocreatine shuttle system. The phosphate from ATP is transferred to creatine (Cr) to form phosphocreatine (PCr) and ADP, a reaction catalysed by the mitochondrial isoform of Cr kinase (CK). PCr is much smaller and less charged than ATP and can rapidly diffuse out of the mitochondria via the shuttle system to the myofibrils, SR, etc. Here, the myofibrillar isoform of CK catalyses the reformation of ATP from PCr, enabling ATP to be utilised by the cell to fuel contraction. The free Cr formed by this reaction diffuses back to the mitochondria for rephosphorylation. Around two thirds of the heart's total Cr pool is phosphorylated to PCr, whereas around one third remains as free Cr. Cr cannot be synthesised by the cardiac myocyte, and enters the cell via the Cr transporter.

The CK system also plays an important role as an energy buffer. When energy demand exceeds supply, such as in bursts of intense activity, PCr can be utilised to maintain ATP levels. However, this results in an increase in the free ADP concentration, inhibiting the function of many intracellular enzymes and

subsequently the contractile function of the heart. Thus, the myocyte is adversely affected by a fall in PCr and increase in ADP levels, even when ATP levels are maintained. The ratio of PCr to ATP gives a good indication of the energetic state of the heart. The CK equilibrium favours ATP synthesis over PCr synthesis. When the demand for ATP surpasses supply, PCr levels decline first and ATP levels only decline when PCr is substantially depleted (Neubauer, 2007).

A number of changes in the CK system have been demonstrated in HF. PCr, Cr and CK levels are reduced (Beer *et al.*, 2002; Kalsi *et al.*, 1999; Nascimben *et al.*, 1996) and down-regulation of the creatine transporter (Neubauer *et al.*, 1999; Ten Hove *et al.*, 2005) contributes to the reduction in the creatine pool. Consequently, ATP transfer within the cell is severely impaired. Taking into account the decrease in PCr:ATP ratio which results from the depleted Cr pool, it is clear that the metabolic reserves are seriously compromised in HF.

1.7.4 Effects of metabolic changes on contractile function

A summary of the metabolic changes that occur over the course of HF progression is shown in Figure 1-12 (Neubauer, 2007). The combination of mitochondrial dysfunction and defects in energy transfer mechanisms that occur in cardiac hypertrophy and HF result in reduced ATP supply and availability. Ultimately the contractile function of the heart will be adversely affected as myofilaments and ion pumps are unable to receive the fuel they require to function effectively. Although a number of studies have described the changes in mitochondrial protein content and activity, very few have looked at how the redox state and hence control of oxidative phosphorylation may be affected in HF.

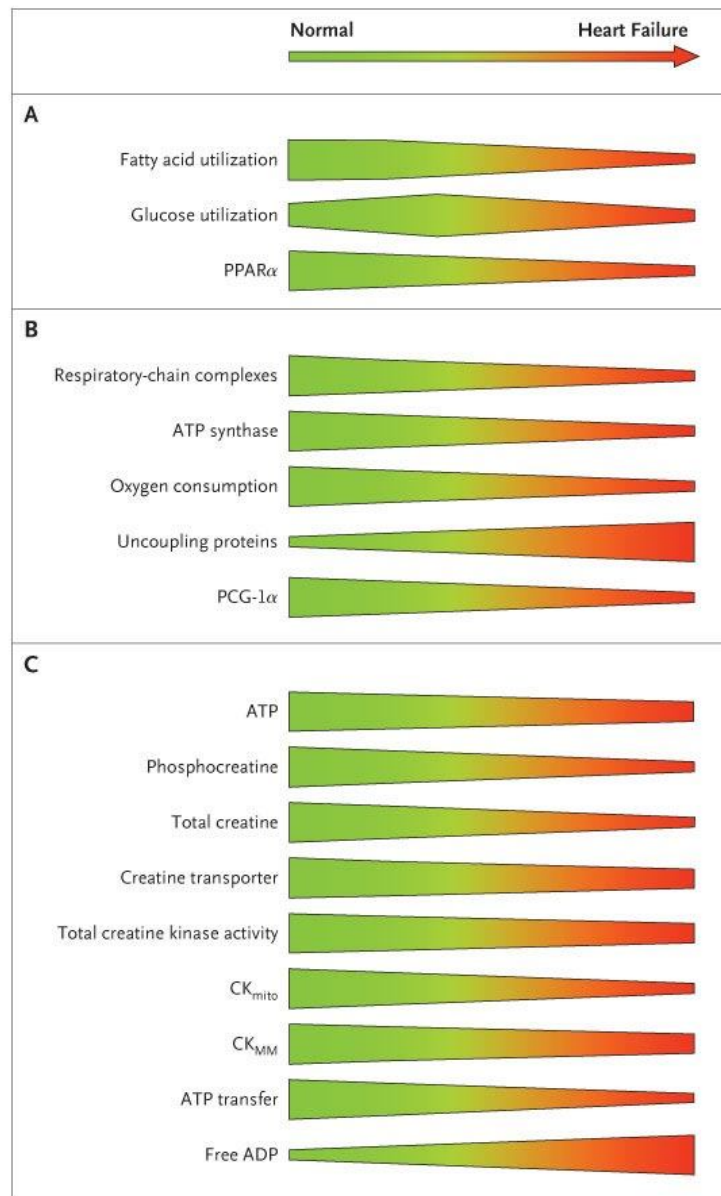


Figure 1-12 Changes in cardiac energy metabolism in HF

Panel A shows changes in substrate utilisation, panel B changes in oxidative phosphorylation and panel C changes in high energy phosphate metabolism in patients with heart failure. PPAR α : Peroxisome proliferator-activated receptor alpha, PCG-1 α : PPAR γ coactivator 1 alpha, CK_{mito}: mitochondrial creatine kinase isoenzyme, CK_{MM}: myofibrillar creatine kinase isoenzyme. Reprinted with permission (Neubauer, S. (2007). The Failing Heart - An Engine Out of Fuel). *The New England Journal of Medicine* 356, 1140-1151). Copyright © [2007] Massachusetts Medical Society. All rights reserved.

1.8 Investigating energy supply and demand matching in animal models of cardiac hypertrophy

A number of different methods are employed to develop animal models of cardiac hypertrophy and HF. These methods include rapid ventricular pacing, myocardial ischaemia and infarction (e.g. by ligation of the coronary artery), use of drugs with cardiac toxicity or by inducing volume or pressure overload (Monnet & Chachques, 2005). The stroke-prone spontaneously hypertensive rat (SHRSP) model is a genetic model of cardiac hypertrophy induced by pressure overload.

1.8.1 The SHRSP model

The spontaneously hypertensive rat (SHR) was developed from the Wistar-Kyoto (WKY) strain by Okamoto and Aoki in the early 1960s (Okamoto & Aoki, 1963). Selection and repeated mating of hypertensive WKY offspring eventually gave rise to a colony of rats which, without exception, developed hypertension. Selective breeding of offspring from SHR rats that died from stroke led to the establishment of the SHRSP strain. SHRSP rats develop hypertension at a younger age than other SHR strains, frequently over 230mmHg, and this is closely related to the high incidence of stroke (Okamoto *et al.*, 1974). These animals develop a number of cardiovascular complications, including endothelial dysfunction, vascular remodelling and LV hypertrophy and fibrosis (Arribas *et al.*, 1999; McIntyre *et al.*, 1999; Dominiczak *et al.*, 1996).

Some studies have also reported mitochondrial dysfunction in these animals. In 24 week old SHRSP rats, levels of isocitrate dehydrogenase (related to the TCA cycle) and cytochrome c oxidase (complex IV of the respiratory chain) were found to be lower compared to WKY controls, suggesting impaired oxidative metabolism in SHRSP hearts. In addition, reduced superoxide dismutase activity in SHRSP hearts, a potent scavenger of free radicals, is likely to result in increased oxidative stress and may be the cause of the abnormalities in SHRSP mitochondrial DNA also reported (Tokoro *et al.*, 1996). Cytochrome c oxidase was also found to be reduced in the hearts of 16 week old SHRSP rats (Chen *et al.*, 1995). Mitochondrial function in SHRSP rat heart has been examined in this

thesis and compared to age matched WKY controls. In these experiments, the focus was on the mitochondrial redox state and energy supply and demand matching, as well as studying differences in contractile function.

1.8.2 Energy supply and demand matching in pressure overload-induced models of LV hypertrophy

Changes in mitochondrial redox state in response to increased work intensity have previously been examined in guinea pig and rat models of cardiac hypertrophy. In both cases, aortic banding was used to induce pressure overload leading to LV hypertrophy. Guinea pig cardiomyocytes were isolated around 6-8 weeks after surgery when a decrease in LV ejection fraction was observed (Liu & O'Rourke, 2008). It was found that failing cells were unable to match energy supply with demand. When workload was increased by increasing stimulation frequency to 4Hz in the presence of isoproterenol, NADH fluorescence dramatically decreased and did not recover when stimulation was stopped, but the redox state was maintained in control cells (Figure 1-13). This difference was attributed to higher $[Na^+]_i$ in failing cells, reducing Ca^{2+} accumulation by the mitochondria due to altered mitochondrial NCX activity. The resultant reduced stimulation of Ca^{2+} -sensitive dehydrogenase enzymes of the TCA cycle limits the rate of NADH production in failing cells, leading to oxidation of the mitochondrial environment when workload and ATP demand is increased.

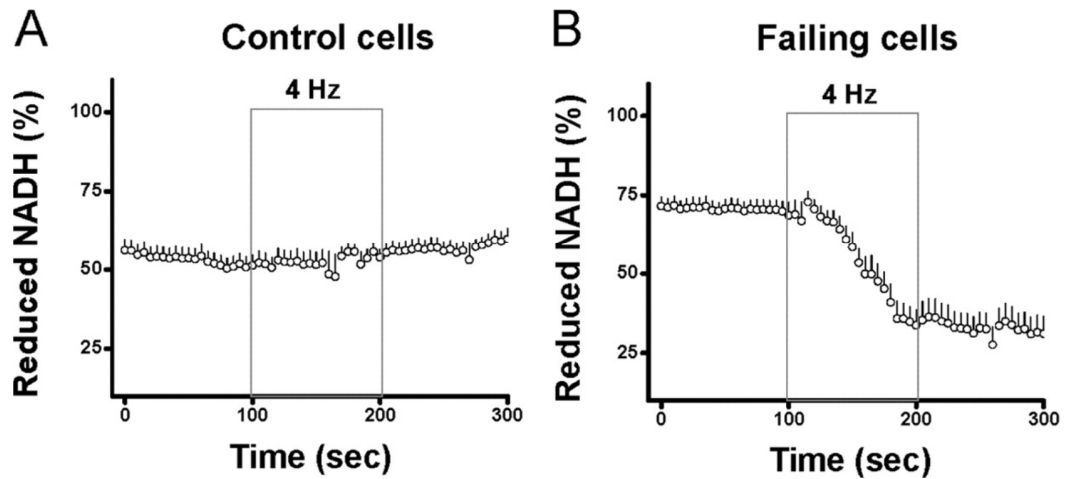


Figure 1-13 NADH fluorescence changes in guinea pig ventricular myocytes in response to increased work intensity

(A) NADH fluorescence is maintained in control cells (B) NADH fluorescence dramatically decreased upon increased stimulation frequency in failing cells. Reprinted by permission from Wolters Kluwer Health: (Liu, T. & O'Rourke, B. (2008). Enhancing Mitochondrial Ca²⁺ Uptake in Myocytes From Failing Hearts Restores Energy Supply and Demand Matching. *Circulation Research* 103, 279-288).

However, similar experiments performed on isolated trabeculae from rat heart produced a somewhat different response (Brandes *et al.*, 1998). In these experiments, trabeculae were isolated 15-18 weeks after aortic banding surgery. Stimulation frequency was increased from 0.25 Hz to 0.5 Hz, 1 Hz and 2 Hz and NADH fluorescence recorded. It was found that immediately after stimulation frequency was increased, the fall in NADH fluorescence was much greater in trabeculae from hypertrophied hearts. NADH fluorescence then recovered towards baseline to around the same steady state level. When stimulation frequency was slowed back to 0.25 Hz, the NADH fluorescence overshoot on recovery was greater in hypertrophied trabeculae (Figure 1-14).

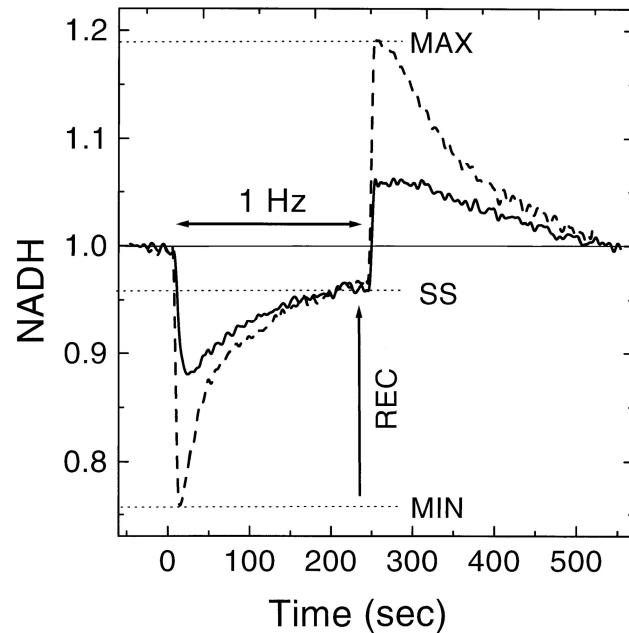


Figure 1-14 NADH fluorescence changes in rat isolated trabeculae in response to increased work intensity

Increasing stimulation frequency to 1Hz results in a fall in NADH fluorescence to minimum levels (MIN). Fluorescence then recovers (REC) to a new steady state (SS) level. When stimulation frequency is slowed back to 0.25Hz, NADH fluorescence overshoots to maximum levels (MAX) before recovering to baseline. Solid line represents response in control trabeculae, dashed line represents response in trabeculae from hypertrophied hearts. NADH reached a lower min and higher max in trabeculae from hypertrophied hearts. Reprinted by permission from Wolters Kluwer Health: (Brandes, R., Maier, L. S., & Bers, D. M. (1998). Regulation of Mitochondrial [NADH] by Cytosolic $[Ca^{2+}]$ and Work in Trabeculae From Hypertrophic and Normal Rat Hearts. *Circulation Research* 82, 1189-1198)

Like Liu & O'Rourke, Brandes *et al.* demonstrate that there is an initial large imbalance between energy production and consumption in cardiac hypertrophy. However, they show that there is compensation for this imbalance, and the recovery mechanism is enhanced in hypertrophic hearts. Thus the effects of cardiac hypertrophy on energy supply and demand matching are inconsistent and remain unclear. Therefore, these responses have been further investigated in a genetic model of cardiac hypertrophy in this thesis.

1.9 Aims of the project

The overall aim of the project was to investigate mitochondrial redox state in myocardial cells and tissue using intrinsic fluorescence methods. Spectral analysis of the endogenous fluorophores NADH and FAD was first performed in order to establish optimal optical settings to simultaneously measure fluorescence from both fluorescent species.

The individual aims of the project were:

- i. To assess the reproducibility and reliability of the method by measuring mitochondrial redox state in isolated LV cells from rabbit hearts using a variety of fluorescence techniques.
- ii. To assess if the enzymatic digestion process used to isolate single cells affects mitochondrial function by comparing mitochondrial redox state in isolated LV cells with intact cardiac tissue preparations.
- iii. To examine the feasibility of using 2P-excitation fluorescence microscopy to image local regions within the myocardium
- iv. To investigate how mitochondrial redox state changes in isolated rabbit LV cells in response to changes in work intensity, i.e. metabolite supply and demand matching.
- v. To investigate metabolite supply and demand matching in a genetic model of pressure overload-induced cardiac hypertrophy in the rat.

2 Methods

Solutions used

2.1.1 Extracellular solutions

Experiments performed on isolated cells used a modified Krebs solution as the physiological extracellular solution. For experiments using whole rabbit heart and the ventricular wedge preparation, a modified Tyrode's solution was used. All chemicals were obtained from Sigma unless otherwise stated.

Modified Krebs solution

120 NaCl, 20 HEPES, 5.40 KCl, 0.52 NaH₂PO₄, 3.50 MgCl₂.6H₂O, 20 taurine, 10 creatine, 11.10 glucose (concentrations in mM).

Modified Tyrode's solution

93 NaCl, 20 NaHCO₃, 1 Na₂HPO₄, 1 MgSO₄.7H₂O, 5 KCl, 20 Na⁺ acetate, 50 glucose (concentrations in mM). Solution contained 1.8mM CaCl₂ unless otherwise stated. The solution was filtered through a 5µm filter (Millipore) and continuously bubbled with a gaseous mixture containing 95% O₂ and 5% CO₂ to maintain pH 7.4

2.1.2 Mitochondrial inhibitors

Carbonyl cyanide *p*-(trifluoromethoxy) phenylhydrazone (FCCP)

Stock solution of FCCP was diluted in water to a concentration of 100µM on each experimental day. This FCCP solution was further diluted in Krebs solution (containing 1.8mM Ca²⁺) to 2µM for cell perfusion.

Sodium cyanide (NaCN)

NaCN was dissolved in water to a concentration of 300mM on each experimental day. This was diluted to 200mM by addition of 1M HEPES solution and pH was adjusted to 7.4 with 1M HCl. The NaCN solution was further diluted in Krebs solution (containing 1.8mM Ca²⁺) to 2mM for cell perfusion.

2.2 Cell isolation

2.2.1 Cell isolation procedure for rabbit ventricular myocytes

Male New Zealand white rabbits were euthanised with 500 IU heparin and an overdose of Na pentobarbitone (100mg/kg), delivered via the left marginal ear vein. Absence of corneal and pain reflexes was confirmed and the thoracic cavity opened. The heart was quickly removed and placed in a beaker of sterile Krebs at room temperature. The heart was then mounted via the aorta on to the cannula of a Langendorff retrograde perfusion system and securely tied in position, ensuring no air bubbles entered the heart. Excess fat and connective tissue was trimmed away and the coronary vessels perfused with Ca^{2+} -free sterile Krebs solution (maintained at 37°C) to remove blood and Ca^{2+} . Perfusion was then switched to Ca^{2+} -free Krebs solution supplemented with 0.66mg/ml collagenase (Worthington Chemicals) and 0.04mg/ml protease. The enzyme solution was collected from the heart after 1 minute and re-circulated once the initial volume of solution had passed through. When the heart became hard, around 2-3 minutes into the digestion process, 0.05mM CaCl_2 was added to the re-circulating enzyme. Enzymatic digestion was continued for 5-7 minutes, or until the right ventricular tissue felt softened to touch. The enzymes were then washed out of the heart by perfusing with 50ml sterile Krebs solution containing 0.1% (w/v) Bovine Serum Albumin (BSA) and 0.075mM CaCl_2 .

The heart was taken off the cannula and atrial tissue removed and discarded. Digested tissue was finely cut up in BSA solution; ensuring that tissue from the LV, right ventricle (RV) and intraventricular septum were kept separate. The myocytes were dissociated by gently triturating the tissue in solution with a Pasteur pipette. Any undigested tissue was removed by filtering through gauze mesh, leaving behind a single-cell solution which was transferred into tubes.

The isolated cells were allowed to settle, the supernatant removed and the cells re-suspended in Krebs solution containing 0.125mM CaCl_2 . This process was repeated 3 times in solutions with progressively higher CaCl_2 concentrations, until a final concentration of 1.0mM CaCl_2 was achieved. All experiments were performed using cells isolated from the LV.

2.2.2 Cell isolation procedure for rat ventricular myocytes

Male WKY and SHRSP rats were stunned by a blow to the head and killed by cervical dislocation. The thoracic cavity was opened and heart removed and placed in ice-cold Krebs solution. The heart was mounted and tied via the aorta on to the cannula of a Langendorff perfusion system and perfused with Krebs solution at 37°C until all the blood had been washed out from the coronary vessels and the perfusate from the heart ran clear. The heart was then perfused with Ca²⁺-free Krebs solution containing 0.66mg/ml collagenase and 0.04mg/ml protease. Enzyme solution was collected from the heart and re-circulated once the initial solution had passed through. Enzyme digestion was continued until the RV tissue felt softened to the touch, at which point perfusion was stopped.

The heart was taken down, divided into LV and RV tissue sections, and cut up finely into Krebs solution containing 0.5% (w/v) BSA. The tissue was gently triturated with a Pasteur pipette in order to dissociate the myocytes, and the supernatant transferred into tubes. The CaCl₂ concentration in the cell solution was gradually increased over time until a final concentration of 1.0mM CaCl₂ was obtained. Experiments were performed on cells isolated from the LV.

2.3 Left ventricular wedge preparation

The arterially perfused LV wedge preparation was first developed in canine hearts (Yan & Antzelevitch, 1996) and is a useful model for electrophysiological studies. The preparation can also be reproduced in rabbit heart (Yan *et al.*, 2001), although is technically more difficult to prepare due to the smaller size. For the purposes of this project, the rabbit LV wedge preparation was used to study mitochondrial redox state in intact tissue.

Male New Zealand white rabbits were euthanised with 500 IU heparin and an overdose of Na pentobarbitone (100mg/kg), delivered via the left marginal ear vein. Absence of pain reflexes was confirmed and the thoracic cavity opened. The heart was rapidly excised and placed in a beaker of ice cold Tyrode's solution and then transferred to a custom-made Perspex chamber. The ascending aorta was opened, the left main coronary ostium identified and the

modified cannula passed into the artery and perfused with oxygenated Tyrode's solution maintained at 37°C. Pressure in the system was continuously monitored with an inline pressure monitor.

Once the cannula was in position, flow rate was increased to 30ml/min. Correct positioning of the cannula was confirmed by observing clearance of blood from the perfused area of myocardium and an increase in pressure in the system (~50-60mmHg). The RV outflow tract was removed and the cannula sutured in position. A bleb and a black suture marker on the cannula identified how deep the cannula needed to be inserted into the vessel. The left and right atria and the RV free wall were removed. Any open vessels that resulted when these tissues were removed were closed up by suturing to ensure that perfusion pressure was maintained. An incision was made through the interventricular septum at the base of the aorta and any unperfused tissue removed. Any open vessels were sutured closed to prevent myocardial perfusion becoming compromised. The wedge preparation was positioned in the chamber, epicardial surface facing upwards, and secured in place with metal pins. Perfusion was then switched to an oxygenated Tyrode's solution containing 10µM blebbistatin (Biomol International) to inhibit contraction. Once contractions had been completely inhibited, the preparation was ready for imaging.

2.4 Langendorff-perfused whole heart preparation

Although the LV wedge preparation had the advantage that it could be studied in a quiescent state, it was technically difficult to prepare. This led to the simplification of the procedure to measure mitochondrial redox state in Langendorff-perfused whole heart.

Male New Zealand white rabbits were euthanised with 500 IU heparin and an overdose of Na pentobarbitone (100mg/kg), delivered via the left marginal ear vein. Absence of corneal and pain reflexes was confirmed and the thoracic cavity opened. The heart was quickly excised and immersed in ice cold Tyrode's solution. The heart was transferred to the custom made Perspex chamber and mounted and tied via the aorta to the cannula (a modified 3-way valve) of a Langendorff retrograde perfusion system. The heart was perfused with

oxygenated Tyrode's solution maintained at 37°C. Flow rate was increased to 30ml/min and any excess fat and connective tissue trimmed away. Pressure in the system was continually monitored using an inline pressure monitor.

Once the blood had been washed from the coronary arteries, a vent was inserted into the LV at the apex to release any excess fluid from the LV cavity. If this resulted in pressure falling below 20mmHg, flow rate was increased to 35ml/min in order to maintain perfusion of the coronary vessels. The solution was then switched to one of oxygenated Tyrode's solution containing 100µM Ca²⁺ and 10mM MgCl₂. The low [Ca²⁺] was used to inhibit contraction of the heart and prevent movement (Hoenicke & Damiano, 2001; Lansman *et al.*, 1986). At very low [Ca²⁺], Na⁺ conductance into the cell through the L-Type Ca²⁺ channel is increased and this can influence the action of the mitochondrial NCX (Maack *et al.*, 2006). The use of high magnesium (Mg²⁺) concentrations in the solution, as well as the use of low (not zero) [Ca²⁺] helped protect against this increase in Na⁺ (Chapman *et al.*, 1984).

The heart was positioned horizontally with the LV facing upwards for imaging (Figure 2.1). Once contractions had been completely abolished, the preparation was ready to be imaged.

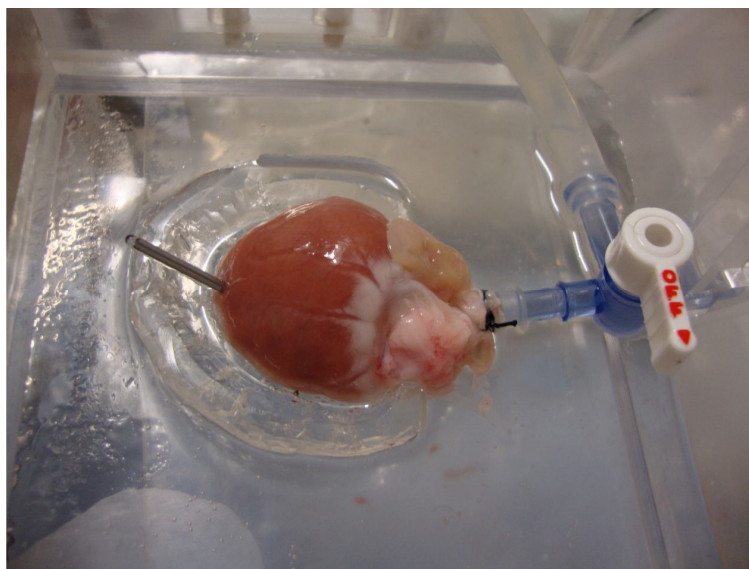


Figure 2-1 Position and orientation of Langendorff-perfused heart for 2P imaging

2.5 Fluorescence spectroscopy

Fluorescence spectroscopy was performed using the Perkin Elmer LS 55 fluorescence spectrometer. Fluorescence spectroscopy allows light intensity to be plotted against wavelength, and thus allows analysis of the spectral properties of fluorescent species. Spectroscopic measurements enabled determination of excitation and emission spectra of pure NADH and FAD in solution, as well as intrinsic fluorescence in cells.

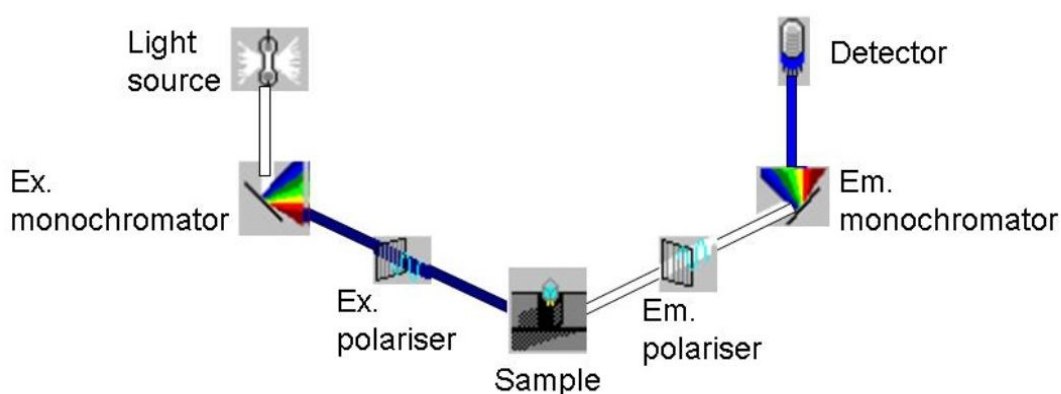


Figure 2-2 LS 55 fluorescence spectrometer setup

Instrument used a xenon lamp as the light source. White light is directed to the excitation monochromator, where it is split into narrow wavebands of light. These individual wavebands are directed to the sample. Any fluorescence emission that results is directed to the emission monochromator, split into narrow wavebands and directed to the photomultiplier detector. Excitation and emission polarisers could be selected if required. (Adapted from Perkin Elmer FL WinLab user's guide)

2.5.1 Determination of excitation spectra

To obtain an excitation spectrum, 2ml of the solution of interest was placed in a plastic cuvette and positioned in the cell holder. The emission wavelength was set as the wavelength where the emission peak was known or expected to occur. Excitation and emission slit widths were set at 10nm; these are the spectral bandwidths of the excitation and emission monochromators. Increasing the excitation slit width resulted in a wider waveband (and thus more light) being directed to the sample. Increasing the emission slit width resulted in a wider waveband of light being directed to the detector. The excitation spectrum

resulting from the scan indicated the range of wavelengths of light that excited fluorescence in the sample, the peak being the wavelength that most effectively excited fluorescence.

2.5.2 Determination of emission spectra

Emission spectra were obtained by a similar procedure. For these measurements, the information obtained from the excitation spectrum of the sample was utilised to set the excitation wavelength. The resultant emission spectrum indicated the range of wavelengths at which fluorescence is emitted, the peak being the wavelength where most fluorescence is emitted.

2.6 Fluorescence microscopy

A number of fluorescence microscopy techniques were performed on single, isolated cells.

2.6.1 1P excitation CLSM

1P excitation CLSM was performed using the Zeiss LSM 510 META inverted confocal microscope. From the lasers available, the 405nm diode laser and the 488nm argon laser were deemed most suitable for exciting NADH and FAD respectively. The high numerical aperture (NA) Zeiss C-Apochromat 40x/1.2 NA water-immersion objective lens was used throughout.

Spectral analysis of intrinsic fluorescence was first performed using the META detector on the system. Emission from the sample is directed onto a wavelength dispersive element and imaged by the META detector, which consists of 32-channels. Each channel consists of a PMT and detects emission within a spectral range of 10.7nm as described below:

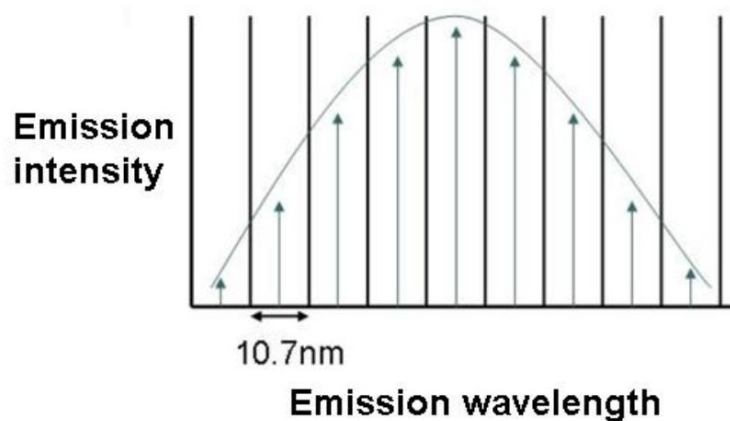


Figure 2-3 Emission fingerprinting using META detector

Each photomultiplier detects emission within a spectral range of 10.7nm (indicated by black lines). Compiling the total emission detected by each photomultiplier builds a picture of the emission spectrum for the sample.

Emission fingerprinting using this system enabled analysis of the intrinsic fluorescence emitted by a single cell and comparison with the emission signal from pure NADH and FAD. This allowed selection of the most suitable dichroic mirrors and emission filters in order to selectively collect fluorescence from NADH and FAD in the cell. The overall configurations chosen are illustrated in Figure 2-4.

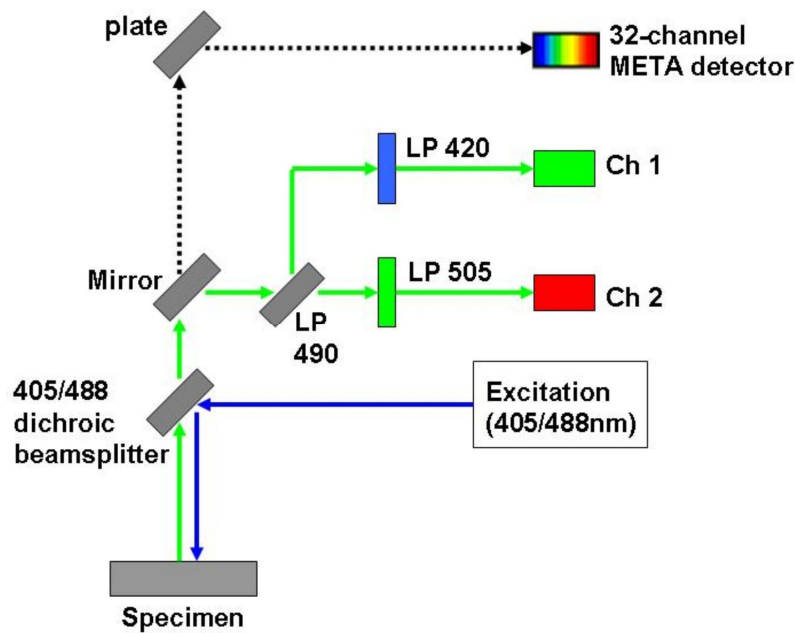


Figure 2-4 Optical settings for 1P CLSM

Excitation light was directed to the specimen and any fluorescence emitted was split from the excitation path with the 405/488nm main dichroic mirror. The emission light was split with a dichroic mirror at 490nm. Light of wavelengths shorter than 490nm was directed towards Ch 1 through a 420nm long-pass emission filter and light of wavelengths longer than 490nm was directed towards Ch 2 through a 505nm long-pass emission filter. This resulted in Ch 1 emission collection at 420-490nm (corresponding to NADH fluorescence) and Ch 2 detecting emission at wavelengths longer than 520nm (FAD fluorescence). The optical path to the 32-channel META PMT array is represented by the dashed arrows (the mirror was removed from the light path). These detectors were only used for emission fingerprinting experiments (in place of Ch 1 and Ch 2).

The time series function enabled multiple fluorescence measurements to be made in series over time. Using the multi-track function on the system, laser excitation of the specimen could be switched alternately between 405nm and 488nm excitation, and emission from NADH and FAD split by wavelength and imaged separately at different channels. The maximum power of the lasers was 30mW, but transmission intensity was set at less than 10% for all experiments in order to minimise photobleaching and photodamage to the cells. In order to maximise fluorescence detection, the PMT gain and pinhole diameter were instead increased as required.

2.6.2 2P laser scanning fluorescence microscopy

2P excitation fluorescence microscopy was performed on isolated cells, as well as on intact tissue preparations. The Zeiss LSM 510 NLO upright microscope

equipped with a Coherent Chameleon Titanium-Sapphire tunable laser was used for all experiments. For experiments performed on cells, excitation wavelengths of 720 and 750nm were used and for tissue experiments, excitation wavelengths of 720 and 740nm were used (depending on where the laser was most stable). The Zeiss Achroplan IR 40x/0.8 NA and the Zeiss Achroplan 10x/0.3 NA water-dipping objectives were used for cell and tissue experiments respectively.

Excitation fingerprinting was performed on cells in order to confirm that NADH and FAD fluorescence could be imaged using 2P-excitation, and the appropriate wavelengths to achieve this. Fluorescence emission was collected as the laser was tuned through a range of excitation wavelengths. The emission measurements were collated to produce a 2P-excitation spectrum for the sample. It was found that FAD fluorescence could not be detected by 2P-excitation, so the dichroic mirrors and filters were set to optimally collect NADH fluorescence (Figure 2-5).

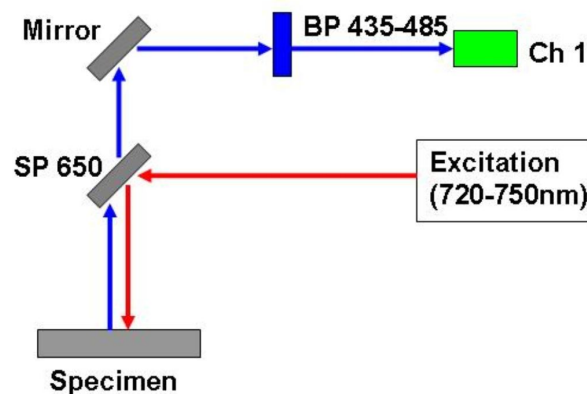


Figure 2-5 Optical settings for 2P excitation fluorescence microscopy

Excitation light was focussed on to the specimen and the emitted fluorescence was split from the excitation path using a 650nm main dichroic mirror. The emitted fluorescence was directed by a mirror to the PMT detector through a 435-485nm band-pass emission filter.

The time series function was used to image fluorescence over time. Maximum laser power at the wavelengths used was ~625mW, but transmission intensity was set at ~20% for cell experiments, as use of higher laser powers usually resulted in cell death. For experiments performed on intact tissue, laser power was set at maximum (although technical adjustments to the laser meant that maximum laser power at the wavelengths used was now ~1250mW). The PMT

gain was increased as required in order to maximise fluorescence detection and signal-to-noise ratio improved by scan averaging over 2 scans.

For experiments involving tissue preparations, the Z-stack mode was used. This involves the laser scanning and imaging a thin plane, then displacing vertically by a specified amount and scanning and imaging again. This process was repeated a specified number of times to build up a 3D-representation of NADH fluorescence in the tissue. Any differences in fluorescence through the different layers of the heart could be investigated in this way.

2.6.3 Wide-field epifluorescence microscopy

Experiments were performed using a Nikon inverted microscope fitted with a Nikon Fluor 40x/1.3 NA oil-immersion objective lens. Epifluorescence measurements were made with a Cairn Optoscan epifluorescence system using a xenon short arc lamp as light source. NADH was excited at 340nm and FAD at 430nm and fluorescence from each detected at two separate PMTs. NADH fluorescence was collected between 455 and 480nm and FAD fluorescence collected between 520 and 600nm. Excitation was alternately switched at 200ms intervals between the two wavelengths by the monochromator. The optical settings used for epifluorescence measurements are described in Figure 2-6.

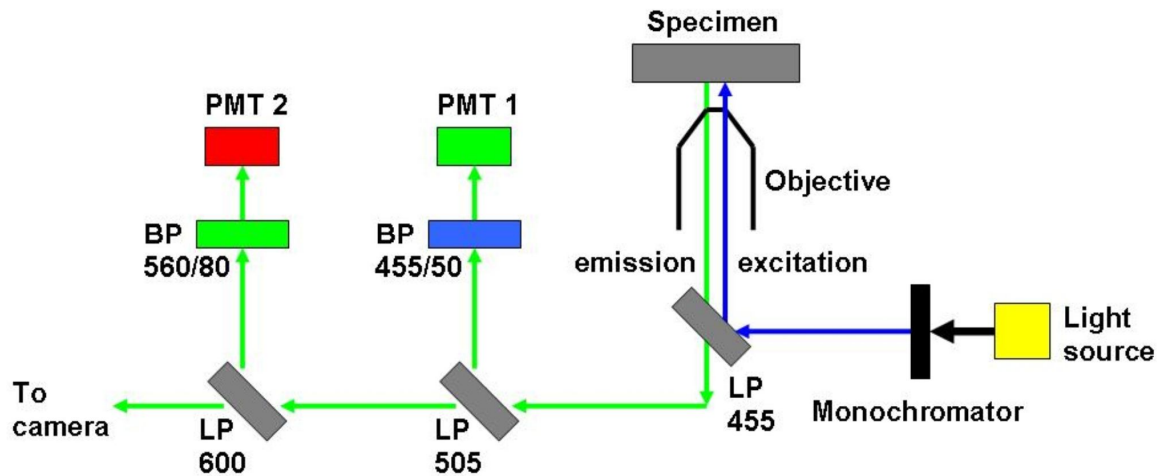


Figure 2-6 Optical settings for epifluorescence microscopy

Light from the xenon lamp was directed to the monochromator where it was split into the excitation wavelengths (340 and 430nm) and directed in sequence to the specimen. Emitted fluorescence was split from the excitation light with a 455nm dichroic mirror. Emission light was split again at 505nm; shorter wavelength light was directed to PMT 1 via a 455/50nm (455 ± 25 nm) emission filter, corresponding to NADH fluorescence. The longer wavelength light was further split at 600nm. Emission light of 505-600nm was directed to PMT 2 via a 560/80nm (560 ± 40 nm) emission filter, corresponding to FAD emission. Light of wavelengths longer than 600nm (from the microscope lamp) was directed to the CCD camera to enable cell edge detection measurements.

A red disc filter was used on the microscope to prevent light from the microscope lamp contaminating the PMT signals. Red coloured room light was used and the microscope and PMT setup were draped in thick cloth to prevent ambient light leak. These precautions were taken in order to reduce signal noise at the PMTs.

The charge coupled device (CCD) camera (IonOptix Limited) captured a video of the cell, which was displayed via the IonWizard software (IonOptix Limited). The iris diaphragm was adjusted so that only one cell was in the optical field.

2.7 Measurements of mitochondrial redox state

To establish the mitochondrial redox state in rabbit myocardial cells and tissue, NADH and FAD fluorescence was calibrated with the mitochondrial inhibitors NaCN and FCCP. These inhibitors induced mitochondrial states of maximal reduction and maximal oxidation respectively. In the maximally reduced mitochondrial state, NADH fluorescence increases and FAD fluorescence decreases, whereas maximal oxidation of the mitochondrial environment has the

opposite effect on NADH and FAD fluorescence. Calibrating NADH and FAD fluorescence in this way gives a measurement of the initial proportion of NAD and FAD in the reduced state i.e. the mitochondrial redox state of the cell or tissue.

2.7.1 Mitochondrial redox state measurements using fluorescence spectroscopy

2ml of cell solution was placed in a plastic cuvette and positioned in the cell holder of the fluorescence spectrometer. Initial NADH and FAD emission spectra were taken at 380nm and 450nm respectively. FCCP was then added to the cuvette at a concentration of 2 μ M and NADH and FAD emission spectra immediately taken. NADH and FAD emission spectra were repeatedly measured over the course of ~6-7mins to ensure that any effect of FCCP on the spectra was recorded. The cell solution was mixed with a pipette between scans to prevent the cells settling at the bottom of the cuvette.

FCCP could not be washed out of the cells in the cuvette, so 2ml of fresh cells from the same heart were placed in a new cuvette and the process repeated with 2mM NaCN. The concentration of cells was the same for both FCCP and NaCN measurements.

2.7.2 Perfusion system for isolated cardiomyocytes

A perfusion system was designed for microscopy experiments to allow fast switching between solutions (Figure 2.7).

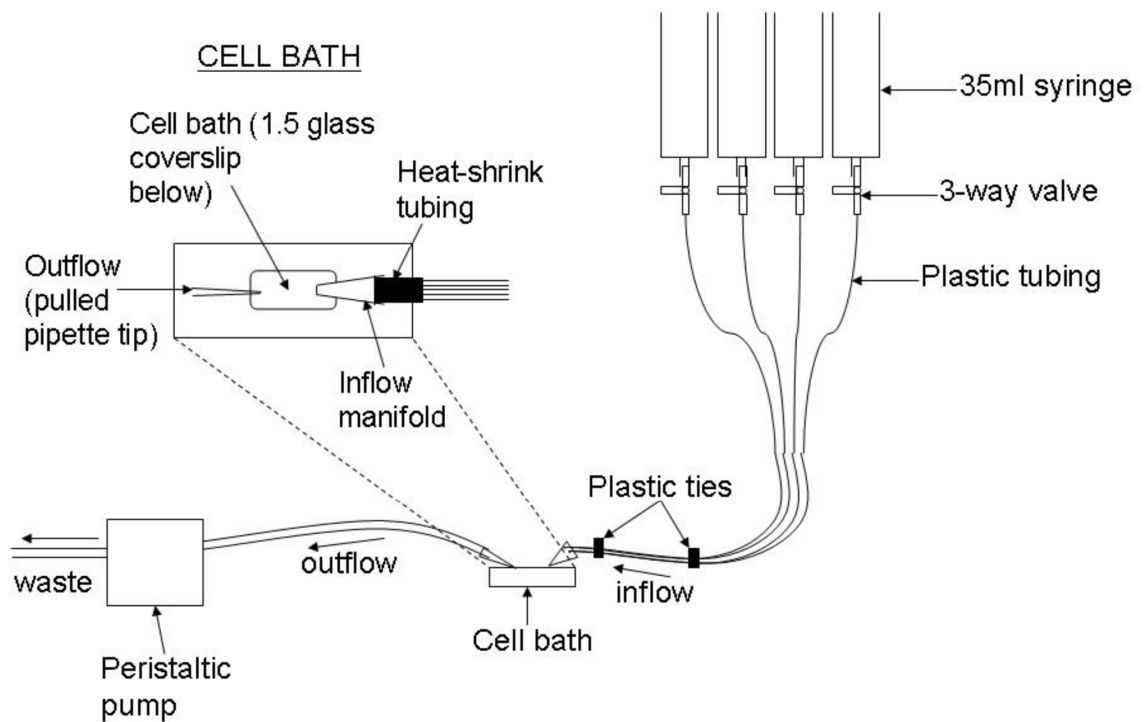


Figure 2-7 Apparatus for perfusion of isolated cardiomyocytes

Each 35ml syringe was filled with solution and perfusion of each solution was controlled by a 3-way valve. Perfusion was gravity driven and solutions were directed to the cell bath by narrow plastic tubes which converged at the inflow manifold. Heat-shrink tubing and silicon were used to create low volume dead space and prevent solution leak at the manifold. Outflow from the bath was driven by peristaltic pump. The angle of orientation of the inflow tip and the narrow outflow tip minimised disruption to the cells.

A Perspex cell bath was used for 1P and 2P experiments. For experiments involving field-stimulation of the cells, a larger aluminium bath was used and inflow was through a hole in the side wall of the bath. This is because these experiments were required to be performed at 37°C, and the aluminium cell bath could be heated to achieve solution flow at this temperature.

In order to avoid contamination, each syringe was designated for use as a reservoir for a particular solution: control, FCCP or NaCN. The remaining tube was used for any other solution. After each experiment, the whole perfusion system was washed through with double de-ionised water.

2.7.2.1 Perfusion protocol for isolated cardiomyocytes

The same perfusion protocol was used to establish mitochondrial redox state in isolated cardiomyocytes using 1P excitation, 2P excitation and epifluorescence techniques.

Cells were placed in the cell bath with the bottom covered by a glass coverslip (thickness 1.5mm); the cell density was such that cells were evenly spread and not overlapping. The cells were allowed to settle and stick to the coverslip. After 2-3 min, perfusion with Krebs solution containing 1.8mM Ca^{2+} (control solution) was started. Any cells that had not stuck down were allowed to wash away before any fluorescence measurements were taken. The focus was set on rod-shaped cells with clear striations that appeared to be well adhered to the coverslip, preferably in the centre of the bath. For experiments performed using 1P and 2P excitation fluorescence microscopy, measurements could be made on more than one cell during each recording. For experiments using epifluorescence, measurements could only be made on one cell at a time.

Intrinsic fluorescence measurements were taken throughout the perfusion protocol. The protocol began by taking baseline fluorescence measurements of cells perfused with control solution. This was continued for ~100s, so that the rate of any fluorescence bleaching that may have occurred could be calculated and corrected for later. Perfusion was then switched to a 2 μM FCCP solution (in 1.8mM Ca^{2+} Krebs solution) and perfusion continued until fluorescence levels had reached a steady state. FCCP was washed out by perfusing with control solution for 200-300s, or until the effects of FCCP on intrinsic fluorescence had been reversed. Perfusion was then switched to 2mM NaCN solution (in 1.8mM Ca^{2+} Krebs solution) and continued until fluorescence levels reached a steady state. Finally, perfusion was switched back to control solution to washout the NaCN solution.

The background fluorescence signal was measured in 1P and 2P experiments by selecting a region of interest (ROI) containing no cells. This background signal was easily subtracted from the fluorescence signals from the cells. For epifluorescence experiments, the background signal had to be taken by moving the focus away from the cell and measuring the fluorescence signal from an

adjacent area free from any cell or debris. This was done a number of times during each recording. The overall background signal was later averaged from this and subtracted from the cellular fluorescence signal.

2.7.3 Delivering mitochondrial inhibitor to tissue preparations

Measurements of mitochondrial redox state in the whole heart and wedge preparations required delivery of mitochondrial inhibitor by a syringe driver (Figure 2.8).

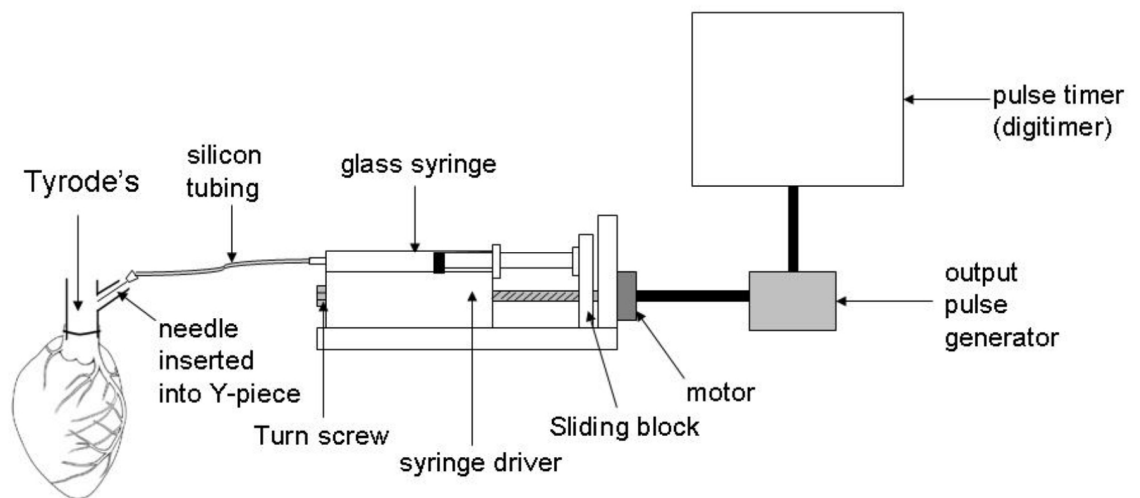


Figure 2-8 Mitochondrial inhibitor delivery system for tissue preparations

A glass syringe was filled with FCCP, NaCN or control solution. A length of silicone tubing connected the end of the syringe to a needle, which was inserted into a Y-piece in the perfusion system. A digitimer triggered the pulse output generator to deliver trigger impulses to the motor on the syringe driver. This turned a screw which moved a sliding block behind the syringe, pushing the plunger and delivering the contents of the syringe. The cycle length (the length of time between trigger impulses) was set on the digitimer to ensure that inhibitor solution was delivered into the perfusing Tyrode's solution at the correct rate in order to achieve the desired concentration in the perfusate.

The control solution in the syringe was the same Tyrode's solution perfusing through the heart. FCCP solution was placed in the syringe at a concentration of 400 μ M and NaCN solution at 400mM. The digitimer cycle length was set at 255ms, which resulted in the syringe contents being delivered at rate of 0.3ml/min. As the heart was being perfused with Tyrode's solution at a rate of 30ml/min, the dilution factor was 100:1. Thus the FCCP and NaCN concentration reaching the coronary arteries was 4 μ M and 4mM respectively, which is double the concentrations used in isolated cells. The higher concentrations were used

so that the effective inhibitor concentration reached the tissue as quickly as possible. 1.5ml of inhibitor or control solution was placed in the syringe, which resulted in delivery for 5 min.

2.7.3.1 Perfusion protocol for tissue preparations

For the first measurement on each preparation, control solution was placed in the syringe. Initial measurements of baseline NADH fluorescence in the tissue layers were made; 4-5 X-Y images of each layer in the Z-stack were taken. Delivery of the syringe contents was then started and carried on for ~5mins. Control solution was also poured into the Perspex chamber to ensure that the heart was immersed in the same solution as was being delivered to the tissue. Once the syringe had emptied and delivery stopped, fluorescence measurements were continued for 5-10mins to record any fluorescence changes during recovery. After recordings were stopped, the syringe was switched to one containing NaCN and the process repeated. The process was repeated again with FCCP. Sufficient time was left between inhibitors to ensure that the inhibitor had been completely washed out of the heart. The solution in the chamber was also replaced with fresh Tyrode's solution.

At the end of the day's experiments, the heart was removed from the chamber and the fluorescence signal from Tyrode's solution alone was measured. The PMT settings and room light conditions were kept the same as those used during the tissue fluorescence measurements. The fluorescence values obtained were taken to be background fluorescence and subtracted from the tissue fluorescence values.

2.7.4 Calculation of mitochondrial redox state

For each experimental recording, background fluorescence measured at each wavelength was subtracted from the cell and tissue fluorescence at the corresponding wavelength. The fluorescence signal was normalised by normalising the initial fluorescence values during control perfusion (or before inhibitor injection in tissue preparations) to 1. If any fluorescence bleaching had taken place, this was corrected for by subtracting the underlying bleach from the trace. The maximum NADH fluorescence was obtained during NaCN perfusion

and the minimum fluorescence during FCCP perfusion. Conversely, the maximum FAD fluorescence was obtained during FCCP perfusion and the minimum fluorescence during NaCN perfusion. The fluorescence values at baseline, minimum and maximum were used to calculate NAD and FAD states (Figures 2-9 and 2-10).

$$\text{NAD}_{\text{state}} = \frac{F_{\text{control}} - F_{\text{FCCP}}}{(F_{\text{CN}} - F_{\text{FCCP}})}$$

Figure 2-9 Calculation for NAD_{state}

NAD_{state} for each cell was calculated using the fluorescence measurements at baseline (F_{control}), minimum (F_{FCCP}) and maximum (F_{CN}).

Calculation of NAD_{state} indicates the proportion of NAD in the reduced state, 1.0 being fully reduced, 0 being fully oxidised.

$$\text{FAD}_{\text{state}} = \frac{F_{\text{control}} - F_{\text{CN}}}{(F_{\text{FCCP}} - F_{\text{CN}})}$$

Figure 2-10 Calculation for FAD_{state}

FAD_{state} for each cell was calculated using the fluorescence measurements at baseline (F_{control}), minimum (F_{CN}) and maximum (F_{FCCP}).

Conversely, calculation of FAD_{state} gives an indication of the proportion of FAD in the *oxidised* state, 1.0 being fully oxidised and 0 being fully reduced.

2.8 Electrical stimulation of isolated cardiomyocytes

Experiments that assessed mitochondrial redox state in response to changes in work intensity required cells to be in the contracting state. Cellular contraction was induced by electrical field stimulation. A thin layer of cell solution was placed on to the coverslip of a metal bath (Figure 2-7). The bath was heated so that the extracellular solution was ~37°C during perfusion. A stimulator generated square wave electrical impulses which were delivered to the cells

through two narrow platinum electrodes on each side of the bath. A digitimer connected to the stimulator set the frequency of stimulus impulses.

Cell shortening measurements were made using a CCD camera with cell edge detection capability (IonOptix Limited). Intrinsic fluorescence measurements were simultaneously made using the Cairn Optoscan epifluorescence system (see section 2.6.3).

2.8.1 Pacing protocol for metabolic challenge in isolated cardiomyocytes

The metabolic challenge was designed to step increase the rate of cellular contraction, and thus level of work, performed by the cell. Analysis of the changes in NADH and/or FAD fluorescence as a result of changes in work intensity indicated how well cells were able to match energy supply with demand.

The pacing protocol for rabbit cardiomyocytes began by stimulating the cells at 0.5Hz for around 100s. Stimulation frequency was step increased to 1Hz and pacing was continued at this rate for ~50s, or until fluorescence levels had reached a steady state. Stimulation frequency was switched back to 0.5Hz and the cell allowed to recover. Stimulation frequency was again increased to 1Hz for ~50s before returning to 0.5Hz stimulation. In the same way, the cell was subjected to 2 bursts of 2Hz stimulation and 2 bursts of 3Hz stimulation. Each burst of fast pacing was interspersed with pacing at 0.5Hz to allow the cell to recover (Figure 2-11). Step increasing the frequency of stimulation in this way abruptly increased the intensity of work performed by the cell.

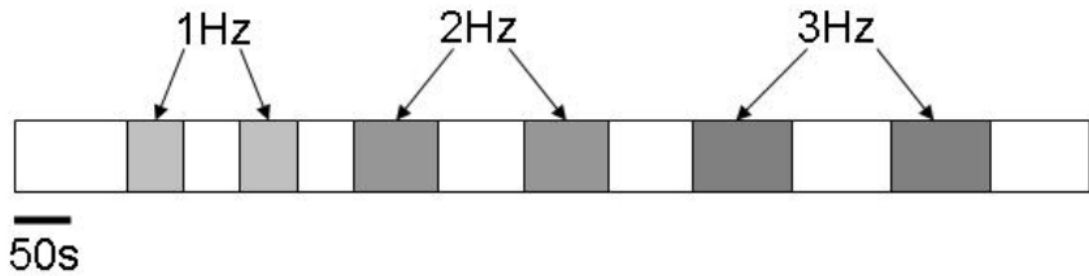


Figure 2-11 Metabolic challenge stimulation protocol in rabbit cells

The stimulation protocol for the metabolic challenge involved subjecting the rabbit cell to burst pacing at 1Hz, 2Hz and 3Hz. Each burst was interspersed with 0.5Hz pacing (white boxes). The length of time the cell was paced at 2Hz and 3Hz was slightly longer, as it took longer for NADH and FAD fluorescence levels to reach a steady state at faster stimulation rates.

A similar protocol was performed in rat cells (Figure 2-12), but faster pacing rates were used. Intrinsic heart rate is faster in rats compared to rabbits, and rat cells can therefore contract at faster rates than rabbit cells.

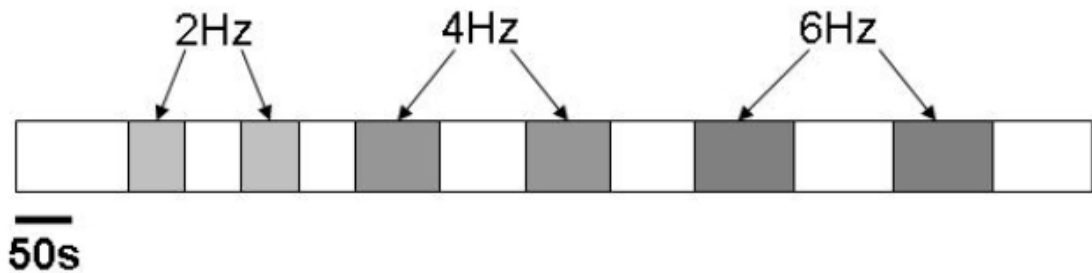


Figure 2-12 Metabolic challenge stimulation protocol in rat cells

Rat cells were burst paced at 2Hz, 4Hz and 6Hz, each burst interspersed with 1Hz stimulation (white boxes).

At the end of the pacing protocol, NADH and FAD fluorescence was calibrated with FCCP and NaCN. A ratio of NADH/FAD fluorescence was also taken in order to minimise artefacts in the fluorescence signals caused by movement, changes in background signal, etc.

2.9 Statistical analysis

Statistical analysis was performed using GraphPad InStat statistical software. All data was presented as mean \pm standard error of the mean (SEM) unless otherwise

stated. Comparison between groups of data was performed by Student's t-test (paired where appropriate). Multiple comparison tests were performed using repeated measures one-way ANOVA with Tukey's multiple comparison post-hoc test. A 2-tailed p-value of less than 0.05 was considered statistically significant.

3 Characterisation of intrinsic fluorescence in ventricular myocytes

3.1 Introduction

It has been established for several decades that cells have autofluorescent properties. The source of this autofluorescence has been mainly attributed to a number of respiratory enzymes and these properties have been extensively studied by Chance and colleagues (Chance, 1952; Chance, 1954; Chance & Williams, 1955a; Chance & Williams, 1955b; Chance & Williams, 1955c; Chance & Williams, 1955d; Chance *et al.*, 1955).

In order to confirm that the major source of intrinsic fluorescence arising from cardiac cells and tissue was NADH and FAD, it was necessary to characterise the excitation and emission properties of this fluorescence. In addition, knowledge of the spectral characteristics of intrinsic fluorescence enabled selection of the most appropriate excitation wavelengths, dichroic mirrors and emission filters to ensure that the maximum fluorescence signal was detected.

3.2 Methods

3.2.1 Fluorescence spectroscopy

3.2.1.1 Preparation of pure metabolites and determination of spectra

NADH and FAD were obtained in the pure state and dissolved in a basic mock intracellular solution containing (in mM) 120 KCl, 1 MgCl₂ and 0.05 EGTA. This was to recreate the intracellular ionic environment and any possible interactions that may occur between the metabolites and ions within the cell. The pH of the NADH solution was adjusted to ~9 as more acidic conditions can cause NADH decomposition. Excitation and emission spectra were determined as previously described. A range of NADH and FAD concentrations were used, but it was found that using excitation and emission slits of 10nm and a scan speed of 500nm/min, the [NADH] of 5µM and [FAD] of 2.5-3µM produced the clearest spectra without saturation of the fluorescence signal.

For experiments involving oxidising and reducing agents, NADH was diluted in a pH 9 buffer solution and FAD was diluted in a HEPES buffered solution at pH 7.

This was to ensure any change in spectral properties upon oxidation or reduction was not due to changes in pH. 2,6-Dimethoxy-1,4-benzoquinone (2,6-DMBQ) was used as an oxidising agent for NADH and sodium dithionite (Na-dithionite) was used as a reducing agent for FAD. 2,6-DMBQ was only freely soluble in glacial acetic acid, and greatly acidified the cuvette contents upon addition. The volume of 10M NaOH solution required to return the pH of 2ml of 5 μ M NADH solution to pH 9 following addition of 0.5mM 2,6-DMBQ was therefore determined, and this was added to the cuvette along with 0.5mM 2,6-DMBQ. Baseline NADH and FAD emission spectra were first recorded and the oxidising/reducing agent was then added to the cuvette and emission spectra recorded again. NADH/NAD⁺ was excited at 340nm and FAD/FADH₂ excited at 450nm. The concentration of 2,6-DMBQ or Na-dithionite was increased in 0.5mM and 0.25mM steps respectively, until the full effect was deemed to have occurred.

3.2.1.2 Spectral measurements of intrinsic fluorescence from isolated ventricular myocytes

Rabbit ventricular myocytes were isolated as previously described and the excitation and emission spectra of the intrinsic fluorescence from aggregates of live and dead cells determined. The same scan settings used for measurements in pure metabolites were used for measurements in cells.

3.2.2 Excitation and emission fingerprinting

3.2.2.1 Emission fingerprinting using 1P-excitation CLSM

Emission fingerprinting was performed using the 1P-excitation confocal microscope. When excitation was with the 405nm laser, the 405/514/594 main dichroic beamsplitter was used. When excitation was with the 488nm laser, the 405/488 main dichroic beamsplitter was used. These dichroic mirrors were chosen so as to cause minimal interference to the transmission of emission light from the samples to the detector. The sample of interest (pure metabolite solution or cell suspension) was placed in the bath and imaged using the 32-channel META detector. A wavelength dispersive element split the emission light into wavebands of around 10nm, each waveband detected by a different PMT

channel. Compilation of the emission detected by all the PMT channels gives a picture of the emission spectral characteristics of the sample. For the cell measurements, emission fingerprinting was performed on individual rod-shaped cells.

3.2.2.2 2P-excitation fingerprinting

In order to assess the 2P-excitation characteristics of NADH and FAD, excitation fingerprinting was carried out on pure NADH and FAD solutions and on the intrinsic fluorescence from single rod-shaped cells. This involved the laser tuning through a range of excitation wavelengths and collecting emission at each wavelength. The laser power was calibrated through the wavelength range and adjusted at each wavelength to ensure that the power remained constant throughout. Collating the emission measurements produced a 2P-excitation spectrum for the sample.

3.3 Results

3.3.1 Pure NADH and FAD spectra

Initial experiments were performed on pure NADH and FAD samples in solution to establish the excitation and emission spectral properties of the metabolites, shown in Figure 3-1. From these measurements, it was found that the excitation peak for NADH was at 340nm and emission peak was at ~460nm. The main excitation peak for FAD was at 450nm and emission peak at 525nm.

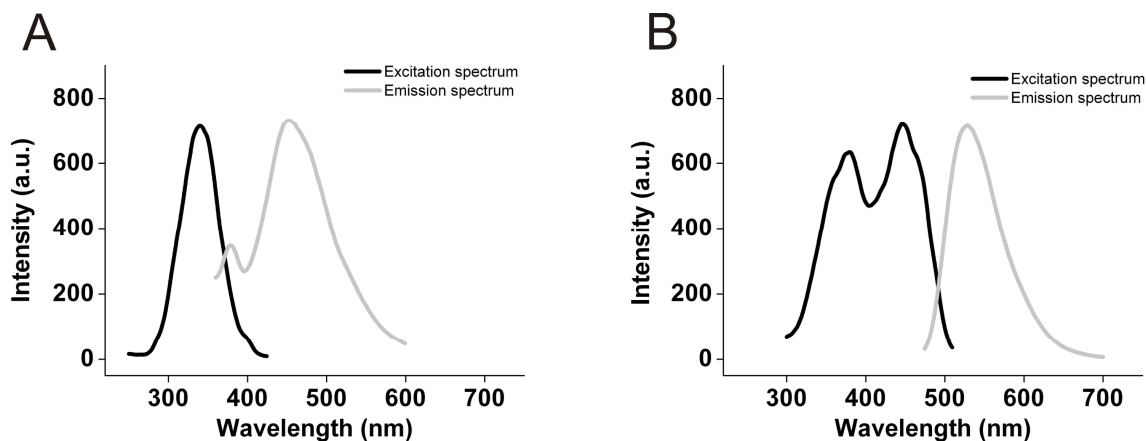


Figure 3-1 Excitation and emission spectra of pure NADH and FAD in solution

Excitation spectrum (black) and emission spectrum (grey) of (A) pure NADH and (B) pure FAD.

3.3.2 Pure NADH and FAD 2P excitation spectra

2P-excitation spectra of pure NADH and FAD in solution were taken using the excitation fingerprinting function of the 2P fluorescence microscope. These 2P spectra were then compared with the predicted 2P-excitation spectra produced by doubling of 1P-excitation wavelengths (Figure 3-2).

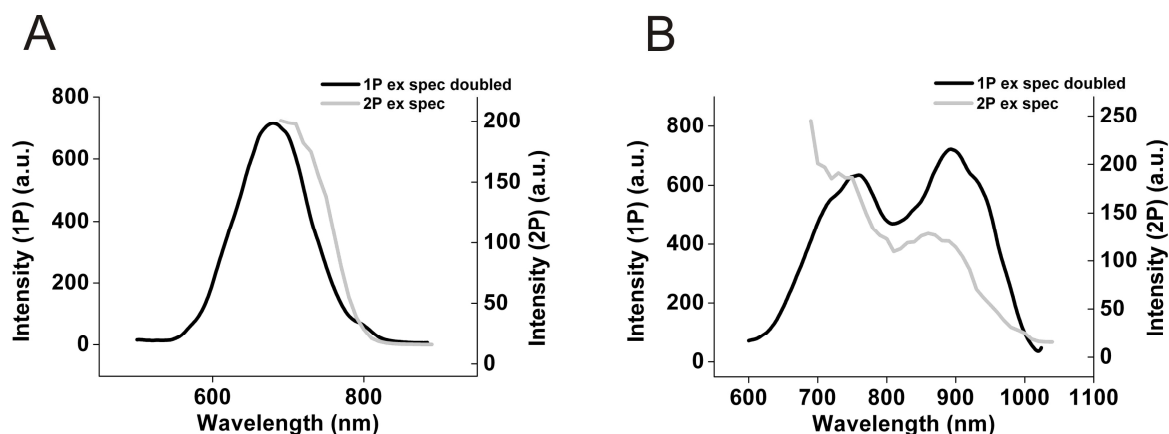


Figure 3-2 2P-excitation spectra of pure NADH and FAD in solution (predicted and measured)

The 2P-excitation spectra of (A) NADH and (B) FAD were predicted by taking 1P-excitation spectra and doubling the wavelengths (black lines). These spectra were compared with measured 2P-excitation spectra obtained by 2P-excitation fingerprinting (grey lines).

Measured 2P-excitation spectra of pure NADH and FAD corresponded well with the 2P spectra predicted for the fluorophores by doubling 1P-excitation spectral

wavelengths. The measured 2P-excitation peak of NADH was red-shifted by ~15-20nm, whereas the measured 2P-excitation peaks of FAD were blue-shifted by ~20-30nm compared to the predicted 2P excitation peaks. However, doubling the wavelengths of the 1P-excitation spectrum only gives an estimation of the 2P-excitation spectrum, and the excitation peaks of the predicted and measured spectra would not necessarily be expected to match exactly (Xu & Webb, 1996).

As with the 1P spectral measurements, there are 2 peaks present in the FAD 2P-excitation spectrum. However, in the 2P-excitation spectrum the first peak is larger than the second peak, whereas the opposite is the case in the 1P-excitation spectrum. The 2P-excitation spectra of pure NADH and FAD obtained in these experiments are consistent with previous reports in the literature (Huang *et al.*, 2002).

3.3.2.1 Effect of oxidising agent on NADH fluorescence

The fluorescent properties of NAD^+ were also assessed by spectrophotometry using the oxidising agent 2,6-DMBQ to oxidise pure NADH to NAD^+ . The emission spectra of NADH taken before and after addition of 2,6-DMBQ are shown in Figure 3-3.

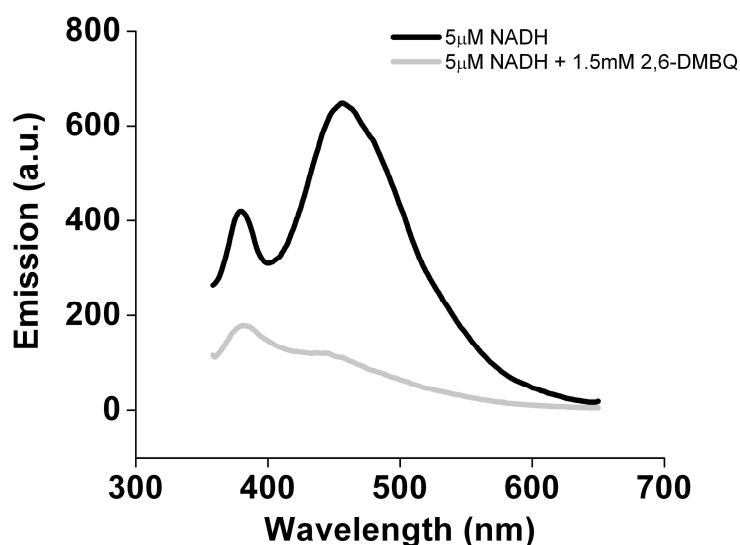


Figure 3-3 NADH emission spectra before and after oxidation

The emission spectrum of pure NADH at excitation 340nm was taken (black line). Addition of 1.5mM of the oxidising agent 2,6-DMBQ to the cuvette oxidised NADH to NAD^+ and decreased fluorescence emission (grey line).

The oxidation of NADH to NAD⁺ results in a considerable decrease in fluorescence emission. Thus NAD⁺ emits little or no fluorescence at an excitation wavelength of 340nm.

3.3.2.2 Effect of reducing agent on FAD fluorescence

The effect of reducing FAD to FADH₂ on the fluorescence signal was also examined using the reducing agent Na-dithionite. The emission spectra of FAD at 450nm excitation, taken before and after addition of Na-dithionite, are shown in Figure 3-4.

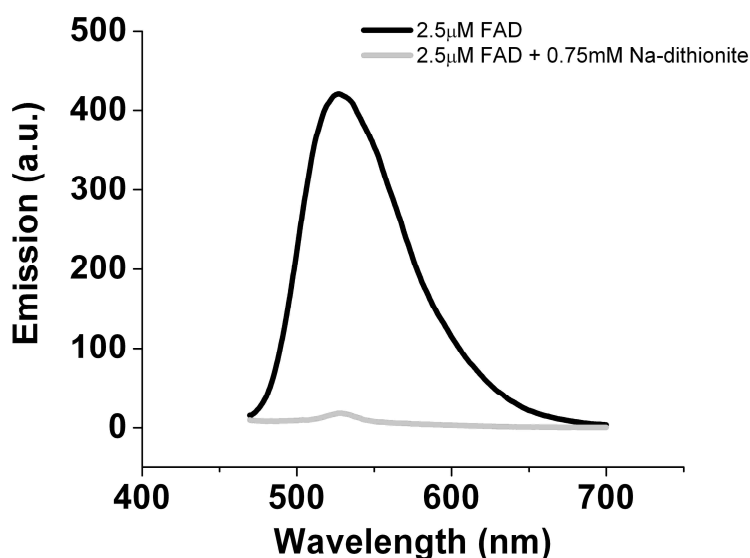


Figure 3-4 FAD emission spectra before and after reduction

The emission spectra of pure FAD at excitation 450nm before (black line) and after (grey line) addition of 0.75mM of the reducing agent Na-dithionite. The reduction of FAD to FADH₂ causes the fluorescence signal to be virtually eliminated.

Reduction of FAD to FADH₂ using the reducing agent Na-dithionite caused the fluorescence signal to be abolished. Thus FAD is only fluorescent in the oxidised state.

3.3.3 Fluorescent properties of NADH-FAD solution mixture

A solution containing both pure NADH and pure FAD was also made up and the excitation and emission spectra taken at the peak excitation and emission

wavelengths for NADH and FAD (Figure 3-5). Pure NADH was used at a concentration of $5\mu\text{M}$ and pure FAD at a concentration of $2.5\mu\text{M}$. The same concentrations were used in the mixture of solutions and the spectra of the pure metabolites were compared with the spectra of the solution mixture. This was to assess whether there were any interactions between the two fluorescent species causing any unexpected shifts in the spectral properties of the individual metabolites.

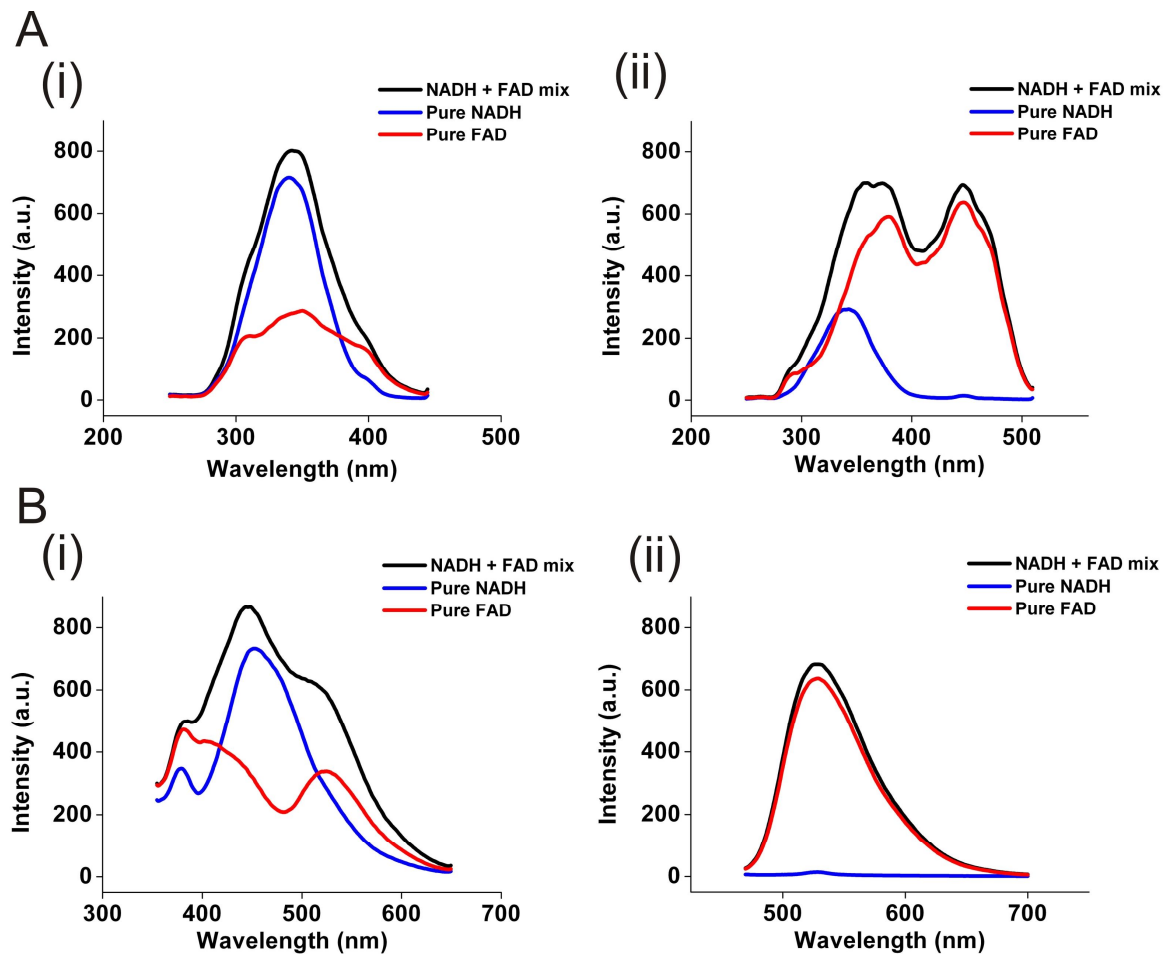


Figure 3-5 Excitation and emission spectra of pure NADH and FAD solution mixture

A: Excitation spectra of pure NADH (blue), pure FAD (red) and a mixture of the two metabolites (black). Panel (i) emission collected at 460nm, (ii) emission collected at 525nm.
B: Emission spectra of pure NADH (blue), pure FAD (red) and a mixture of the two metabolites (black). Panel (i) excitation at 340nm, (ii) excitation at 450nm.

The excitation and emission spectra of the NADH-FAD solution mixture did not show any spectral shifts compared to the excitation and emission spectra of pure NADH and pure FAD alone. The spectral effects are additive: where both

metabolites are fluorescent at a particular wavelength, the fluorescent peaks in the solution mixture represent the peaks seen in both NADH and FAD.

3.3.4 Comparison of intrinsic fluorescence in cells with pure NADH and FAD fluorescence

3.3.4.1 Spectrophotometer measurements

It was necessary to confirm that the intrinsic fluorescence arising from ventricular myocytes was indeed due to NADH and FAD fluorescence. In order to do this, excitation and emission spectra of intrinsic fluorescence were taken at peak excitation and emission wavelengths for NADH and FAD and compared to the spectra taken of the pure metabolites (Figure 3-6).

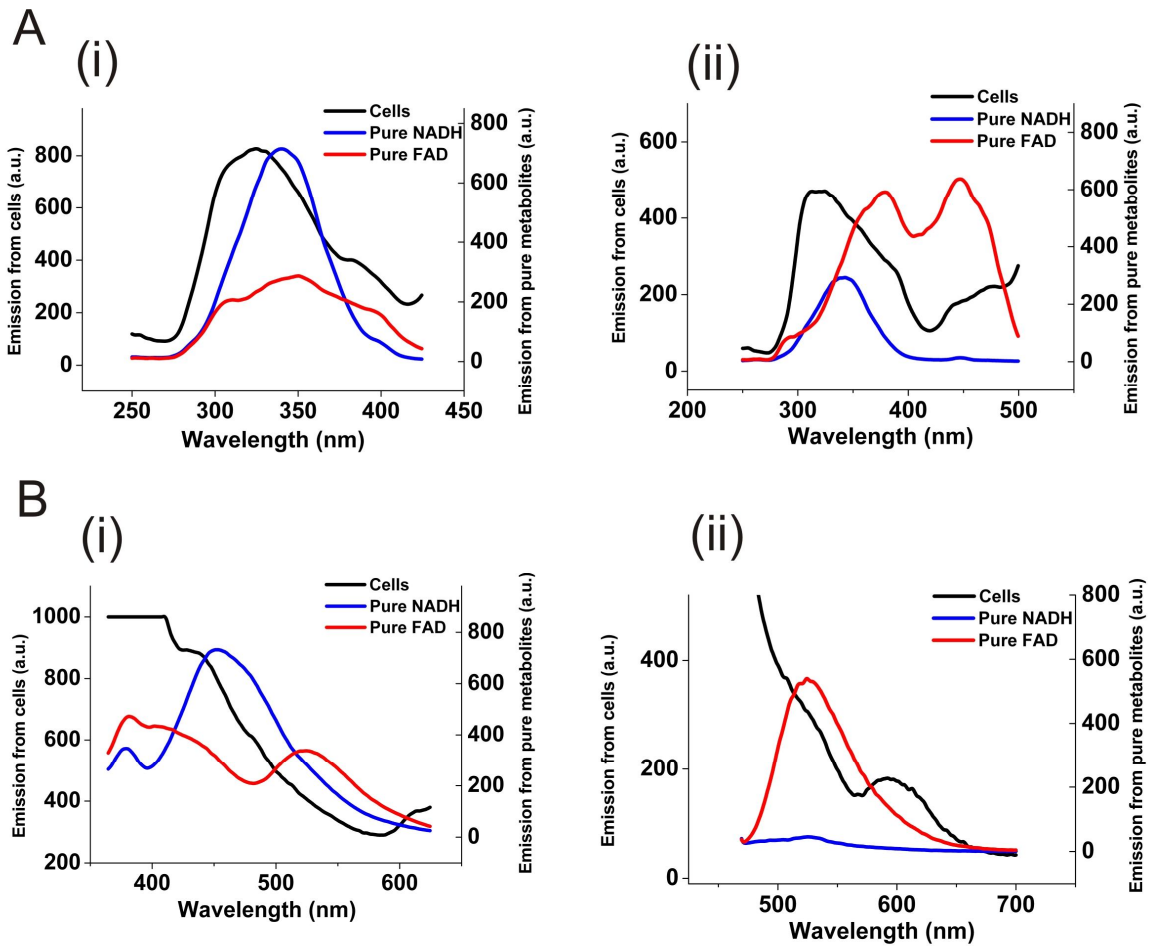


Figure 3-6 Spectrophotometric comparison of cellular intrinsic fluorescence with pure NADH and FAD

A: Excitation spectra of intrinsic fluorescence from cells (black), pure NADH (blue) and pure FAD (red). Panel (i) emission collected at 460nm, (ii) emission collected at 525nm.

B: Emission spectra of intrinsic fluorescence (black), pure NADH (blue) and pure FAD (red). Panel (i) excitation at 340nm, (ii) excitation at 450nm.

The Y-axis scale was adjusted for the intrinsic fluorescence spectra to ensure that the height of the peaks from cell measurements coincided with the height of the peak for the metabolite most fluorescent at that particular wavelength. This allowed for easier spectral comparison.

Although the excitation and emission peaks from intrinsic fluorescence arising from aggregates of live and dead cells seem to correspond to NADH and FAD, the peaks do not match exactly. In particular, the excitation and emission peaks likely to correspond to NADH are left-shifted (i.e. at shorter wavelengths) in the cells compared to the pure solution. Furthermore, it was found that the turbid cell suspension caused excessive light scattering. This was most apparent at FAD

excitation wavelengths, and clear intrinsic fluorescence emission spectra could not be obtained. The emission peak visible at ~590nm is likely to be due to lipofuscin, a pigment associated with aging produced by lysosomes (Gao *et al.*, 1994), although this was not investigated further and could not be conclusively confirmed. Due to the lack of clarity in the spectrophotometer measurements, additional spectral analysis of intrinsic fluorescence was performed using the META detector on the 1P confocal microscope.

3.3.4.2 Emission fingerprinting using 1P confocal methods

Emission fingerprinting was performed on single rod-shaped cells and compared with the emission characteristics of pure NADH and FAD (Figure 3-7).

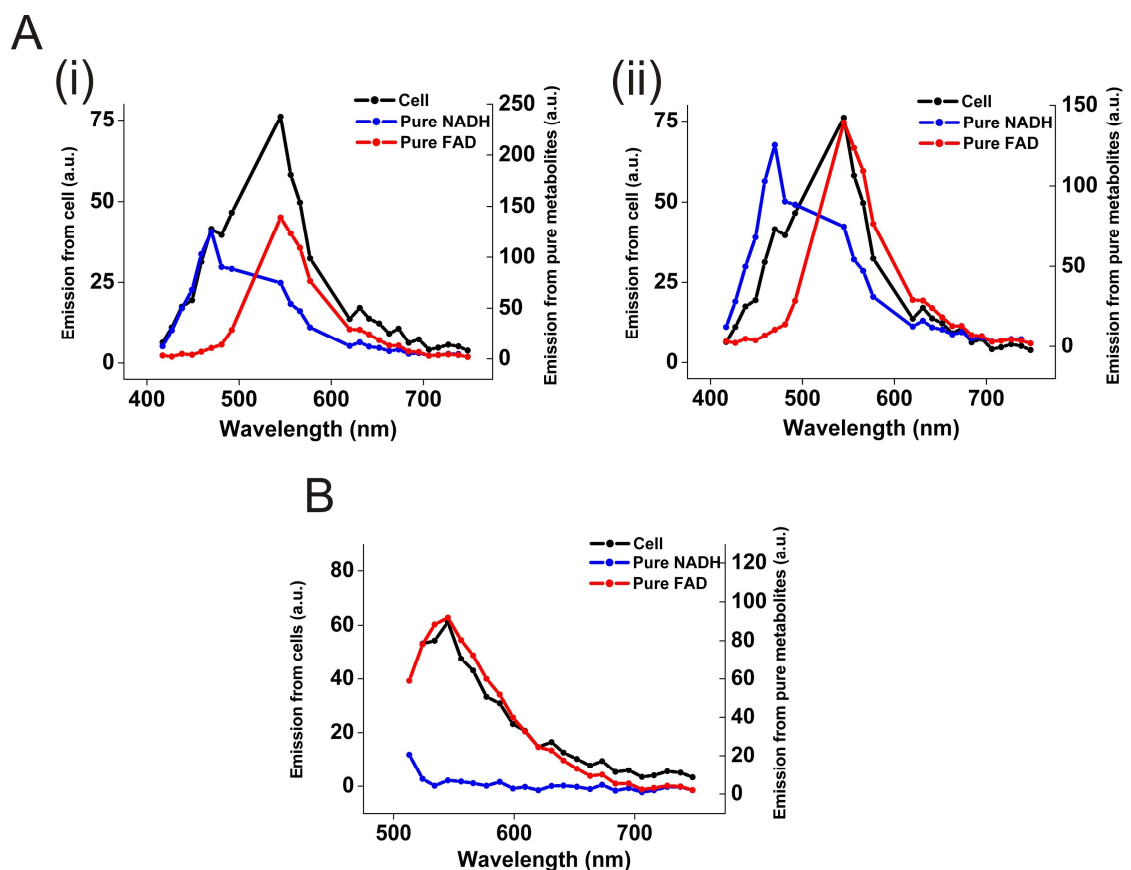


Figure 3-7 Comparison of cellular intrinsic fluorescence with pure NADH and FAD emission characteristics using the META detector

A: Emission fingerprinting of intrinsic fluorescence from a single cell (black), pure NADH (blue) and pure FAD (red) using a 405nm laser for excitation. Y-axis scales have been adjusted to compare (i) pure NADH peak emission and (ii) pure FAD peak emission with intrinsic fluorescence emission peaks. **B:** Emission fingerprinting using a 488nm laser for excitation.

Excitation of intrinsic fluorescence using the 405nm laser results in emission peaks corresponding to both NADH and FAD. At wavelengths shorter than ~480nm, intrinsic fluorescence corresponds solely to NADH. At longer wavelengths, the intrinsic fluorescence emission signal correlates with FAD fluorescence. Excitation at 405nm is suboptimal for NADH, but the lasers available on the 1P confocal system meant that this was the only wavelength present that could excite NADH. For future experiments, it was therefore important to ensure that the emission filters selected collect fluorescence only from NADH. When the 488nm laser is used, intrinsic fluorescence arises only from FAD.

A number of points have been excluded from the emission traces obtained by 405nm excitation. This was because the 405/514/594nm main dichroic beamsplitter was used to split the excitation light from the emission path. This dichroic mirror was chosen as it caused the least interference at the wavelengths where the NADH emission peak was expected. However, it prevented a substantial amount of emission light from being transmitted to the detectors at and around 514nm and 594nm, thus altering the shape of the emission spectra. The points between 492 and 545nm and 577 and 620nm were therefore removed to prevent confusion arising. However, this meant that some details concerning emission could not be detected (e.g. the FAD emission peak), as the dichroic beamsplitter makes it impossible to collect all the emission light from the full wavelength range. Ultimately, 405nm was the wavelength used for exciting NADH, so it was deemed more important to obtain the emission characteristics of this fluorophore.

3.3.4.3 Excitation fingerprinting using 2P-excitation methods

The 2P-excitation characteristics of intrinsic fluorescence from single rod-shaped cells were assessed using excitation fingerprinting. This was to confirm the source of intrinsic fluorescence, as well as to select the most appropriate wavelengths for 2P-excitation. The 2P-excitation spectrum from the cell was compared to the 2P-excitation spectra of pure NADH and FAD solutions (Figure 3-8).

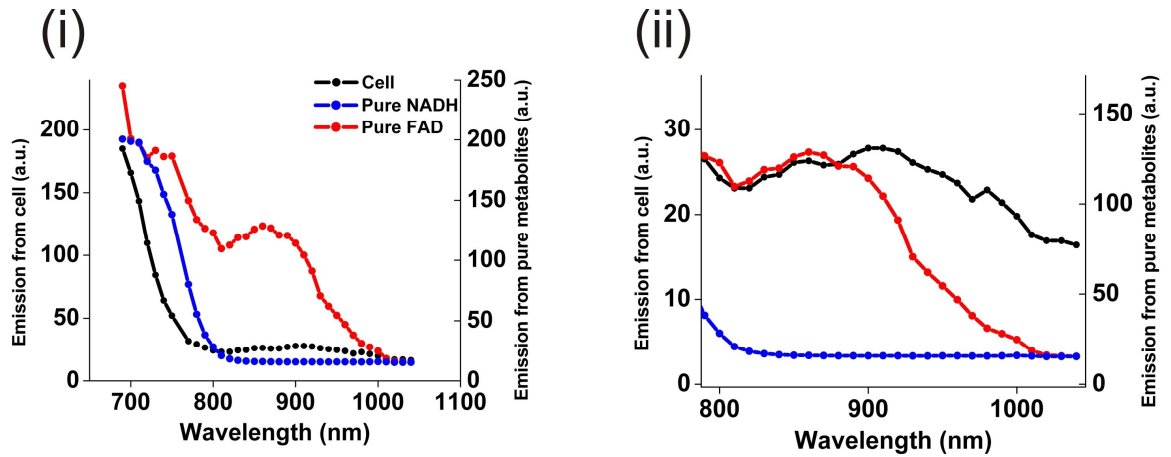


Figure 3-8 Comparison of cellular intrinsic fluorescence with pure NADH and FAD 2P-excitation characteristics

(i) 2P-excitation fingerprinting of intrinsic fluorescence from a cell (black), pure NADH (blue) and pure FAD (red). (ii) Enlarged view of spectral region encompassing second FAD excitation peak. Y-axes scales have been adjusted to compare excitation peak from intrinsic fluorescence with pure FAD excitation peak. Broadband emission was collected between 400nm and 650nm.

The 2P-excitation spectrum from cellular intrinsic fluorescence seems to correlate with NADH, although as with the spectrophotometer measurements, the cell spectrum is left-shifted. The slight increase in intrinsic fluorescence when excited between 800 and 1000nm (which is not present in the NADH solution spectrum) corresponds well to the second peak in the FAD excitation spectrum. However, there appears to be a further source of intrinsic fluorescence at wavelengths longer than 900nm. This is possibly arising from lipofuscin granules.

3.4 Discussion

The purpose of this set of experiments was to characterise the excitation and emission spectra of NADH and FAD in the pure state and to confirm that the intrinsic fluorescence from cardiac myocytes corresponded to these metabolites. As well as confirming the source of intrinsic fluorescence, these experiments also provided information about the possibility to simultaneously (but separately) visualise NADH and FAD fluorescence from the cells using a variety of fluorescence techniques, and the most suitable optical settings to achieve this.

A number of problems were encountered when measuring excitation and emission spectra from intrinsic fluorescence using the spectrophotometer. Firstly, when emission spectra were taken at 340nm excitation, an additional peak can be seen at 380nm. This was attributed to an instrument artefact, as it was evident even in non-fluorescent solutions such as water. Secondly, these measurements were made on 2ml volumes of cell suspension containing a mixture of live and dead cells in a cuvette. The turbidity of this suspension meant that light scattering was a problem, and clear, precise excitation and emission spectra could not be obtained. This was particularly a problem when an emission spectrum was taken from the cells at 450nm excitation, and it was not possible to see an emission peak from cellular intrinsic fluorescence that corresponded to FAD. However, 1P-excitation emission fingerprinting performed using the META detector on the confocal system revealed close correlation between the emission spectra of intrinsic fluorescence excited at 488nm and pure FAD fluorescence, with no contribution from NADH fluorescence.

Excitation and emission peaks from intrinsic fluorescence did seem to correspond to NADH fluorescence, although in both cases this peak was left-shifted by ~20nm in the cells. A possible explanation for this could be protein-binding of NADH within the mitochondria of the cells, a situation that does not arise with the pure metabolite in solution (Blinova *et al.*, 2005; Avi-Dor *et al.*, 1962; Chance & Baltscheffsky, 1958; Duysens & Ames, 1957). This left-shifting of NADH fluorescence was also evident in the 2P-excitation spectrum of intrinsic fluorescence from single cells. However, this was not apparent in 1P emission fingerprinting. A possible reason for this could be because there are 11nm gaps between each measured point in the emission spectrum with 1P emission fingerprinting using the META detectors. Thus, the peak intrinsic NADH fluorescence from the cell may indeed be left-shifted compared to pure NADH, but this is not visible because the exact wavelengths where the emission peaks arise could have been missed.

Although 2P-excitation fingerprinting revealed FAD as a source of intrinsic fluorescence in the cell, this fluorescence signal was so small that it was not possible to separately measure both FAD and NADH signals. All 2P experiments were therefore designed to optimise intrinsic fluorescence measurements of NADH in cardiac myocytes and tissue.

There are a number of limitations with this spectral analysis that need to be taken into consideration. Firstly, mitochondrial inhibitors may cause small changes in intracellular pH which could influence the spectral properties of NADH and FAD and haven't been taken into account in these measurements. Secondly, the spectral properties of NADPH were not measured here. However, it is known that they are almost identical to the spectral properties of NADH (Koenig & Schneckenburger, 1994), but as discussed previously, the majority of fluorescence is likely to arise from mitochondrial NADH (Eng *et al.*, 1989; Jöbsis & Duffield, 1967; Avi-Dor *et al.*, 1962; Estabrook, 1962). Finally, although spectral measurements were made on NADH and FAD solution mixtures, this may not be a true reflection of the interactions occurring intracellularly. Within the cell, the close proximity of transiently bound NADH and covalently bound FAD in flavoproteins such as lipoamide dehydrogenase, together with the overlap of the NADH emission spectrum and FAD excitation spectrum may enable fluorescence resonance energy transfer (FRET) to take place. In this situation, energy emitted by one chromophore may excite fluorescence in another chromophore located in very close proximity (~1-10nm). The occurrence of FRET from NADH to FAD may vary depending on the redox state of the mitochondria, influencing the fluorescence emission from FAD. However, no evidence could be obtained from the literature to support this theory.

The spectral analysis performed in this work could have been improved if spectral measurements were made of NADH in the fully reduced state, FAD in the fully oxidised state, as well as measurement of these metabolites in intermediate redox states. This would provide a better representation of the intrinsic fluorescence arising from these metabolites in their intracellular state.

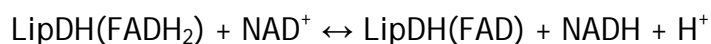
4 Establishing mitochondrial redox state in isolated rabbit ventricular myocytes

4.1 Introduction

The mitochondrial redox state provides a valuable index for assessing mitochondrial function in cells and tissue. These measurements reflect the balance between reduced and oxidised forms of the NAD and FAD pools, and provide information about O₂ availability/consumption, availability of substrate and ATP turnover (Mayevsky & Barbiro-Michaely, 2009; Duchen *et al.*, 2003; Huang *et al.*, 2002; Eng *et al.*, 1989). The major application of measurements of redox state is to monitor changes in these factors during experimental manipulations and different cellular conditions, such as in cancer. However, initial experiments were performed on quiescent cells in order to establish the resting redox state.

4.1.1 Intrinsic fluorescence arising from cellular flavins

In the previous chapter, pure FAD was used as a standard for comparison with cellular intrinsic fluorescence. However, the fluorescence excited by blue light arises from a number of flavoenzymes. Early studies in isolated rat liver mitochondria attributed the majority of this fluorescence to the NAD-linked flavoprotein α -lipoamide dehydrogenase (LipDH) in the oxidised state (Kunz & Kunz, 1985). LipDH is a component of a number of dehydrogenase enzymes, including the pyruvate dehydrogenase complex. The redox state of LipDH is in direct equilibrium with the redox state of NAD⁺ by the following simplified reaction mechanism:



The fluorescence intensity of LipDH thus reflects the redox state of NAD. An increase in NADH levels results in a change in the redox state of LipDH towards the reduced form and hence a decrease in LipDH fluorescence (Rocheleau *et al.*, 2004).

Electron transferring flavoprotein (ETF) was also shown to contribute to flavoprotein fluorescence. ETF is reducible in a non-NAD-linked reaction and is a component of the fatty acid oxidising system. It has a redox association with the

ETC through Q. More recent work in isolated rat cardiomyocytes spectrally unmixed the intrinsic fluorescence arising from cellular flavins to identify individual sources of fluorescence. This identified flavin fluorescence arising from bound FAD in the form of LipDH and ETF, as well as from free FAD (Chorvat *et al.*, 2004; Chorvat & Chorvatova, 2006; Chorvat *et al.*, 2005). FAD fluorescence is blue-shifted when protein bound. However, treatment with the mitochondrial uncoupler 2,4 dinitrophenol (DNP), which resulted in an increase in oxidised flavin fluorescence, found the emission peak to be shifted to closely match the emission peak of oxidised free FAD. This demonstrates the contribution of free FAD to cellular flavin fluorescence, as well as its redox contact with the respiratory chain. However, the exact location of free FAD within the mitochondria is not clear. Henceforth, any reference to FAD fluorescence will encompass the fluorescence arising from the FAD cofactor in the free and bound (flavoprotein) forms.

4.1.2 Intrinsic fluorescence measurements as an indicator of mitochondrial function

The main benefit of using intrinsic fluorescence measurements to assess mitochondrial function is that it eliminates the need for exogenous dyes and labels, which may themselves interfere with normal mitochondrial functioning. Most indicators for measuring mitochondrial membrane potential, for example, have direct toxic effects on the mitochondria (Duchen *et al.*, 2003). TMRE, TMRM and rhodamine 123 all decrease the rate of coupled respiration as they accumulate in the mitochondria (Scaduto & Grotyohann, 1999), and rhodamine 123 is known to have inhibitory effects on F_1F_0 -ATP synthase at high concentrations (Emaus *et al.*, 1986; Modica-Napolitano *et al.*, 1984).

To determine the resting mitochondrial redox state, NADH and FAD fluorescence signals in the maximally oxidised and maximally reduced state were established to allow for calibration of resting fluorescence levels. This was achieved using the mitochondrial inhibitors FCCP and NaCN. Utilising the fluorescence values at baseline, minimum and maximum, the resting NAD_{state} and FAD_{state} could be calculated.

4.1.3 Mechanism of action of mitochondrial inhibitors

4.1.3.1 FCCP

FCCP is a mitochondrial uncoupler. It acts as a proton ionophore and carries protons across the inner mitochondrial membrane. The mitochondrial membrane potential is abolished, because the inner membrane is no longer impermeable to H^+ ions. NADH and $FADH_2$ are continuously oxidised in an attempt to restore the membrane potential and O_2 consumption increases, but this is no longer coupled to the phosphorylation of ADP due to the loss of the proton gradient (Figure 4-1). This results in a fall in NADH fluorescence and an increase in FAD fluorescence.

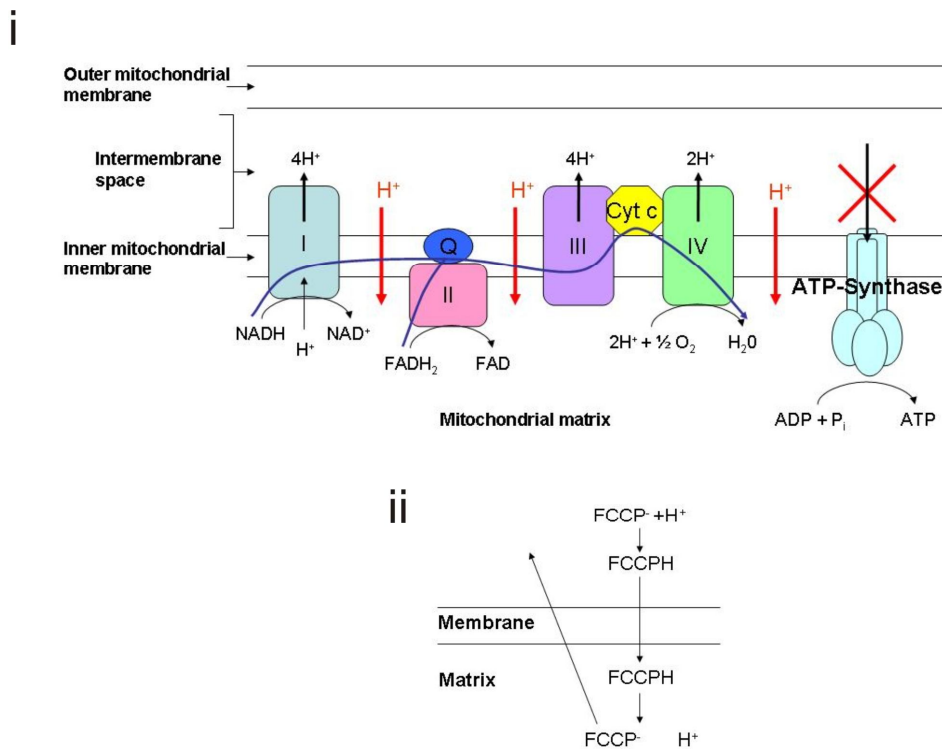


Figure 4-1 Mechanism of FCCP action on the respiratory chain

(i) The actions of FCCP are shown in red. The direction of electron transfer is shown by the blue arrow. FCCP causes the inner mitochondrial membrane to become freely permeable to protons, abolishing the mitochondrial membrane potential and inhibiting ATP synthesis. (ii) FCCP is protonated on the positive side of the membrane and moves across the membrane in the neutral form. In the mitochondrial matrix, FCCP loses its proton and in its negative form, it is driven back across the membrane by the mitochondrial membrane potential. This process can be repeated millions of times, which leads to dissipation of the mitochondrial membrane potential.

4.1.3.2 NaCN

The cyanide anion (CN^-) acts directly on the respiratory chain by combining with iron in cytochrome a_3 , a component of cytochrome c oxidase (complex IV). This binding is of high affinity, with a dissociation constant (K_d) of less than 50nM (Wainio & Greenlees, 1960; Jones *et al.*, 1984). Inhibition of complex IV prevents the oxidation of NADH and FADH_2 , electron transfer is blocked and reducing equivalents accumulate (Figure 4-2). The result is an increase in NADH fluorescence and a decrease in FAD fluorescence. Disruption of electron transfer, and thus proton pumping across the inner mitochondrial membrane, means that the cell can no longer produce ATP aerobically.

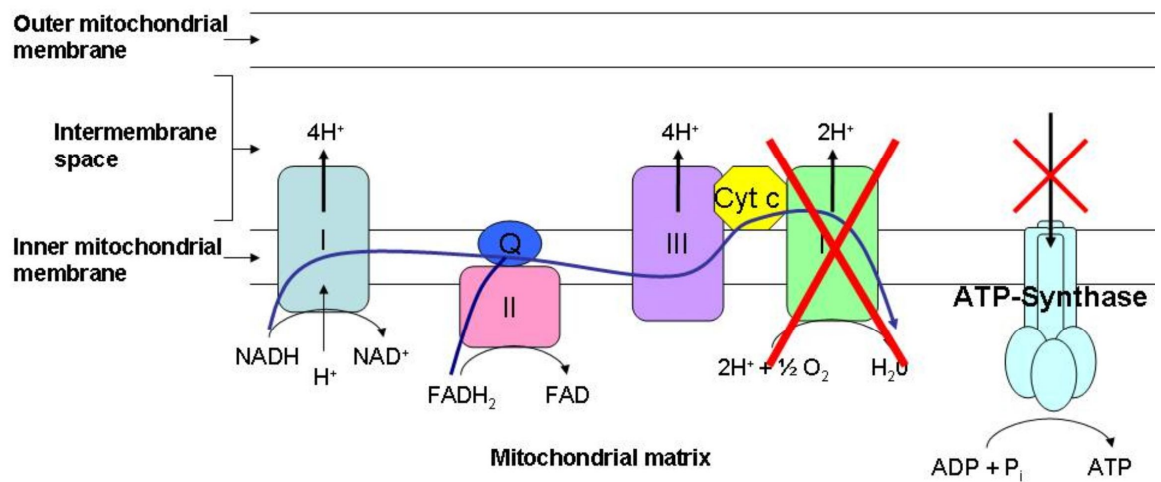


Figure 4-2 Mechanism of CN^- action on the respiratory chain

CN^- inhibits complex IV of the respiratory chain, blocking electron transfer (blue arrow) and causing accumulation of reducing equivalents.

4.1.4 Aims of the chapter

The main aim of this chapter was to establish mitochondrial redox state in isolated rabbit ventricular myocytes under quiescent conditions. A number of different fluorescent techniques were employed, allowing comparison of NAD and FAD state values in order to assess the reproducibility and reliability of the method.

4.2 Methods

All experiments were performed on rabbit ventricular myocytes isolated from the heart using the enzymatic digestion procedure described in Section 2.2.1.

4.2.1 Fluorescence spectroscopy

Following the isolation procedure, cells were suspended in Krebs solution containing 0.125mM CaCl₂ and 0.1% BSA. It was found that BSA has fluorescent properties, so the cells were spun down and the pellet re-suspended in a BSA-free Krebs solution.

4.2.1.1 Cell counting

The concentration of cells was calculated using an Improved Neubauer Haemocytometer (BDH Laboratory Supplies, Poole, England). The haemocytometer is a modified microscope slide with two polished sides, each displaying a precisely ruled, subdivided grid. Around 30µl of freshly isolated cardiac myocytes was loaded into the haemocytometer. Each of the two chambers was filled individually by the capillary action created between the haemocytometer and coverslip. Care was taken to ensure that the chambers were not overfilled and no solution had spread to the lateral grooves. At 100x magnification, the number of rod-shaped cells (cells with intact membranes) and ball-shaped cells (hyper-contracted cells with damaged membranes) were counted using the grid, and added to give a total cell count (number of cells per ml). The proportion of cells with intact membranes was also recorded.

4.2.1.2 Calculating mitochondrial redox state from spectral measurements

The mitochondrial redox state of cell aggregates containing a known concentration of rod-shaped and ball-shaped cells was taken as described in section 2.7.1. The fluorescence value at the peak emission wavelength prior to the addition of FCCP or NaCN (hereafter referred to as CN) was normalised to 1. The subsequent change in fluorescence following treatment with FCCP and CN was measured, and the normalised values at baseline, minimum and maximum were used to calculate NAD_{state} (Figure 2-9). The mean NAD_{state} was calculated

using the NAD_{state} values obtained from cell aggregates from each heart and are presented \pm standard deviation (SD).

4.2.2 Fluorescence microscopy

4.2.2.1 Excitation and emission settings in relation to NADH and FAD spectra

4.2.2.1.1 1P-excitation CLSM

The optical settings used for 1P-excitation CLSM are described in Figure 2-4. The excitation wavelengths used and emission wavelengths detected by the PMTs (due to the dichroic mirrors and emission filters used) in relation to the excitation and emission spectra of pure NADH and pure FAD are illustrated in Figure 4-3.

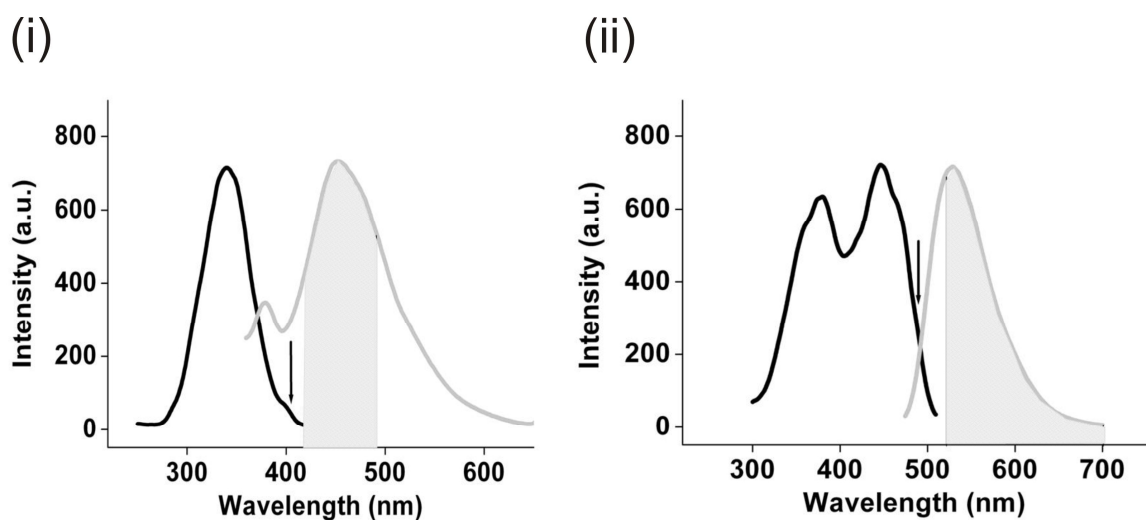


Figure 4-3 Excitation wavelengths used and emission wavelengths detected with 1P CLSM in relation to NADH and FAD spectra

Arrows indicate excitation wavelengths used corresponding to (i) NADH and (ii) FAD excitation spectra (black lines). NADH was excited at 405nm and FAD at 488nm. Shaded areas on emission spectra (grey lines) indicate emission wavelengths detected by the two PMTs as a result of the selected dichroic mirrors and emission filters. NADH fluorescence was collected at 420-490nm by one PMT and FAD fluorescence at wavelengths longer than 520nm by another PMT.

4.2.2.1.2 2P-excitation fluorescence microscopy

2P-excitation of the cells was performed using a Coherent Chameleon Titanium-Sapphire tunable laser. NADH was excited at 720nm and 750nm, but FAD fluorescence could not be detected in the cells. The wavelengths used for NADH

excitation and the emission wavelengths collected during experiments with 2P-excitation fluorescence microscopy are shown corresponding to the NADH excitation and emission spectra in Figure 4-4

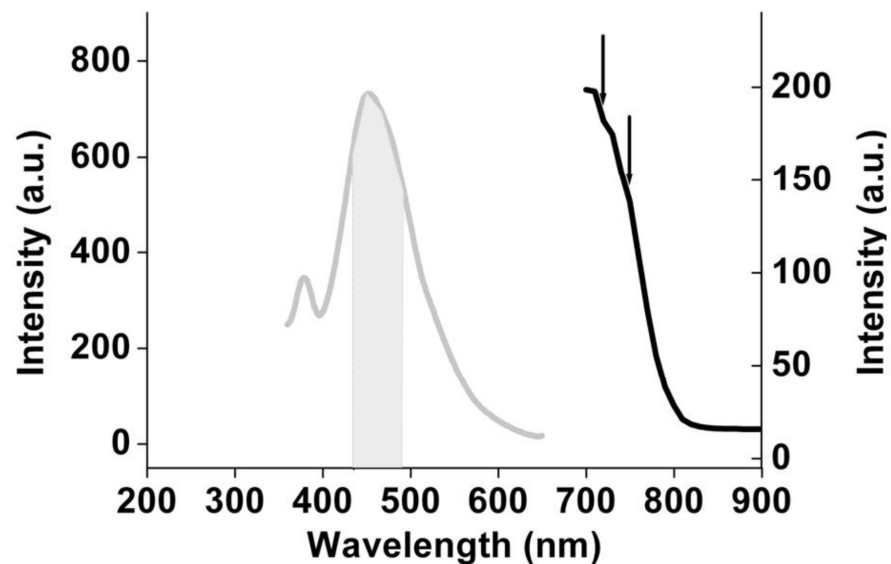


Figure 4-4 Excitation wavelengths used and emission wavelengths detected with 2P excitation fluorescence microscopy

Arrows on 2P excitation spectrum (black line) indicate 2P excitation wavelengths used to excite NADH (720nm and 750nm). Shaded area on NADH emission spectrum (grey line) indicates emission wavelengths detected by the PMT (435-485nm). Right Y-axis corresponds to fluorescence intensity of excitation spectrum, left Y-axis corresponds to fluorescence intensity of emission spectrum.

4.2.2.1.3 Wide-field epifluorescence microscopy

Unlike with laser scanning microscopy, where the excitation wavelength used is determined by the lasers present on the system, wide-field epifluorescence microscopy uses a xenon lamp as a light source, which provides intense broadband illumination. The excitation light could be adjusted (using a monochromator) to any wavelength within the near ultraviolet and visible range. The excitation wavelengths used in these experiments are therefore much closer to the excitation peaks for NADH and FAD, thus exciting more fluorescence. This compensated for the fact that the emission wavelengths detected, particularly for NADH fluorescence, had to be of a narrower waveband due to the dichroic mirrors and emission filters that were required in order to measure fluorescence

from both NADH and FAD. The excitation wavelengths used and emission wavelengths detected by the PMTs are shown in Figure 4-5.

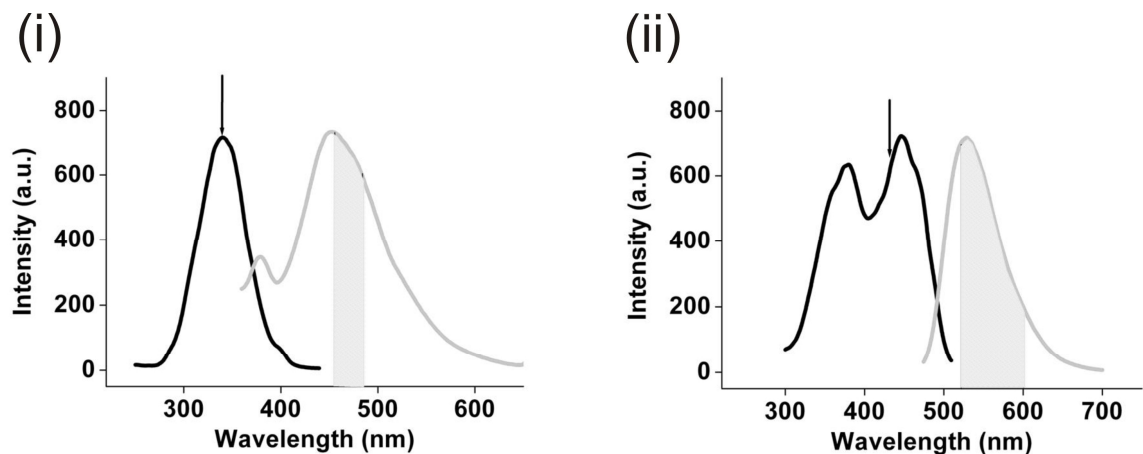


Figure 4-5 Excitation wavelengths used and emission wavelengths detected with wide-field epifluorescence methods in relation to NADH and FAD spectra

Arrows indicate excitation wavelengths used corresponding to (i) NADH and (ii) FAD excitation spectra (black lines). NADH was excited at 340nm and FAD at 430nm. Shaded areas on emission spectra (grey lines) indicate emission wavelengths detected by the 2 PMTs as a result of the selected dichroic mirrors and emission filters. NADH fluorescence was collected at 455-480nm by one PMT and FAD fluorescence at 520-600nm by another PMT.

4.2.2.2 Calculating mitochondrial redox state in single cells

Experiments involving microscopy enabled the fluorescence signal from individual cells to be measured. With 1P and 2P-excitation laser scanning microscopy, this was achieved by selecting a ROI consisting of an individual rod-shaped cell. With wide-field epifluorescence microscopy, a diaphragm was adjusted so that light could only be collected from a single rod-shaped cell.

The perfusion protocol for delivering mitochondrial inhibitors to the cells is described in section 2.7.2.1. The background subtracted normalised fluorescence values at baseline, minimum and maximum were used to calculate NAD_{state} and FAD_{state} (Figures 2-9 and 2-10). The mean NAD and FAD states were calculated using the NAD_{state} and FAD_{state} values obtained individually for each cell and are presented \pm SD.

4.3 Results

4.3.1 Mitochondrial redox state of cell aggregates assessed by fluorescence spectrometry

The mitochondrial redox state of cell aggregates containing both rod-shaped and hyper-contracted cells was assessed by fluorescence spectrometry. Clear emission spectra corresponding to FAD fluorescence could not be detected using this method due to problems with light scattering (see Chapter 3). The focus was therefore directed towards measurements of NADH fluorescence. The effects of FCCP and CN on the emission spectrum of NADH at the excitation wavelength (λ) 380nm were assessed by measuring changes in the amplitude of the emission peak following treatment (Figure 4-6).

The effects of FCCP and CN are shown in separate batches of cells, but the number of cells in each cuvette is the same and both batches of cells were isolated from the LV of the same heart.

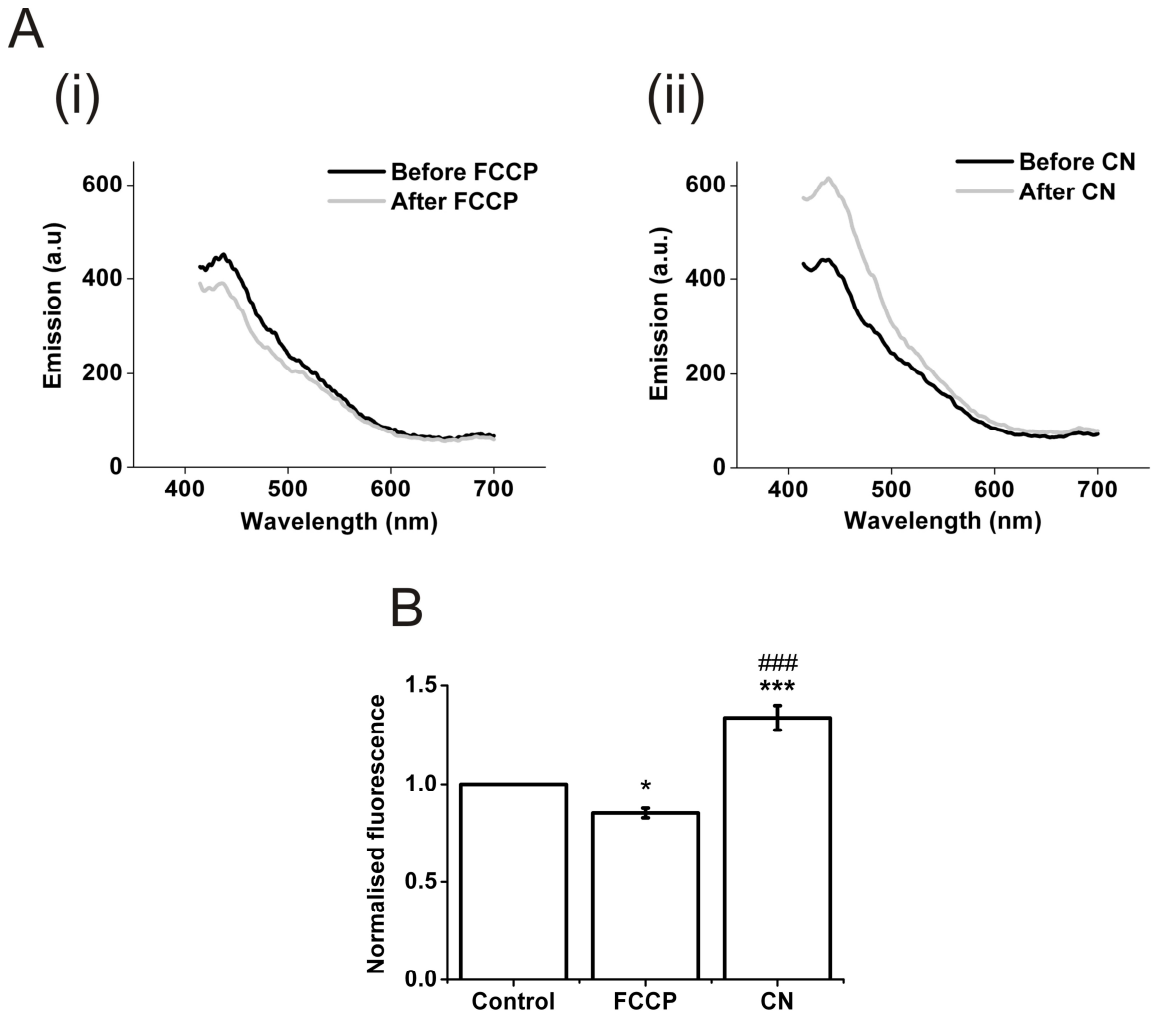


Figure 4-6 Effect of FCCP and CN on NADH emission spectrum

A: Example traces showing the effects of FCCP and CN on the NADH emission spectrum. The NADH emission spectrum before addition of mitochondrial inhibitor is shown by the black line. The effect of (i) 2 μ M FCCP and (ii) 2mM CN on NADH emission is shown by the grey line. Total cell number was 5.75×10^5 (20.9% rods). **B:** Mean effect of FCCP and CN on normalised NADH fluorescence (n=7 hearts). * P<0.05 versus control; *** P<0.001 versus control; ### P<0.001 versus FCCP.

FCCP and CN both have effects on the NADH emission spectrum. Prior to treatment, the baseline fluorescence emission was normalised to 1. FCCP causes a small decrease in NADH fluorescence, the mean normalised fluorescence value was found to be 0.85 ± 0.07 . CN has a slightly larger effect, causing NADH fluorescence to increase. The mean normalised fluorescence value following CN treatment was found to be 1.34 ± 0.16 . The mean NAD_{state} from cell aggregates isolated from 7 hearts was calculated to be 0.33 ± 0.15 . This means that 33% of the NAD pool is in the reduced state.

4.3.2 Mitochondrial redox state of single cells assessed by fluorescence microscopy

The mitochondrial redox state of single isolated rabbit ventricular myocytes was assessed by 1P and 2P-excitation laser scanning microscopy and by wide-field epifluorescence microscopy.

4.3.2.1 1P-excitation CLSM

Both the $\text{NAD}_{\text{state}}$ and the $\text{FAD}_{\text{state}}$ could be measured with 1P-excitation CLSM. The effects of FCCP and CN on NADH and FAD fluorescence from single cells are shown in Figure 4-7. The mean normalised minimum NADH fluorescence value obtained following FCCP treatment was found to be 0.67 ± 0.07 and the mean normalised maximum fluorescence value obtained following CN treatment was found to be 1.23 ± 0.13 . In 22 single cells with intact membranes, the mean $\text{NAD}_{\text{state}}$ was found to be 0.58 ± 0.16 (58% of the NAD pool in the reduced state). The mean normalised minimum FAD fluorescence value after CN treatment was found to be 0.58 ± 0.14 and the mean normalised maximum fluorescence value after FCCP treatment was 2.94 ± 0.53 . The mean $\text{FAD}_{\text{state}}$ in the same cells was found to be 0.18 ± 0.07 (18% of the FAD pool in the oxidised state, 82% reduced).

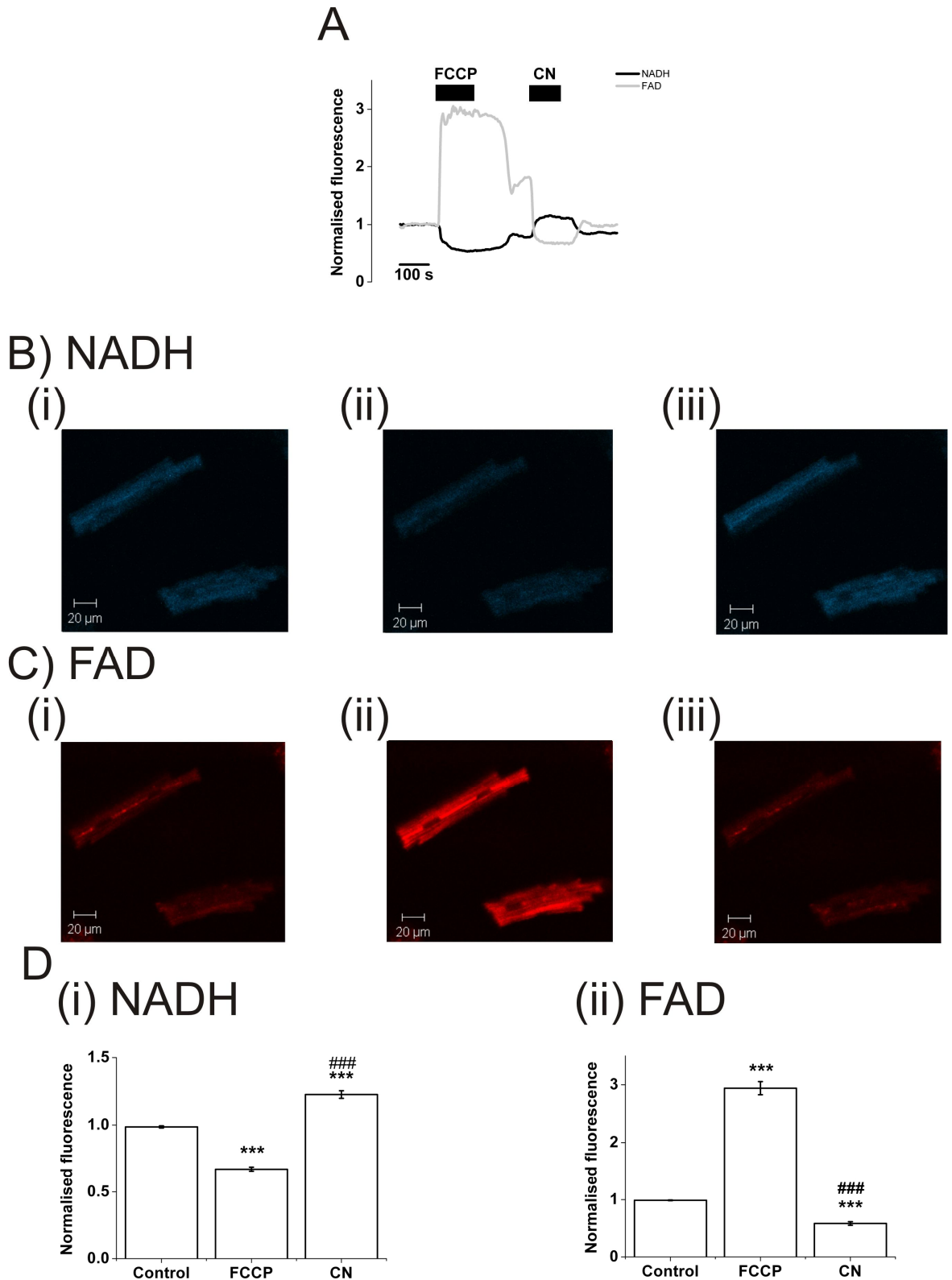


Figure 4-7 Effect of FCCP and CN on intrinsic fluorescence measured by 1P CLSM

A: An example trace showing the effect of FCCP and CN on normalised NADH fluorescence (black line) and FAD fluorescence (grey line) in a single rod-shaped cell. Images show intensity of **(B)** NADH fluorescence (ex λ 405nm) and **(C)** FAD fluorescence (ex λ 488nm) during each treatment. **(i)** control **(ii)** FCCP **(iii)** CN. **D:** Mean effect of FCCP and CN on normalised **(i)** NADH fluorescence and **(ii)** FAD fluorescence (n=22 cells from 5 hearts). *** $P < 0.001$ versus control; ### $P < 0.001$ versus FCCP.

4.3.2.2 2P-excitation fluorescence microscopy

Mitochondrial redox state measurements were also made using 2P-excitation fluorescence microscopy. FAD fluorescence could not be clearly detected, so only the $\text{NAD}_{\text{state}}$ could be established by this method. The effects of the mitochondrial inhibitors on NADH fluorescence in a single rod-shaped cell are shown in Figure 4-8. The mean normalised fluorescence value obtained after FCCP treatment was 0.47 ± 0.11 and after CN treatment was 1.41 ± 0.35 . In 20 cells, the mean $\text{NAD}_{\text{state}}$ was calculated to be 0.57 ± 0.18 , i.e. 57% in the reduced state.

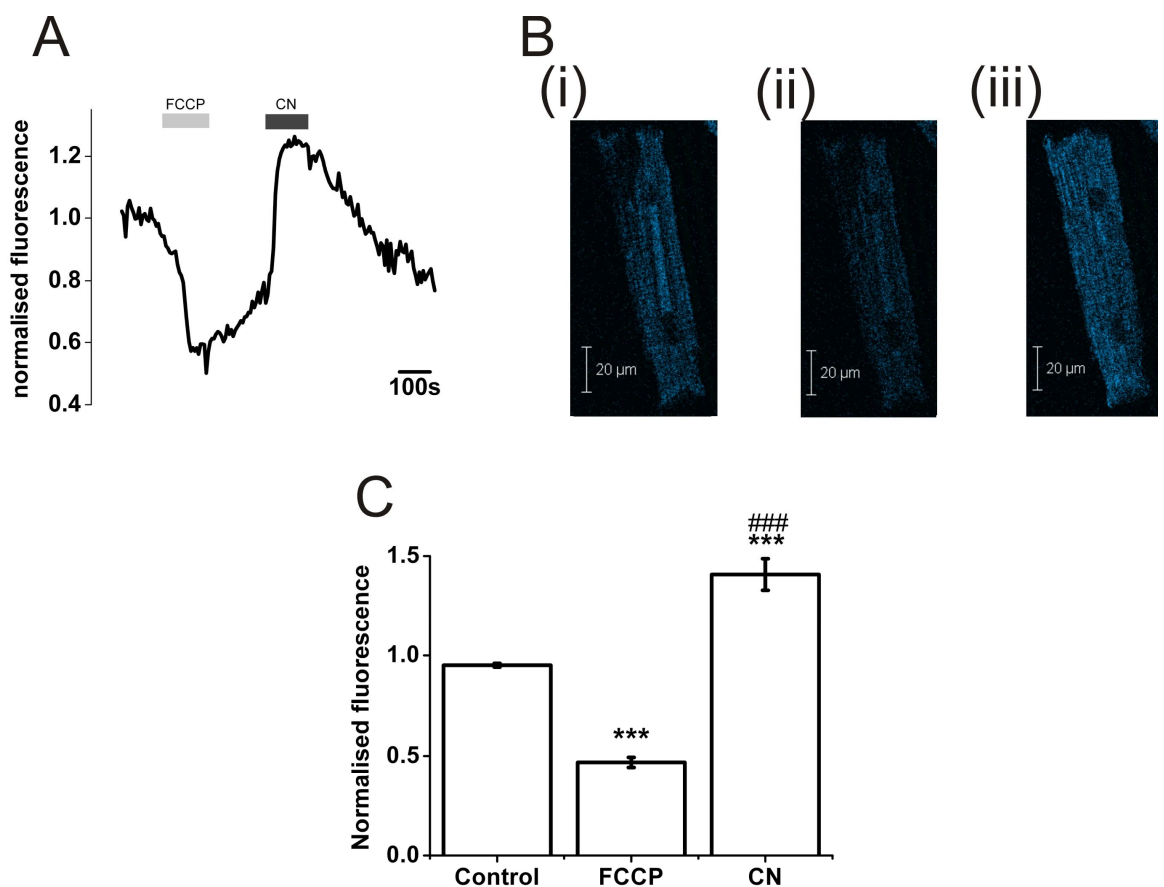


Figure 4-8 Effect of FCCP and CN on NADH fluorescence measured by 2P-excitation fluorescence microscopy

Panel A: Representative trace showing changes in normalised NADH fluorescence from a single cardiomyocyte over time following each treatment (excitation λ 720nm). **Panel B:** Images demonstrate intensity of NADH fluorescence during each treatment. (i) Perfused with control solution, (ii) decrease in NADH fluorescence following treatment with 2 μM FCCP solution and (iii) increase in NADH fluorescence following treatment with 2mM CN solution. **Panel C** shows mean effect of FCCP and CN on normalised NADH fluorescence (n=20 cells from 7 hearts). *** $P < 0.001$ versus control. ### $P < 0.001$ versus FCCP.

4.3.2.3 Wide-field epifluorescence microscopy

Finally, the mitochondrial redox state of single cells was measured using wide-field epifluorescence methods. As with 1P-excitation CLSM, both NADH and FAD fluorescence could be detected and simultaneously measured, thus enabling the establishment of both $\text{NAD}_{\text{state}}$ and $\text{FAD}_{\text{state}}$ from the fluorescence responses to FCCP and CN (Figure 4-9). Following FCCP treatment, the mean normalised NADH fluorescence value was found to be 0.38 ± 0.11 and following CN treatment, was found to be 1.55 ± 0.46 . Mean normalised FAD fluorescence was found to be 2.23 ± 0.29 in FCCP and 0.75 ± 0.13 in CN. The mean $\text{NAD}_{\text{state}}$ was found to be 0.59 ± 0.17 and $\text{FAD}_{\text{state}}$ was 0.17 ± 0.10 .

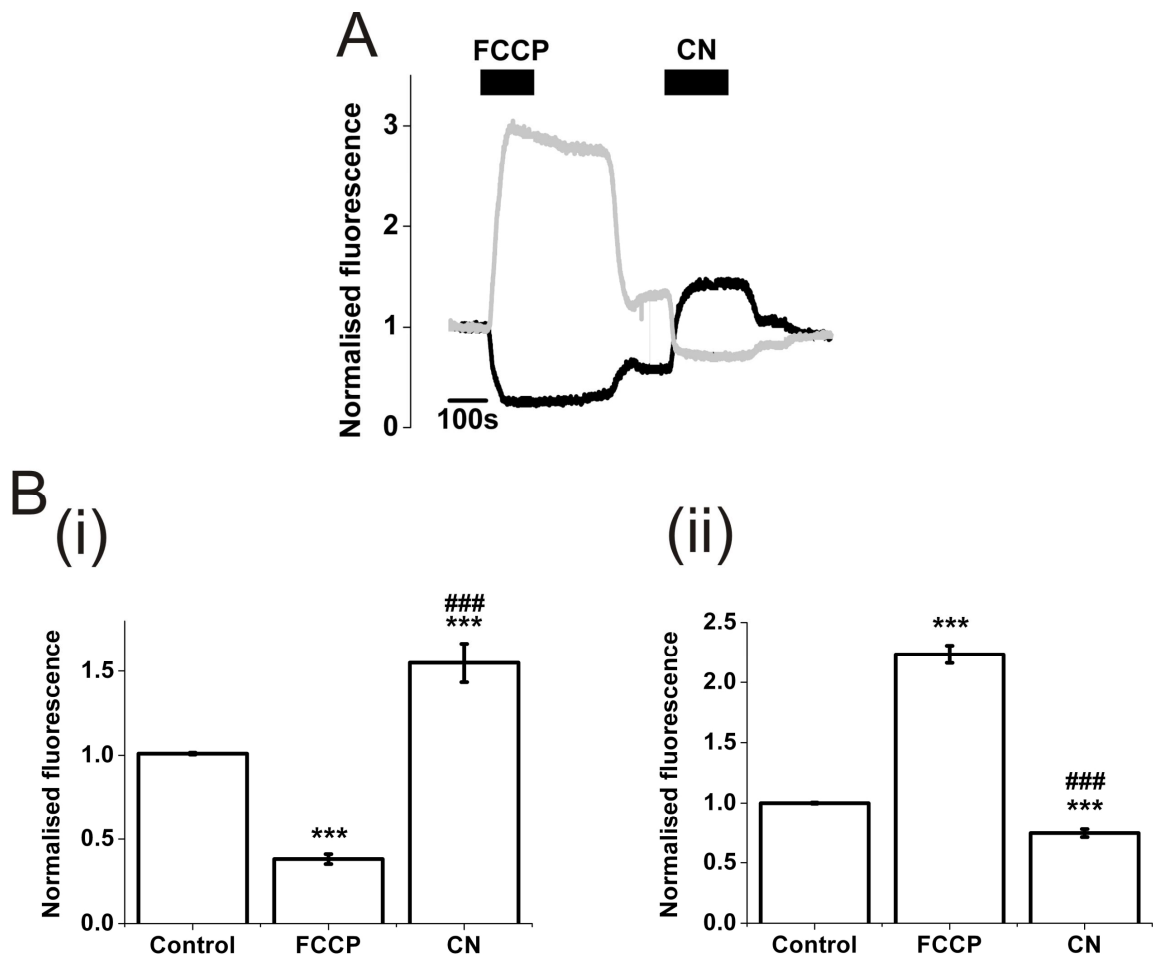


Figure 4-9 Effect of FCCP and CN on intrinsic fluorescence measured by wide-field epifluorescence microscopy

A: An example trace showing the effect of FCCP and CN on normalised NADH fluorescence (black line) and FAD fluorescence (grey line) in a single cardiac myocyte over time. **C:** Mean effect of FCCP and CN on normalised (i) NADH fluorescence and (ii) FAD fluorescence ($n=16$ cells from 11 hearts). *** $P < 0.001$ versus control. ### $P < 0.001$ versus FCCP.

4.3.3 Summary of mitochondrial redox state values assessed by intrinsic fluorescence methods

Table 4-1 summarises the values obtained for $\text{NAD}_{\text{state}}$ and $\text{FAD}_{\text{state}}$ using the fluorescence methods described. Experiments on cell aggregates contained both rod-shaped cells with intact membranes and hyper-contracted cells with damaged membranes, whereas single cell measurements were only performed on rod-shaped cells.

Fluorescence method	Cell aggregates/ single cell	$\text{NAD}_{\text{state}}$	$\text{FAD}_{\text{state}}$
Fluorescence spectrometry	Aggregates	0.33 ± 0.06 n=7	-
1P-excitation	Single cell	0.58 ± 0.03 n=22	0.18 ± 0.01 n=22
2P-excitation	Single cell	0.57 ± 0.04 n=20	-
Epifluorescence	Single cell	0.59 ± 0.04 n=16	0.17 ± 0.03 n=16

Table 4-1 Summary of mitochondrial redox state values obtained using each fluorescence technique

4.4 Discussion

4.4.1 Reproducibility of technique

The mitochondrial redox state values obtained in single rod-shaped cells by fluorescence microscopy are comparable between all the fluorescence

techniques used. The mean $\text{NAD}_{\text{state}}$ was found to be between 0.57 and 0.59 using 1P and 2P laser excitation and epifluorescence methods. Mean $\text{FAD}_{\text{state}}$, measured by 1P laser excitation and epifluorescence methods, was between 0.17 and 0.18. This confirms the reproducibility of the technique to measure mitochondrial redox state, and also shows that there is little variation in mitochondrial function between individual live cells.

However, the mean $\text{NAD}_{\text{state}}$ value achieved using fluorescence spectrometry was considerably lower, suggesting that the mitochondrial NAD^+ pool is in a more oxidised state in these cells. The most likely reason for this difference is that these measurements were performed on cell aggregates, containing a heterogeneous population of live, dead and dying cells. In the example trace shown in Figure 4-6, only 20.9% of the cells were live. The dead cells are no longer metabolically active, and the mitochondrial inhibitors will therefore have no effect on these cells. However, some cells may be dying, but may have some residual metabolic activity, as was observed in some hyper-contracted cells by 1P confocal microscopy. These cells are likely to be in a more oxidised state and their response to the metabolic inhibitors will reflect this. Consequently, the overall $\text{NAD}_{\text{state}}$ value obtained by spectrophotometry will not be a reflection of an entirely healthy population of cells and comparable redox values to those obtained in single, healthy cells would not necessarily be expected. In addition, the emission spectra produced by this technique are not particularly clear, most probably due to the effects of light scattering in the turbid cell suspension. As a result, the changes in fluorescence may not be quantitatively accurate enough to calculate $\text{NAD}_{\text{state}}$. However, the qualitative responses to FCCP and CN confirm the source of this intrinsic fluorescence to be NADH.

4.4.2 Comparison with redox state values in the literature

The values obtained for $\text{NAD}_{\text{state}}$ in single ventricular myocytes are comparable to other values quoted in the literature for cardiac cells or tissue (Brandes & Bers, 1996; Duchen & Biscoe, 1992; Esumi *et al.*, 1991; Eng *et al.*, 1989). The redox state of these cells at rest corresponds to state 3 respiration in isolated mitochondria. This indicates that the cells are actively respiring in aerobic conditions with high levels of substrate and ADP availability (Chance & Williams,

1955c; Mayevsky & Barbiro-Michaely, 2009). However, isolated mitochondria cannot really be compared to cardiac myocytes in terms of relative NAD and FAD states. This is because the substrate is in excess in isolated mitochondria and thus the limitation of NADH supply is less, leading to a more reduced NAD state at the same rate of ATP synthesis and therefore does not reflect the physiological situation in intact cells.

The results show that the FAD pool is in a more reduced state than the NAD⁺ pool. Flavoprotein redox state has been reported to be ~50% reduced in the Langendorff-perfused whole heart (Pasdois *et al.*, 2008). No FAD_{state} values have been reported in isolated cells. However, studies performed on cardiac myocytes, in which flavoprotein autofluorescence and its response to mitochondrial inhibitors and uncouplers was measured, suggest that the mitochondrial flavoproteins are predominantly in the reduced state at rest (Sedlic *et al.*, 2010; Chorvat *et al.*, 2004; Kato *et al.*, 2002; Romashko *et al.*, 1998).

4.4.3 Possible sources of residual fluorescence

Some residual fluorescence remains even when the ETC is in the completely reduced and completely oxidised state. In the completely reduced state, in the presence of CN, the residual fluorescence probably originates from other flavoproteins with fluorescent properties, but not in redox contact with the respiratory chain (Kunz, 1986). This may be attributed to enzymes of fatty acid β -oxidation (Chorvat *et al.*, 2005). In the oxidised state (following FCCP treatment) the remaining fluorescence is likely to be arising from cytosolic NADH and NADPH, which have similar optical properties to mitochondrial NADH, but are relatively unaffected by uncoupling of the mitochondria. Cytosolic NADH produced by glycolysis may be indirectly affected by mitochondrial uncoupling primarily due to the presence of the malate-aspartate shuttle. This complex cycle involves a number of metabolites that leads to the transfer of electrons from cytosolic NADH to mitochondrial NAD⁺. The cytosolic NAD⁺ that results can be recycled for glycolytic use and in the mitochondria, NADH can enter the ETC for ATP production. Oxidation of mitochondrial NADH with FCCP may shift this equilibrium to increase the activity of the shuttle, potentially increasing the rate

of NADH transfer from cytosol to mitochondria. This would contaminate the mitochondrial $\text{NADH}_{\text{state}}$ measurements obtained by calibration with FCCP and CN with cytosolic NADH signal. However, there is evidence to suggest that uncoupling agents, including FCCP, have inhibitory effects on this shuttle (LaNoue & Williamson, 1971), in which case the contribution of cytosolic NADH to the calibrated NADH signal would be expected to be small.

Another factor that should be taken into consideration is that the NAD^+/NADH and $\text{NADP}^+/\text{NADPH}$ redox couples are also linked via the pyridine nucleotide transhydrogenase enzyme. This enzyme catalyses electron transfer from NADH to NADPH, which can then act as an electron donor in antioxidant mechanisms such as the glutathione peroxidase reaction. However, if NADP^+ reduction through this enzyme depends on NADH and the protonmotive force (Kohlhaas *et al.*, 2010; Liu & O'Rourke, 2009), the presence of FCCP would inhibit this reaction and thus there would be no additional contribution expected to arise from NADPH fluorescence (over and above any baseline NADPH fluorescence) when the mitochondria are uncoupled. However, if oxidation of NADH during FCCP treatment subsequently leads to oxidation of NADPH, this would mean that the NADH signal calibrated with FCCP would have some contribution from NADPH fluorescence. As NADPH is also maintained in the reduced state via the malic enzyme and isocitrate dehydrogenase reactions, it is likely that although some NADPH oxidation may occur, its contribution to the calibrated signal is expected to be small.

The $\text{NAD}_{\text{state}}$ and $\text{FAD}_{\text{state}}$ values were calculated for each cell/batch of cells using the normalised fluorescence values in control, FCCP and CN. The mean NAD and $\text{FAD}_{\text{state}}$ were obtained by taking an average of these values, as opposed to using the values for average responses to FCCP and CN. The 2 methods for calculating mean $\text{NAD}/\text{FAD}_{\text{state}}$ produce slightly different values. However, taking the average from individual cells meant that any slight differences in conditions between the cells (for example, differences in the rate of fluorescence bleaching at the start of the experiment which could affect the baseline fluorescence value) were taken into account when the $\text{NAD}/\text{FAD}_{\text{state}}$ was calculated.

4.4.4 Relationship between NAD and FAD states

The results of these experiments have demonstrated that FAD is in a more reduced state at rest compared to NAD^+ . These results agree with what would be expected; as the standard reduction potential of FAD is more positive compared to NAD^+ (see Table 1-1), FAD would be expected to be more reduced than NAD^+ at any given mitochondrial state.

These experiments have demonstrated the reproducibility of the technique for assessing mitochondrial function through measurements of redox state in isolated rabbit ventricular myocytes. Using 1P-excitation and epifluorescence methods, both NADH and FAD fluorescence could be measured, but only NADH fluorescence was visible using 2P-excitation and spectroscopic methods. In the following chapters, intrinsic fluorescence measurements were used to assess mitochondrial redox state in intact tissue preparations and to assess energy supply and demand matching in isolated cells.

5 Establishing mitochondrial redox state in intact ventricular tissue preparations

5.1 Introduction

The cell isolation procedure involves the dissociation of cardiac myocytes from ventricular tissue using the protein digesting enzymes collagenase and protease. The crude activity of these enzymes gives rise to the possibility that the mitochondria may be damaged by this process. In order to investigate this, mitochondrial function in intact ventricular tissue preparations, not exposed to the digestion procedure, was assessed using measurements of mitochondrial redox state. This would then be compared to mitochondrial redox state values in single, isolated ventricular cells in order to establish if there is any difference, and thus if the isolation procedure has an effect on mitochondrial function. In addition, if measurements of mitochondrial redox state could be achieved in different areas and layers of tissue, variations in the metabolic status of local regions within the myocardium could be investigated.

Two intact tissue preparations from the rabbit heart were used in these experiments. In the ventricular wedge preparation, the LV is isolated from the rest of the heart and the coronary circulation perfused by cannulation of the left coronary orifice. The horizontal Langendorff preparation utilises the whole heart, retrogradely perfused through the aorta to perfuse the coronary vessels. The preparation is placed horizontally and an area of the LV tissue is imaged.

Imaging of the tissue preparations was made possible with 2P-excitation fluorescence microscopy, which enables greater imaging penetration depth due to the lack of detector pinhole and reduced scattering of the excitation light (Rubart, 2004; Huang *et al.*, 2002; Centonze & White, 1998; Denk *et al.*, 1990). However, earlier experiments using isolated cardiomyocytes have shown that the use of 2P-excitation methods meant that only measurements of NADH fluorescence could be made.

5.1.1 LV wedge preparation

The arterially perfused LV wedge preparation was first developed in canine heart (Yan & Antzelevitch, 1996) and has since been reproduced in the rabbit heart (Yan *et al.*, 2001). As it is directly perfused through the left coronary artery, the

tissue remains viable for up to 7 hours (Chen *et al.*, 2006). This preparation has predominantly been used in electrophysiological studies, as its transmural surface enables the investigation of electrical heterogeneity within the different layers of the myocardium. The rationale behind using the LV wedge for investigating mitochondrial function is that the relatively flat ventricular epicardial surface that results once the preparation is securely pinned down produces the ideal surface for imaging. Another advantage of this preparation is that the absence of regions of automaticity means that the wedge is not spontaneously active and therefore quiescent cardiac preparations can be studied without motion artifact (although blebbistatin was still used as a precaution).

5.1.2 Horizontal Langendorff preparation

The horizontal Langendorff preparation utilises the principle of retrograde perfusion of the aorta in order to perfuse the coronary arteries, but instead of hanging vertically, the preparation is placed horizontally. Although it is more difficult to find a suitably flat ventricular surface for imaging, this preparation requires no dissection of the heart, and is thus easier and quicker to set up than the arterially perfused LV wedge preparation, and no cut surfaces are left exposed. However, spontaneous activity cannot be avoided. To counter this, but retain a metabolically active tissue, inhibitors of contractile function were required. The loss of contractile function will mean that the rate of respiration will be very much lower than in the physiological situation where the heart would be beating and the metabolic demand will be higher. However, this allowed comparisons of redox state between inactive intact tissue preparations and inactive cells to be made.

5.1.3 Inhibitors of contraction

Contractile function in the cardiac tissue preparation needs to be inhibited in order to suppress movement which causes motion artefacts and interferes with imaging. This can be achieved pharmacologically using motion uncouplers.

5.1.3.1 2,3-Butanedione monoxime

2,3-Butanedione monoxime (BDM) is a reversible inhibitor of myofibrillar ATPase and is commonly used as an agent to reduce contractile force. However, there are reports of BDM having effects on the electrical activity of cardiac muscle at concentrations used experimentally. BDM effects on conduction velocity, action potential duration and electrical restitution have been reported (Kettlewell *et al.*, 2004; Baker *et al.*, 2000; Riccio *et al.*, 1999). More importantly for this study, BDM has also been reported to have effects on mitochondrial function. It has been shown to suppress state 3 respiration, having an inhibitory effect on complex I of the ETC even at concentrations below 10mM (Scaduto & Grotyohann, 2000). Inhibition of ATP transport across the mitochondrial membrane by BDM has also been reported (Stapleton *et al.*, 1998; Mojon *et al.*, 1993). For these reasons, BDM was not used as a movement uncoupler in these experiments.

5.1.3.2 Blebbistatin

Blebbistatin is a recently discovered movement uncoupler which selectively inhibits myosin II ATPase in an actin-detached state (Kovács *et al.*, 2004; Straight *et al.*, 2003). Unlike BDM, it has been shown to have no effect on the electrical activity of the heart (Fedorov *et al.*, 2007) and no direct effects on mitochondrial function have been reported. However, blebbistatin can be inactivated by illumination with UV and visible blue light (Kolega, 2004; Sakamoto *et al.*, 2004). In addition, blebbistatin has fluorescent properties which can interfere with the fluorescence signal of interest. The excitation and emission spectra of blebbistatin are shown in Figure 5-1. Blebbistatin has 3 excitation peaks, the main peak being at 330nm. Peak emission is at ~500nm. These fluorescent properties overlap with those of NADH, and the weak intrinsic fluorescence signal is likely to be masked by blebbistatin fluorescence. However, the fluorescent properties of blebbistatin were not initially known, and the experiments performed on the LV wedge preparation used blebbistatin as a movement uncoupler.

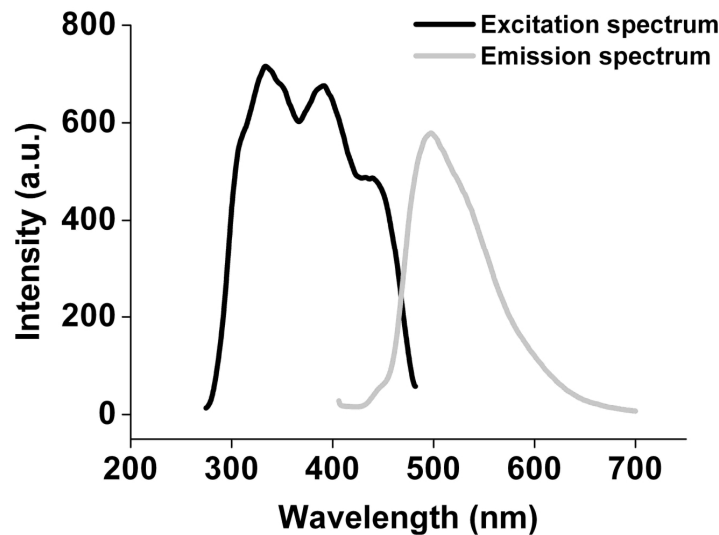


Figure 5-1 Spectral properties of blebbistatin

Excitation spectrum (black line, emission measured at 500nm) and emission spectrum (grey line, excitation at 390nm) of a 10 μ M blebbistatin solution.

5.1.3.3 Low Ca²⁺ solution

In order to avoid the difficulties resulting from the use of pharmacological agents to inhibit contractile activity, no external movement uncoupler was added during the horizontal Langendorff experiments. In its place, a low extracellular [Ca²⁺] of 100 μ M (instead of 1.8mM) was used. If a Ca²⁺ free Tyrode's solution had been used, any subsequent exposure of the heart to solutions with higher [Ca²⁺] would result in the "Ca²⁺ paradox" and cell death. The [Ca²⁺] used in these experiments is too low for contraction of cardiac myocytes to occur, but together with 10mM MgCl₂, protects against the calcium paradox taking place (Hoenicke & Damiano, 2001; Suleiman & Chapman, 1993; Chapman & Tunstall, 1987; Lansman *et al.*, 1986). In addition, by preventing the increase in Na⁺ conductance via the L-Type Ca²⁺ channel that can occur in low extracellular [Ca²⁺] conditions, the use of high extracellular [Mg²⁺] also ensures that functioning of mitochondrial NCX is not influenced by high intracellular [Na⁺] (Maack *et al.*, 2006; Chapman *et al.*, 1984). Any effect of the altered ion concentrations on mitochondrial redox state was evaluated by assessing NAD_{state} and FAD_{state} in a few isolated ventricular cells (n=5) using an extracellular solution containing 100 μ M CaCl₂ and 10mM MgCl₂. The values were found to be similar to those seen in isolated cardiomyocytes using normal Krebs solution, and

use of this low Ca^{2+} , high Mg^{2+} solution was deemed to be a suitable means to inhibit contraction in the tissue preparation.

5.1.4 Inner filter effect on NADH fluorescence transmission

In the thick tissue preparation, the fluorescence emission of NADH may interact with other cellular constituents with light absorption capabilities, potentially affecting the fluorescence signal being directed to the PMT detector. This inner filter effect complicates the interpretation of the changes in the NADH emission signal during mitochondrial inhibition. In addition, if the mitochondrial inhibitors affect the optical properties of the tissue, this could also potentially influence fluorescence detection of NADH.

Earlier experiments examining the excitation and emission spectrum of FAD show that changes in FAD absorption could affect NADH fluorescence transmission through the tissue and subsequently its detection. Myoglobin (Mb) also strongly absorbs light at wavelengths corresponding to NADH emission wavelengths. Mb is an O_2 -binding haemoprotein found in striated muscle which acts as an intracellular storage site for O_2 . Upon periods of O_2 deprivation, oxymyoglobin (MbO_2) releases its O_2 , which can then be used by the cell for aerobic metabolism. The Mb absorption spectrum is known to shift depending on whether it is in the oxygenated or deoxygenated state (Brandes *et al.*, 1994; Leisey *et al.*, 1994). Thus the inner filtering effects of Mb would complicate interpretation of NADH fluorescence measurements if experimental conditions were changing between normoxia and hypoxia/anoxia, as the variation in light absorption by Mb at the different conditions would influence the amount of NADH emission light reaching the detector.

5.1.5 Aims of the chapter

The main aims of this chapter were to establish mitochondrial redox state in intact cardiac tissue preparations which could then be compared to redox state values obtained in isolated cells to assess if the enzymatic dissociation process has an effect on mitochondrial function. In addition the feasibility of using 2P-excitation fluorescence microscopy to image metabolic state in local regions within the myocardium was examined.

5.2 Methods

5.2.1 Preparation and imaging of tissue

5.2.1.1 Arterially perfused LV wedge preparation

The LV wedge preparation was set up as described in section 2.3. A glass coverslip was attached to a Perspex slide with an ellipsoidal-shaped section cut out, and placed on the tissue to create a flat imaging surface. The preparation was imaged by 2P-excitation fluorescence microscopy and NADH was excited at 720nm. The optical settings used are described in Figure 2-5. A 3D-representation of the tissue was created by sampling images down the Z-stack. This involved the laser scanning and imaging a thin plane, displacing vertically by 20-25 μm and rescanning and imaging. This was repeated until around 10 layers had been scanned, giving a cross-sectional fluorescence representation through around 200 μm . These layers included the epicardial surface and a number of myocardial layers, as well as images 50-100 μm above the surface of the tissue to get an indication of the background fluorescence signal.

5.2.1.2 Horizontal Langendorff preparation

The horizontally positioned Langendorff-perfused whole heart preparation was set up as described in section 2.4. The Perspex slide was placed on the heart to hold it in position, but this time without the coverslip attached. This was because of the possibility that the pressure of the coverslip over the coronary vessels may cause occlusion of the vessels, preventing flow of the mitochondrial inhibitor to the area of tissue being imaged.

The preparation was excited at 720nm and the optical settings used were the same as those described for the experiments on the LV wedge (Figure 2-5). Occasionally, the laser would not mode-lock at 720nm, in which case excitation was performed at 740nm. As with the wedge preparation, the Z-stack function was utilised to sample the fluorescence signal through the myocardial layers. For this preparation, the distance between each layer was 50 μm . This meant that more images could be taken from above and deep within the tissue than with the wedge preparation, without extending the time taken to scan through all the

layers. In total, the Z-scan spanned around 400 μ m for these experiments, encompassing myocardial and epicardial tissue layers, as well as up to 150 μ m above the tissue surface. The background fluorescence was obtained at the end of the experimental day after the heart had been removed from the chamber. The fluorescence signal from Tyrode's solution alone (under the same ambient light conditions, laser power and PMT settings used during tissue fluorescence measurements) was taken and subtracted from the tissue fluorescence values.

5.2.2 Delivery of mitochondrial inhibitors

The mitochondrial inhibitors FCCP and CN were delivered to the tissue preparations as described in section 2.7.3. For the experiments performed on the LV wedge, the same concentration of FCCP (2 μ M) and CN (2mM) were used as was used in isolated cells. For the whole heart experiments, the concentration of both inhibitors was doubled to ensure that effective inhibitor concentrations were reaching the area of tissue being imaged as quickly as possible. The same concentration of inhibitor was also added to the bathing solution surrounding the preparation to achieve maximum exposure to the inhibitor. Between each experimental run, the solution in the chamber was removed and fresh Tyrode's solution added.

5.2.3 Normalisation of fluorescence

The fluorescence signal arising from the tissue alone was obtained by subtracting the background fluorescence signal. For each layer in the Z-stack, the mean baseline fluorescence value prior to the delivery of mitochondrial inhibitor was determined and normalised to 1. The same method of normalisation was used for both the LV wedge and Langendorff perfused whole heart preparations.

5.2.4 Assessing perfusion through the coronary vessels

In order to confirm that the coronary vessels were being perfused adequately and that the mitochondrial inhibitor was reaching the area of tissue being imaged, the fluorescent indicator 5(6)-carboxyfluorescein was used as a tracer. Excitation was at 800nm and fluorescence collected at 500-550nm. 100 μ M of dye was injected through the injection port by the syringe driver into the perfusing

solution, resulting in a dye concentration of 1 μ M being delivered to the tissue. The appearance of the dye in the vessels and tissue confirmed that the vessels were being perfused and the myocardial tissue was receiving an adequate supply of perfusate. In addition, any effect of the mitochondrial inhibitor on vascular tone was indirectly assessed by injecting inhibitor together with the dye. If the presence of the inhibitor prevented or slowed dye uptake by the tissue, this would suggest that the inhibitor was causing constriction of the coronary vessels and restricting flow. Consequently, this would suggest that the inhibitor was not being delivered to the area of tissue being imaged.

5.2.5 Assessing the effects of mitochondrial inhibitors on light transmission through the tissue

To investigate whether the mitochondrial inhibitors were directly affecting the optical properties of the tissue, light transmission through the ventricular myocardium was measured. A blue light emitting diode (LED), emitting light at 450-490nm (corresponding to peak NADH emission) was inserted into the ventricle and the effect of the mitochondrial inhibitors on light transmission to the PMT detectors was assessed. An additional green LED, emitting light at 500-550nm was also inserted into the heart. This emission corresponds to the downward slope of the NADH emission spectrum, but unlike the blue LED, it does not overlap with the FAD excitation spectrum (which could potentially interact with NADH emission). The wavebands emitted by these LEDs are spectrally adjacent, as light scattering is affected by wavelength. Any change in the LED emission signal detected by the PMTs during perfusion with the mitochondrial inhibitors would suggest that the inhibitor is affecting transmission of light through the tissue, therefore complicating the interpretation of the oxidative status of NADH.

These experiments were performed in the whole heart. The horizontal Langendorff-perfusion was setup and contraction was inhibited by perfusing with low Ca²⁺ solution. The measurements were made in both the RV and the LV. The LEDs were inserted into the RV through a slit cut into the right atrium. An opening was cut at the apex of the heart to allow the LEDs to be inserted into the LV. The heart was positioned with either the RV or LV facing upwards, and

orientated in a manner so that light from both LEDs could be simultaneously detected (Figure 5-2). No laser was used in these experiments. Blue light was detected at one PMT using a 435-485nm filter. Green light was detected at another PMT using a 505nm long-pass filter.

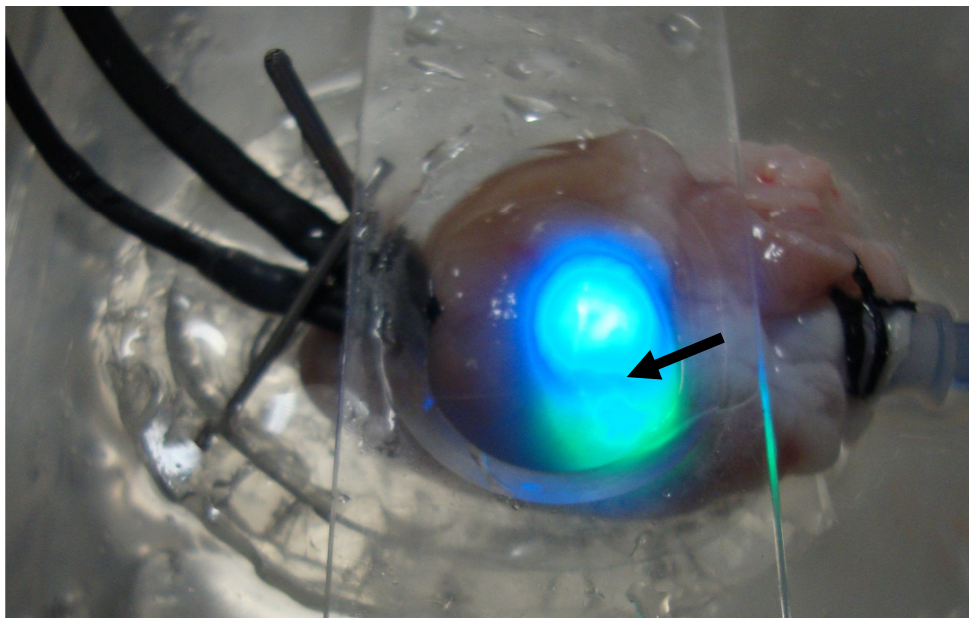


Figure 5-2 Positioning of LEDs in the LV of the horizontal Langendorff preparation

The LEDs were inserted into an opening cut at the apex of the LV and pinned into position. The heart was imaged in an area where light from both LEDs could be detected by the PMTs (indicated by black arrow).

5.2.6 FAD absorption measurements

The absorption spectrum of FAD was verified using a Shimadzu UV-2401PC UV-VIS recording spectrophotometer. 0.1mM of pure FAD was dissolved in a mock intracellular solution containing (in mM) 120 KCl, 1 MgCl₂, 0.05 EGTA and 25 HEPES with the pH adjusted to 7.2. The absorption spectrum of 2ml of pure FAD was recorded between 300 and 700nm. 1mM Na-dithionite was added to this solution to reduce FAD to FADH₂, simulating the effect of CN treatment in the tissue preparation. The absorption spectrum of the solution was recorded again, enabling comparison of absorption profiles of FAD and FADH₂.

5.2.7 Mb absorption measurements

Another cellular component potentially capable of complicating intrinsic fluorescence measurements due to inner filtering effects is Mb (Brandes *et al.*, 1994; Leisey *et al.*, 1994). To examine this, Mb from equine heart (Sigma) was dissolved in the same mock intracellular solution used in FAD absorption measurements. 2ml of Mb at a concentration of 0.01mM was placed in a cuvette and the absorption spectrum between 300nm and 700nm was recorded. 4mM NaCN was added to the cuvette and the absorption spectrum recorded again to assess any effect of CN on the absorption spectrum of Mb.

5.3 Results

5.3.1 Mitochondrial inhibitor responses in the LV wedge preparation

An example image of the localisation of NADH fluorescence in intact tissue is shown in Figure 5-3.

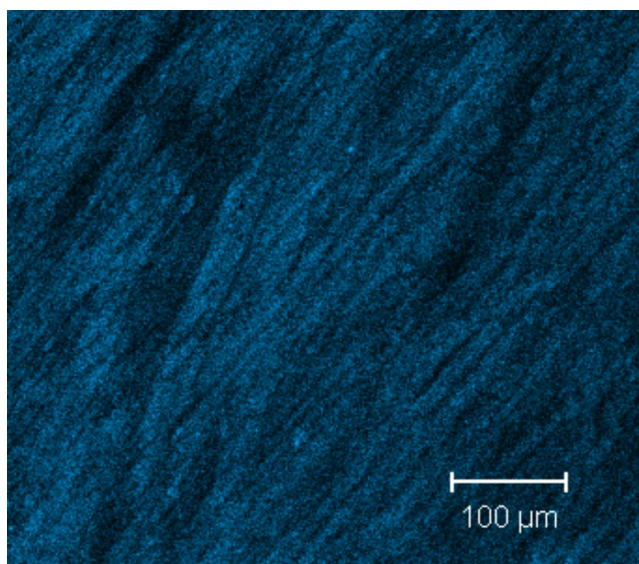


Figure 5-3 NADH fluorescence localisation in intact tissue

NADH fluorescence can be clearly seen throughout the myocardial structure; here indicated by the blue pseudocolour. At this scale (using a 10x objective), individual cells cannot be identified. Image was taken ~50µm below the tissue surface. Excitation was at 740nm, emission was collected at 435-485nm.

The responses to FCCP and CN in the LV wedge preparation were difficult to quantify due to continuous upward movement of the preparation. This meant that the plane of focus was constantly changing, resulting in fluorescence changes due to areas of tissue coming into/going out of focus, and not due to the effect of the mitochondrial inhibitor. No clear response to FCCP was seen in any of the preparations (data not shown). However, in some preparations, a transient increase in NADH fluorescence in response to CN infusion was seen. An example of this response is shown in Figure 5-4. This transient response was only apparent in the myocardial tissue layers; images taken from above the tissue surface (essentially background fluorescence) did not display the same response. This suggests that this response was not simply an artefact due to movement of the tissue, and was likely to be a true biological response to CN. Out of four LV wedge preparations, this transient response to CN was seen in two. In the other preparations, no clear changes in fluorescence could be observed over and above those caused by movement of the tissue.

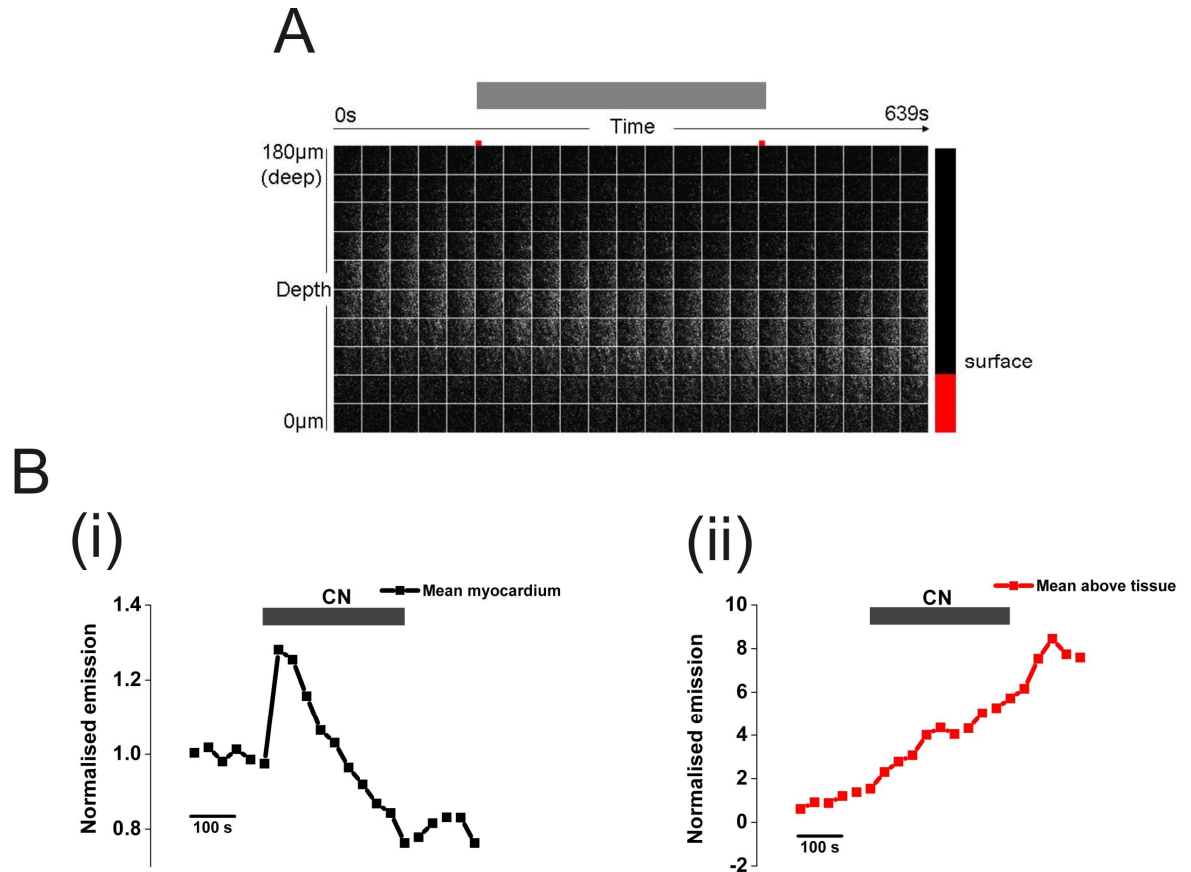


Figure 5-4 NADH fluorescence response to CN in LV wedge preparation

Panel A shows changes in NADH fluorescence and the effect of 2mM CN over time at different tissue depths. The difference between each Z-layer is 20µm. The grey bar indicates the time period during which CN was delivered. The plane of focus appears to be changing over time, suggesting upward movement of the preparation. Black and red bars on right indicate images arising from myocardial tissue and above the surface of the tissue respectively (at the start of the experiment before any movement of the tissue had occurred). B: Collating the mean normalised fluorescence in all the myocardial layers (i) indicates a transient response to CN, not seen in the mean normalised fluorescence from layers above the tissue surface (ii).

5.3.2 Confirmation of coronary artery perfusion in the horizontal Langendorff preparation

The technical difficulty of preparing the LV wedge, and the lack of consistency in the responses to the mitochondrial inhibitors, led to the decision to use the horizontal Langendorff preparation for intact tissue experimentation.

It was necessary to check that the coronary vessels were being effectively perfused in this preparation, as inadequate perfusion would result in the tissue becoming ischaemic as well as prevent the mitochondrial inhibitors being

delivered to the tissue. This was achieved by perfusing with the tracer dye 5(6)-carboxyfluorescein, which is easily washed into and out of the heart. Perfusion of the vessels is illustrated in Figure 5-5. Dye uptake by the tissue can be clearly seen in all 3 images, indicating that coronary perfusate was supplying deeper layers as well as surface tissue. The tissue surface is not completely flat, and the lower part of this image includes areas from above the surface of the tissue. This consists of dye in solution which has washed out of the heart and the lack of detail in this area distinguishes it from tissue images, where myocardial structure is visible.

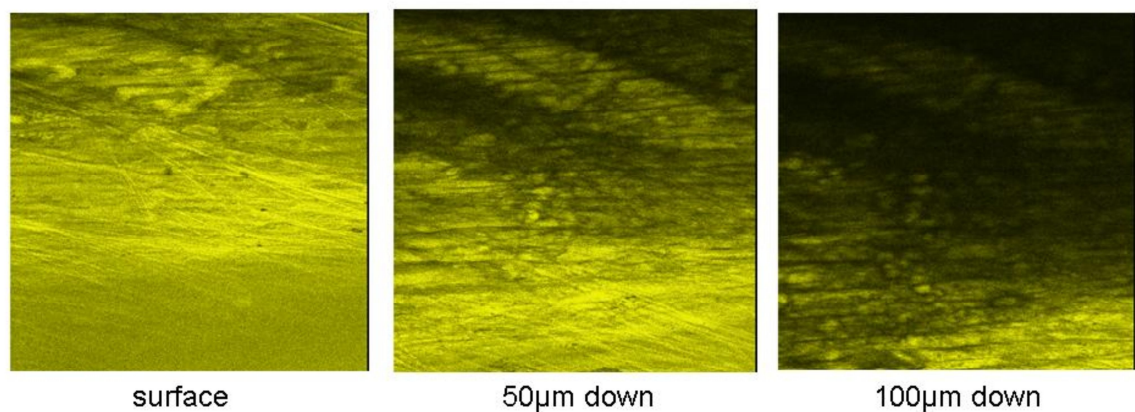


Figure 5-5 Perfusion of the coronary vessels imaged with 5(6)-carboxyfluorescein

Presence of the dye within the myocardium shows that the vessels are being perfused and the myocardial tissue is receiving an adequate supply of perfusate. Images were taken at the tissue surface and 50 and 100µm below the surface.

To investigate whether the mitochondrial inhibitors themselves had any effect on vascular tone, the vessels were perfused with 5(6)-carboxyfluorescein dye together with 4mM NaCN or 4µM FCCP. Any difference in the rate of tissue uptake and washout of the dye in the presence of the inhibitors would suggest an effect on vascular tone. Traces showing uptake and washout of the dye alone, and in the presence of FCCP and CN, are shown in Figure 5-6.

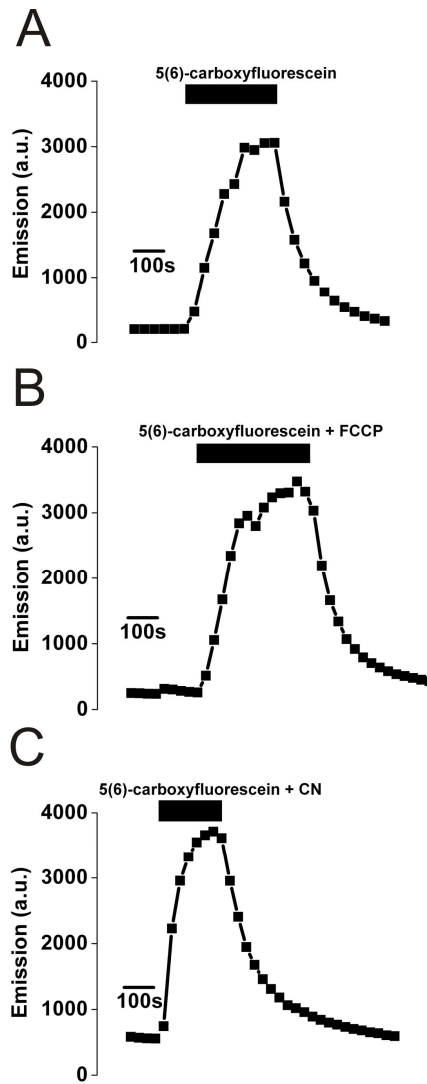


Figure 5-6 5(6)-Carboxyfluorescein uptake and washout in presence and absence of mitochondrial inhibitors

Panel A: Representative trace showing perfusion with 5(6)-carboxyfluorescein alone caused an increase in fluorescence as the dye was taken up by the tissue. When perfusion was stopped, the fluorescence signal decreased as the dye was washed out of the tissue. Similar dye uptake and washout profiles were produced when perfusion of the dye was combined with (B) 4 μ M FCCP and (C) 4mM CN. Black bars indicate period during which dye/dye + inhibitor perfusion took place. All traces show dye uptake and washout profiles in a single myocardial layer from the same heart.

The dye uptake and washout profiles in the presence and absence of the mitochondrial inhibitors were similar between the three conditions. This indicated that FCCP and CN did not cause constriction of the coronary vessels and therefore did not prevent flow to the tissue.

5.3.3 Mitochondrial inhibitor responses in the horizontal Langendorff preparation

Movement of the tissue was still a problem in the Langendorff-perfused preparation, making quantifiable measurements of the NADH response to the mitochondrial inhibitors difficult to interpret. In addition, no FCCP responses could be elicited in the tissue. The fluorescence changes that took place were associated with upward movement of the tissue, as the decrease in fluorescence in the myocardial layers corresponded to increasing fluorescence in Z-layers initially above the tissue surface, indicating a shift in the focal plane (Figure 5-7). However, a transient increase in fluorescence in response to CN occurred consistently in this preparation, and this response was slightly more sustained than in the wedge preparation (Figure 5-8). Once again, this response was only seen in the myocardial layers, not above the tissue, indicating that this was a true biological response to CN and not an optical artefact. In the same heart, control treatment (Tyrode's solution alone delivered by syringe driver) produced no change in fluorescence signal over and above the changes caused by tissue movement (Figure 5-9).

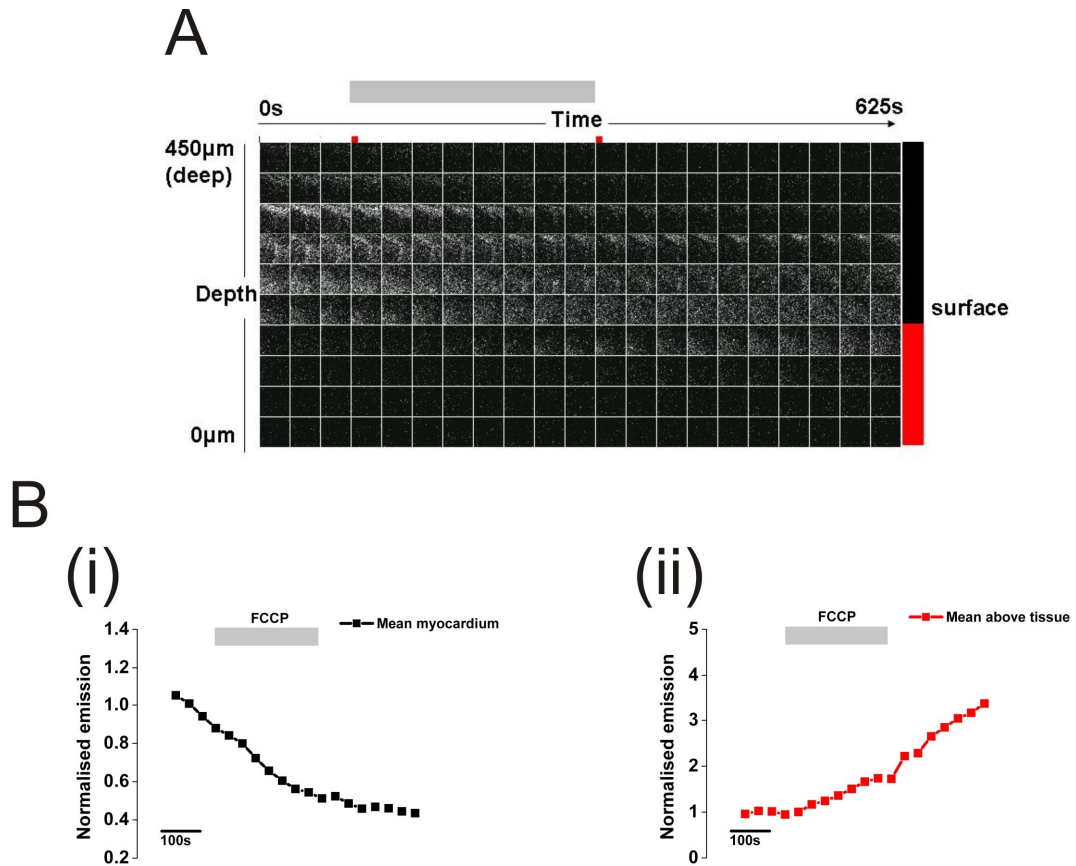


Figure 5-7 NADH fluorescence response to FCCP in the horizontal Langendorff preparation

Panel A shows changes in NADH fluorescence and the effect of $4\mu\text{M}$ FCCP over time at different tissue depths. The difference between each Z-layer is $50\mu\text{m}$. The grey bar indicates the time period during which FCCP was delivered. Black and red bars on right indicate images arising from myocardial tissue and above the surface of the tissue respectively (at the start of the experiment). B: The mean normalised fluorescence in all the myocardial layers was collated (i), demonstrating an overall decrease in fluorescence that corresponded to an increase in fluorescence seen in the collated mean normalised fluorescence from above the tissue surface (ii).

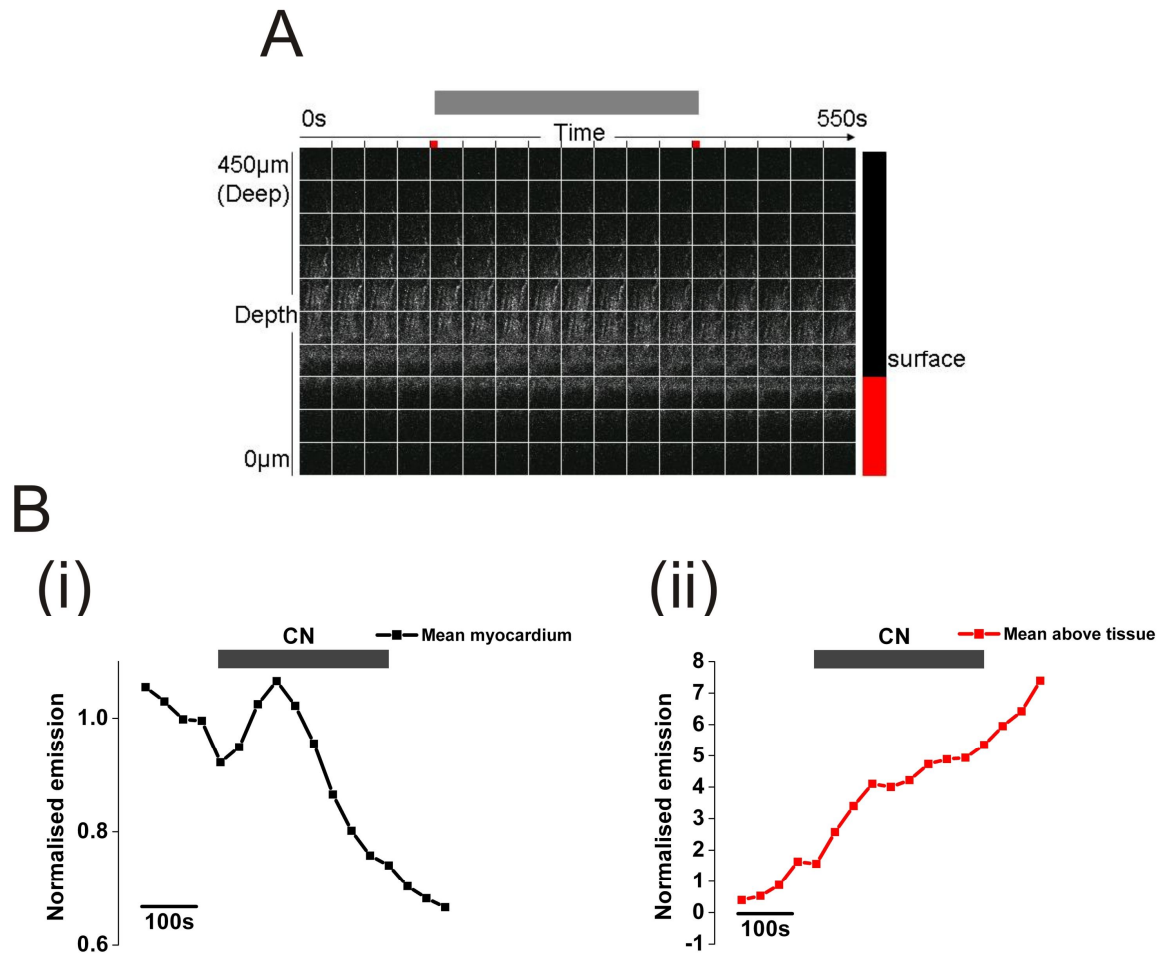


Figure 5-8 NADH fluorescence response to CN in the horizontal Langendorff preparation

Panel A shows changes in NADH fluorescence and the effect of 4mM CN over time at different tissue depths. The difference between each Z-layer is 50µm. The grey bar indicates the time period during which CN was delivered. Black and red bars on right indicate images arising from myocardial tissue and above the surface of the tissue respectively (at the start of the experiment). B: Collating the mean normalised fluorescence in all the myocardial layers (i) indicates a transient response to CN, not seen in the mean normalised fluorescence from layers above the tissue surface (ii).

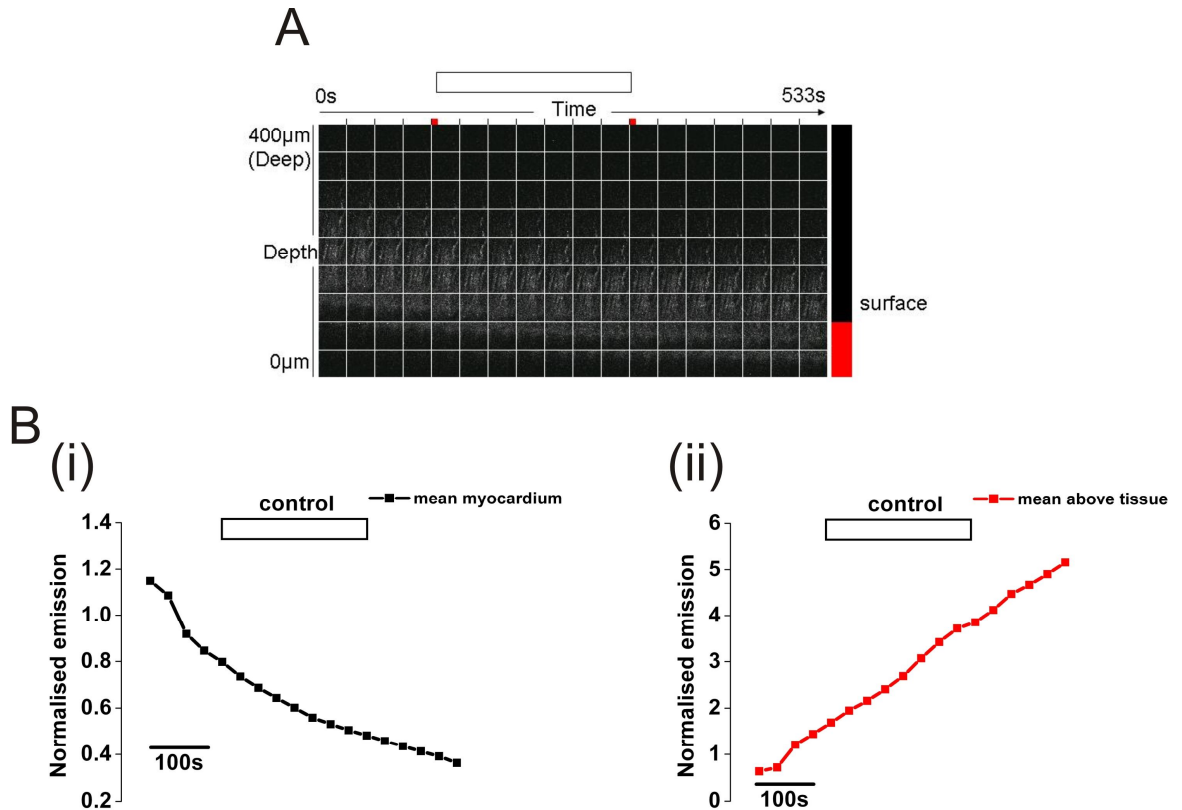


Figure 5-9 NADH fluorescence response to control in the horizontal Langendorff preparation
Panel A shows changes in NADH fluorescence and the effect of control infusion over time at different tissue depths. The difference between each Z-layer is 50µm. The white bar indicates the time period during which control solution was delivered by the syringe driver. The plane of focus is changing over time, suggesting upward movement of the preparation. Black and red bars on right represent images arising from myocardial tissue and above the surface of the tissue respectively (at the start of the experiment before movement has occurred). **B**: No additional change in fluorescence can be seen during control treatment in **(i)** the myocardial layers or **(ii)** above the surface of the tissue.

The decrease in fluorescence over time in the myocardial layers was associated with upward movement of the preparation causing the focal plane to shift to deeper layers of tissue, where light scattering is greater and fluorescence detection is subsequently reduced. In layers that were initially above the surface of the tissue, upward movement of the preparation caused the fluorescence signal to increase with time as myocardial tissue came into focus.

After correcting for the fluorescence changes associated with movement of the preparation, the mean normalised maximum fluorescence value obtained following CN treatment in 3 hearts was found to be 1.19 ± 0.03 .

5.3.4 Transmission of emission light through the tissue

The reason for the difference in the profile of response to CN in the intact tissue preparation compared to isolated cells was considered to be most likely due to inner filter effects that are associated with the use of thicker preparations.

Transmission of light through the ventricular tissue at wavelengths corresponding to NADH emission was therefore examined using LEDs inserted into the ventricular chamber. Two LEDs were used - a blue LED (peak emission at 450nm), the emission from which corresponded to the FAD excitation spectrum and a green LED (peak emission at 500nm), which did not correspond to the FAD excitation spectrum. The LEDs were orientated to emit light directly to the PMTs through the ventricular tissue. Measurements were made in both the RV and the LV. The effect of addition of 4mM CN solution on light transmission through the tissue at the two emission wavebands was assessed and compared to addition of control (Tyrode's) solution. The effects of CN on transmission of blue light through the LV and RV tissue are shown in Figure 5-10.

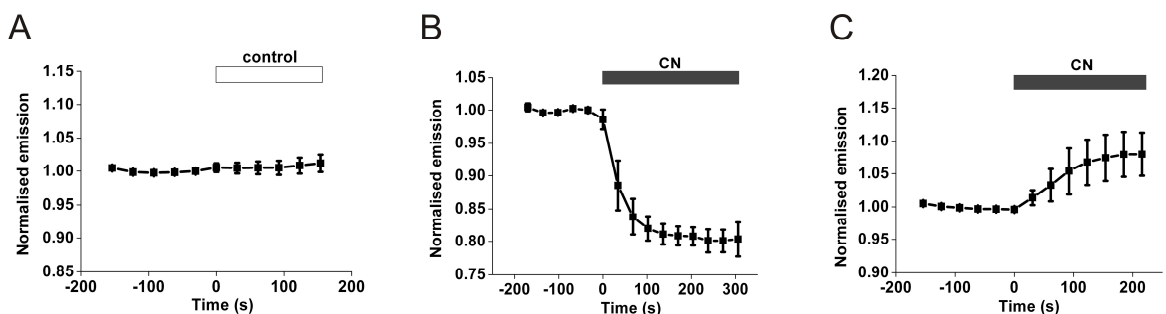


Figure 5-10 Mean effects of CN on transmission of blue emission light through LV and RV tissue

Panel A: Addition of control solution had no effect on transmission of blue LED light through the RV or LV tissue (n=5). **Panel B:** CN caused a decrease in blue light transmission through LV tissue (n=4), but in the majority of experiments caused an increase in transmission through RV tissue (panel C, n=4)

Blue light transmission through the LV tissue significantly decreased in response to CN treatment. This effect was not seen to be fully reversible in the timescale during which measurements were made (up to 15 minutes after CN removal, data not shown). In the majority of experiments, treatment with CN caused a small, reversible increase in transmission of blue light through the RV tissue. Figure 5-10C shows the mean response from these 4 experiments. However, on 2

occasions, a biphasic response was observed, in which both a decrease and increase in transmission of blue light occurred upon CN treatment (Figure 5-11).

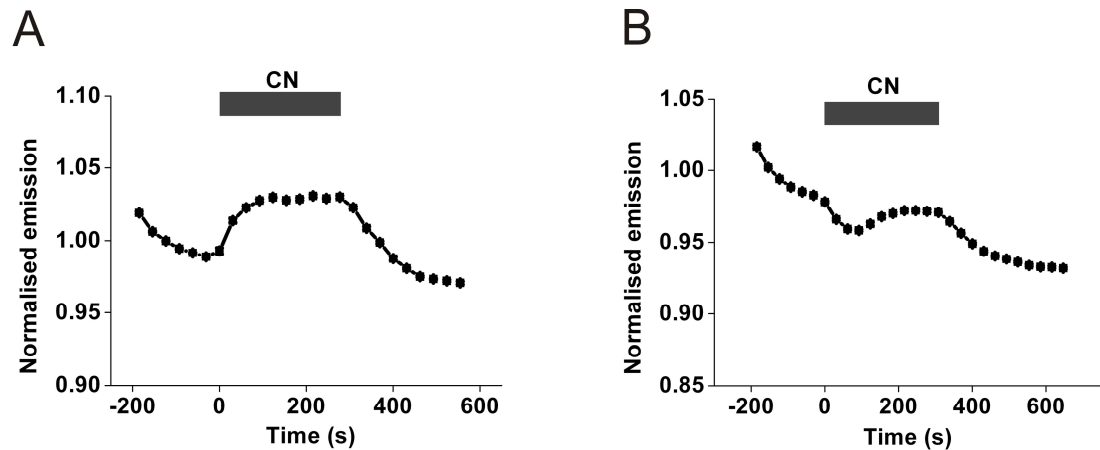


Figure 5-11 Alternative transmission responses to CN treatment in the RV

In the majority of experiments ($n=4$), a small increase in blue light transmission through the RV occurred in response to CN treatment. Panel A shows an example of such a response. However, in a small number of experiments ($n=2$), a biphasic response took place, where an initial decrease in transmission upon CN treatment was followed by an increase in transmission (Panel B).

No significant change in green light transmission was found in response to CN treatment in the RV or LV tissue (Figure 5-12).

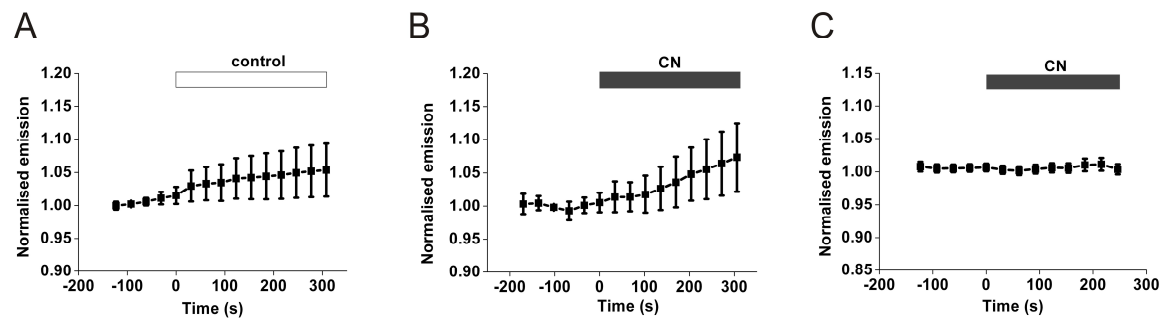


Figure 5-12 Mean effects of CN on transmission of green emission light through the left and right ventricular tissue

Addition of control solution to the RV and LV (panel A, $n=3$), CN to the LV (panel B, $n=2$) and CN to the RV (panel C, $n=5$) did not cause a significant change to green light transmission through the tissue.

5.3.5 FAD absorption properties

The absorption properties of FAD in the oxidised and reduced state were measured to assess if FAD absorption could have any influence on the NADH fluorescence changes in response to CN. The absorption spectra of 0.1mM FAD and FADH₂ (following addition of 1mM Na-dithionite) are shown in Figure 5-13.

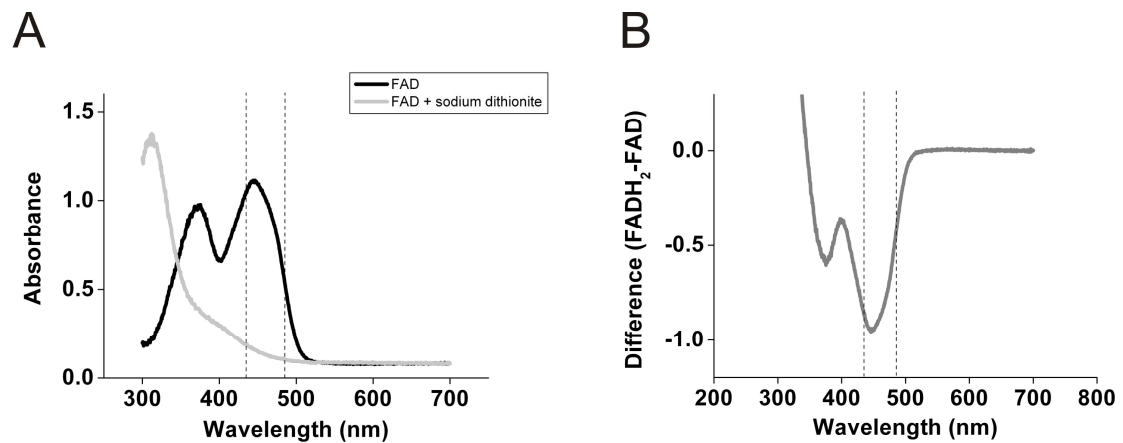


Figure 5-13 FAD absorption spectra in the oxidised and reduced state

Panel A: FAD absorption before (black line) and after addition of the reducing agent Na-dithionite (grey line). Dashed lines indicate wavelengths at which NADH fluorescence is measured. **Panel B:** Absorption difference between FAD in the reduced and oxidised states (FADH₂-FAD). At shorter wavelengths (below ~400nm), light absorption by Na-dithionite contaminates the trace. However at the wavelengths at which NADH fluorescence was collected, clear differences in absorption between FAD in the oxidised and reduced states can be seen with little contribution from Na-dithionite absorption.

The absorption peak of FAD is at 450nm. This coincides with the wavelengths at which NADH emits fluorescence, measured using a 435-485nm band pass emission filter. This means that NADH fluorescence is likely to be absorbed by FAD in the tissue before it is transmitted to the detector. When FAD is reduced to FADH₂, as would be the case following CN treatment, absorption at 435-485nm is virtually eliminated. Treatment with CN causes an increase in NADH fluorescence, but the simultaneous decrease in FADH₂ absorption would also lead to an increase in NADH fluorescence transmission and thus increased fluorescence detection. Therefore the anticipated change in NADH fluorescence following CN treatment is unclear.

5.3.6 Mb absorption spectra

The Mb absorption spectrum is known to shift depending on whether Mb is in the oxygenated or deoxygenated state. However, there are no reports of how infusion of CN in a whole heart preparation might affect Mb absorbance and subsequently complicate the interpretation of NADH fluorescence and thus measurements of metabolic state. There is some evidence to show that binding of CN modifies the absorption spectrum of Mb (Legako *et al.*, 2003; Bowen, 1949). In order to confirm this, the direct effect of 4mM CN on the absorption spectrum of 0.01mM Mb in a mock intracellular solution was examined (Figure 5-14).

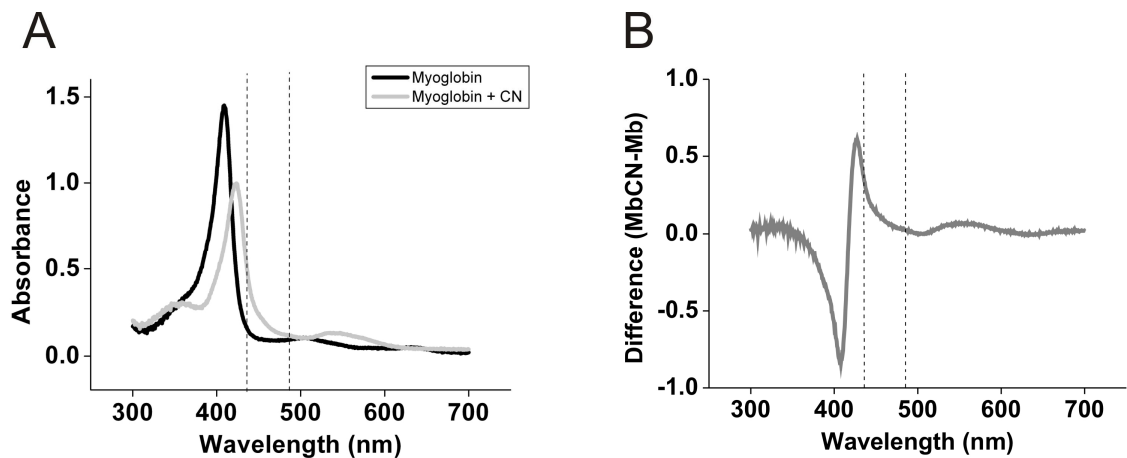


Figure 5-14 Mb absorption spectra in the presence and absence of CN

Panel A: Mb absorption before (black line) and after (grey line) addition of CN. Dashed lines indicate wavelengths at which NADH fluorescence is measured. Panel B: Absorption difference between Mb and Mb+CN (MbCN-Mb).

The absorption spectrum of Mb changes on addition of 4mM CN. At the wavelength range where NADH fluorescence is measured, absorption of Mb bound to CN is clearly greater than the absorption of Mb alone. Therefore treatment with CN will lead to increased Mb absorption at 435-485nm, decreased transmission of NADH fluorescence and subsequently decreased NADH fluorescence detection. Consequently, Mb absorption further complicates the interpretation of the NADH fluorescence response to CN in the intact tissue preparation.

5.4 Discussion

Values for mitochondrial redox state could not be established in the intact tissue preparations. The use of 2P-excitation methods, which were required for experiments in thick tissue sections, meant that only $\text{NAD}_{\text{state}}$ could be investigated. However, these measurements were more difficult to achieve in tissue than in isolated cells. This was due to changes in the focal plane associated with movement of the preparation, as well as inner filter effects complicating the interpretation of the fluorescence signal. Finally, with FCCP, there appeared to be additional difficulties with delivery of the inhibitor. It was therefore found to be unfeasible at this stage to image metabolic state within local regions of the myocardium.

5.4.1 Movement of the preparation

Movement of the tissue occurred in virtually every preparation and complicated the interpretation of the fluorescence signal. The movement was likely to be due to progressive oedema of the tissue, resulting in the focal plane shifting. This meant that the fluorescence signal was continuously decreasing in deeper Z-sections due to increasing light scattering as the focus moved deeper into the tissue. The fluorescence signal would simultaneously increase in the upper Z-sections as myocardial and epicardial tissue came into focus in Z-layers that were initially above the tissue surface.

We were unable to completely prevent this movement taking place, although in some preparations it was less pronounced than in others. The fluorescence changes occurring due to movement were taken into account when interpreting the effects of the mitochondrial inhibitors. Images from at least 50-100 μm above the surface of the tissue were included in the Z-stack to ensure that even if the tissue moved upwards, there was still a margin before the layers of tissue in focus moved above the limits of the Z-stack.

5.4.1.1 Viability of the preparation

In the early stages of developing the horizontal Langendorff preparation, a number of problems with the viability of the preparation were experienced. This

was likely to be due to the orientation and positioning of the heart occluding outflow from the vessels resulting in excessive oedema and progressive increases in pressure. To combat this, the moulded nest on which the heart was placed in the chamber was manipulated to provide support for the heart with minimal restriction to coronary outflow. Insertion of a vent in the apex of the LV also eased pressure increases.

5.4.2 Measurements in the LV wedge preparation

Blebbistatin was used as a movement uncoupler in the experiments performed in the LV wedge preparation. However, we were unaware at this point of the highly fluorescence properties of blebbistatin (Figure 5-1). The excitation spectrum of blebbistatin overlaps with the excitation spectrum of NADH, thus fluorescence emission from the tissue is likely to include both blebbistatin and NADH fluorescence. As the intrinsic fluorescence signal of NADH is relatively weak in comparison to blebbistatin fluorescence, the proportion of the signal arising from NADH was likely to have been small. Thus any changes in NADH fluorescence during treatment with FCCP and CN may have been too small to be detected.

In addition, a glass coverslip was attached to the Perspex slide and placed on the surface of the heart. This was in order to produce a flat imaging surface; however, as the tissue swelled, the coverslip may have applied excessive pressure on the tissue and could have compressed the surface coronary vessels. Consequently, solution flow through the vessels and delivery of inhibitor may have been restricted at the area of tissue being imaged.

On two occasions, apparent transient responses to CN were observed. The increase in NADH fluorescence that took place following application of CN was short-lived and recovery was almost immediate. These responses were not observed consistently in every preparation, and this may have been due to the influence of vessel compression due to the use of the coverslip. However, FCCP responses were not observed in any of the tissue preparations.

5.4.3 NADH responses to FCCP in intact tissue preparations

In contrast to single isolated ventricular cells, no NADH response to FCCP treatment could be elicited in the intact tissue preparation. A possible reason for this could be if FCCP was acting on the coronary vessels and inducing vasoconstriction, thereby restricting delivery of the inhibitor to the area of tissue being imaged. To investigate if this was the case, uptake of the tracer dye 5(6)-carboxyfluorescein was measured in the presence of 4 μ M FCCP (Figure 5-6B). It was found that FCCP did not prevent dye uptake, and was therefore not causing substantial vasoconstriction. However, FCCP is a lipophilic drug and is likely to be taken up by any cell it makes contact with. It may be that all the FCCP in the perfusing solution is being absorbed by the vascular tissue and the concentrations reaching the myocardial tissue could be too low to have any effect.

Attempts were made to inject a bolus of FCCP directly into the region of ventricular tissue being imaged. However, this approach was found to be unfeasible, as the needle had to be inserted as close to the imaging surface as possible and the pressure of the needle piercing the tissue distorted the image to the extent that fluorescence measurements could no longer be made.

Ultimately, we were unable to elicit FCCP responses and thus could not calculate mitochondrial redox state in the intact tissue preparations. Other groups have successfully introduced FCCP to intact tissue preparations (Brennan *et al.*, 2006; Zurbier *et al.*, 2003; Rouslin & Broge, 1996), although these were not confocal measurements, so targeted FCCP delivery to particular areas of tissue were not as critical in these contexts.

5.4.4 NADH responses to CN in intact tissue preparations

NADH responses to CN in the intact tissue preparations differed from those seen in isolated cells. In cells, treatment with CN leads to an increase in NADH fluorescence which is maintained until CN is washed out. In tissue preparations, CN treatment caused an increase in NADH fluorescence, but this response was only transient and the fluorescence signal returned to baseline whilst CN was still being perfused. A possible explanation for this could be that CN caused

constriction of the coronary vessels, restricting further flow of the inhibitor to the area of tissue being imaged. However, uptake of 5(6)-carboxyfluorescein dye by the tissue was not prevented in the presence of 4mM CN in the Langendorff perfused preparation (Figure 5.6C); hence CN was not inhibiting coronary flow.

It is possible that that the contribution of NADPH fluorescence to the NADH fluorescence signal may be influencing the observed fluorescence response. CN causes an increase in ROS (King *et al.*, 2003), which causes oxidation of NADPH to keep ROS levels in the cell low. This increase in ROS may be due to CN inhibition of catalase (which is involved in H₂O₂ clearance) (Kanthasamy *et al.*, 1997). However, the increase in ROS demonstrated by King *et al.* occurred mainly during CN washout. This would still not explain the transient effects of CN on NAD(P)H fluorescence as fluorescence fell while CN was still being perfused with no obvious changes in NAD(P)H fluorescence during washout.

Another possibility was that the altered CN response may have been due to the influence of the inner filter effects in the thick tissue preparation. The absorption properties of myocardial tissue were therefore studied and any effect of CN on these properties was investigated.

5.4.5 Examining the influence of inner filter effects on NADH fluorescence measurements

Tissue inner filter effects were examined by inserting LEDs into the left and right ventricles and any change in light transmission through the tissue to the PMT detectors was assessed. The most likely cellular components to affect NADH fluorescence measurements due to inner filter absorbance is Mb (Fralix *et al.*, 1990; Tamura *et al.*, 1978). This is due to the high concentration of Mb present in the heart and the overlap of Mb absorption bands and NADH emission wavelengths. The absorption properties of Mb and the effect of CN on Mb absorbance were investigated using purified Mb from equine heart and it was found that CN caused shifts in the Mb absorption spectrum (Figure 5-14).

5.4.5.1 Mb transmission properties

The shift in the Mb absorption spectrum in the presence of CN suggests that Mb absorption would interfere with any measurements of NADH redox state.

However, the relationship between light absorption and transmission is non-linear. Therefore, in order to understand the responses to LED emission light transmission through the tissue, the absorption properties of Mb expressed in terms of light transmission needed to be examined. The transmission profile of 0.01mM Mb and the effect of 4mM CN on transmission are shown together with the emission profiles of the LEDs (Figure 5-15).

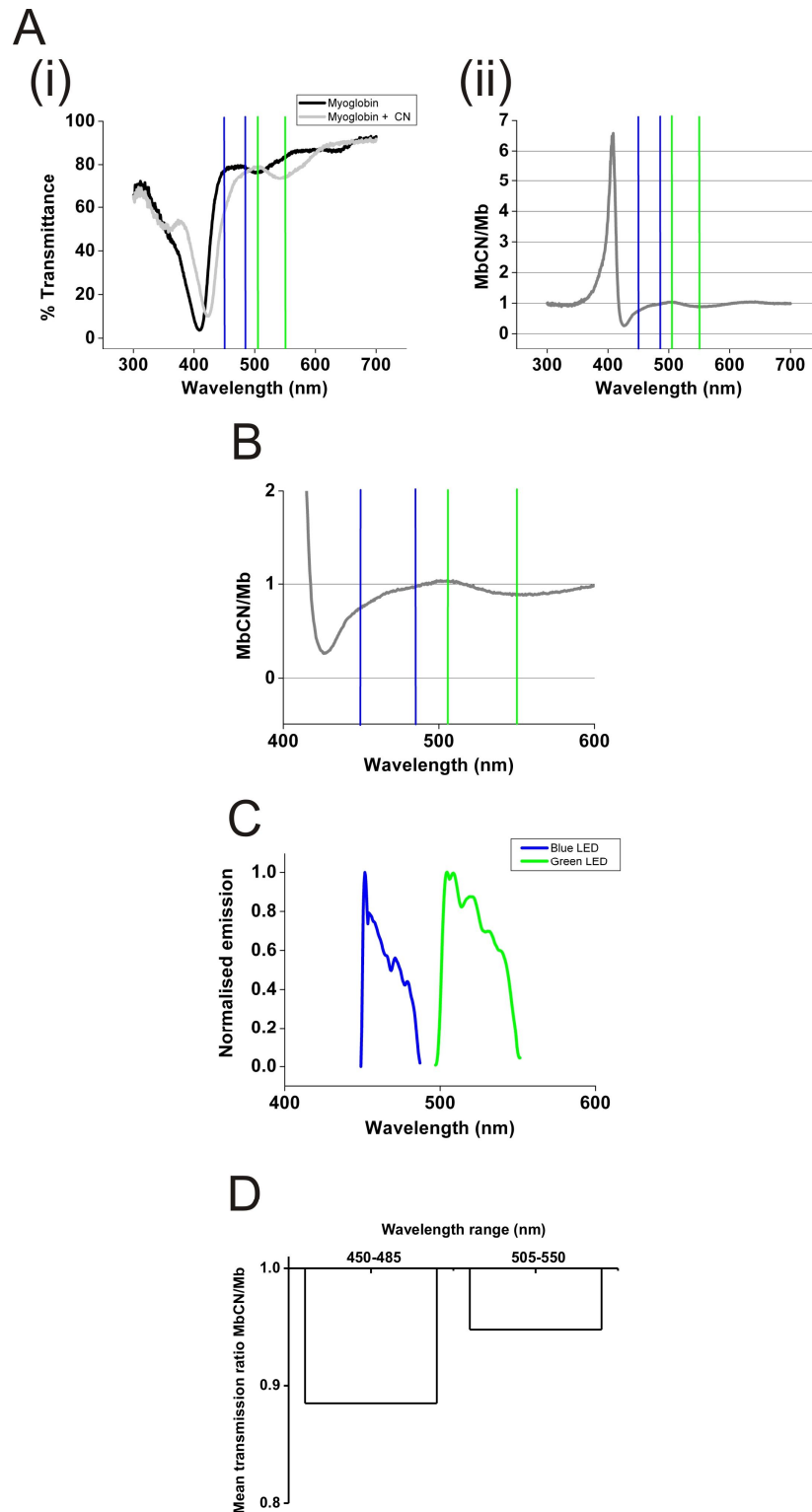


Figure 5-15 Transmission profile of Mb compared with LED emission profiles

Panel A: (i) Transmittance of 0.01mM Mb expressed in terms of % light transmittance before (black line) and after (grey line) addition of 4mM CN. (ii) Transmission ratio between Mb and Mb+CN (MbCN/Mb). **Panel B:** Transmission ratio enlarged between wavelength range of 400-600nm. Blue lines indicate wavelength range where blue LED light is detected using a 435-485nm band pass filter and green lines indicate range where green LED light is detected using a 505nm long pass filter. **Panel C:** Normalised emission profiles of blue (blue line) and green (green line) LEDs on the same x-axis scale over the same wavelength range. **Panel D:** Comparison of mean transmission ratio (MbCN/Mb) at the wavelength ranges where blue and green LED emission light is detected.

In the LV tissue, transmission of blue light decreases upon perfusion with CN (Figure 5-10B). This is most likely due to increased absorption of light at these wavelengths by Mb when bound to CN, leading to decreased light transmission through the tissue to the detector. However, in the LV, no significant change in green light transmission is seen following treatment with CN (Figure 5-12B), despite differences in the transmission profiles of Mb in the presence and absence of CN in the green spectral region. There are likely to be two reasons for this. Firstly, mean transmission ratio in the presence and absence of CN is greater over the wavelength range that blue LED light is detected compared to the range at which green LED light is detected (Figure 5-15D). Secondly, the greatest difference in transmission over the blue spectral region occurs where blue LED emission is at its highest (at shorter wavelengths, closer to 450nm); but over the green spectral region, occurs where green LED emission is at its lowest (at longer wavelengths, closer to 550nm). Consequently, the difference in transmission of Mb (before and after CN) over the green LED spectral range is most probably too small to be detected as a change in transmission of light through the LV tissue.

It should be acknowledged that the measurements of Mb absorption were made in purified Mb extracts. It is not clear whether any shifts in the absorption spectrum of Mb occur within the tissue where interactions with other cellular components may take place. It is known that the Mb spectrum shifts depending on whether it is in the oxygenated or deoxygenated state, so the absorption effects of CN binding to Mb when the tissue is in different oxygenation states will be even more complicated, but remains to be investigated.

5.4.5.2 Sources contributing to inner filter effects arising from the mitochondria

The major absorption peak of FAD coincides with the emission peak of NADH. Reduction of FAD to FADH₂ almost completely eliminates light absorption (Figure 5-13, the increase in absorbance in the UV region is due to Na-dithionite absorbance). Thus FAD is likely to be influencing tissue transmittance of NADH fluorescence and subsequently fluorescence detection. In contrast to Mb, FAD absorbs less light in the presence of CN, and tissue transmittance is increased. This may explain the trend seen in the RV in which detection of blue LED

emission increased during CN treatment (Figure 5-10C). This small increase in transmission was generally reversible upon CN removal, as shown in Figure 5-11A, which concurs with the reversible FAD response to CN observed in the isolated cells. Similar changes in green LED transmission were not observed because FAD does not absorb light at the green LED emission waveband. In two experiments, a biphasic transmission response to CN was observed in the RV (Figure 5-11B), where transmission initially decreased and then increased. This may be a result of opposing effects of changes in Mb and FAD concentrations on tissue absorbance.

The cytochromes of the electron transport chain also have absorption properties (Chance, 1954; Dixon *et al.*, 1931), and they may also contribute to the inner filter effects of the tissue. However, at the wavelength at which NADH is measured, this contribution is likely to be much less than that of Mb (Tamura *et al.*, 1978).

5.4.5.3 Influence of light scattering

When light propagates through biological tissue, interaction with cellular structures with different refractive indexes causes the direction of the light path to change. This results in scattering of light. The cellular components which contribute most to these local variations in refractive index are thought to be the nuclei, cytoplasmic organelles (such as the mitochondria) and connective tissue fibres (Schmitt & Kumar, 1998; Wilson & Jacques, 1990). However, the optical changes that affect tissue transmittance when CN is perfused are most likely to be mainly due to changes in tissue absorbance and not light scattering. If CN was causing a major increase in light scattering in the thicker LV tissue, resulting in decreased detection of blue light, similar changes would be expected with green light and this was not the case. Light scattering is wavelength dependent and is more prominent at shorter wavelengths. However, the emission wavebands of the two LEDs are close together on the spectrum (~450-490nm and ~500-550nm), so any great change in light scattering at one waveband would be expected to be seen, at least in part, at the other.

Nevertheless, light scattering is a complex phenomenon, and it cannot be ruled out that it plays some role in the differences in transmittance that occur upon

CN perfusion. This would be particularly important if CN causes changes in the structure/size of the mitochondria or other cellular components. There is some evidence to suggest that this is indeed the case and anoxia, as well as mitochondrial inhibition with CN, causes the mitochondrial matrix to shrink (Fujii *et al.*, 2004).

5.4.5.4 Overall effect on transmission of NADH specific wavelengths

The Beer-Lambert law states that absorption is proportional to the concentration of absorbing species and the light path length. Thus the differences in LED light transmission observed in the RV and LV may be due to varying concentrations of Mb, FAD and other absorbing species in the two tissue types, or may be influenced by the difference in tissue thickness.

The net effect of CN on transmission of blue light (corresponding to NADH emission wavelengths) is likely to be due to the combination of absorbance by Mb, FAD and the cytochromes. The differing transmission effects seen in LV and RV tissue suggest that different absorbing species predominate in each tissue type. In the LV, the decrease in transmittance following CN treatment implies that Mb absorbance effects predominate, as CN was shown to cause an increase in Mb absorbance, hence reducing transmission of light through the tissue. Indeed higher concentrations of Mb have been reported in the LV compared to the RV of rat hearts (Frolkis, 1967) and other mammals (Alexander, 1975) due to the higher workloads and subsequently greater O₂ demands in the LV. Using the Beer-Lambert law, the effect of this difference in [Mb] on Mb absorption (and hence transmission of light through the tissue) is illustrated in Figure 5-16. The molar extinction coefficient value for Mb of $12000\text{M}^{-1}\text{cm}^{-1}$ was obtained from Bowen (1949). The LV [Mb] of $300\mu\text{M}$ was used (Wittenberg & Wittenberg, 2003) and the RV [Mb] of $180\mu\text{M}$ was used to reflect that Mb concentrations have been measured to be ~40% less in RV compared to LV (Frolkis, 1967).

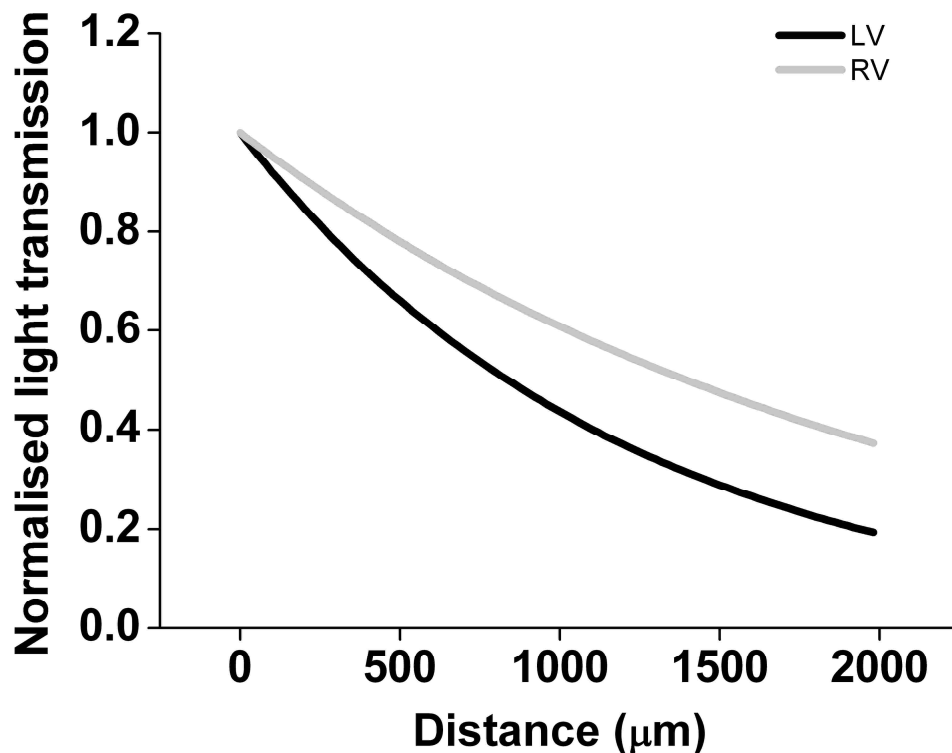


Figure 5-16 Effect of Mb absorption in the LV and RV on light transmission through the tissue

Absorption of light by Mb results in a decrease in the amount of light that is transmitted through the tissue (maximum light transmission was normalised to 1). As the light path distance increases, more light is absorbed by Mb and thus less light is transmitted. Absorption of light through the LV (black trace) is greater than in the RV (grey trace) due to the higher concentration of Mb in the LV. Hence transmission is less at a given light path distance in the LV compared to the RV.

In contrast, CN caused a small increase in tissue transmittance in the RV, suggesting a slight reduction in inner filter effects. This would indicate that FAD absorbance predominates in the RV, as CN treatment causes FAD to be reduced to FADH₂, effectively eliminating absorption by FAD.

5.4.6 Effects of absorption on NADH fluorescence changes in response to CN

All experiments examining the effects of CN on NADH fluorescence were performed in the LV, thus only the effect of CN on tissue transmission in the LV needed to be taken into account. The decrease in transmission of light at wavelengths corresponding to NADH emission following perfusion with CN is likely to mean that the increase in NADH fluorescence in response to CN will be

underestimated in the tissue preparation. CN caused a mean increase in NADH fluorescence of ~19%, but transmission was reduced by ~19% on average. The interactions that occur within the tissue in terms of the inner filter effects and light scattering events at different tissue depths are complicated and difficult to predict. However, using these values, the true increase in NADH fluorescence following CN treatment will be ~38%. Converted to a mean normalised fluorescence of 1.38, this value is similar to the mean normalised fluorescence value of 1.41, which was obtained in isolated cells following CN treatment measured by 2P excitation fluorescence microscopy.

It was hoped that the effects of CN on light transmission through the tissue may be able to explain the transient NADH response to CN observed in the tissue. However the rapid timescale of changes in light transmission appear to be too fast to explain the decrease in NADH fluorescence, which occurs 90-150s after CN perfusion is started. However, as the relationship between light transmission and absorption is non-linear, the time course of changes in absorption will be different to transmission, and it is unclear how this will affect the NADH fluorescence response.

5.4.7 Conclusions

We were unable to obtain measurements of mitochondrial redox state in intact tissue preparations to allow comparison with isolated cells or within local regions of the myocardium. The main reason for this was that no NADH fluorescence response to FCCP could be elicited, and a minimum NADH fluorescence value could not be established. In addition, the responses to CN were influenced by the inner filter effects of the tissue, complicating the interpretation of maximum NADH fluorescence. Measurements of redox state in isolated cells are not complicated by the inner filter effect because the light path distance through the isolated cell is comparatively much smaller (~10 μ m). As shown in Figure 5-17B, Mb absorption causes a negligible decrease in light transmission at depths relevant to isolated cells.

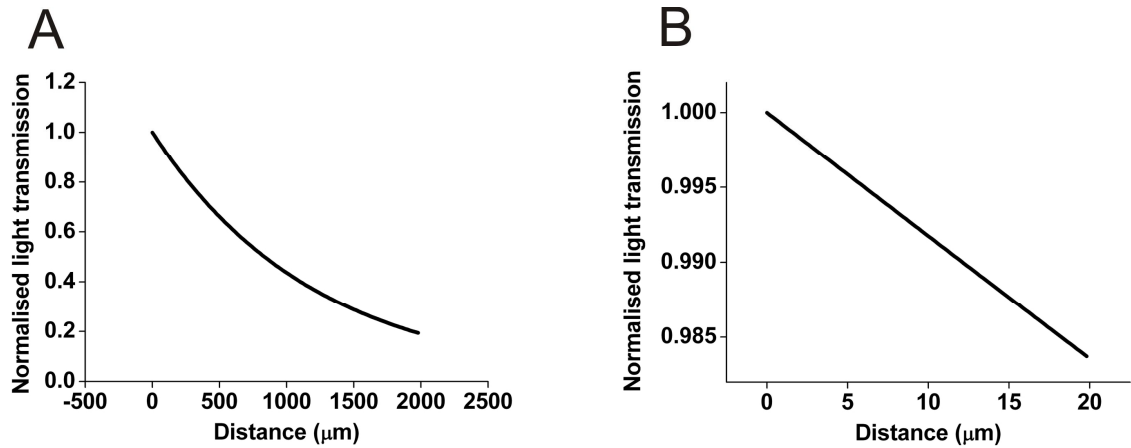


Figure 5-17 Effect of Mb absorption on light transmission at distances relevant to tissue and isolated cell measurements

Effect of Mb absorption on transmission of light through light path distances relevant to (A) tissue measurements and (B) cell measurements. Maximum light transmission was normalised to 1 with no transmission equivalent to 0.

However, if the effects of CN on light transmission through the tissue are taken into account, the value obtained for mean maximum normalised NADH fluorescence by 2P excitation fluorescence microscopy in the horizontal Langendorff preparation (~ 1.38) is similar to the value obtained in isolated cells (1.41).

6 Mitochondrial redox response to increased work intensity in rabbit ventricular myocytes

6.1 Introduction

The heart is a highly metabolic organ and the process of E-C coupling requires a constant supply of ATP to power contractile shortening and ion pumps. ATP stores within the cardiac myocyte are relatively small, and only sufficient to provide energy for a few beats (Ingwall, 2009; Stanley *et al.*, 2005). Any increase in myocardial energy demand due to increased force or frequency of contraction will therefore require an increase in ATP production to fulfil this demand. ATP production by oxidative phosphorylation requires a continuous supply of reducing equivalents in order to proceed. If the rate of ATP production is increased, a concomitant increase in the rate of the TCA cycle is needed to maintain this supply. By measuring changes in oxidative status simultaneously with changes in work intensity (by altering the stimulation frequency), energy flux and the cell's ability to match energy supply with demand can be assessed.

Previous studies, using measurements of NADH fluorescence alone, have found a variety of responses in cardiac cells and tissue to changes in work intensity. Some studies have reported no change in oxidative status (Griffiths *et al.*, 1998; Heineman & Balaban, 1993). Others report oxidation of the cellular environment (Ashruf *et al.*, 1995; Chapman, 1972; Heinzel *et al.*, 2006; White & Wittenberg, 1993; White & Wittenberg, 2000), whereas others still report an increase in NADH fluorescence in response to increased work intensity (Griffiths *et al.*, 1997; Katz *et al.*, 1987). In a series of experiments, Brandes *et al.* demonstrated an initial decrease in NADH fluorescence in rat cardiac trabeculae in response to an increase in stimulation frequency, followed by a mitochondrial Ca^{2+} dependent increase in fluorescence (though not to control levels) during rapid pacing (Brandes & Bers, 1996; Brandes & Bers, 1997; Brandes *et al.*, 1998; Brandes & Bers, 1999; Brandes & Bers, 2002). These findings were supported in later work performed on guinea pig ventricular myocytes (Jo *et al.*, 2006).

The reason for this lack of consistency in responses is unclear. It is unlikely to be due to species difference, as all four responses have been reported in the rat. One possibility is that it is due to differences in the preparations used, as factors such as O_2 and substrate supply could influence the metabolic response, particularly in tissue preparations.

6.1.1 Advantages of simultaneously measuring NADH and FAD fluorescence

All of the studies mentioned above used NADH fluorescence measurements alone to assess mitochondrial redox state responses to changes in work intensity. The major advantage of our approach is that the NADH and FAD fluorescence signals respond oppositely to oxidation and reduction of the cellular environment. When a ratio of the two fluorescence signals is taken, true biological responses can be distinguished from signal noise and movement artefacts.

6.1.2 PCr as an energy buffer

In addition to a small amount of ATP, the cell also possesses PCr stores. PCr acts as an energy buffer during acute changes in energy demand. It can be rapidly broken down to produce ATP by the following reaction:



Phosphate is transferred from PCr to ADP, forming Cr and ATP. This is a reversible reaction catalysed by CK. PCr is formed when ATP levels are high and these stores are sufficient to power around 15 beats (Levick, 2003).

6.1.3 Aim of the chapter

The main aim of this chapter was to assess the mitochondrial redox response to increased work intensity in isolated rabbit ventricular myocytes. From this, the cell's ability to match metabolite supply with demand could be determined.

6.2 Methods

All experiments were performed on single rabbit ventricular myocytes isolated from the heart using the enzymatic digestion process described in Section 2.2.1. Following the isolation procedure, the cells were suspended in Krebs solution containing 1mM CaCl₂.

6.2.1 Stimulation protocol for metabolic challenge

Cellular contraction was induced by electrical field stimulation. A thin layer of cells was placed in the bath and allowed to settle on the coverslip. The cells were then perfused with Krebs solution containing 1.8mM CaCl₂ using the apparatus described in Figure 2-7. Inflow was through a hole in the side of the aluminium bath, which was heated to ensure the temperature of extracellular solution in the bath was ~37 °C. A stimulator generated square wave electrical impulses of 10ms duration which were delivered to the cells through two narrow platinum electrodes attached to parallel sides of the bath. Cells were stimulated at suprathreshold current intensities (threshold + ~5%). A digitimer connected to the stimulator set the frequency of stimulus impulses.

Cells were deemed suitable for imaging if they had intact membranes, clear striations, free edges (no overlapping cells) and if they contracted consistently upon stimulus. The selected cell was imaged using a CCD camera with edge detection software (IonOptix Limited), allowing cell shortening measurements to be made. Simultaneous epifluorescence measurements of NADH and FAD were made using the optical settings described in Section 2.6.3.

The cells were initially stimulated at 0.5Hz for around 100s. The frequency of stimulation was then increased to 1Hz for ~50s or until fractional shortening and fluorescence levels were judged to have reached a steady state. Pacing frequency was returned to 0.5Hz to allow the cell to recover, before delivering another burst of 1Hz stimulation for ~50s. This burst pacing was repeated at 2Hz and 3Hz (Figure 2-11), each burst interspersed with 0.5Hz pacing. These abrupt increases in stimulation frequency constitute rapid increases in work intensity and thus increased metabolic demand. The oxidative response to these changes demonstrates how well the cell can increase metabolite supply in response to an increase in demand.

The NADH and FAD fluorescence signals were calibrated at the end of the pacing protocol by perfusing with 2µM FCCP to induce complete oxidation and 2mM CN to induce complete reduction of the mitochondrial environment.

6.2.2 Analysis of rate of oxidative change and work performed by the cell

The rate of oxidative change within the cell upon transitions in workload, expressed as the NADH/FAD ratio, was analysed using a program written in house (LabTalk, Origin 6.1). The rate of change in the NADH/FAD fluorescence ratio at 2Hz and 3Hz stimulation, and the rate of recovery when stimulation rate was decreased back to 0.5Hz was analysed by interpolating the time points at which 10%, 50% and 90% fluorescence change took place, as well as the time at which the new level of work was initiated and terminated. In addition, the mean cell length was taken at these time points as an index of contractile work performed by the cell. Relative work performed by the cell was expressed as the inverse of mean cell length. Contraction of the cell causes a decrease in cell length; hence shorter mean cell length would indicate more time spent in the contractile state, and consequently more work performed.

6.2.3 Verifying the mitochondrial origin of the intrinsic fluorescence response

In order to confirm that the fluorescence changes observed during changes in metabolic demand were mitochondrial in origin, the cells were metabolically challenged in the presence of mitochondrial inhibitors. Initially, the cells were perfused with Krebs solution and a metabolic challenge (2 bursts of 3Hz pacing) was delivered in this control state. Between each burst of fast pacing, cells were stimulated at 0.5Hz. Cells were then perfused with 2mM CN to induce a completely reduced mitochondrial state, during which they were subjected to the same metabolic challenge. CN was washed out and the cells were allowed to recover. Following recovery, a completely oxidised mitochondrial state was induced in the cells by perfusion with 2 μ M FCCP and the metabolic challenge was again delivered in this state (Figure 6-1). Throughout this protocol, NADH and FAD fluorescence emissions were recorded as previously described.

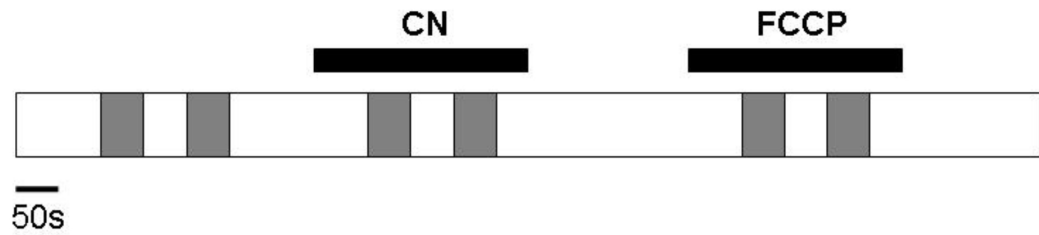


Figure 6-1 Pacing protocol to establish mitochondrial origin of intrinsic fluorescence response to increased work intensity

The cells were metabolically challenged by delivering bursts of 3Hz pacing (represented by grey boxes) in the presence of CN and FCCP. Each burst of fast pacing was interspersed with 0.5Hz stimulation (white boxes). In the absence of mitochondrial inhibitor, cells were perfused with control Krebs solution.

6.2.4 Verifying contractile work to be the source of metabolic demand

In order to confirm that the increased metabolic demand was induced by contractile work, metabolic challenges (during which pacing was step increased to 3Hz) were performed in the presence and absence of the movement uncoupler cytochalasin D (cyto D) (Figure 6-2). Cyto D inhibits contraction by impairing actin filament polymerisation (Kettlewell *et al.*, 2004). Cyto D was used at a concentration of 20 μ M, which was sufficient to reduce fractional shortening to ~2% at 3Hz stimulation. Complete inhibition of contraction was not induced because the residual contractile function was a useful indicator that the cells were still electrically active and responding to stimulus impulse.

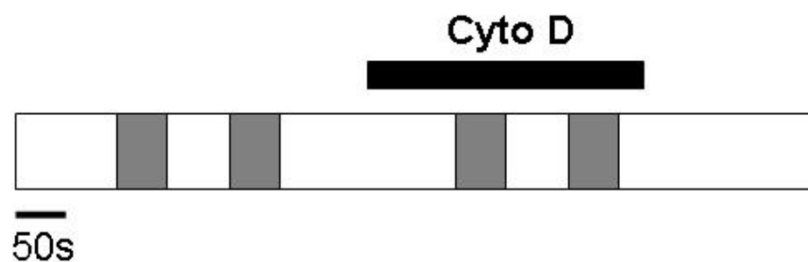


Figure 6-2 Pacing protocol to establish contractile work as source of metabolic demand

The cells were given 2 burst of 3Hz pacing (grey boxes) under control conditions and then during inhibition of contraction with cyto D. At low work intensities, pacing was reduced to 0.5Hz (white boxes). Changes in intrinsic fluorescence were recorded throughout.

6.2.5 Assessing possible role of PCr in energy supply and demand matching

The role of PCr in energy buffering during increases in work intensity was also investigated. CK catalyses the reversible transfer of a high-energy phosphate moiety between creatine and ADP. Inhibition of CK thus prevents PCr functioning as an energy store. The oxidative response of the cells to increased work intensity in the absence of PCr stores was assessed using two inhibitors of CK - iodoacetamide and cyclocreatine. Iodoacetamide is an alkylating reagent for histidine and cysteine residues. Inhibition by iodoacetamide is irreversible and not specific to CK. It also inhibits the glycolytic enzyme glyceraldehyde-3-phosphate dehydrogenase, although even when glyceraldehyde-3-phosphate dehydrogenase was significantly inhibited, it has been shown that glycolysis continues to proceed at the same rate (Tian *et al.*, 1997). In contrast, cyclocreatine acts as a competitive inhibitor. It is an efficient substrate for CK and is phosphorylated to generate cyclocreatine phosphate. Cyclocreatine phosphate is turned-over 160 fold less efficiently than PCr and thus leads to reduced ATP generation by the PCr-Cr system (Teicher *et al.*, 1995).

Iodoacetamide was used at a concentration of 0.4mM, which has been shown to reduce CK activity to 3% of control values (Harrison *et al.*, 1999). Initially, the cell was perfused with control solution and the metabolic challenge of step increasing stimulation frequency from 0.5Hz to 3Hz for 2-3 bursts was delivered. The cell was then perfused with iodoacetamide for 10min and the protocol was repeated in the presence of the inhibitor. The same procedure was carried out using 10mM cyclocreatine instead of iodoacetamide. However, the period of time required for cyclocreatine to have its full effect was not known, so some cells were also incubated for 1-2 hours with 10mM cyclocreatine prior to the metabolic challenge being performed.

6.3 Results

6.3.1 Intrinsic fluorescence response to metabolic challenge

A typical response to the metabolic challenge protocol in a single left ventricular cardiomyocyte is shown in Figure 6-3.

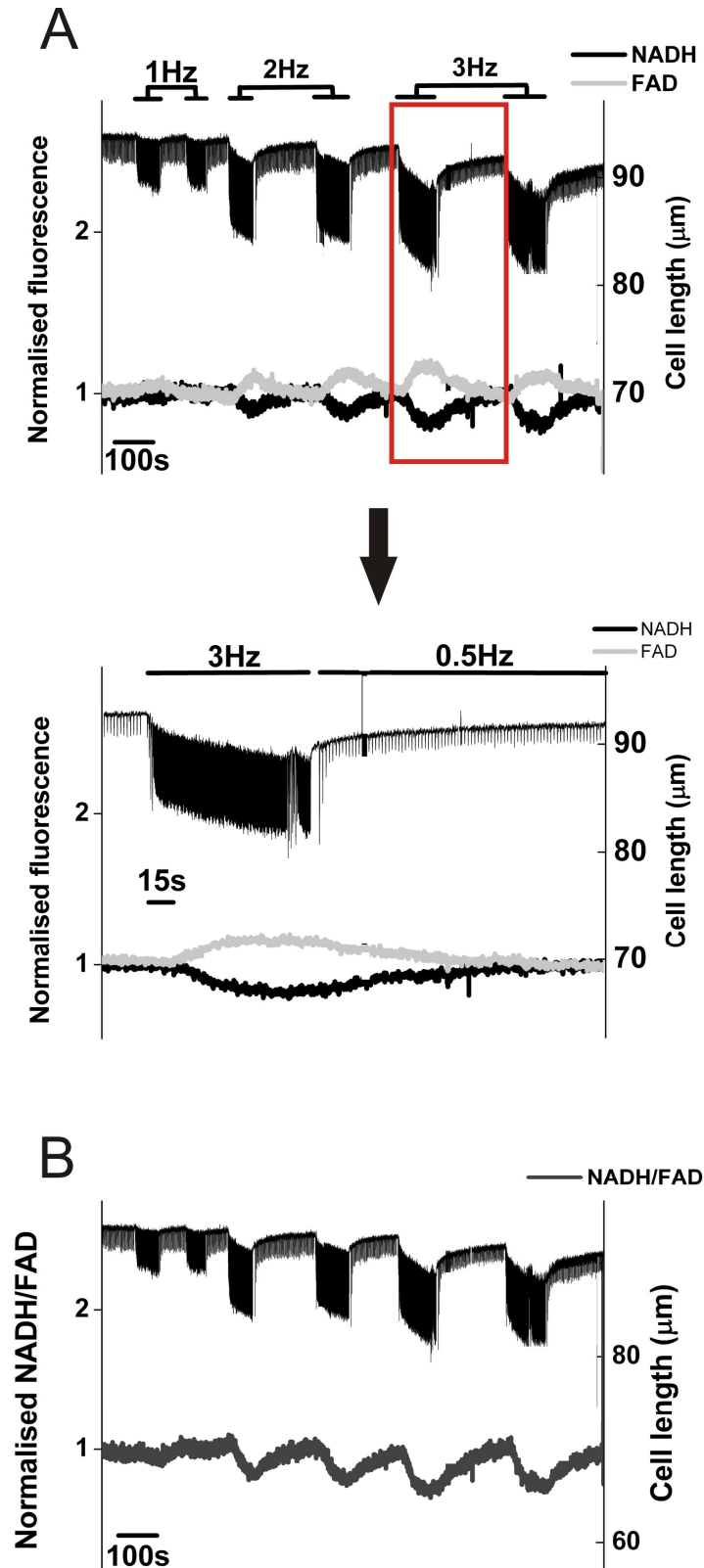


Figure 6-3 Representative trace showing effects of metabolic challenge on intrinsic fluorescence

A: Effect of changing stimulation frequency on fractional shortening (upper trace, black), NADH fluorescence (lower trace, black) and FAD fluorescence (lower trace, light grey). Red box indicates region of trace which has been magnified to show the effect of step increasing work intensity to 3Hz in more detail. **B:** NADH fluorescence signal divided by the FAD fluorescence signal to give NADH/FAD ratio (dark grey trace).

Increasing stimulation frequency also causes an increase in fractional shortening due to the positive force-frequency relationship (Bowditch effect) that occurs in rabbit cardiac myocytes. Thus metabolic demand will be enhanced due to the increased force and frequency of contractions. As the stimulation frequency is increased from 0.5Hz to 2Hz and 0.5Hz to 3Hz, NADH fluorescence clearly decreases and FAD fluorescence simultaneously increases, represented by a decrease in the NADH/FAD ratio. This indicates oxidation of the cell environment and suggests energy supply is not matching demand upon transitions in workload. When stimulation frequency is slowed back to 0.5Hz, NADH and FAD fluorescence returns to baseline levels, demonstrating recovery of the oxidative status of the cell. The mean changes in NADH, FAD and NADH/FAD fluorescence levels at each stimulation frequency are shown in Figure 6-4.

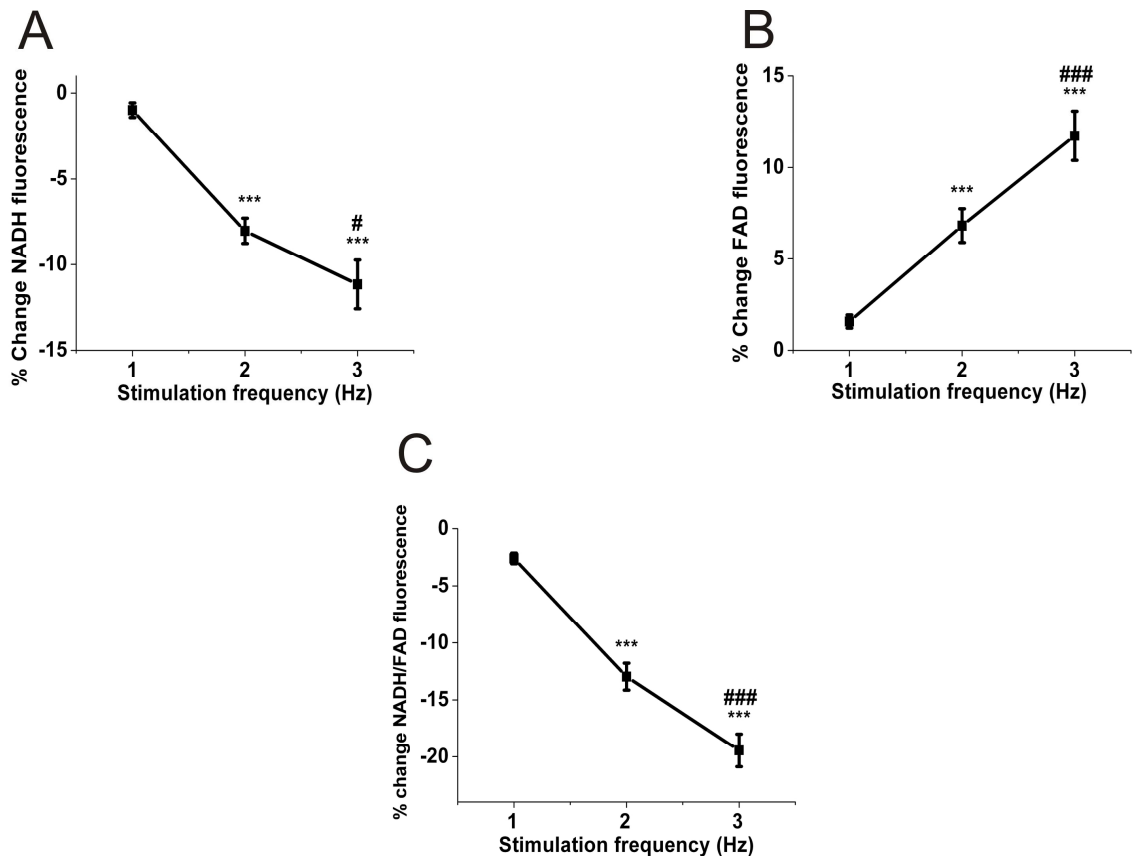


Figure 6-4 Mean effect of step increasing stimulation frequency on intrinsic fluorescence levels

Mean % change in (A) NADH fluorescence (B) FAD fluorescence and (C) NADH/FAD fluorescence ratio upon increasing stimulation frequency from 0.5Hz to 1Hz, 2Hz and 3Hz (n=22). ***p<0.001 versus 1Hz. # p<0.05 versus 2Hz, ### p<0.001 versus 2Hz.

6.3.2 Relationship between work and mitochondrial oxidative response

The time taken to reach 10%, 50%, 90% and 100% fluorescence change (in terms of the NADH/FAD fluorescence ratio) was established following step increase and decrease in workload. The values obtained at 2Hz and 3Hz stimulation were compared to assess if the greater metabolic demand expected at 3Hz stimulation had any effect on the rate of oxidative response. The rate of recovery was also analysed following step down to 0.5Hz stimulation from 2Hz and 3Hz stimulation. The relative and normalised fluorescence change over time at 2Hz and 3Hz stimulation, as well as the relative and normalised work performed, are shown in Figure 6-5.

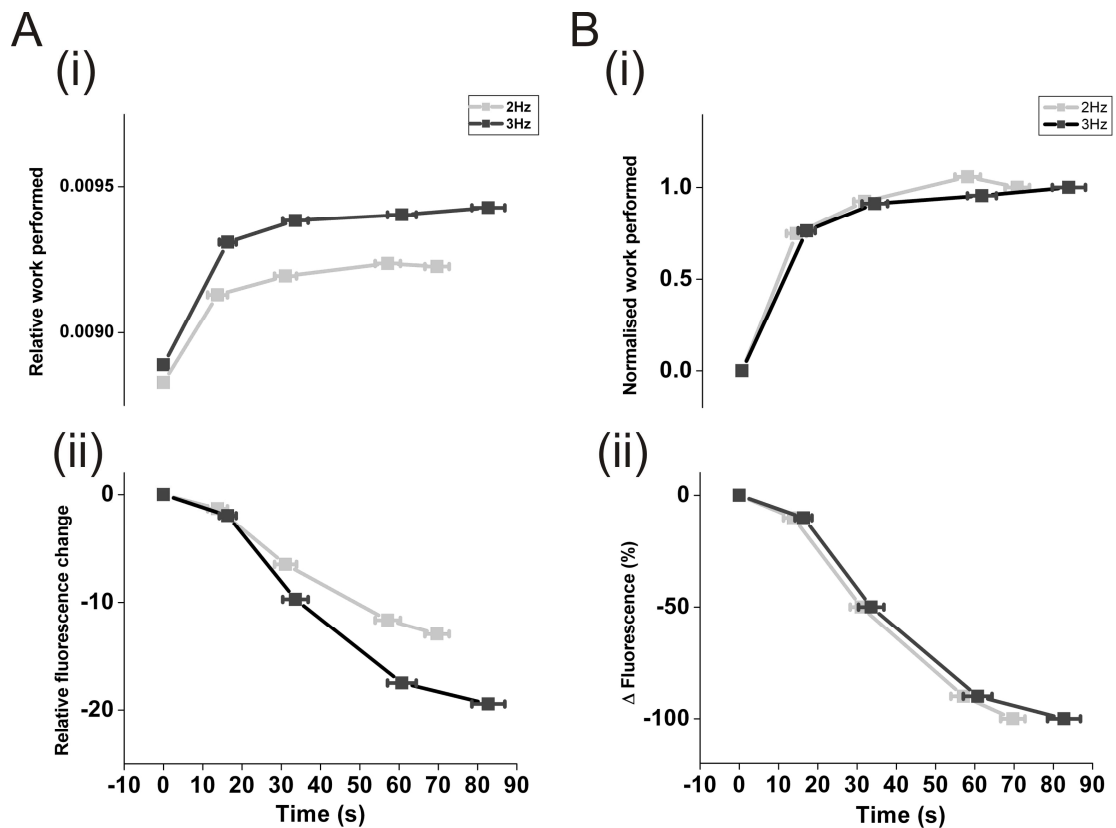


Figure 6-5 Time course of fluorescence change and work performed upon increase in work intensity to 2Hz and 3Hz pacing

Panel A (i) Mean work performed, expressed as inverse of cell length, during pacing at 2Hz (light grey line) and 3Hz (dark grey line). **(ii)** Against the same timescale, mean relative NADH/FAD fluorescence change taking into account the average total fluorescence change at 2Hz and 3Hz stimulation (from Figure 6-4). **Panel B (i)** Normalised work performed with work at T_0 (onset of increase in stimulation frequency) set as 0 and T_{100} (termination of stimulus train) set as 1. **(ii)** Against the same timescale, normalised fluorescence expressed as percentage of overall fluorescence change during stimulus train ($n=20$). In all panels, points are marked at times where 0, 10, 50, 90 and 100% changes in fluorescence occurred.

Figure 6-5 shows that the level of work performed by the cell appears to have essentially reached a steady state during the trains of 2 and 3Hz pacing. Fluorescence levels also appear to be approaching a steady state, although it is unclear if a completely steady state has been reached. Between T_0 (onset of increased workload) and T_{10} (time point at which 10% of overall fluorescence change during stimulus train occurred), there is a large increase in work for a relatively small change in fluorescence. It is during this initial period that the cell is thought to utilise PCr as a temporal buffer to fulfil ATP demand, and so the mitochondrial oxidative response to the increased work is initially slow. Following this, the stable level of work performed indicates that ATP supply is matching demand and contractile function is maintained. However, fluorescence levels change at a faster rate as the mitochondria are unable to match NADH and $FADH_2$ production with the increased rate of their oxidation in order to produce sufficient ATP by oxidative phosphorylation, thus leading to progressive oxidation of the mitochondrial environment.

Relative work performed was calculated from the mean cell length over a 5s period at each time point. The inverse of mean cell length gives an indication of the degree of fractional shortening as well as the length of time spent in the contracted state (i.e. performing work). As expected, the level of work performed was significantly higher at 3Hz compared to 2Hz when the data was paired for each cell ($p < 0.001$).

When the work performed was normalised to 0 at T_0 and 1 at T_{100} (time at which train of stimulation was terminated), the rate at which work increased was comparable between 2 and 3Hz. Similarly, when fluorescence change was expressed as a percentage of overall fluorescence (0% at T_0 , 100% at T_{100}), the time course of fluorescence change was virtually identical for 2 and 3Hz.

Analogous analysis was carried out during the recovery period when stimulation frequency was stepped down to 0.5Hz and is shown in Figure 6-6.

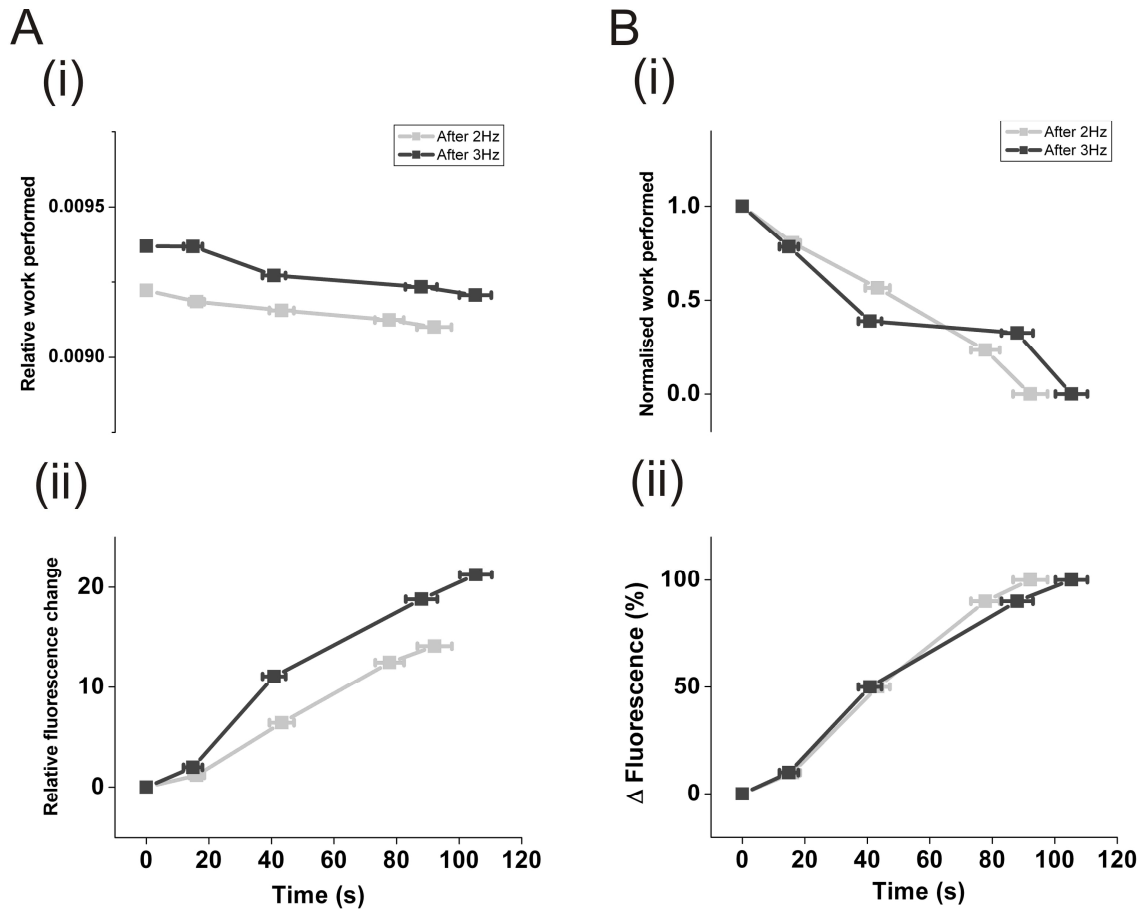


Figure 6-6 Time course of fluorescence change and work performed upon decrease in work intensity from 2Hz and 3Hz pacing to 0.5Hz pacing

Panel A (i) Mean work performed, expressed as inverse of cell length, during pacing at 0.5Hz following stimulation at 2Hz (light grey line) and 3Hz (dark grey line). **(ii)** Against the same timescale, mean relative fluorescence change taking into account the mean initial NADH/FAD fluorescence level immediately after 2Hz and 3Hz stimulation. **Panel B (i)** Normalised work performed with work at T_0 (onset of 0.5Hz stimulation) set as 1 and T_{100} (termination of stimulus train) set as 0. **(ii)** Against the same timescale, normalised fluorescence expressed as percentage of overall NADH/FAD fluorescence change during stimulus train ($n=16$). In all panels, points are marked at times where 0, 10, 50, 90 and 100% changes in fluorescence occurred

The time scale for recovery of fluorescence and work performed is slower following decrease in workload compared to the rate of changes when workload is increased. In Figure 6-6, fluorescence and work do not appear to have reached a steady state, despite continuing low intensity work for almost 2 min. The relative work performed at 0.5Hz is higher following 3Hz pacing compared to 2Hz. This is because work performed by the cells starts at a higher level following 3Hz pacing and remains higher throughout the 0.5Hz stimulus train due to the slow recovery.

Expressing fluorescence change over the recovery period in percentage terms (T_0 being 0% and T_{100} being 100%) there is an overlap in time course for recovery following 2 and 3Hz stimulation. However, during late recovery, the rate of fluorescence change shows a trend towards slower fluorescence recovery at 3Hz. The rate of fluorescence change over the period of increased and decreased stimulation frequency was further analysed and is shown in Figure 6-7.

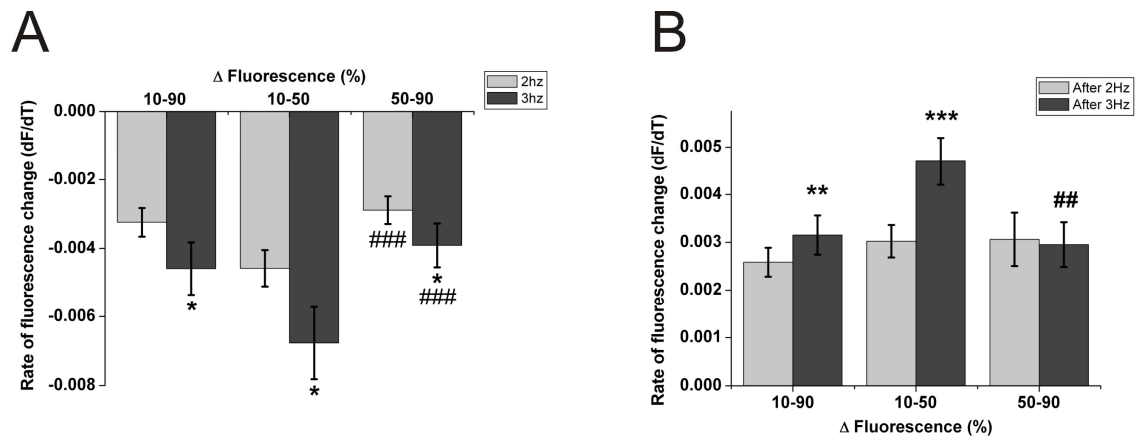


Figure 6-7 Rate of fluorescence change following increased and decreased workload

Panel A: Rate of fluorescence change following increase in stimulation frequency to 2Hz (light grey bars) and 3Hz (dark grey bars) ($n=20$). **Panel B:** Rate of fluorescence change during recovery following 2Hz (light grey bars) and 3Hz (dark grey bars) stimulation ($n=17$). Overall rate of fluorescence change (10-90%), as well as during the early response (10-50%) and the late response (50-90%) are shown. * $p<0.05$ versus 2Hz; ** $p<0.01$ versus 2Hz; *** $p<0.001$ versus 2Hz. ## $p<0.01$ versus 10-50%; ### $p<0.001$ versus 10-50%.

The overall rate of fluorescence change (between T_{10} and T_{90}) was faster when work intensity was increased to 3Hz compared to 2Hz pacing. When the rate of the early fluorescence response to increased work intensity (between T_{10} and T_{50}) is compared to the late response (between T_{50} and T_{90}), it becomes clear that the rate of change is non-linear through the entire response and is significantly faster at the start. The greatest difference in rate of fluorescence change between the 2 workloads is seen in the early response.

The rate of fluorescence change was faster when pacing was slowed to 0.5Hz following pacing at 3Hz compared to 2Hz during early recovery. The late response in fact shows a trend towards slower recovery at 3Hz (although this was not significant).

6.3.3 Mitochondrial origin of fluorescence changes

To confirm that the changes in intrinsic fluorescence were originating from the mitochondria, the cells were metabolically challenged with 2 bursts of 3Hz stimulation in the presence of the mitochondrial inhibitors FCCP and CN. Example and mean responses to the metabolic challenge under control and mitochondrially inhibited conditions are shown in Figure 6-8, expressed as the NADH/FAD ratio.

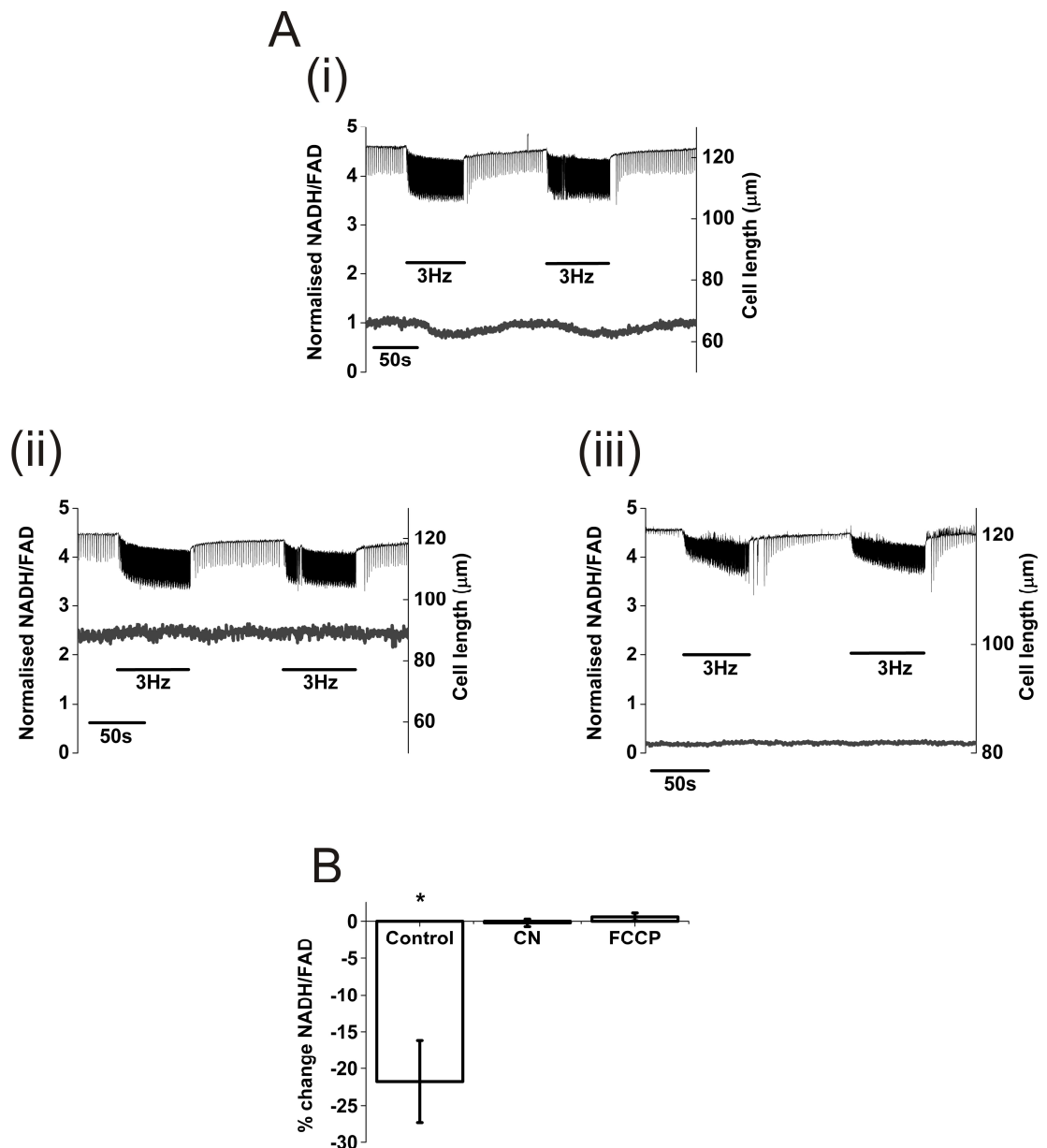


Figure 6-8 Fluorescence responses to 3Hz stimulation in control conditions and in the presence of mitochondrial inhibitors

A: Example trace showing change in fractional shortening (upper black trace) and normalised NADH/FAD fluorescence ratio (lower grey trace) during 3Hz stimulation in (i) control conditions and in the presence of (ii) 2mM CN and (iii) 2µM FCCP. **B:** Mean % change in NADH/FAD ratio during 3Hz stimulation with each treatment (n=4). *p<0.05.

The % change in NADH/FAD fluorescence ratio upon 3Hz stimulation was found to be significant only under control conditions following 1-sample t-test ($p < 0.05$). When the mitochondria are maximally reduced in the presence of 2mM CN or maximally oxidised with 2 μ M FCCP, there is no significant change in NADH or FAD fluorescence when the cell is metabolically challenged. Consequently, the fluorescence changes occurring under control conditions must be arising from NADH and FAD originating from the mitochondria.

6.3.4 Contractile work as source of increased metabolic demand

To verify that the intrinsic fluorescence changes are a response to increased metabolic demand, and that the source of this increased demand was indeed contractile work, contractile function was inhibited with the movement uncoupler cyto D (cyto D itself did not observably have any effect on basal fluorescence). The metabolic challenge of 2 bursts of 3Hz stimulation was delivered to the cell and oxidative responses recorded. The same metabolic challenge was repeated following treatment of the cells with 20 μ M cyto D and the oxidative responses compared between control and cyto D treated cells (Figure 6-9).

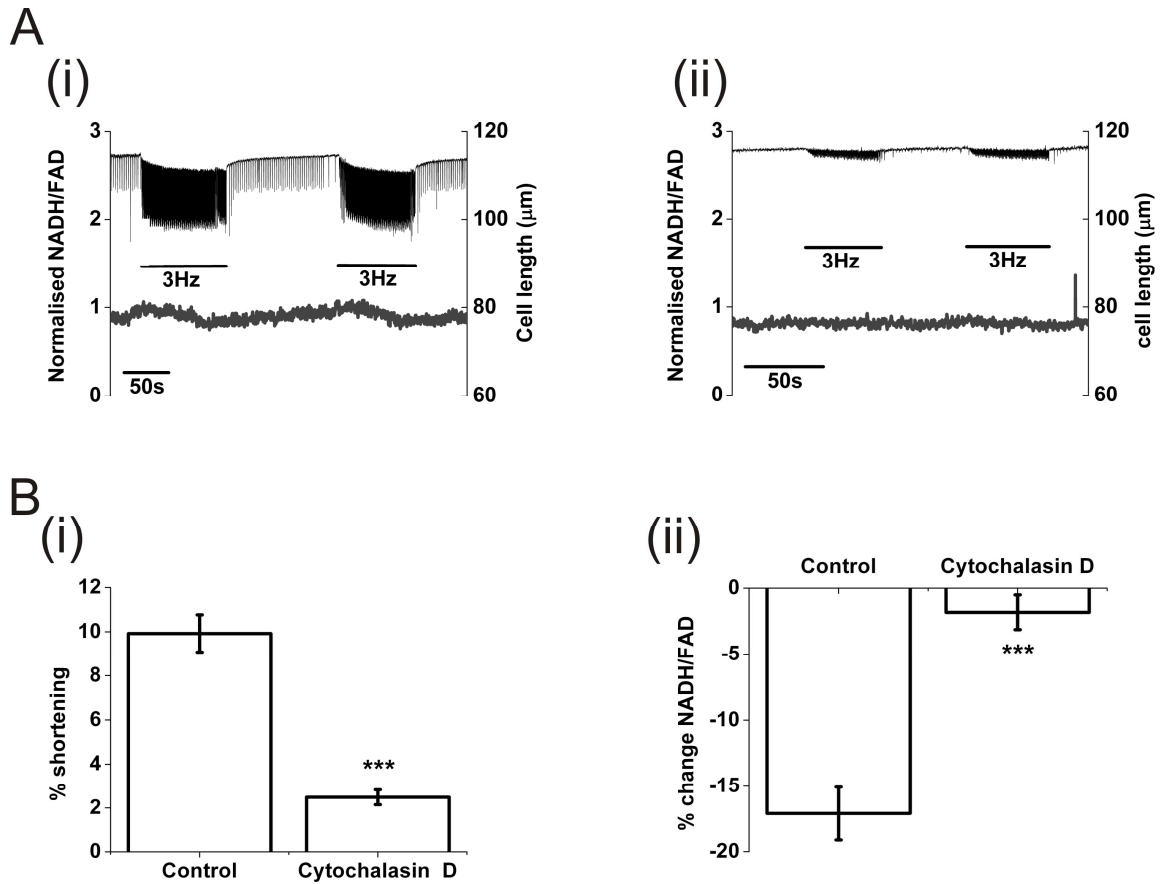


Figure 6-9 Example and mean fluorescence responses to 3Hz stimulation in control conditions and with contractile function inhibited with cyto D

A: Example trace showing change in fractional shortening (upper black trace) and normalised NADH/FAD fluorescence ratio (lower grey trace) during 3Hz stimulation under (i) control conditions and (ii) in the presence of 20μM cyto D. **B:** (i) Mean % shortening at 3Hz stimulation (ii) mean % change in NADH/FAD ratio during 3Hz stimulation with each treatment (n=6). ***p<0.001 versus control.

Fractional shortening was on average ~2.5% at 3Hz following cyto D treatment, compared to on average ~10% in the same cells prior to treatment. This residual contraction in the presence of cyto D demonstrated that the cells were still electrically active and it was only the contractile machinery of the cell that was inhibited. The percentage change in NADH/FAD ratio when work intensity is increased to 3Hz is significantly less in the cells following cyto D treatment compared to the same cells prior to treatment. Thus when contractile function is inhibited, metabolic demand does not increase sufficiently to cause changes in the oxidative status of the cell. This indicates that the source of increased metabolic demand is indeed contractile work.

6.3.5 Interpreting the cause of the delayed oxidative response to increased work intensity

In the majority of cells, there was a delay of up to 25s after stimulation frequency was step increased before the redox status of the cell changed. This can be seen in Figure 6-3, where there is a delay of ~15s before NADH fluorescence decreased and FAD fluorescence simultaneously increased. This is consistent with the idea that the cell is initially coping with the increased metabolic demand, and indicates that other (non-mitochondrial) sources of ATP are immediately utilised to fulfil the increased energy requirements before mitochondrial ATP production takes over.

In cardiac muscle, the CK/PCr system acts both as a high-energy phosphate shuttle and as a temporal energy buffer (Wallimann *et al.*, 1992; Jacobus, 1985). The PCr pool is therefore the most likely initial source of ATP upon abrupt increases in energy demand. To investigate this, the CK/PCr system was inhibited to determine if this eliminated the initial delay prior to the occurrence of mitochondrial oxidative changes.

Iodoacetamide was used as a CK inhibitor, thereby preventing PCr acting as an energy store. The time delay prior to oxidative changes taking place following increased workload, and the magnitude of these changes, was measured under control conditions and following iodoacetamide treatment (Figure 6-10). Iodoacetamide did not affect contractile function or basal fluorescence when used at a concentration of 0.4mM, but did cause oxidation of the cell at higher concentrations (see Section 6.4.4).

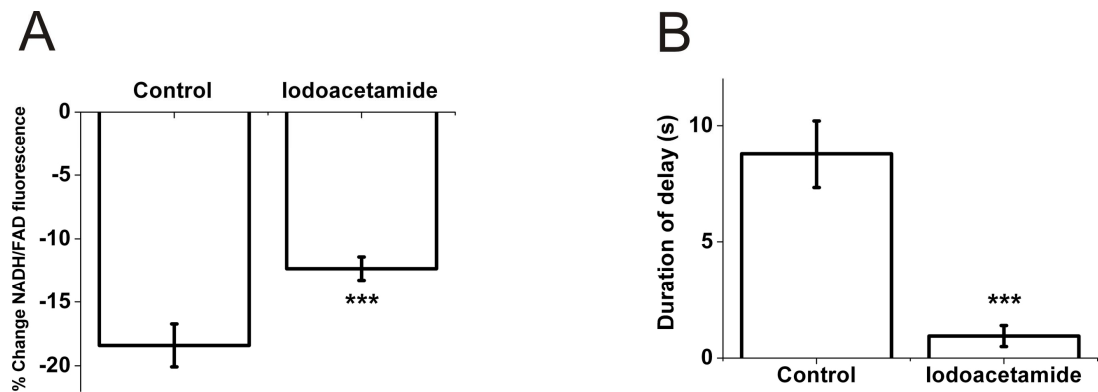


Figure 6-10 Effect of iodoacetamide on fluorescence responses to 3Hz stimulation

A: Mean % change in NADH/FAD fluorescence under control conditions and following 10 min perfusion with 0.4mM iodoacetamide. **B:** Mean duration of delay between initiation of 3Hz stimulation and occurrence of fluorescence changes under control conditions and in the presence of iodoacetamide. *** $p < 0.001$ versus control (n=11).

Inhibition of CK with iodoacetamide caused a decrease in the duration of the delay between the initiation of 3Hz stimulation and the point at which intrinsic fluorescence changes begin to occur. However, the magnitude of these changes was also significantly reduced following iodoacetamide treatment compared to controls.

These differences in the magnitude of intrinsic fluorescence change and duration of the delay were not caused by an experimental artefact, for example, due to the length of the protocol or the process of solution change. The 3Hz metabolic challenge was delivered to the cell whilst perfusing with control Krebs solution and intrinsic fluorescence changes measured. The perfusate was then switched to the same control solution from an alternative reservoir, and the cells perfused for 10 min prior to delivering the same metabolic challenge. No significant difference was found in the magnitude of NADH/FAD response or delay prior to fluorescence changes occurring during the metabolic challenge before and after the solution change (Figure 6-11).

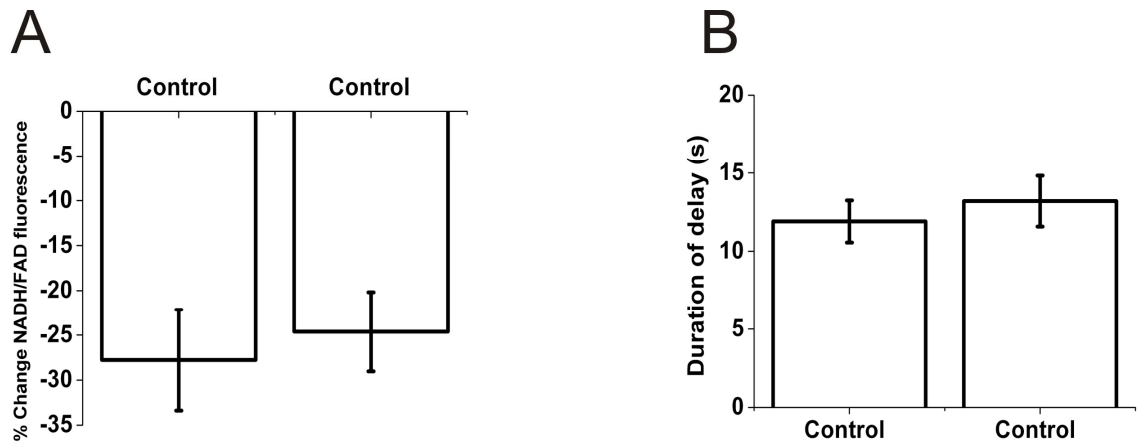


Figure 6-11 Effect of switching between control solutions on fluorescence response to 3Hz stimulation

A: Mean % change in NADH/FAD fluorescence ratio during 3Hz stimulation under control conditions and following switching of perfusing solution to the same control solution from a different reservoir. Cells were perfused for 10 min before second metabolic challenge was performed. **B:** Mean duration of delay prior to occurrence of fluorescence changes following initiation of 3Hz stimulation (n=5).

Another possible reason for the difference in magnitude of fluorescence change following treatment with iodoacetamide could be if the effects of iodoacetamide are not limited to inhibition of CK, as iodoacetamide is a non-specific alkylating agent for cysteine and histidine residues in proteins (Smythe, 1936). To investigate this, the same protocol was repeated, but iodoacetamide was replaced with 10mM cyclocreatine, a more specific inhibitor of CK. Cyclocreatine did not affect basal fluorescence or contraction at the concentrations used. As the period of time required for inhibition of CK with cyclocreatine was not known, groups of cells were also incubated with 10mM cyclocreatine for 1-2 hours prior to performing the metabolic challenge. However, with these cells, it was not possible to measure the response to increased work intensity before and after CK inhibition. The mean magnitude of redox change and the duration of delay prior to these changes occurring are shown in Figure 6-12.

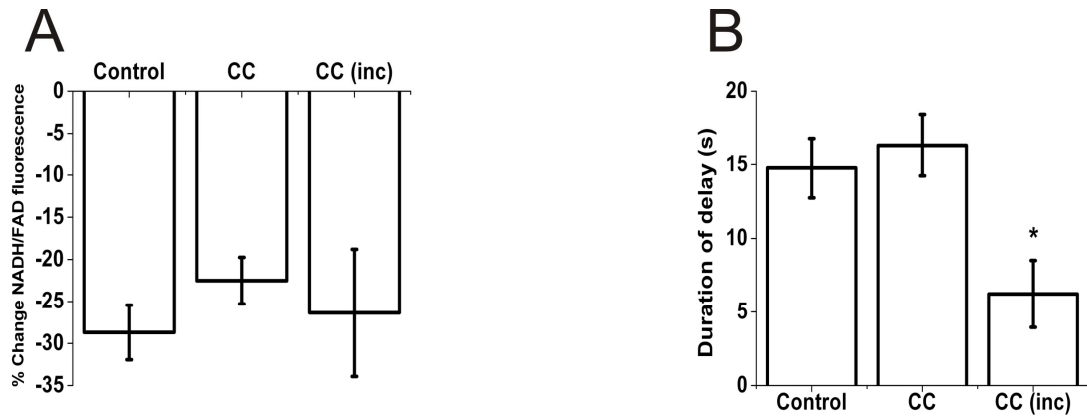


Figure 6-12 Effect of cyclocreatine on fluorescence responses to 3Hz stimulation

A: Mean % change in NADH/FAD fluorescence ratio during 3Hz stimulation under control conditions, following 10 min of perfusion with 10mM cyclocreatine (CC) and (in different cells) following incubation with 10mM cyclocreatine for 1-2 hours (CC (inc)). **B:** Mean duration of delay prior to occurrence of fluorescence changes following initiation of 3Hz stimulation (n=4); * p<0.05.

There was no significant difference in the magnitude or duration of delay in the redox response following increase in workload before and after perfusion with 10mM cyclocreatine. However, in a different group of cells, which had been incubated with 10mM cyclocreatine for 1-2 hours, the duration of delay was significantly reduced (though not eliminated). The magnitude of fluorescence change was not significantly different between these groups. This suggests that the initial delay in mitochondrial oxidative response is due to PCr metabolism, and CK is partially (but not completely) inhibited by incubation with cyclocreatine for 1-2 hours, resulting in a reduction in the duration of the delay. The lack of significant change in the magnitude of oxidative response suggests that mitochondrial function has not been affected by cyclocreatine treatment. Perfusing the cells for 10 min with cyclocreatine does not seem to inhibit CK sufficiently to have any effect on the delayed oxidative response.

6.4 Discussion

6.4.1 Energy supply and demand matching in rabbit ventricular myocytes

The results of these experiments demonstrate that in isolated rabbit ventricular myocytes, increasing work intensity causes an initial oxidation of the mitochondrial environment before reaching an essentially steady redox state. This indicates that there is a mismatch between energy supply and demand upon transition to increased workload. Decreasing work intensity back to initial stimulation rates causes the redox status of the cell to recover to baseline values. There is a linear relationship between the magnitude of oxidative response and the level of work performed, with the largest oxidative responses taking place at the highest work intensity (3Hz). Surprisingly, this mismatch between energy supply and demand occurred at physiological heart rates in the rabbit, which suggests that the heart is permanently in a delicate state of metabolic balance.

The intensity of work performed by the heart does not remain constant and frequently changes over time. An increase in workload requires an increase in ATP supply in order for the heart to maintain function. The mitochondria achieve this by increasing the rate of flux of electrons through the ETC. As NADH and FADH₂ are the sources of these electrons, an increase in the rate of ATP production must be accompanied by an increase in the rate of substrate dehydrogenation through the reactions of the TCA cycle in order to maintain the supply of reducing equivalents. If the rate of production of reducing equivalents does not match the rate of mitochondrial ATP production, the mitochondrial environment will become progressively oxidised and the loss of redox potential will eventually result in the cessation of mitochondrial ATP synthesis.

The results of these experiments demonstrate that in isolated rabbit ventricular myocytes, the rate of oxidative phosphorylation is not well matched with the rate of substrate dehydrogenation. However, the cell does not become completely oxidised and reaches an essentially steady redox state, despite continuous high intensity work. This may be due to the rate of oxidative

phosphorylation reaching a steady state that matches the rate of substrate dehydrogenation by the TCA cycle. Alternatively, it may be due to control mechanisms taking effect, which increase the rate of production of reducing equivalents to match the increased rate of their oxidation at the ETC. The exact mechanisms by which this may be occurring were not investigated in this project. However, one possible mechanism is through an increase in mitochondrial $[Ca^{2+}]$ ($[Ca^{2+}]_m$) in response to increased stimulation frequency.

Mitochondrial Ca^{2+} plays an important role in the regulation of mitochondrial ATP production (Balaban, 2009; Griffiths & Rutter, 2009; Nguyen *et al.*, 2007; Cortassa *et al.*, 2006; Balaban, 1990). Three rate limiting dehydrogenases (pyruvate dehydrogenase, 2-oxoglutarate dehydrogenase and NAD^+ isocitrate dehydrogenase), critical elements of substrate metabolism are regulated by mitochondrial Ca^{2+} (Denton *et al.*, 1978; Denton *et al.*, 1972; McCormack & Denton, 1979). An increase in $[Ca^{2+}]_m$ stimulates mitochondrial dehydrogenase activity, increasing the rate of production of reducing equivalents by the TCA cycle.

During cytosolic Ca^{2+} transients, the mitochondria accumulate and subsequently release Ca^{2+} . However, whether the transduction of cytosolic Ca^{2+} transients occurs slowly by accumulation over a number of beats, or rapidly, on a beat-to-beat basis is a contentious issue (Huser *et al.*, 2000). The slow integration of rapid cytosolic Ca^{2+} transients leading to the slow accumulation Ca^{2+} by the mitochondria may explain the initial oxidation upon increased workload, prior to the fluorescence levels reaching a steady redox state. It may take tens of seconds before $[Ca^{2+}]_m$ has increased enough to stimulate dehydrogenase activity sufficiently to prevent further oxidation of the mitochondrial environment. This temporal integration of cytosolic Ca^{2+} transients by cardiac mitochondria has been demonstrated in a number of studies (Brandes & Bers, 2002; Zhou *et al.*, 1998; Leisey *et al.*, 1993; Miyata *et al.*, 1991).

However, the close proximity of the mitochondria to SR Ca^{2+} release channels, demonstrated by electron microscopy (Sharma *et al.*, 2000) would suggest that there is preferential coupling of Ca^{2+} transport between the SR and mitochondria, and the mitochondria are actually exposed to microdomains of very high cytosolic $[Ca^{2+}]$. This may mean that beat-to-beat oscillations in

$[Ca^{2+}]_m$ are possible, and indeed a number of studies have demonstrated this in cardiomyocytes (Maack *et al.*, 2006; Robert *et al.*, 2001; Szalai *et al.*, 2000; Duchen *et al.*, 1998). In addition, recent work using a Ca^{2+} sensitive protein sensor targeted to the mitochondria demonstrated mitochondrial Ca^{2+} sequestration was a combination of beat-to-beat oscillations and slow integration of mean cytosolic $[Ca^{2+}]$ (Kettlewell *et al.*, 2009).

The redox response to increased work intensity demonstrated in this study, and the time course of fluorescence changes, would suggest that mitochondrial Ca^{2+} uptake corresponding to the slow integration model may be stimulating NADH production by the TCA cycle and preventing complete oxidation of the mitochondrial environment at high intensity workloads. However, as measurements of mitochondrial Ca^{2+} were not made in this study, it is not possible to say for certain that this was the case.

A summary diagram showing the postulated sequence of metabolic events that take place when work intensity is increased is shown in Figure 6-13. The initial time delay shown in ATP supply from the mitochondria is consistent with the findings of Eijgelshoven *et al.* (1994), who demonstrated that the decrease in [PCr] occurred significantly faster than the increase in O_2 consumption (representing mitochondrial ATP production) when heart rate was doubled in isolated perfused isovolumically contracting rabbit hearts (Eijgelshoven *et al.*, 1994).

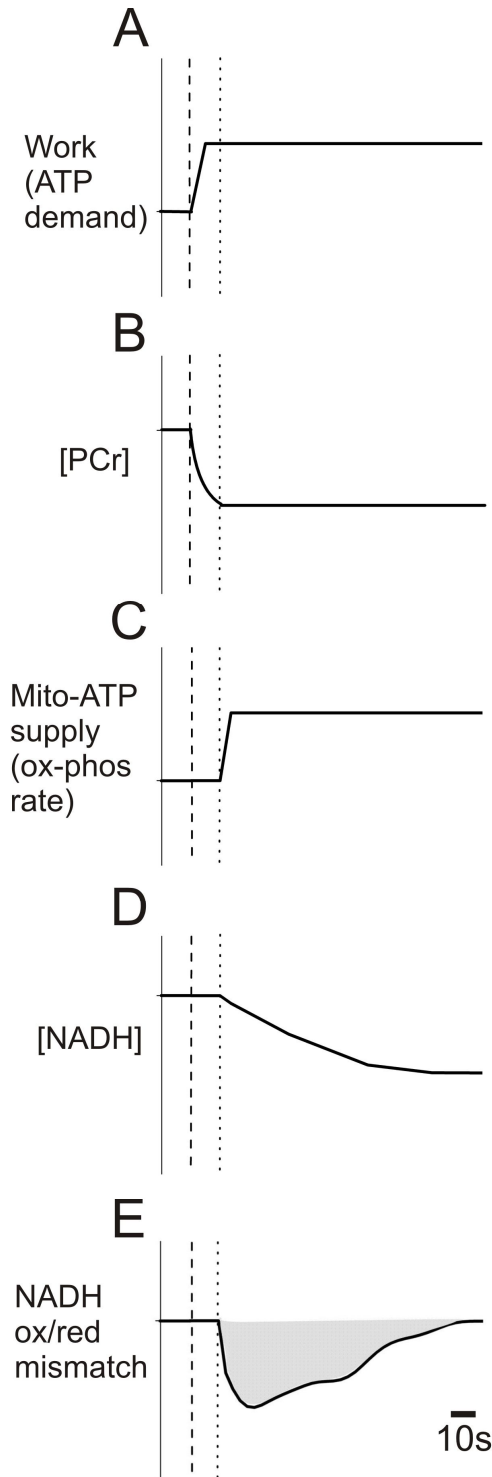


Figure 6-13 Summary of postulated sequence of metabolic events that take place upon increases in work intensity, as observed in the current study

Step increase in work intensity (represented by dashed line) results in an increase in ATP demand (A). This ATP demand is initially fulfilled by metabolism of PCr stores, and [PCr] falls (B). Mitochondrial regulatory mechanisms then take effect and ATP supply from the mitochondria increases by increased rate of oxidative phosphorylation (C). This is achieved by increased rate of flux of electrons from NADH and FADH₂ through the ETC (i.e. increased rate of oxidation). This results in an initial net oxidation of the mitochondrial environment and a fall in [NADH] (D) and [FADH₂] (not shown). However, the rate of fall of [NADH] slows and eventually reaches a steady state, indicating that the rate of NADH and FADH₂ oxidation by oxidative phosphorylation is now matching the rate of NAD⁺ and FAD reduction by the TCA cycle. The period and extent of mismatch between oxidation and reduction is represented by the shaded area in (E), obtained by differentiation of trace D.

6.4.1.1 Regulation of oxidative phosphorylation

The control mechanisms that increase the rate of oxidative phosphorylation and ATP production upon increases in workload have been studied for many years, but as yet, have not been unequivocally shown. The classical feedback regulation mechanism was first proposed in the 1950s and states that an increase in concentration of the products of ATP hydrolysis (ADP and P_i) stimulates an increase in the rate of oxidative phosphorylation. This proposal was in response to the observation that in isolated liver mitochondria, addition of P_i (Lardy & Wellman, 1952) and ADP (Chance & Williams, 1955c) caused an increase in O_2 consumption, indicating increased rate of oxidative phosphorylation. When ADP and P_i concentrations fell, the rate of O_2 consumption also fell. However, measurements of ATP, PCr, ADP and P_i levels using ^{31}P -NMR in intact hearts during workload transitions have revealed conflicting results. Some studies report an increase in ADP and P_i concentrations and a fall in PCr when work intensity was increased (Eijgelshoven *et al.*, 1994; Elliott *et al.*, 1994), whereas others report no significant change in metabolite concentration (Katz *et al.*, 1989; Katz *et al.*, 1987). If no change in phosphate metabolites occurs during workload transitions, this would suggest that the feedback regulation model would not adequately explain the increased rate of oxidative phosphorylation upon increased work.

An alternative theory is that an increase in the NADH/NAD⁺ redox potential (secondary to Ca²⁺ dependent activation of TCA cycle dehydrogenases) stimulates an increase in the rate of oxidative phosphorylation (Katz *et al.*, 1987). However, in order for this to be the primary regulator of oxidative phosphorylation, an increase in workload must be accompanied by an immediate increase in the NADH/NAD⁺ ratio. Few studies demonstrate this (Griffiths *et al.*, 1997; Katz *et al.*, 1987) and this therefore seems to be an unlikely primary control mechanism for oxidative phosphorylation.

The results of our experiments also do not support this theory, as NADH fluorescence falls when workload is increased. However, the primary trigger for increased ATP production by oxidative phosphorylation could be an increase in ADP, causing initial NADH and FADH₂ oxidation. The rate of oxidative phosphorylation may then be maintained by stimulation of Ca²⁺ dependent

dehydrogenases, preventing complete oxidation of NADH (as discussed earlier). What is clear is that the regulation of oxidative phosphorylation is complex and more than one control mechanism is likely to be involved (Bell *et al.*, 2006; Cortassa *et al.*, 2006; Jo *et al.*, 2006; Korzeniewski *et al.*, 2005).

6.4.1.2 Comparison of results with previous studies

Previous studies assessing energy supply and demand matching in cardiac cells and tissue have demonstrated a variety of responses. The results of this study most closely replicate the results of Heinzl *et al.* (2006), White & Wittenberg (2000), Ashruf *et al.* (1995), White & Wittenberg (1993) and Chapman (1972). However, in contrast to these studies, which only measured NADH fluorescence as an indicator of redox state, our study benefited from the advantages of simultaneously measuring both NADH and FAD fluorescence responses.

It is not known why similar experiments have produced different results in other studies. It is unlikely to be due to species difference alone, as a number of different oxidative responses upon transitions in workload have been reported in rat cardiac myocytes and tissue preparations (White & Wittenberg, 2000; Griffiths *et al.*, 1998; Griffiths *et al.*, 1997; Brandes & Bers, 1996; Ashruf *et al.*, 1995; White & Wittenberg, 1993; Katz *et al.*, 1987). The most likely explanation for these variable results would be due to differences in the preparations used and experimental conditions. Factors such as limited O₂ supply, particularly in tissue preparations, would lead to a misleading increase in NADH fluorescence upon increased work intensity caused by decreased mitochondrial ATP synthesis and not increased NADH production. In addition, limited substrate availability would slow down the production of reducing equivalents by the TCA cycle, resulting in oxidation of the cell if ATP supply is maintained.

A possible weakness in this study is that although a constant perfusion of glucose was maintained throughout, the perfusing medium was not supplemented with pyruvate to ensure that endogenous substrate supply was not limiting. There are conflicting reports about the effect of endogenous pyruvate supplementation on the response to workload transitions. White and Wittenburg (2000) report that the presence of 2mM pyruvate in a superfusing medium containing 5.4mM glucose prevented the fall in NADH fluorescence observed upon increased work

intensity in isolated rat heart cells. Conversely, Ashruf *et al.* (1995) report that in Langendorff perfused rat hearts, addition of 10mM pyruvate to a Tyrode's solution containing 5.5mM glucose caused an increase in baseline NADH fluorescence levels, but did not change the oxidative response upon increased work intensity. However, in White and Wittenburg's study, contractile function was reduced when substrate availability was limited. The fact that contractile function did not diminish at high intensity work suggests that ATP supply was continuously maintained and endogenous substrate supply was not limited to any great extent in our study. However, our study could be improved by use of a bicarbonate based extracellular solution, which would have recreated more physiological conditions. In addition, the solution should be supplemented with better physiological substrates such as fatty acids or lactate.

The intensity of work performed may also determine the redox response to workload transitions. In this study, pacing at 3Hz was used as the highest intensity workload, as this was the maximum stimulation rate that could be achieved with isolated rabbit cardiac myocytes at 37°C. At higher frequencies the cell is unable to contract on stimulus. A range of stimulation frequencies were used to increase work intensity in other studies. The highest intensity workload achievable is dependent on species as well as the type of preparation used - intact tissue preparations are capable of higher stimulation frequencies than isolated cells. The work performed in a contracting Langendorff-perfused heart (with fluid-filled balloon in the LV), working heart or intact trabeculae preparation will also be higher. In these situations contraction is against a load, whereas this is not the case with cells. It could therefore be argued that increasing stimulation frequency in isolated cells does not significantly increase work. However, Heinzel *et al.* (2006) have shown that despite the unloaded conditions, an increase in stimulation frequency is accompanied by an increase in O₂ consumption (indicating stimulation of oxidative phosphorylation and higher ATP production) in isolated cardiomyocytes. Thus, although the work intensity may not be as high as in hearts under *in vivo* or more physiological conditions, workload is still being increased in the isolated cells. The advantage of using isolated cell preparations is that substrate and O₂ delivery can be more rigorously controlled than in tissue preparations.

Finally, in some studies no oxidative response to transitions in workload was observed without the use of inotropic agents such as norepinephrine and isoproterenol to further increase workload (Liu & O'Rourke, 2008; Maack *et al.*, 2006; Griffiths *et al.*, 1997). It is therefore difficult to compare the conditions of high intensity work in the various studies and may be a reason why a diverse range of responses were observed.

6.4.2 Analysing the kinetics of oxidative responses upon transitions in work intensity

The time course for changes in intrinsic fluorescence and work performed was analysed for each train of 2Hz and 3Hz stimulation, as well as the recovery phase immediately following this, during which time the cells were stimulated at 0.5Hz. It was found that step increasing work intensity to a greater extent i.e. up to 3Hz pacing compared to 2Hz pacing, resulted in a greater oxidative response from the cells. However, when the data was normalised to percentage fluorescence change (during each stimulation frequency), the rate of change was almost identical for both work intensities. The difference in the rate of fluorescence change only became clear when the magnitude of oxidative response at each work intensity was taken into account. This difference was greater in the early response (10-50% fluorescence change) compared to the late response (50-90% fluorescence change).

6.4.2.1 Problems associated with the protocol

During the experimental procedure, stimulus frequency was changed when fractional shortening and fluorescence levels were judged (by eye) to have reached a steady state. The length of this period varied from cell to cell, but upon increase in stimulation frequency was always longer than 45s at 2Hz and 55s at 3Hz pacing. In order to increase the chances of successfully completing the protocol, the metabolic challenge was kept as short as possible. However, closer analysis of the fluorescence changes during each stimulus train revealed that rate of change in fluorescence levels and work performed had slowed, but may not have reached a completely steady state before the stimulation frequency was changed. This was particularly apparent during the recovery

period, even though the length of time the cells were given to recover was longer than the period of high intensity work and as much as 2 min in length. This may have led to an accumulation of metabolic deficit over the period of the protocol; further metabolically compromising the cells. However, as work intensity was increased incrementally (starting at 1Hz) and only two bursts of each frequency was delivered, the overall accumulation would be expected to be small and not substantially affect subsequent responses to high intensity work. In addition, similar responses to 3Hz stimulation were seen even when this was the first level of high intensity work delivered to the cell. This would suggest that a possible metabolic deficit does not adversely affect subsequent cellular responses to increased workload.

6.4.3 Confirming the cause of increased metabolic demand and source of fluorescence changes

The mitochondrial origin of the fluorescence responses was confirmed by performing the metabolic challenge in the presence of mitochondrial inhibitors. Under these conditions, where oxidative phosphorylation by the mitochondria was blocked, no change in intrinsic fluorescence was observed during high intensity work. This demonstrates that the changes in intrinsic fluorescence seen under control conditions during transition in workload are arising from the mitochondria. It also indicates that under control conditions, the mitochondria are the major source of ATP for the cell. Interestingly, inhibition of mitochondrial function with CN does not substantially affect contractile activity. Under these conditions, the cell must be utilising other, non-mitochondrial, sources of ATP to supply contractile fibres, such as glycolysis and PCr metabolism.

The cause of increased metabolic demand was shown to be increased contractile work. When contractile function was inhibited with cyto D, the redox changes during increased frequency of stimulation were abolished. This was not simply due to the design of the protocol allowing the cell to adapt during the long period of low intensity work whilst cyto D took effect. When cells were given a 10 min period of low intensity work whilst being perfused with control solution, the redox changes that took place when work intensity was increased were not

significantly different to those prior to this 10min period of low work intensity (Figure 6-11).

6.4.4 Investigating the delayed oxidative response following workload transitions

The onset of increased work intensity was associated with a time delay of varying length prior to the occurrence of intrinsic fluorescence changes. This indicated that non-mitochondrial sources of ATP were utilised in order to fulfil the initial increase in energy demand before mitochondrial ATP production takes over. The most likely source of this ATP supply is PCr, and the blockade of PCr metabolism with CK inhibitors went some way towards conforming this. However, problems were encountered with the use of these inhibitors.

Initially, iodoacetamide was used as a CK inhibitor at concentrations of 0.4mM. It was found that perfusion with iodoacetamide at this concentration for 10 min almost completely abolished the time delay between workload transition and onset of oxidative response. However, iodoacetamide also unexpectedly caused a significant decrease in the magnitude of fluorescence response. The reasons for this were not completely clear. It may be that the effects of iodoacetamide were not specific to CK inhibition, and it may have been having effects on mitochondrial and/or glycolytic metabolism. Indeed, when higher iodoacetamide concentrations of 1.2mM or greater were tried, complete oxidation of the cell took place, before an increase in work intensity was even instigated. Alternatively, these effects may actually be a direct result of the loss of PCr metabolism, and may not be due to the non-specific action of iodoacetamide. To investigate this, the more specific CK inhibitor cyclocreatine was used.

The same protocol that was used for iodoacetamide treatment was repeated with 10mM cyclocreatine. However, it was found that 10 min perfusion with cyclocreatine did not cause any significant reduction in duration of delay following workload transition. Cells were also incubated with 10mM cyclocreatine for 1-2 hours before the metabolic challenge was carried out. This method was found to reduce (but not abolish) the delay, without significantly affecting the magnitude of oxidative response. Use of cyclocreatine in the

literature has been largely limited to studies investigating its role in inhibiting tumour growth due to its effects on CK. In these studies, cyclocreatine is either included in the diet for a number of weeks, or cancer cell lines are cultured in the presence of cyclocreatine for a period of several days. It was therefore difficult to establish suitable cyclocreatine concentrations and incubation periods in order to acutely inhibit CK dependent ATP generation. The concentrations and incubation periods chosen were based on a study performed in macrophages in which CK was not completely inhibited (Kuiper *et al.*, 2008). However, from the results of the cyclocreatine experiments, it appears that the additional effects of iodoacetamide, apart from the abolition of the delay, are due to the non-specific actions of the inhibitor.

6.4.5 Conclusions

The results of these experiments demonstrate that increasing work intensity by increasing stimulation frequency in isolated rabbit ventricular myocytes results in oxidation of the cellular environment, indicating a mismatch between metabolite supply and demand. This response was shown to be mitochondrial in origin and the increase in energy demand was shown to be due to an increase in contractile work performed by the cell. The initial delay that precedes the oxidative response following transition to higher workload was found to be most likely due to metabolism of PCr stores as the initial source of ATP. The degree of oxidative response correlated well with the level of work performed by the cell, with the oxidative response at 3Hz being greater than at 2Hz pacing.

7 Mitochondrial redox response to increased work intensity in a rat model of cardiac hypertrophy

7.1 Introduction

The previous chapter demonstrated that metabolite supply is not well matched with demand when work intensity is increased in isolated rabbit ventricular myocytes. These experiments were performed in normal, healthy rabbits. The following chapter describes similar experiments performed in isolated rat cardiac myocytes from a genetic model of cardiac hypertrophy induced by pressure overload, and the normotensive control model.

7.1.1 SHRSP model of cardiac hypertrophy

The SHR rat strain is the most commonly used genetic model of hypertension (Pinto *et al.*, 1998), which was generated by selection and inbreeding of WKY rats with the highest blood pressure (Okamoto & Aoki, 1963). This strain was further developed to produce the SHRSP sub-strain. SHRSP rats develop even higher blood pressure and have a strong tendency to die from stroke (Okamoto *et al.*, 1974). The pressure overload induced by hypertension results in pathological remodelling of the heart in the form of cardiac hypertrophy.

7.1.2 Effects of cardiac hypertrophy on mitochondrial function

Sustained pressure overload on the heart due to chronic hypertension or aortic stenosis leads to the LV undergoing concentric hypertrophy, in which the ventricular wall grows thicker (due to increase in myocyte size), with no increase in chamber size. This is a compensatory mechanism to normalise the persistently elevated wall stress that occurs under these conditions, and leads to an increase in contractile force. However, over time these compensatory mechanisms become insufficient and deterioration to decompensation and failure may result.

Mitochondrial dysfunction has been reported in a number of models of cardiac hypertrophy induced by pressure overload. Experimental models of hypertrophy produced by constriction (banding) of the ascending aorta have shown impaired ETC activity in neonatal rabbits with both compensated and decompensated LV hypertrophy (LVH) (Griffiths *et al.*, 2010). In addition, LVH induced by the same

method in rats has been associated with reduced mitochondrial density, impaired substrate oxidation and changes in mitochondrial protein levels 20 weeks after aortic constriction (Bugger *et al.*, 2010). Impaired fatty acid oxidation has been observed as early as 2 weeks after the aortic banding procedure in rats, followed by a progressive decrease in glucose oxidation. However, respiratory capacity was only significantly reduced after 20 weeks when HF had developed and ejection fraction (EF) was impaired (Doenst *et al.*, 2010).

Changes in mitochondrial activity have also been reported in genetic models of pressure overload induced cardiac hypertrophy. Respiratory assays have shown reduced respiratory capacity in 20 month old SHR hearts compared to WKY controls, as well as changes in mitochondrial proteins (Jullig *et al.*, 2008). In addition, mitochondrial dysfunction has been demonstrated in 12 month old non-failing SHR hearts after intense work (Hickey *et al.*, 2009). Morphological changes have also been reported, with decreases in mitochondria/myofibril volume ratios reported in both genetic and experimentally induced models of cardiac hypertrophy (Anversa *et al.*, 1979; Lund & Tomanek, 1978). Indeed, impaired oxidative metabolism and increased oxidative stress have also been observed in SHRSP hearts (Chen *et al.*, 1995; Tokoro *et al.*, 1996).

7.1.3 Aim of the chapter

Previous studies have suggested that energy supply and demand matching is adversely affected in hypertrophic hearts induced by aortic banding (Liu & O'Rourke, 2008; Brandes *et al.*, 1998) (See section 1.8.2). The aim of this chapter was to investigate the mitochondrial redox response to increased work intensity in the SHRSP model of cardiac hypertrophy. Comparison of these responses with redox responses in the WKY control model would allow assessment of how mitochondrial function may be affected in this genetic model of cardiac hypertrophy.

7.2 Methods

Cardiac myocytes were isolated from 16 week old SHRSP hearts and age-matched normotensive WKY control hearts as described in Section 2.2.2.

7.2.1 Cell sizing

Cells were viewed under the microscope and cell size measurements were made using an eyepiece graticule. Around 60 cells from each heart were selected randomly and the length and width of each cell was read off the graticule. This procedure was repeated for each heart in the SHRSP and WKY groups.

7.2.2 Stimulation protocol for metabolic challenge

A similar stimulation and perfusion protocol was used for rat cells as was used for rabbit cardiac myocytes (Section 6.2.1). However, as rat hearts are capable of pacing at faster rates, the baseline stimulation frequency was set at 1Hz and step increased to 2Hz, 4Hz and 6Hz in order to metabolically challenge the cells. At the end of the stimulation protocol, NADH and FAD fluorescence signals were calibrated with FCCP and CN. However, the cell did not always survive the full protocol and a calibrated signal could not always be obtained.

Isolation of cardiomyocytes from SHRSP hearts revealed heterogeneity in cell size, with some (but not all) cells displaying obvious hypertrophy. As this study was specifically investigating the effect of hypertrophy on energy supply and demand matching, only cells with hypertrophic appearance were selected for imaging.

Analysis of contractile work and rate of fluorescence change upon workload transitions was performed using the same program as described in Section 6.2.2.

7.2.3 Statistical analysis

All statistical analysis comparing SHRSP and WKY cells was performed by 2 sample t-test.

7.3 Results

7.3.1 Measurements of cell size

Mean cell size (length and width) was measured in cardiac myocytes isolated from WKY and SHRSP hearts and is shown in Figure 7-1 (Data kindly provided by Dr Sarah Kettlewell).

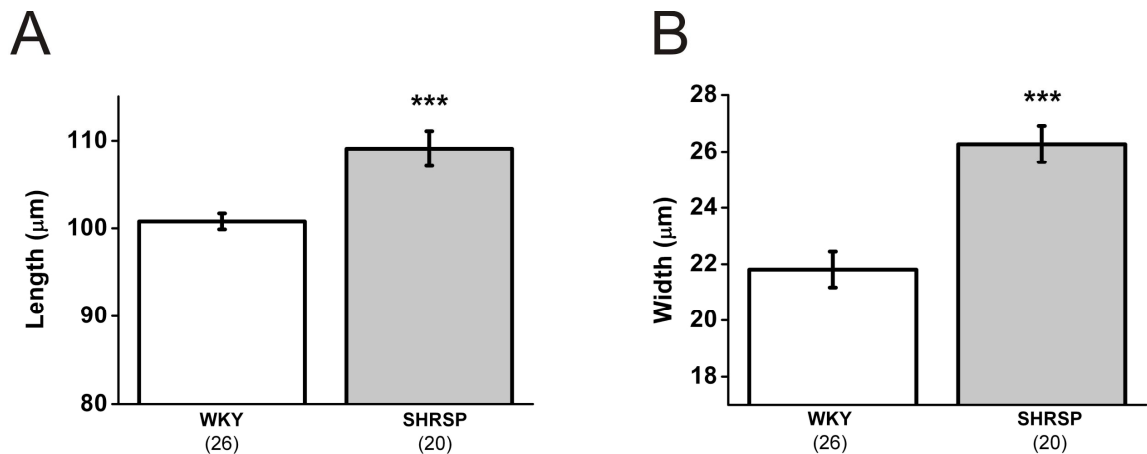


Figure 7-1 Mean cardiac myocyte size isolated from WKY and SHRSP hearts

Mean (A) length and (B) width of cells isolated from hearts from the 2 strains. Sample size in brackets represents the number of hearts, with ~60 cells from each heart measured. * $p < 0.001$ versus WKY.**

SHRSP cardiac myocytes displayed significant hypertrophy compared to WKY controls. This is characteristic of pathological concentric hypertrophy, with myocyte width increasing more than length (Heineke & Molkenin, 2006). Mean SHRSP myocyte width was ~18% longer than mean WKY myocytes width, whereas length was only ~9% longer. Although mean myocyte size was increased in SHRSP hearts, a heterogeneous population of hypertrophic and non-hypertrophic myocytes was observed. Thus, it may be that hypertrophy does not occur equally in all areas and/or layers of the ventricle.

7.3.2 Redox response to increased work intensity

The metabolic challenge of step increasing stimulation frequency was carried out in hypertrophic cardiac myocytes isolated from SHRSP hearts and non-

hypertrophic myocytes from WKY control hearts. The mean magnitude of intrinsic fluorescence response to each level of work is shown in Figure 7-2.

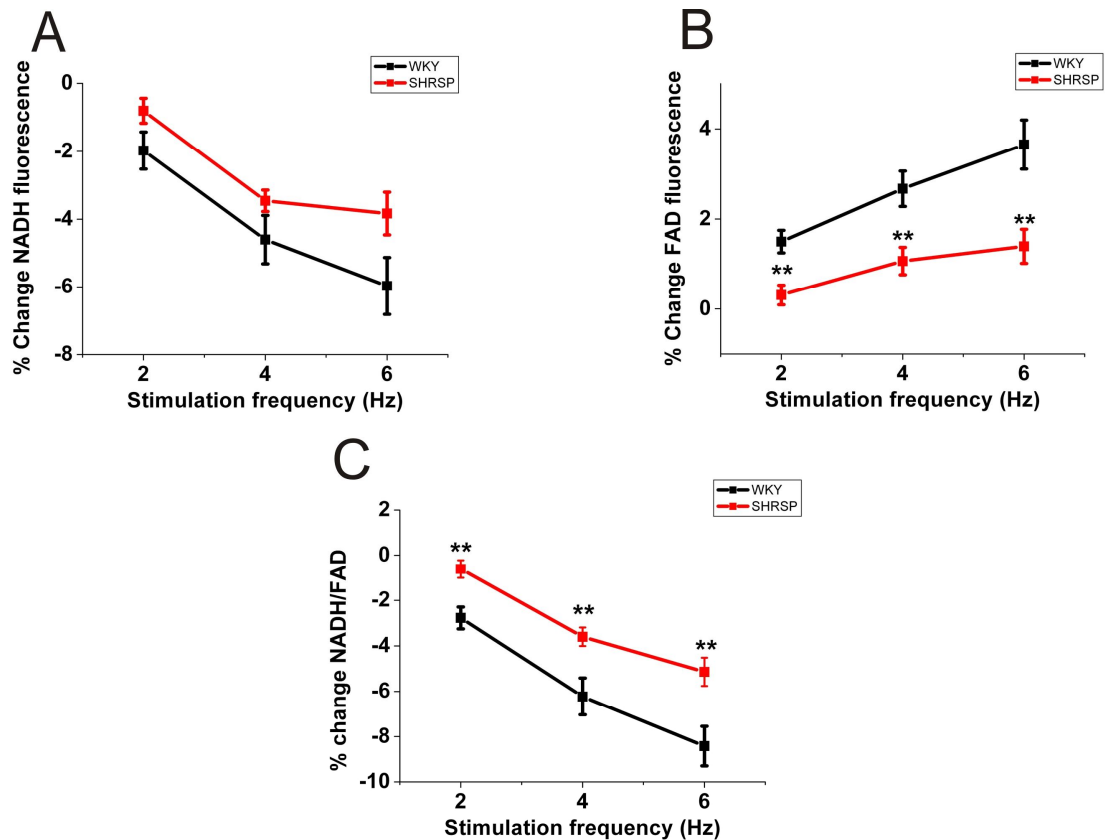


Figure 7-2 Mean effect of step increasing stimulation frequency on intrinsic fluorescence levels in cardiomyocytes isolated from WKY and SHRSP hearts

Mean percentage change in (A) NADH fluorescence (B) FAD fluorescence and (C) NADH/FAD fluorescence ratio following step increase in stimulation frequency (relative to basal fluorescence at 1Hz stimulation). Black lines represent mean effect in myocytes isolated from WKY hearts and red lines represent myocytes isolated from SHRSP hearts (n=13 for each group). ** p<0.01 versus WKY.

In both groups of cells, increasing stimulation frequency causes a small decrease in NADH fluorescence and a small increase in FAD fluorescence, indicating slight oxidation of the mitochondrial environment when work intensity is increased. This percentage change in FAD fluorescence and the NADH/FAD fluorescence ratio is significantly greater in WKY cells and indicates a bigger oxidative response. This would suggest that energy supply is better matched with demand in SHRSP hearts. However, it may also be that the level of contractile work performed by the SHRSP cardiomyocytes is not as great as that performed by WKY myocytes. The level of contractile work performed by each group of cells was therefore also examined.

7.3.3 Comparison of work performed by WKY and SHRSP cardiomyocytes

The method of interpreting work performed by the cell as the inverse of cell length is only valid when assessing different levels of work performed by the same cell. When work needs to be compared between different cells, the fact that the initial cell length at rest varies between cells (and SHRSP myocytes have been shown to be longer than WKY myocytes), means that using this method would misleadingly suggest that SHRSP cells performed less work. Instead, work was expressed as the mean cell length at each frequency in proportion to the initial cell length at rest. Smaller values represent more time spent in the contractile state and thus more work performed. The mean cell length in proportion to resting length for each rat strain at each stimulation frequency is shown in Figure 7-3.

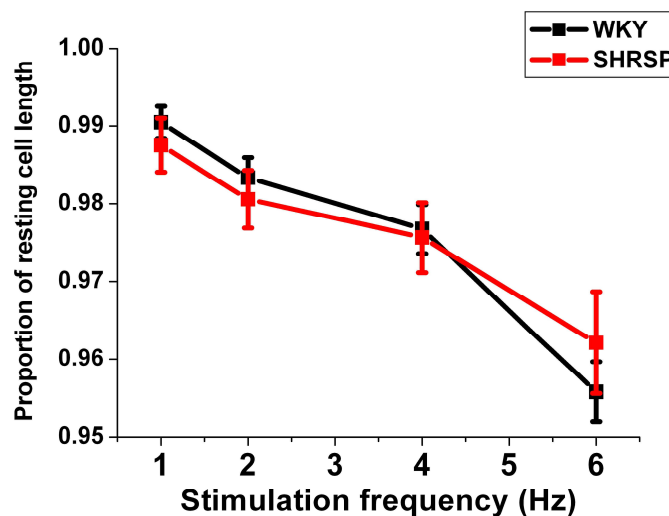


Figure 7-3 Comparison of work performed by cardiomyocytes isolated from WKY and SHRSP hearts

Mean work performed by each rat strain expressed as mean cell length in proportion to resting cell length at each stimulation frequency (WKY n=9, SHRSP n=8).

As stimulation frequency is increased, mean cell length in proportion to resting cell length decreases. This means that mean cell length gets shorter at higher pacing rates and indicates more contractile work performed. However, statistical analysis found no difference in work performed by cardiomyocytes isolated from WKY and SHRSP hearts. Thus the difference in intrinsic

fluorescence changes upon transition in workload cannot be explained by differences in the amount of work performed.

7.3.4 Analysis of rate of fluorescence change in response to transitions in workload

The rate of fluorescence change upon increase in workload was compared between cardiomyocytes from WKY and SHRSP hearts. The time taken to reach 10%, 50%, 90% and 100% fluorescence change (in terms of the NADH/FAD fluorescence ratio) when work was increased to 4Hz and 6Hz was plotted to assess if there was any difference in the profile of the fluorescence response between the two groups. The rate of recovery response when workload was reduced to 1Hz was also analysed (Figure 7-4).

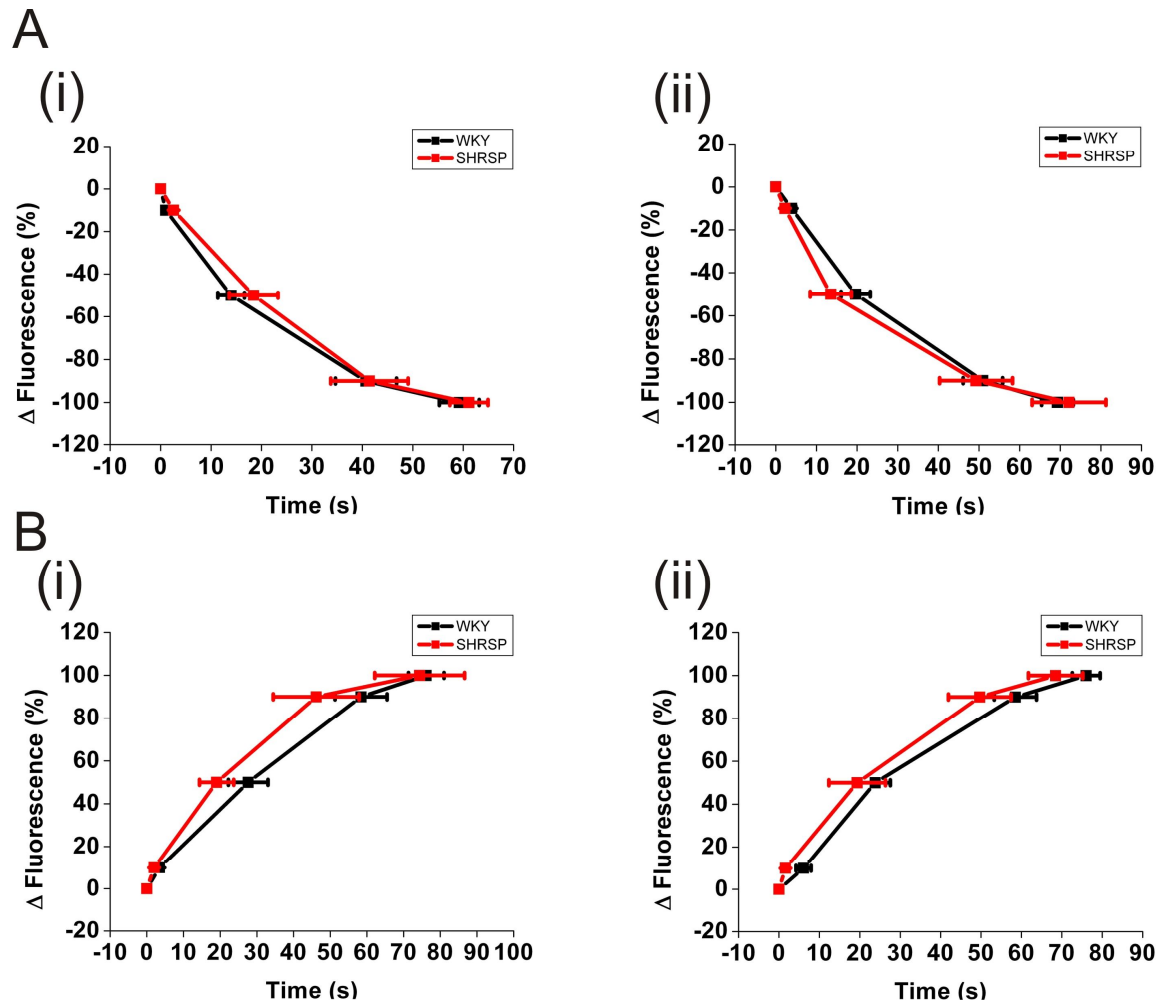


Figure 7-4 Mean time course of fluorescence changes following workload transitions in WKY and SHRSP cardiomyocytes

Panel A: Mean time taken for 0, 10, 50, 90 and 100% fluorescence changes to occur (as indicated by points) in a single stimulus train in WKY and SHRSP cardiomyocytes when pacing was increased to (i) 4Hz and (ii) 6Hz. **Panel B:** Time taken for fluorescence to recover when work intensity was reduced to 1Hz pacing from (i) 4Hz and (ii) 6Hz. WKY n=10, SHRSP n=8.

There is no difference in the rate of normalised fluorescence changes that take place in WKY and SHRSP cardiomyocytes following increase in stimulation frequency to 4Hz and 6Hz. In both groups of cells, fluorescence changes take place as soon as work intensity is increased, with no delay, and the time courses of fluorescence changes that follow are virtually identical. There was no significant difference in the rate of fluorescence recovery when workload was reduced to 1Hz pacing, although there was a trend towards faster recovery by SHRSP cells.

As the magnitude of fluorescence response differed between the two groups, the rate of fluorescence change (10-90%) was also compared with the magnitude of fluorescence change taken into account (Figure 7-5).

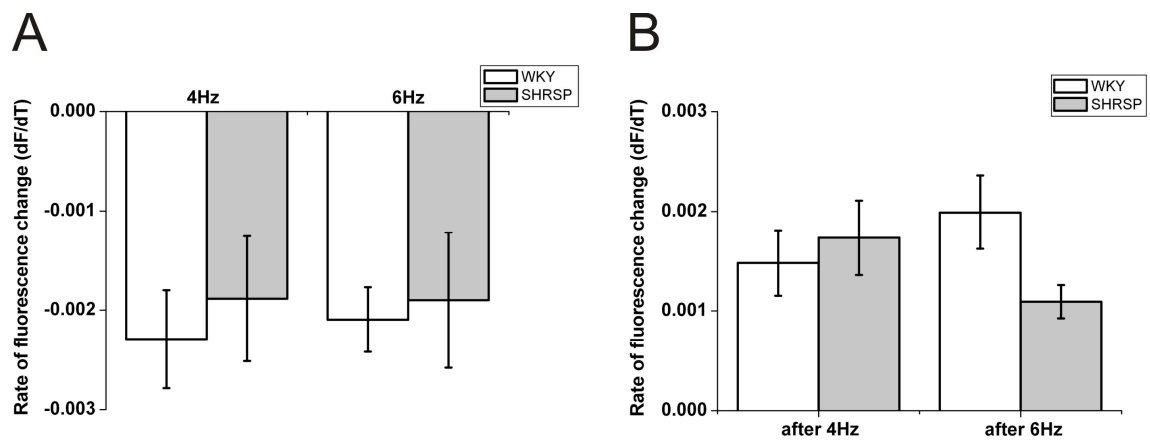


Figure 7-5 Mean rate of fluorescence changes in WKY and SHRSP cardiomyocytes following workload transitions

Panel A: Mean rate of decrease in NADH/FAD fluorescence ratio when workload is increased to 4Hz and 6Hz in WKY and SHRSP cardiomyocytes. Panel B: Mean rate of NADH/FAD fluorescence recovery when pacing is slowed to 1Hz following stimulation at 4Hz and 6Hz. WKY (open bars) n=10, SHRSP (grey bars) n=8.

Taking into account the differences in magnitude of fluorescence changes that take place during workload transitions, there is still no difference in the rate of NADH/FAD fluorescence change in WKY and SHRSP myocytes when work intensity is modified. The rate of fluorescence recovery appears to be slower in SHRSP cardiomyocytes when work intensity is reduced following pacing at 6Hz. However, this difference was found to be not significant following 2 sample t-test ($p > 0.05$).

7.4 Discussion

Investigation into the redox response to increased work intensity found that energy supply and demand matching was not impaired in cardiac myocytes isolated from hypertrophic SHRSP hearts compared to WKY controls. In fact, energy supply and demand was found to be better matched in SHRSP myocytes, with a significantly smaller mean oxidative response to increased work intensity observed in these cells compared to WKY control cells. The rate of fluorescence

changes upon transition in workload and the amount of work performed by the cells was not different between the two strains.

The reason for this unexpected observation may be that at 16 weeks the SHRSP hearts are still in a phase of compensated cardiac hypertrophy. Although mitochondrial dysfunction has been shown in some models of cardiac hypertrophy prior to the development of HF (Griffiths *et al.*, 2010), other studies have found that respiratory capacity is maintained until HF develops with impaired EF (Doenst *et al.*, 2010). Indeed, maximal respiratory capacity was significantly greater in mitochondria isolated from hypertrophic cells prior to the development of HF compared to controls. Fibres from non-failing SHR hearts also showed higher maximal respiratory flux rates and marginally higher state 3 respiration than fibres from WKY hearts (Hickey *et al.*, 2009). This suggests that the mitochondria adapt in response to pressure overload induced hypertrophy, and in the early stages mitochondrial function may even be improved. Protein expression of a number of enzymes of the TCA cycle was found to be elevated in mitochondria from failing SHR hearts (Jullig *et al.*, 2008). At this stage, the activity of these enzymes was found to be reduced. However, if in the early stages of compensated cardiac hypertrophy protein expression is increased without substantial decrease in enzyme activity, this could potentially explain why energy supply and demand are better matched in SHRSP cardiomyocytes compared to WKY controls. Indeed, SHRSP cells are working against a greater pressure than WKY cells *in vivo*, but this is not the case when the cells are isolated. Thus any compensatory increase in mitochondrial function in the SHRSP cells will give a greater respiratory reserve in the isolated cells, as observed here.

7.4.1 Comparison with guinea pig model of cardiac hypertrophy

Liu *et al.* (2008) clearly demonstrated that in their guinea pig model of pressure overload induced LVH, energy supply and demand was well matched in controls but poorly matched in hypertrophic cardiomyocytes. In hypertrophic cells, NADH fluorescence fell upon increased work intensity, with no recovery of fluorescence when returned to resting state (Figure 1-13). There are a number of reasons for the difference in response observed in this model compared to

those seen in our rat model of hypertrophy. Firstly, cells were only isolated from guinea pig hearts when a decrease in EF was observed during echocardiography, demonstrating that the heart was in a failing state. This was around 6-8 weeks after the aortic constriction procedure.

Secondly, impaired energy supply and demand matching was attributed to an increase in intracellular $[\text{Na}^+]_i$ ($[\text{Na}^+]_i$) from ~5mmol/L in control cells to ~17mmol/L in failing cells. This increase in $[\text{Na}^+]_i$ would cause the mitochondrial NCX pump to increase Ca^{2+} extrusion from the mitochondria due to the altered Na^+ gradient, thus limiting the Ca^{2+} stimulated activity of mitochondrial dehydrogenase enzymes. The result of this would be an inadequate increase in the production of reducing equivalents by the TCA cycle to match the increased rate of oxidative phosphorylation when work was increased. Consequently, net oxidation of the mitochondrial environment occurred, observed by a decrease in NADH fluorescence.

However, $[\text{Na}^+]_i$ is known to be much higher in rat cardiac myocytes, in the range of 10-15mmol/L (Bers *et al.*, 2003; Despa *et al.*, 2002; Donoso *et al.*, 1992; Shattock & Bers, 1989). The activity of the mitochondrial NCX exchanger is therefore likely to be different in rat compared to guinea pig cardiomyocytes. No reports of measured differences in $[\text{Na}^+]_i$ in WKY and SHRSP cardiac myocytes could be found in the literature, but it is unlikely that any difference between the two models would be to the same extent as in the guinea pig model of cardiac hypertrophy.

7.4.2 Comparison with rat model of cardiac hypertrophy induced by aortic banding

Brandes *et al.* (1998) also reported altered control of mitochondrial [NADH] in their model of cardiac hypertrophy induced by aortic banding in the rat. They demonstrated in isolated trabeculae that increasing work intensity from 0.25Hz to 0.5Hz, 1Hz and 2Hz resulted in a greater fall in NADH fluorescence compared to controls. The overshoot in NADH fluorescence when workload was reduced was also enhanced in the hypertrophic trabeculae, indicative of a compensatory response to this imbalance (Figure 1-14).

Experiments were performed 15-18 weeks after the banding procedure, at which point hypertension, LVH and impaired cardiac function was evident. Unlike in the SHRSP model of hypertrophy, the initial fall in NADH fluorescence upon increased work intensity was larger in the hypertrophic hearts. The impaired cardiac function following aortic banding indicates that these hearts had progressed to decompensated hypertrophy, and may explain the difference in these findings compared to our own.

Possible explanations suggested by the investigators for the larger imbalance in [NADH] in hypertrophic trabeculae include reduced NADH production, increased NADH consumption (possibly due to higher [ADP] in hypertrophic cells causing increased stimulation of oxidative phosphorylation), or a higher rate of uncoupled respiration by mitochondria in hypertrophic cells. In addition, a decrease in mitochondrial versus myofilament volume has been shown in this model of hypertrophy (Anversa *et al.*, 1979; Lund & Tomanek, 1978). Therefore, an increase in ATP consumption by myofilaments may be expected to result in a greater fall in [NADH] due to the presence of relatively fewer mitochondria.

Interestingly, NADH recovery when work intensity was decreased showed a greater overshoot in hypertrophic trabeculae compared to controls. The investigators propose that this is due to increased $[Ca^{2+}]_m$ or increased sensitivity to $[Ca^{2+}]_m$ in hypertrophic cells, causing greater stimulation of dehydrogenase enzymes and greater NADH production. However, this is in direct contrast to the explanations of Liu *et al.* (2008), who propose that stimulation of dehydrogenase enzymes by mitochondrial Ca^+ is reduced in hypertrophic hearts.

7.4.3 Comparison of intrinsic fluorescence responses to increased workload in rat and rabbit cardiac myocytes

The profile of intrinsic fluorescence response to increased work intensity showed some differences in rat and rabbit cardiomyocytes.

7.4.3.1 Differences in magnitude of oxidative response

The magnitude of response was much greater in rabbit cardiomyocytes, with a mean NADH/FAD fluorescence decrease of ~20% at the highest stimulation

frequency (3Hz) in rabbit cells compared to ~8% at the highest stimulation frequency (6Hz) in WKY rat cells. A possible reason for this disparity could be due to the amount of work performed by the cells. Most mammalian cardiac myocytes, including rabbit, demonstrate a positive force-frequency relationship due to the Bowditch effect. This means that as frequency of stimulation is increased, the force of contraction also increases. Both of these factors contribute to the amount of work performed by the cell. Conversely, cardiac myocytes from the rat tend to demonstrate a negative force-frequency relationship (Hoffman & Kelly, Jr., 1959), as was the case with the vast majority of cells isolated from rat hearts in our experiments.

The positive force-frequency relationship observed in rabbit myocardium is thought to be due to an increase in $[Na^+]_i$ that has been shown to occur as stimulation rate is increased (Cohen *et al.*, 1982). Efflux of Ca^{2+} via the sarcolemmal NCX decreases due to the reduced Na^+ gradient, and Ca^{2+} uptake by the SR via the SERCA pump predominates (Maier *et al.*, 2000). Consequently, increased SR Ca^{2+} load allows for increased systolic SR Ca^{2+} release and greater force of contraction at higher stimulation frequencies. In rat cells that exhibit a negative force frequency relationship, little or no increase in intracellular Na^+ activity was found in response to faster pacing, and the duration of the $[Ca^{2+}]_i$ transient was found to be shorter, with no change or a decrease in the amplitude of the transient (Frampton *et al.*, 1991).

Thus the negative force-frequency relationship exhibited by rat cardiac myocytes will limit the increase in contractile work performed when stimulation frequency is increased. This may help explain why the oxidative response is smaller upon increased pacing rate in rat compared to rabbit cardiac myocytes. However, it may also be that subtle differences in the control of energy metabolism exist between species, and the magnitude of oxidative response would not necessarily be expected to be the same in rat and rabbit cells. Indeed the mean initial NAD and FAD states were more oxidised in rat compared to rabbit. Mean NAD_{state} assessed by epifluorescence methods was 0.59 in rabbit myocytes compared to 0.46 in rat and mean FAD_{state} was 0.17 in rabbit myocytes compared to 0.28 in rat (WKY and SHRSP combined). It may be that the more oxidised initial redox state in rat cells influences the extent of oxidation and timescale for oxidative control mechanisms to take effect when workload is

increased. There is also some evidence to suggest that beat-to-beat mitochondrial Ca^{2+} transients may be species dependent (Griffiths, 1999), with beat-to-beat oscillations occurring in guinea pig but not rat cardiomyocytes. Beat-to-beat oscillations have also been demonstrated in rabbit cardiomyocytes (Kettlewell *et al.*, 2009; Trollinger *et al.*, 1997; Chacon *et al.*, 1996). If differences in mitochondrial Ca^{2+} uptake exist, this could mean differences in control of oxidative phosphorylation exist between species. Thus, the same response to increases in stimulation frequency would not necessarily be expected in rat and rabbit cardiac myocytes.

7.4.3.2 Delay in oxidative response following increase in work intensity

Another difference observed in the profile of oxidative responses to increased workload was that in rabbit cardiomyocytes, a clear delay of up to 25s occurred following increase in stimulation frequency before any changes in intrinsic fluorescence occurred. This was attributed to initial metabolism of PCr stores as an ATP source before changes in mitochondrial ATP production were effected. However, this delay was not present in rat cardiac myocytes (Figure 7-6).

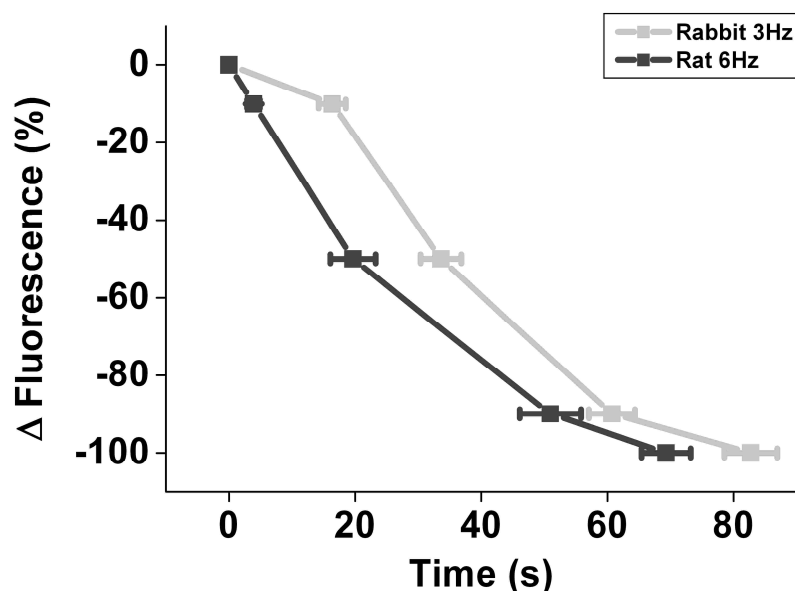


Figure 7-6 Comparison of time course of intrinsic fluorescence response to increased workload in rabbit and rat cardiomyocytes

Mean time taken for 0, 10, 50, 90 and 100% fluorescence changes to occur (as indicated by points) in a single stimulus train in rabbit and WKY rat cardiomyocytes following increase in stimulation frequency to the highest level of work (3Hz in rabbit cells, 6Hz in rat cells). Rabbit n=16, rat n=10.

The lack of delay in rat cardiac myocytes would suggest that PCr energy stores are much smaller in these cells following the isolation procedure. However, ^{31}P -NMR studies suggest that comparable levels of PCr and ATP exist in rat and rabbit hearts (Gard *et al.*, 1985; Hoerter *et al.*, 1988). Other possible reasons for the lack of delay in rat cardiomyocytes could be if irreversible depletion of PCr stores or inactivation of the CK enzyme occurs in isolated rat myocytes.

7.4.4 Problems encountered

The isolation procedure for rat cardiomyocytes produced a very low yield of live cells. The procedure itself would usually give sufficient numbers of live cells. However, these cells had very low Ca^{2+} tolerance, and increasing $[\text{Ca}^{2+}]$ led to the majority of cells dying off. This limited the number of cells that could be used for experimentation and on several occasions, no usable cells remained after Ca^{2+} had been increased to the required concentration. As a consequence, the number of cells obtained from both WKY and SHRSP hearts from which measurements could be made was very low.

Ideally, a greater number of cells would have improved the reliability of the results. However, the availability of animals and time constraints meant that this was not possible. In addition, a number of cell shortening traces could not be analysed due to the loss of edge tracking in some cells (although fluorescence measurements could still be made). This reduced the sample size for comparison of certain factors even further.

7.4.5 Conclusions

These experiments examined metabolite supply and demand matching in cardiomyocytes from the SHRSP model of cardiac hypertrophy in comparison to cardiomyocytes from control WKY hearts. Previous studies had shown that cardiac hypertrophy was associated with mitochondrial dysfunction and a decrease in mitochondria/myofibril volume ratio, as well as effects on the oxidative response to increased work intensity. It was therefore hypothesised that cardiac myocytes from SHRSP hearts would demonstrate impaired metabolite supply and demand matching compared to controls.

However, the results in fact demonstrated the opposite. SHRSP cells exhibited better metabolite supply and demand matching than WKY cells, with similar amounts of contractile work performed by both groups. This is likely to be due to the SHRSP hearts being in a state of compensated hypertrophy at 16 weeks of age when the myocytes were isolated. It is probable that at this early stage the mitochondria are still functioning well, and may even show improved function as a compensatory response to hypertrophy.

7.4.6 Future Studies

In the future these experiments could be performed in older SHRSP animals, where compensated hypertrophy has progressed to HF. This would provide a better comparison with other studies investigating the oxidative response to increased work intensity in models of cardiac hypertrophy induced by aortic constriction.

8 General Discussion

This thesis describes the use of intrinsic fluorescence measurements as a technique to study mitochondrial redox state in cardiac muscle. The intrinsic fluorescent properties of the metabolites NADH and FAD enabled redox state to be established in isolated ventricular myocytes and these measurements were also attempted in intact tissue preparations. Measurements of redox state in isolated ventricular myocytes were correlated with contractile shortening to assess the cell's ability to match metabolite supply with demand. Finally, the ability of the SHRSP model of cardiac hypertrophy to match metabolite supply with demand was examined.

8.1 Establishing mitochondrial redox state in isolated rabbit ventricular myocytes

The mitochondrial redox state was established in ventricular myocytes isolated from the rabbit heart by a standard enzymatic dissociation procedure. Characterisation of the intrinsic fluorescence arising from the cells by spectrophotometry and excitation and emission fingerprinting confirmed that the major source of fluorescence was NADH (reduced) and FAD (oxidised). This characterisation of NADH and FAD fluorescence also enabled selection of the most effective excitation wavelengths and emission filters and dichroic mirrors required to simultaneously measure fluorescence signals from both metabolites by a variety of fluorescence techniques. It was found that FAD fluorescence could not be detected by 2P-excitation methods. The reason for this is unclear, but not all fluorophores are easily excited by 2P methods (Xu *et al.*, 1996), and it may be that FAD in the cellular environment is just not as easily accessible to 2P-excitation as it is to 1P-excitation or in the pure state in solution.

Calibration of NADH and FAD fluorescence signals with the mitochondrial inhibitors FCCP and CN allowed for calculation of NAD and FAD redox states. Any fluorescence arising from non-mitochondrial sources such as lipofuscin or cytosolic NAD(P)H should not respond to the mitochondrial inhibitors to any great extent. Thus by calibrating fluorescence with FCCP and CN, the fluorescence arising from mitochondrial origins can be isolated and measurements of redox state are therefore a specific indicator of mitochondrial function.

Mitochondrial redox state of cell aggregates containing a heterogeneous population of live, dead and dying cells was established by fluorescence spectrometry. Mitochondrial redox state of individual rod-shaped cells with intact membranes was performed by fluorescence microscopy using 1P, 2P and epifluorescence methods. Using fluorescence spectrometry, NAD_{state} was calculated to be 0.33 (33% of the NAD pool in the reduced state). This value was lower than those calculated in individual cells and this difference is likely to be due to the presence of a large population of cells of varying metabolic state. As a result, the overall NAD_{state} value obtained by spectrophotometry will not be a reflection of an entirely healthy population of cells and comparable redox values to those obtained in single, healthy cells would not necessarily be expected. However, calculation of NAD_{state} in single rod shaped cells by fluorescence microscopy produced similar values by all three techniques. The range of these NAD_{state} values was between 0.57 and 0.59 (57-59% in the reduced state). FAD_{state} values established by 1P confocal and epifluorescence methods were also similar, calculated as 0.17 and 0.18 (17% and 18% of the FAD pool in the oxidised state, i.e. 83% and 82% in the reduced state). The similarity of the values obtained for NAD_{state} and FAD_{state} by different fluorescence methods confirmed the reproducibility and reliability of the technique to establish mitochondrial redox state. These values were also similar to those quoted in the literature (Brandes & Bers, 1996; Duchen & Biscoe, 1992; Esumi *et al.*, 1991; Eng *et al.*, 1989).

8.2 Establishing mitochondrial redox state in intact tissue preparations from rabbit heart

Similar measurements of mitochondrial redox state were attempted in the isolated LV wedge preparation and the Langendorff perfused whole heart using 2P excitation fluorescence microscopy. However, it was found that these measurements were greatly complicated by movement of the preparation and the inner filter effect produced in the thick tissue preparation by other cellular constituents with light absorption properties. In addition, no response to FCCP could be elicited in the tissue, and thus calculations of NAD_{state} were not possible. We were therefore unable to compare mitochondrial redox state in intact tissue and isolated cells to assess if the enzymatic digestion procedure has

a detrimental effect on mitochondrial function. However, if the mean effect of CN in the tissue preparations was corrected for movement and the mean inner filter effect in the LV was taken into account, a similar mean magnitude of increase in fluorescence would result in both tissue and isolated cell preparations (~38% and 41% increase respectively).

8.3 Mitochondrial redox responses to increased work intensity in isolated rabbit ventricular myocytes

Real time monitoring of NADH and FAD fluorescence signals in synchrony with measurements of contractile work enabled energy supply and demand matching to be assessed in ventricular myocytes. The ability of the mitochondria to match production of reducing equivalents through the reactions of the TCA cycle with their consumption by oxidative phosphorylation is crucial in order to maintain an adequate redox potential to continue ATP production at the required rate.

It was found that step increasing work intensity by increasing stimulation frequency resulted in oxidation of the cellular environment. This was demonstrated by a decrease in NADH fluorescence and a simultaneous increase in FAD fluorescence. The magnitude of the oxidative response was related to the intensity of work performed, with the largest responses taking place at the highest work intensities. This indicates that the production of reducing equivalents by the TCA cycle was not well matched to the increased rate of their consumption in order to produce the required supply of ATP at higher workloads. However, complete oxidation of the cellular environment did not take place and NADH and FAD signals reached an essentially steady state whilst workload was still high. This may either be due to the rate of oxidative phosphorylation reaching a steady state, or may be due to the presence of some sort of control mechanism, increasing the rate of TCA cycle reactions in order to maintain redox potential. It is thought that this may be due to increased uptake of Ca^{2+} by the mitochondria, stimulating a number of dehydrogenase enzymes and increasing the rate of NADH and FADH_2 production. When the intensity of work was reduced, the oxidative status of the cell recovered to initial levels. The reversibility of this response demonstrates that the fluorescence changes are

caused by a temporary metabolite imbalance and that the cell is not permanently damaged by the experimental manipulation.

Prolonged periods of oxidation may have detrimental effects on the cell, as NADH plays a role in antioxidant control mechanisms through the maintenance of glutathione in the reduced state via NADPH (Section 1.6.2). A fall in [NADH] and sustained periods of mitochondrial oxidation could therefore result in an increase in oxidative stress and the harmful effects associated with this (Knopp *et al.*, 2009; Liu & O'Rourke, 2009; Heinzl *et al.*, 2006).

No consistent oxidative response to increased work intensity has been reported in the literature. However, the results presented in this thesis are in closest agreement with those of Heinzl *et al.* (2006), White & Wittenberg (2000), Ashruf *et al.* (1995), White & Wittenberg (1993) and Chapman (1972). Previous studies looking at the oxidative response to transitions in workload only measured changes in NADH fluorescence. However, in this study, fluorescence measurements were optimised to monitor both NADH and FAD, and this has the additional advantage of enabling a fluorescence ratio of the signals to be taken. As a result, the signal to noise ratio was increased and the effects of movement and other artefacts associated with single wavelength measurements were minimised.

8.4 Mitochondrial redox responses to increased work intensity in cardiac myocytes from the SHRSP model of cardiac hypertrophy compared to WKY controls

The mitochondrial redox response to increased work intensity was also investigated in the SHRSP genetic model of hypertension. Rats of this strain demonstrate clear cardiac hypertrophy as a consequence of sustained pressure overload. It was hypothesised that cardiac myocytes from these animals would show impaired energy supply and demand matching for a number of reasons. Firstly, mitochondrial dysfunction has been reported in cardiac myocytes from SHRSP rats (Chen *et al.*, 1995; Tokoro *et al.*, 1996). Secondly, changes in the oxidative response to increased work intensity have been shown in models of cardiac hypertrophy induced by aortic banding (Brandes *et al.*, 1998; Liu &

O'Rourke, 2008). Finally, the reduced mitochondria/myofibril volume ratio reported in both genetic and experimentally induced models of cardiac hypertrophy (Anversa *et al.*, 1979; Lund & Tomanek, 1978) would suggest that energy supply and demand matching would be detrimentally affected in cardiac hypertrophy due to the presence of relatively fewer mitochondria.

However, it was found that this was not the case and indeed the mitochondrial oxidative response to increased work intensity was less in SHRSP rat hearts compared to WKY controls, indicating improved matching of metabolite supply to demand. This is most probably due to the SHRSP hearts being in a state of compensated hypertrophy when the cells were isolated at 16 weeks of age. In this state, mitochondrial dysfunction may not have yet occurred, and any changes in mitochondrial function may actually be a compensatory improvement.

8.5 Further work

The results of this investigation could be further developed to examine the cellular mechanisms of matching metabolic supply with demand. In particular, simultaneous measurements of redox state with $[Ca^{2+}]_m$ would provide more insight into the role of mitochondrial Ca^{2+} uptake in regulating mitochondrial metabolism. This could be achieved using a targeted mitochondrial Ca^{2+} probe developed in our lab (Kettlewell *et al.*, 2009), although currently this probe is transfected into freshly isolated myocytes and cultured for 48 hours before use. This situation is not ideal, as by this stage mitochondrial function may have deteriorated. Alternatively, mitochondrial Ca^{2+} measurements could be made with synthetic fluorescent Ca^{2+} indicators such as Rhod-2, Indo-1 or Fluo-3, although precautions would need to be taken when using these dyes to avoid contamination with the cytosolic Ca^{2+} signal. In addition, simultaneous measurements of redox state with mitochondrial membrane potential or O_2 consumption would add another dimension to the measurements and would provide a clearer picture of the mitochondrial functional changes occurring during transitions in workload. Mitochondrial membrane potential can be measured using fluorescent indicators such as TMRM and TMRE (but should be used at very low concentrations to avoid affecting mitochondrial function

(Scaduto & Grotyohann, 1999)). However, real time measurements of O_2 consumption in isolated single cells are extremely difficult to achieve.

Experiments examining the effects of cardiac hypertrophy on energy supply and demand matching were performed in hearts in a state of compensated hypertrophy. These experiments could be repeated in older animals, where progression to decompensated hypertrophy and HF has taken place. Furthermore, other models of HF could be used, such as the rabbit model of myocardial infarction induced by coronary artery ligation. This would help improve our understanding of how energy metabolism is affected in HF.

8.6 Summary of conclusions

The majority of intrinsic fluorescence from isolated heart cells could be attributed to the metabolic coenzymes NADH and FAD. Metabolic inhibition enabled modulation of the oxidative status of these enzymes, allowing for calculation of relative redox state in isolated ventricular myocytes. However, similar measurements of mitochondrial redox state could not be made in intact tissue preparations, mainly due to difficulties directing mitochondrial inhibitor to the area of tissue being imaged and to the inner filter effect that exists when thicker specimens are imaged. Simultaneous measurements of redox status and fractional shortening in field-stimulated cells have demonstrated that rabbit ventricular myocytes become oxidised when work rates are increased, suggesting a transient mismatch between metabolite supply and demand. Cardiac myocytes isolated from hypertrophic SHRSP hearts did not demonstrate impaired matching of metabolite supply with demand compared to WKY control cardiomyocytes and in fact, smaller oxidative responses were observed in these cells. However, these hearts were still in a state of compensated hypertrophy and at this stage it may be too early for any deleterious effects on mitochondrial function to have taken place.

References

- Akki, A., Smith, K., & Seymour, A. M. L. (2008). Compensated cardiac hypertrophy is characterised by a decline in palmitate oxidation. *Molecular and Cellular Biochemistry* **311**, 215-224.
- Aldakkak, M., Stowe, D. F., Heisner, J. S., Spence, M., & Camara, A. K. S. (2008). Enhanced Na^+/H^+ exchange during ischemia and reperfusion impairs mitochondrial bioenergetics and myocardial function. *Journal of Cardiovascular Pharmacology* **52**, 236-244.
- Aldakkak, M., Stowe, D. F., Lesnefsly, E. J., Heisner, J. S., Chen, Q., & Camara, A. K. S. (2009). Modulation of mitochondrial bioenergetics in the isolated guinea pig beating heart by potassium and lidocaine cardioplegia: Implications for cardioprotection. *Journal of Cardiovascular Pharmacology* **54**, 298-309.
- Alexander, K. M. (1975). Biochemical studies on mammalian cardiac muscles: I. distribution pattern of myoglobin in different chambers of the heart of some mammals. *Tower International Technomedical - Journal of Life sciences* **5**, 61-64.
- Amos, W. B. (2000). Instruments for fluorescence imaging. In *Protein Localization by Fluorescence Microscopy*, ed. Allan, V. J., pp. 67-108. Oxford University Press.
- Anversa, P., Olivetti, G., Melissari, M., & Loud, A. V. (1979). Morphometric study of myocardial hypertrophy induced by abdominal aortic-stenosis. *Laboratory Investigation* **40**, 341-349.
- Arribas, S. M., Costa, R., Salomone, S., Morel, N., Godfraind, T., & McGrath, J. C. (1999). Functional reduction and associated cellular rearrangement in SHRSP rat basilar arteries are affected by salt load and calcium antagonist treatment. *Journal of Cerebral Blood Flow & Metabolism* **19**, 517-527.
- Ashruf, J. F., Coremans, J. M., Bruining, H. A., & Ince, C. (1995). Increase of cardiac work is associated with decrease of mitochondrial NADH. *American Journal of Physiology-Heart and Circulatory Physiology* **269**, H856-H862.
- Avi-Dor, Y., Olson, J. M., Doherty, M. D., & Kaplan, N. O. (1962). Fluorescence of pyridine nucleotides in mitochondria. *Journal of Biological Chemistry* **237**, 2377-2383.
- Baker, L. C., London, B., Choi, B. R., Koren, G., & Salama, G. (2000). Enhanced dispersion of repolarization and refactoriness in transgenic mouse hearts promotes reentrant ventricular tachycardia. *Circulation Research* **86**, 396-407.

- Balaban, R. S. (1990). Regulation of oxidative phosphorylation in the mammalian cell. *American Journal of Physiology - Cell Physiology* **258**, C377-C389.
- Balaban, R. S. (2009). Domestication of the cardiac mitochondrion for energy conversion. *Journal of Molecular and Cellular Cardiology* **46**, 832-841.
- Barger, P. M. & Kelly, D. P. (2000). PPAR signaling in the control of cardiac energy metabolism. *Trends in Cardiovascular Medicine* **10**, 238-245.
- Barlow, C. H. & Chance, B. (1976). Ischemic areas in perfused rat hearts: measurement by NADH fluorescence photography. *Science* **193**, 909-910.
- Barth, E., Stämmler, G., Speiser, B., & Schaper, J. (1992). Ultrastructural quantitation of mitochondria and myofilaments in cardiac muscle from 10 different animal species including man. *Journal of Molecular and Cellular Cardiology* **24**, 669-681.
- Beer, M., Seyfarth, T., Sandstede, J. o., Landschutz, W., Lipke, C., Kostler, H., von Kienlin, M., Harre, K., Hahn, D., & Neubauer, S. (2002). Absolute concentrations of high-energy phosphate metabolites in normal, hypertrophied, and failing human myocardium measured noninvasively with ³¹P-SLOOP magnetic resonance spectroscopy. *Journal of the American College of Cardiology* **40**, 1267-1274.
- Bell, C. J., Bright, N. A., Rutter, G. A., & Griffiths, E. J. (2006). ATP Regulation in Adult Rat Cardiomyocytes: Time resolved decoding of rapid mitochondrial calcium spiking imaged with targeted photoproteins. *Journal of Biological Chemistry* **281**, 28058-28067.
- Berg, J. M., Tymoczko, J. L., & Stryer, L. (2006). Oxidative phosphorylation. In *Biochemistry*, ed. W.H.Freeman & Co, pp. 502-540.
- Bers, D. M. (2002). Cardiac excitation-contraction coupling. *Nature* **415**, 198-205.
- Bers, D. M., Barry, W. H., & Despa, S. (2003). Intracellular Na⁺ regulation in cardiac myocytes. *Cardiovascular Research* **57**, 897-912.
- Blinova, K., Carroll, S., Bose, S., Smirnov, A. V., Harvey, J. J., Knutson, J. R., & Balaban, R. S. (2005). Distribution of mitochondrial NADH fluorescence lifetimes: steady-state kinetics of matrix NADH interactions. *Biochemistry* **44**, 2585-2594.
- Bowen, W. J. (1949). The absorption spectra and extinction coefficients of myoglobin. *Journal of Biological Chemistry* **179**, 235-245.

- Brandes, R. & Bers, D. M. (1996). Increased work in cardiac trabeculae causes decreased mitochondrial NADH fluorescence followed by slow recovery. *Biophysical Journal* **71**, 1024-1035.
- Brandes, R., Figueredo, V. M., Camacho, S. A., & Weiner, M. W. (1994). Compensation for changes in tissue light absorption in fluorometry of hypoxic perfused rat hearts. *American Journal of Physiology-Heart and Circulatory Physiology* **266**, H2554-H2567.
- Brandes, R. & Bers, D. M. (1997). Intracellular Ca^{2+} increases the mitochondrial NADH concentration during elevated work in intact cardiac muscle. *Circulation Research* **80**, 82-87.
- Brandes, R. & Bers, D. M. (1999). Analysis of the mechanisms of mitochondrial NADH regulation in cardiac trabeculae. *Biophysical Journal* **77**, 1666-1682.
- Brandes, R. & Bers, D. M. (2002). Simultaneous measurements of mitochondrial NADH and Ca^{2+} during increased work in intact rat heart trabeculae. *Biophysical Journal* **83**, 587-604.
- Brandes, R., Maier, L. S., & Bers, D. M. (1998). Regulation of mitochondrial [NADH] by cytosolic [Ca^{2+}] and work in trabeculae from hypertrophic and normal rat hearts. *Circulation Research* **82**, 1189-1198.
- Brennan, J. P., Southworth, R., Medina, R. A., Davidson, S. M., Duchon, M. R., & Shattock, M. J. (2006). Mitochondrial uncoupling, with low concentration FCCP, induces ROS-dependent cardioprotection independent of KATP channel activation. *Cardiovascular Research* **72**, 313-321.
- Bugger, H., Schwarzer, M., Chen, D., Schrepper, A., Amorim, P. A., Schoepe, M., Nguyen, T. D., Mohr, F. W., Khalimonchuk, O., Weimer, B. C., & Doenst, T. (2010). Proteomic remodelling of mitochondrial oxidative pathways in pressure overload-induced heart failure. *Cardiovascular Research* **85**, 376-384.
- Centonze, V. E. & White, J. G. (1998). Multiphoton excitation provides optical sections from deeper within scattering specimens than confocal imaging. *Biophysical Journal* **75**, 2015-2024.
- Chacon, E., Lemasters, J. J., Ohata, H., Harper, I. S., Trollinger, D. R., & Herman, B. (1996). Mitochondrial free calcium transients during excitation-contraction coupling in rabbit cardiac myocytes. *FEBS Letters* **382**, 31-36.
- Chance, B. (1952). Spectra and reaction kinetics of respiratory pigments of homogenized and intact cells. *Nature* **169**, 215-221.

Chance, B., Jöbsis, F., Schoener, B., & Cohen, P. (1962). Intracellular oxidation-reduction states in vivo. *Science* **137**, 499-508.

Chance, B., Salkovitz, I. A., & Kovach, A. G. (1972). Kinetics of mitochondrial flavoprotein and pyridine nucleotide in perfused heart. *American Journal of Physiology - Legacy* **223**, 207-218.

Chance, B. & Schoener, B. (1962). Correlation of oxidation-reduction changes of intracellular reduced pyridine nucleotide and changes in electroencephalogram of rat in anoxia. *Nature* **195**, 956-958.

Chance, B., Schoener, B., Oshino, R., Itshak, F., & Nakase, Y. (1979). Oxidation-reduction ratio studies of mitochondria in freeze-trapped samples - NADH and flavoprotein fluorescence signals. *Journal of Biological Chemistry* **254**, 4764-4771.

Chance, B. (1954). Spectrophotometry of intracellular respiratory pigments. *Science* **120**, 767-775.

Chance, B. & Baltscheffsky, H. (1958). Respiratory enzymes in oxidative phosphorylation. VII. Binding of intramitochondrial reduced pyridine nucleotide. *Journal of Biological Chemistry* **233**, 736-739.

Chance, B. & Williams, G. R. (1955a). Respiratory enzymes in oxidative phosphorylation: I. Kinetics of oxygen utilization. *Journal of Biological Chemistry* **217**, 383-394.

Chance, B. & Williams, G. R. (1955b). Respiratory enzymes in oxidative phosphorylation: II. Difference spectra. *Journal of Biological Chemistry* **217**, 395-408.

Chance, B. & Williams, G. R. (1955c). Respiratory enzymes in oxidative phosphorylation: III. The steady state. *Journal of Biological Chemistry* **217**, 409-428.

Chance, B. & Williams, G. R. (1955d). Respiratory enzymes in oxidative phosphorylation: IV The respiratory chain. *Journal of Biological Chemistry* **217**, 429-438.

Chance, B., Williams, G. R., Holmes, W. F., & Higgins, J. (1955). Respiratory enzymes in oxidative phosphorylation: V. A mechanism for oxidative phosphorylation. *Journal of Biological Chemistry* **217**, 439-452.

Chapman, J. B. (1972). Fluorometric studies of oxidative metabolism in isolated papillary muscle of the rabbit. *Journal of General Physiology* **59**, 135-154.

Chapman, R. A., Rodrigo, G. C., Tunstall, J., Yates, R. J., & Busselen, P. (1984). Calcium paradox of the heart: a role for intracellular sodium ions. *American Journal of Physiology - Heart and Circulatory Physiology* **247**, H874-H879.

Chapman, R. A. & Tunstall, J. (1987). The calcium paradox of the heart. *Progress in Biophysics and Molecular Biology* **50**, 67-96.

Chen, L. Y., Tian, X. O., & Song, L. F. (1995). Biochemical and biophysical characteristics of mitochondria in the hypertrophic hearts from hypertensive rats. *Chinese Medical Journal* **108**, 361-366.

Chen, X., Cordes, J. S., Bradley, J. A., Sun, Z., & Zhou, J. (2006). Use of arterially perfused rabbit ventricular wedge in predicting arrhythmogenic potentials of drugs. *Journal of Pharmacological and Toxicological Methods* **54**, 261-272.

Chorvat, D. & Chorvatova, A. (2006). Spectrally resolved time-correlated single photon counting: a novel approach for characterization of endogenous fluorescence in isolated cardiac myocytes. *European Biophysics Journal with Biophysics Letters* **36**, 73-83.

Chorvat, D., Bassien-Capsa, V., Cagalinec, M., Kirchnerova, J., Mateasik, A., Comte, B., & Chorvatova, A. (2004). Mitochondrial autofluorescence induced by visible light in single rat cardiac myocytes studied by spectrally resolved confocal microscopy. *Laser Physics* **14**, 220-230.

Chorvat, D., Kirchnerova, J., Cagalinec, M., Smolka, J., Mateasik, A., & Chorvatova, A. (2005). Spectral unmixing of flavin autofluorescence components in cardiac myocytes. *Biophysical Journal* **89**, L55-L57.

Christe, M. E. & Rodgers, R. L. (1994). Altered glucose and fatty-acid oxidation in hearts of the spontaneously hypertensive rat. *Journal of Molecular and Cellular Cardiology* **26**, 1371-1375.

Cohen, C. J., Fozzard, H. A., & Sheu, S. S. (1982). Increase in intracellular sodium ion activity during stimulation in mammalian cardiac muscle. *Circulation Research* **50**, 651-662.

Cortassa, S., Aon, M. A., O'Rourke, B., Jacques, R., Tseng, H. J., Marban, E., & Winslow, R. L. (2006). A computational model integrating electrophysiology, contraction, and mitochondrial bioenergetics in the ventricular myocyte. *Biophysical Journal* **91**, 1564-1589.

Cunningham, M. L., Johnson, J. S., Giovanazzi, S. M., & Peak, M. J. (1985). Photosensitized production of superoxide anion by monochromatic (290-405 nm)

ultraviolet-irradiation of NADH and NADPH coenzymes. *Photochemistry and Photobiology* **42**, 125-128.

D'Autreaux, B. & Toledano, M. B. (2007). ROS as signalling molecules: mechanisms that generate specificity in ROS homeostasis. *Nature Reviews Molecular Cell Biology* **8**, 813-824.

Das, A. M. & Harris, D. A. (1990). Control of mitochondrial ATP synthase in heart-cells - inactive to active transitions caused by beating or positive inotropic agents. *Cardiovascular Research* **24**, 411-417.

Davila-Roman, V., Vedala, G., Herrero, P., las Fuentes, L., Rogers, J. G., Kelly, D. P., & Gropler, R. J. (2002). Altered myocardial fatty acid and glucose metabolism in idiopathic dilated cardiomyopathy. *Journal of the American College of Cardiology* **40**, 271-277.

Deluca, H. F. & Engstrom, G. W. (1961). Calcium uptake by rat kidney mitochondria. *Proceedings of the National Academy of Sciences of the United States of America* **47**, 1744-1750.

Denk, W., Piston, D. W., & Webb, W. W. (2006). Multi-photon molecular excitation in laser-scanning microscopy. In *Handbook of Biological Confocal Microscopy*, ed. Pawley, J. B., pp. 535-549. Springer, New York.

Denk, W., Strickler, J. H., & Webb, W. W. (1990). Two-photon laser scanning fluorescence microscopy. *Science* **248**, 73-76.

Denton, R. M., Randle, P. J., & Martin, B. R. (1972). Stimulation by calcium-ions of pyruvate dehydrogenase phosphate phosphatase. *Biochemical Journal* **128**, 161-163.

Denton, R. M., Richards, D. A., & Chin, J. G. (1978). Calcium-ions and the regulation of NAD⁺-linked isocitrate dehydrogenase from the mitochondria of rat-heart and other tissues. *Biochemical Journal* **176**, 899-906.

Despa, S., Islam, M. A., Pogwizd, S. M., & Bers, D. M. (2002). Intracellular [Na⁺] and Na⁺ pump rate in rat and rabbit ventricular myocytes. *Journal of Physiology* **539**, 133-143.

Dhalla, N. S. (1969). Excitation-contraction coupling in heart .1. Comparison of calcium uptake by sarcoplasmic reticulum and mitochondria of rat heart. *Archives Internationales de Physiologie et de Biochimie* **77**, 916-934.

- Dixon, M., Hill, R., & Keilin, D. (1931). The absorption spectrum of the component c of cytochrome. *Proceedings of the Royal Society of London, Series B* **109**, 29-34.
- Doenst, T., Pytel, G., Schreppe, A., Amorim, P., Färber, G., Shingu, Y., Mohr, F. W., & Schwarzer, M. (2010). Decreased rates of substrate oxidation ex vivo predict the onset of heart failure and contractile dysfunction in rats with pressure overload. *Cardiovascular Research* **86**, 461-470.
- Dominiczak, A. F., Devlin, A. M., Lee, W. K., Anderson, N. H., Bohr, D. F., & Reid, J. L. (1996). Vascular smooth muscle polyploidy and cardiac hypertrophy in genetic hypertension. *Hypertension* **27**, 752-759.
- Donoso, P., Mill, J. G., O'Neill, S. C., & Eisner, D. A. (1992). Fluorescence measurements of cytoplasmic and mitochondrial sodium concentration in rat ventricular myocytes. *Journal of Physiology* **448**, 493-509.
- Duchen, M. R. & Biscoe, T. J. (1992). Mitochondrial function in type I cells isolated from rabbit arterial chemoreceptors. *Journal of Physiology* **450**, 13-31.
- Duchen, M. R., Surin, A., & Jacobson, J. (2003). Imaging mitochondrial function in intact cells. *Methods in Enzymology* **361**, 353-389.
- Duchen, M. R., Leyssens, A., & Crompton, M. (1998). Transient mitochondrial depolarizations reflect focal sarcoplasmic reticular calcium release in single rat cardiomyocytes. *Journal of Cell Biology* **142**, 975-988.
- Duysens, L. N. M. & Ames, J. (1957). Fluorescence spectrophotometry of reduced phosphopyridine nucleotide in intact cells in the near-ultraviolet and visible region. *Biochimica et Biophysica Acta* **24**, 19-26.
- Eijgelshoven, M. H., van Beek, J. H., Mottet, I., Nederhoff, M. G., van Echteld, C. J., & Westerhof, N. (1994). Cardiac high-energy phosphates adapt faster than oxygen consumption to changes in heart rate. *Circulation Research* **75**, 751-759.
- Elliott, A. C., Smith, G. L., & Allen, D. G. (1994). The metabolic consequences of an increase in the frequency of stimulation in isolated ferret hearts. *The Journal of Physiology* **474**, 147-159.
- Elrod, J. W., Wong, R., Mishra, S., Vagnozzi, R. J., Sakthivel, B., Goonasekera, S. A., Karch, J., Gabel, S., Farber, J., Force, T., Heller Brown, J., Murphy, E., & Molkentin, J. D. (2010). Cyclophilin D controls mitochondrial pore-dependent Ca²⁺ exchange, metabolic flexibility, and propensity for heart failure in mice. *The Journal of Clinical Investigation* **120**, 3680-3687.

- Emaus, R. K., Grunwald, R., & Lemasters, J. J. (1986). Rhodamine 123 as a probe of transmembrane potential in isolated rat-liver mitochondria: spectral and metabolic properties. *Biochimica et Biophysica Acta - Bioenergetics* **850**, 436-448.
- Eng, J., Lynch, R. M., & Balaban, R. S. (1989). Nicotinamide adenine-dinucleotide fluorescence spectroscopy and imaging of isolated cardiac myocytes. *Biophysical Journal* **55**, 621-630.
- Estabrook, R. W. (1962). Fluorometric measurement of reduced pyridine nucleotide in cellular and subcellular particles. *Analytical Biochemistry* **4**, 231-245.
- Esumi, K., Nishida, M., Shaw, D., Smith, T. W., & Marsh, J. D. (1991). NADH measurements in adult rat myocytes during simulated ischemia. *American Journal of Physiology - Heart and Circulatory Physiology* **260**, H1743-H1752.
- Fedorov, V. V., Lozinsky, I. T., Sosunov, E. A., Anyukhovskiy, E. P., Rosen, M. R., Balke, C. W., & Efimov, I. R. (2007). Application of blebbistatin as an excitation-contraction uncoupler for electrophysiologic study of rat and rabbit hearts. *Heart Rhythm* **4**, 619-626.
- Fralix, T. A., Heineman, F. W., & Balaban, R. S. (1990). Effects of tissue absorbance on NAD(P)H and Indo-1 fluorescence from perfused rabbit hearts. *FEBS Letters* **262**, 287-292.
- Frampton, J. E., Harrison, S. M., Boyett, M. R., & Orchard, C. H. (1991). Ca^{2+} and Na^{+} in rat myocytes showing different force-frequency relationships. *American Journal of Physiology - Cell Physiology* **261**, C739-C750.
- Frolkis, R. A. (1967). Changes in myoglobin content in heart in experimental myocardial infarction and atherosclerosis. *Bulletin of Experimental Biology and Medicine, Ussr* **64**, 1054-&.
- Fujii, F., Nodasaka, Y., Nishimura, G., & Tamura, M. (2004). Anoxia induces matrix shrinkage accompanied by an increase in light scattering in isolated brain mitochondria. *Brain Research* **999**, 29-39.
- Funada, J., Betts, T. R., Hodson, L., Humphreys, S. M., Timperley, J., Frayn, K. N., & Karpe, F. (2009). Substrate utilization by the failing human heart by direct quantification using arterio-venous blood sampling. *PLoS ONE* **4**, e7533.
- Gao, G., Johansson, U., Rundquist, I., & Öllinger, K. (1994). Lipofuscin-induced autofluorescence of living neonatal rat cardiomyocytes in culture. *Mechanisms of Ageing and Development* **73**, 79-86.

Gard, J. K., Kichura, G. M., Ackerman, J. J., Eisenberg, J. D., Billadello, J. J., Sobel, B. E., & Gross, R. W. (1985). Quantitative ^{31}P nuclear magnetic resonance analysis of metabolite concentrations in Langendorff-perfused rabbit hearts. *Biophysical Journal* **48**, 803-813.

Garnier, A., Fortin, D., Deloménie, C., Momken, I., Veksler, V., & Ventura-Clapier, R. (2003). Depressed mitochondrial transcription factors and oxidative capacity in rat failing cardiac and skeletal muscles. *Journal of Physiology* **551**, 491-501.

Griffiths, E. J. (1999). Species dependence of mitochondrial calcium transients during excitation-contraction coupling in isolated cardiomyocytes. *Biochemical and Biophysical Research Communications* **263**, 554-559.

Griffiths, E. J., Lin, H., & Suleiman, M. S. (1998). NADH fluorescence in isolated guinea-pig and rat cardiomyocytes exposed to low or high stimulation rates and effect of metabolic inhibition with cyanide. *Biochemical Pharmacology* **56**, 173-179.

Griffiths, E. J. & Rutter, G. A. (2009). Mitochondrial calcium as a key regulator of mitochondrial ATP production in mammalian cells. *Biochimica et Biophysica Acta - Bioenergetics* **1787**, 1324-1333.

Griffiths, E. J., Wei, S. K., Haigney, M. C. P., Ocampo, C. J., Stern, M. D., & Silverman, H. S. (1997). Inhibition of mitochondrial calcium efflux by clonazepam in intact single rat cardiomyocytes and effects on NADH production. *Cell Calcium* **21**, 321-329.

Griffiths, E. R., Friehs, I., Scherr, E., Poutias, D., McGowan, F. X., & del Nido, P. J. (2010). Electron transport chain dysfunction in neonatal pressure-overload hypertrophy precedes cardiomyocyte apoptosis independent of oxidative stress. *Journal of Thoracic and Cardiovascular Surgery* **139**, 1609-1617.

Gunter, T. E., Gunter, K. K., Sheu, S. S., & Gavin, C. E. (1994). Mitochondrial calcium transport: physiological and pathological relevance. *American Journal of Physiology - Cell Physiology* **267**, C313-C339.

Harrison, G. J., van Wijhe, M. H., de Groot, B., Dijk, F. J., & van Beek, J. H. (1999). CK inhibition accelerates transcytosolic energy signaling during rapid workload steps in isolated rabbit hearts. *American Journal of Physiology - Heart and Circulatory Physiology* **276**, H134-H140.

Heineke, J. & Molkentin, J. D. (2006). Regulation of cardiac hypertrophy by intracellular signalling pathways. *Nature Reviews Molecular Cell Biology* **7**, 589-600.

Heineman, F. W. & Balaban, R. S. (1993). Effects of afterload and heart rate on NAD(P)H redox state in the isolated rabbit heart. *American Journal of Physiology - Heart and Circulatory Physiology* **264**, H433-H440.

Heinzel, F. R., Luo, Y., Dodoni, G., Boengler, K., Petrat, F., Di Lisa, F., de Groot, H., Schulz, R., & Heusch, G. (2006). Formation of reactive oxygen species at increased contraction frequency in rat cardiomyocytes. *Cardiovascular Research* **71**, 374-382.

Hickey, A. J. R., Chai, C. C., Choong, S. Y., Freitas Costa, S., Skea, G. L., Phillips, A. R. J., & Cooper, G. J. S. (2009). Impaired ATP turnover and ADP supply depress cardiac mitochondrial respiration and elevate superoxide in nonfailing spontaneously hypertensive rat hearts. *American Journal of Physiology - Cell Physiology* **297**, C766-C774.

Hoenicke, E. M. & Damiano, R. J. (2001). Superior 12-hour heart preservation with pinacidil hyperpolarizing solution compared to University of Wisconsin solution. *Journal of Heart and Lung Transplantation* **20**, 1106-1114.

Hoerter, J. A., Lauer, C., Vassort, G., & Gueron, M. (1988). Sustained function of normoxic hearts depleted in ATP and phosphocreatine: a ³¹P-NMR study. *American Journal of Physiology - Cell Physiology* **255**, C192-C201.

Hoffman, B. F. & Kelly, J. J., Jr. (1959). Effects of rate and rhythm on contraction of rat papillary muscle. *American Journal of Physiology - Legacy* **197**, 1199-1204.

Huang, S., Heikal, A. A., & Webb, W. W. (2002). Two-photon fluorescence spectroscopy and microscopy of NAD(P)H and flavoprotein. *Biophysical Journal* **82**, 2811-2825.

Huser, J., Blatter, L. A., Sheu, s., & Sheu, S. S. (2000). Mitochondrial calcium in heart cells: beat-to-beat oscillations or slow integration of cytosolic transients? *Journal of Bioenergetics and Biomembranes* **32**, 27-33.

Ingwall, J. S. (2009). Energy metabolism in heart failure and remodelling. *Cardiovascular Research* **81**, 412-419.

Ingwall, J. S. & Weiss, R. G. (2004). Is the failing heart energy starved?: On using chemical energy to support cardiac function. *Circulation Research* **95**, 135-145.

Jacobus, W. E. (1985). Respiratory control and the integration of heart high-energy phosphate-metabolism by mitochondrial creatine-kinase. *Annual Review of Physiology* **47**, 707-725.

Jo, H., Noma, A., & Matsuoka, S. (2006). Calcium-mediated coupling between mitochondrial substrate dehydrogenation and cardiac workload in single guinea-pig ventricular myocytes. *Journal of Molecular and Cellular Cardiology* **40**, 394-404.

Jöbsis, F. F. & Duffield, J. C. (1967). Oxidative and glycolytic recovery metabolism in muscle. *Journal of General Physiology* **50**, 1009-1047.

Jones, M. G., Bickar, D., Wilson, M. T., Brunori, M., Colosimo, A., & Sarti, P. (1984). A re-examination of the reactions of cyanide with cytochrome-c oxidase. *Biochemical Journal* **220**, 57-66.

Jullig, M., Hickey, A. J. R., Chai, C. C., Skea, G. L., Middleditch, M. J., Costa, S., Choong, S. Y., Philips, A. R. J., & Cooper, G. J. S. (2008). Is the failing heart out of fuel or a worn engine running rich? A study of mitochondria in old spontaneously hypertensive rats. *Proteomics* **8**, 2556-2572.

Kalsi, K. K., Smolenski, R. T., Pritchard, R. D., Khaghani, A., Seymour, A. M. L., & Yacoub, M. H. (1999). Energetics and function of the failing human heart with dilated or hypertrophic cardiomyopathy. *European Journal of Clinical Investigation* **29**, 469-477.

Kanthasamy, A. G., Ardelt, B., Malave, A., Mills, E. M., Powley, T. L., Borowitz, J. L., & Isom, G. E. (1997). Reactive oxygen species generated by cyanide mediate toxicity in rat pheochromocytoma cells. *Toxicology Letters* **93**, 47-54.

Kapus, A., Szaszi, K., Kaldi, K., Ligeti, E., & Fonyo, A. (1991). Is the mitochondrial Ca^{2+} uniporter a voltage-modulated transport pathway? *FEBS Letters* **282**, 61-64.

Katoh, H., Nishigaki, N., & Hayashi, H. (2002). Diazoxide opens the mitochondrial permeability transition pore and alters Ca^{2+} transients in rat ventricular myocytes. *Circulation* **105**, 2666-2671.

Katz, L. A., Swain, J. A., Portman, M. A., & Balaban, R. S. (1989). Relation between phosphate metabolites and oxygen consumption of heart in vivo. *American Journal of Physiology - Heart and Circulatory Physiology* **256**, H265-H274.

Katz, L. A., Koretsky, A. P., & Balaban, R. S. (1987). Respiratory control in the glucose perfused heart: A ^{31}P NMR and NADH fluorescence study. *FEBS Letters* **221**, 270-276.

Kay, M., Swift, L., Martell, B., Arutunyan, A., & Sarvazyan, N. (2008). Locations of ectopic beats coincide with spatial gradients of NADH in a regional model of

low-flow reperfusion. *American Journal of Physiology - Heart and Circulatory Physiology* **294**, H2400-H2405.

Kettlewell, S., Cabrero, P., Nicklin, S. A., Dow, J. A. T., Davies, S., & Smith, G. L. (2009). Changes of intra-mitochondrial Ca^{2+} in adult ventricular cardiomyocytes examined using a novel fluorescent Ca^{2+} indicator targeted to mitochondria. *Journal of Molecular and Cellular Cardiology* **46**, 891-901.

Kettlewell, S., Walker, N. L., Cobbe, S. M., Burton, F. L., & Smith, G. L. (2004). The electrophysiological and mechanical effects of 2,3-butane-dione monoxime and cytochalasin-D in the Langendorff perfused rabbit heart. *Experimental Physiology* **89**, 163-172.

King, N., McGivan, J. D., Griffiths, E. J., Halestrap, A. P., & Suleiman, M.-S. (2003). Glutamate loading protects freshly isolated and perfused adult cardiomyocytes against intracellular ROS generation. *Journal of Molecular and Cellular Cardiology* **35**, 975-984.

Kirsch, M. & de Groot, H. (2001). NAD(P)H, a directly operating antioxidant? *FASEB Journal* **15**, 1569-1574.

Knopp, A., Kohlhaas, M., & Maack, C. (2009). Blocking mitochondrial Ca^{2+} uptake increases matrix reactive oxygen species during excitation-contraction coupling in cardiac myocytes. *Biophysical Journal* **96**, 514a.

Koenig, K. & Schneckenburger, H. (1994). Laser-induced autofluorescence for medical diagnosis. *Journal of Fluorescence* **4**, 17-40.

Kohlhaas, M., Liu, T., Knopp, A., Zeller, T., Ong, M. F., Bohm, M., O'Rourke, B., & Maack, C. (2010). Elevated cytosolic Na^+ increases mitochondrial formation of reactive oxygen species in failing cardiac myocytes. *Circulation* **121**, 1606-1613.

Kolega, J. (2004). Phototoxicity and photoinactivation of blebbistatin in UV and visible light. *Biochemical and Biophysical Research Communications* **320**, 1020-1025.

König, K. (2000). Multiphoton microscopy in life sciences. *Journal of Microscopy-Oxford* **200**, 83-104.

König, K. (2006). Cell damage during multi-photon microscopy. In *Handbook of Biological Confocal Microscopy*, ed. Pawley, J. B., pp. 680-689. Springer, New York.

- Korzeniewski, B., Noma, A., & Matsuoka, S. (2005). Regulation of oxidative phosphorylation in intact mammalian heart in vivo. *Biophysical Chemistry* **116**, 145-157.
- Kovács, M., Tóth, J., Hetényi, C., Málnási-Csizmadia, A., & Sellers, J. R. (2004). Mechanism of blebbistatin inhibition of myosin II. *Journal of Biological Chemistry* **279**, 35557-35563.
- Krebs, H. A., Salvin, E., & Johnson, W. A. (1938). The formation of citric and α -ketoglutaric acids in the mammalian body. *Biochemical Journal* **32**, 113-117.
- Kuiper, J. W. P., Pluk, H., Oerlemans, F., van Leeuwen, F. N., de Lange, F., Franssen, J., & Wieringa, B. (2008). Creatine kinase - mediated ATP supply fuels actin-based events in phagocytosis. *PLoS Biology* **6**, 568-580.
- Kunz, W. S. (1986). Spectral properties of fluorescent flavoproteins of isolated rat liver mitochondria. *FEBS Letters* **195**, 92-96.
- Kunz, W. S. & Kunz, W. (1985). Contribution of different enzymes to flavoprotein fluorescence of isolated rat liver mitochondria. *Biochimica et Biophysica Acta - General Subjects* **841**, 237-246.
- LaNoue, K. F. & Williamson, J. R. (1971). Interrelationships between malate-aspartate shuttle and citric acid cycle in rat heart mitochondria. *Metabolism* **20**, 119-140.
- Lansman, J. B., Hess, P., & Tsien, R. W. (1986). Blockade of current through single calcium channels by Cd^{2+} , Mg^{2+} , and Ca^{2+} . Voltage and concentration dependence of calcium entry into the pore. *Journal of General Physiology* **88**, 321-347.
- Lardy, H. A. & Wellman, H. (1952). Oxidative phosphorylations: Role of inorganic phosphate and acceptor systems in control of metabolic rates. *Journal of Biological Chemistry* **195**, 215-224.
- las Fuentes, L., Herrero, P., Peterson, L. R., Kelly, D. P., Gropler, R. J., & Davila-Roman, V. G. (2003). Myocardial fatty acid metabolism: independent predictor of left ventricular mass in hypertensive heart disease. *Hypertension* **41**, 83-87.
- Legako, J. A., White, B. J., & Harmon, H. J. (2003). Detection of cyanide using immobilized porphyrin and myoglobin surfaces. *Sensors and Actuators B: Chemical* **91**, 128-132.

Lei, B., Lionetti, V., Young, M. E., Chandler, M. P., d'Agostino, C., Kang, E., Altarejos, M., Matsuo, K., Hintze, T. H., Stanley, W. C., & Recchia, F. A. (2004). Paradoxical downregulation of the glucose oxidation pathway despite enhanced flux in severe heart failure. *Journal of Molecular and Cellular Cardiology* **36**, 567-576.

Leisey, J. R., Grotyohann, L. W., Scott, D. A., & Scaduto, R. C., Jr. (1993). Regulation of cardiac mitochondrial calcium by average extramitochondrial calcium. *American Journal of Physiology - Heart and Circulatory Physiology* **265**, H1203-H1208.

Leisey, J. R., Scott, D. A., Grotyohann, L. W., & Scaduto, R. C., Jr. (1994). Quantitation of myoglobin saturation in the perfused heart using myoglobin as an optical inner filter. *American Journal of Physiology - Heart and Circulatory Physiology* **267**, H645-H653.

Levick, J. R. (2003). *An Introduction to Cardiovascular Physiology*, 4th Edition ed. Arnold, London.

Lin, L., Sharma, V., & Sheu, S. S. (2007). Mechanisms of reduced mitochondrial Ca^{2+} accumulation in failing hamster heart. *Pflügers Archiv - European Journal of Physiology* **454**, 395-402.

Liu, J., Wang, C., Murakami, Y., Gong, G., Ishibashi, Y., Prody, C., Ochiai, K., Bache, R. J., Godinot, C., & Zhang, J. (2001). Mitochondrial ATPase and high-energy phosphates in failing hearts. *American Journal of Physiology - Heart and Circulatory Physiology* **281**, H1319-H1326.

Liu, T. & O'Rourke, B. (2008). Enhancing mitochondrial Ca^{2+} uptake in myocytes from failing hearts restores energy supply and demand matching. *Circulation Research* **103**, 279-288.

Liu, T. & O'Rourke, B. (2009). Regulation of mitochondrial Ca^{2+} and its effects on energetics and redox balance in normal and failing heart. *Journal of Bioenergetics and Biomembranes* **41**, 127-132.

Lund, D. D. & Tomanek, R. J. (1978). Myocardial morphology in spontaneously hypertensive and aortic-constricted rats. *American Journal of Anatomy* **152**, 141-151.

Maack, C., Cortassa, S., Aon, M. A., Ganesan, A. N., Liu, T., & O'Rourke, B. (2006). Elevated cytosolic Na^+ decreases mitochondrial Ca^{2+} uptake during excitation-contraction coupling and impairs energetic adaptation in cardiac myocytes. *Circulation Research* **99**, 172-182.

- Maier, L. S., Bers, D. M., & Pieske, B. (2000). Differences in Ca²⁺-handling and sarcoplasmic reticulum Ca²⁺-content in isolated rat and rabbit myocardium. *Journal of Molecular and Cellular Cardiology* **32**, 2249-2258.
- Marin-Garcia, J., Goldenthal, M. J., & Moe, G. W. (2001). Abnormal cardiac and skeletal muscle mitochondrial function in pacing-induced cardiac failure. *Cardiovascular Research* **52**, 103-110.
- Mayevsky, A. & Barbiro-Michaely, E. (2009). Use of NADH fluorescence to determine mitochondrial function in vivo. *International Journal of Biochemistry & Cell Biology* **41**, 1977-1988.
- Mayevsky, A. & Rogatsky, G. G. (2007). Mitochondrial function in vivo evaluated by NADH fluorescence: from animal models to human studies. *American Journal of Physiology - Cell Physiology* **292**, C615-C640.
- McCormack, J. G. & Denton, R. M. (1979). Effects of calcium-ions and adenine-nucleotides on the activity of pig-heart 2-oxoglutarate dehydrogenase complex. *Biochemical Journal* **180**, 533-544.
- McIntyre, M., Bohr, D. F., & Dominiczak, A. F. (1999). Endothelial function in hypertension : the role of superoxide anion. *Hypertension* **34**, 539-545.
- Minezaki, K. K., Suleiman, M. S., & Chapman, R. A. (1994). Changes in mitochondrial function induced in isolated guinea-pig ventricular myocytes by calcium overload. *Journal of Physiology* **476**, 459-471.
- Minsky, M. (1988). Memoir on inventing the confocal scanning microscope. *Scanning* **10**, 128-138.
- Mitchell, P. (1961). Coupling of phosphorylation to electron and hydrogen transfer by a chemi-osmotic type of mechanism. *Nature* **191**, 144-148.
- Miyata, H., Silverman, H. S., Sollott, S. J., Lakatta, E. G., Stern, M. D., & Hansford, R. G. (1991). Measurement of mitochondrial free Ca²⁺ concentration in living single rat cardiac myocytes. *American Journal of Physiology - Heart and Circulatory Physiology* **261**, H1123-H1134.
- Modica-Napolitano, J. S., Weiss, M. J., Chen, L. B., & Aprille, J. R. (1984). Rhodamine 123 inhibits bioenergetic function in isolated rat liver mitochondria. *Biochemical and Biophysical Research Communications* **118**, 717-723.
- Mojon, D., Zhang, W. Q., & Oetliker, H. (1993). Inhibition by 2,3-butanedione-monoxime of mitochondrial ADP-dependent respiration and muscle-contraction. *Biochemistry and Molecular Biology International* **31**, 501-507.

- Monnet, E. & Chachques, J. C. (2005). Animal models of heart failure: what is new? *Annals of Thoracic Surgery* **79**, 1445-1453.
- Murray, A. J., Anderson, R. E., Watson, G. C., Radda, G. K., & Clarke, K. (2004). Uncoupling proteins in human heart. *Lancet* **364**, 1786-1788.
- Nascimben, L., Ingwall, J. S., Pauletto, P., Friedrich, J., Gwathmey, J. K., Saks, V., Pessina, A. C., & Allen, P. D. (1996). Creatine kinase system in failing and nonfailing human myocardium. *Circulation* **94**, 1894-1901.
- Neubauer, S. (2007). The failing heart - an engine out of fuel. *New England Journal of Medicine* **356**, 1140-1151.
- Neubauer, S., Remkes, H., Spindler, M., Horn, M., Wiesmann, F., Prestle, J., Walzel, B., Ertl, G., Hasenfuss, G., & Wallimann, T. (1999). Downregulation of the Na⁺-creatine cotransporter in failing human myocardium and in experimental heart failure. *Circulation* **100**, 1847-1850.
- Nguyen, M. H., Dudycha, S. J., & Jafri, M. S. (2007). Effect of Ca²⁺ on cardiac mitochondrial energy production is modulated by Na⁺ and H⁺ dynamics. *American Journal of Physiology - Cell Physiology* **292**, C2004-C2020.
- Nuutinen, E. M. (1984). Subcellular origin of the surface fluorescence of reduced nicotinamide nucleotides in the isolated perfused rat-heart. *Basic Research in Cardiology* **79**, 49-58.
- Nuutinen, E. M., Hiltunen, J. K., & Hassinen, I. E. (1981). The glutamate dehydrogenase system and the redox state of mitochondrial free nicotinamide adenine dinucleotide in myocardium. *FEBS Letters* **128**, 356-360.
- Okamoto, K. & Aoki, K. (1963). Development of a strain of spontaneously hypertensive rats. *Japanese Circulation Journal* **27**, 282-293.
- Okamoto, K., Yamori, Y., & Nagaoka, A. (1974). Establishment of stroke-prone spontaneously hypertensive rat (SHR). *Circulation Research* **34(Suppl. 1)**, I143-I153.
- Opie, L. H. & Owen, P. (1975). Effects of increased mechanical work by isolated perfused rat-heart during production or uptake of ketone-bodies - assessment of mitochondrial oxidized to reduced free nicotinamide-adenine dinucleotide ratios and oxaloacetate concentrations. *Biochemical Journal* **148**, 403-415.
- Osorio, J. C., Stanley, W. C., Linke, A., Castellari, M., Diep, Q. N., Panchal, A. R., Hintze, T. H., Lopaschuk, G. D., & Recchia, F. A. (2002). Impaired

myocardial fatty acid oxidation and reduced protein expression of retinoid X receptor- α in pacing-induced heart failure. *Circulation* **106**, 606-612.

Paolisso, G., Gambardella, A., Galzerano, D., D'Amore, A., Rubino, P., Verza, M., Teasuro, P., Varricchio, M., & D'Onofrio, F. (1994). Total-body and myocardial substrate oxidation in congestive heart failure. *Metabolism* **43**, 174-179.

Pasdois, P., Beauvoit, B., Tariosse, L., Vinassa, B., Bonoron-Adele, S., & Santos, P. D. (2008). Effect of diazoxide on flavoprotein oxidation and reactive oxygen species generation during ischemia-reperfusion: a study on Langendorff-perfused rat hearts using optic fibers. *American Journal of Physiology - Heart and Circulatory Physiology* **294**, H2088-H2097.

Pavlov, E., Grigoriev, S. M., Dejean, L. M., Zweihorn, C. L., Mannella, C. A., & Kinnally, K. W. (2005). The mitochondrial channel VDAC has a cation-selective open state. *Biochimica et Biophysica Acta - Bioenergetics* **1710**, 96-102.

Penna, C., Mancardi, D., Rastaldo, R., & Pagliaro, P. (2009). Cardioprotection: A radical view: Free radicals in pre and postconditioning. *Biochimica et Biophysica Acta - Bioenergetics* **1787**, 781-793.

Petrat, F., Pindiur, S., Kirsch, M., & de Groot, H. (2003). NAD(P)H, a primary target of $^1\text{O}_2$ in mitochondria of intact cells. *Journal of Biological Chemistry* **278**, 3298-3307.

Pinto, Y. M., Paul, M., & Ganten, D. (1998). Lessons from rat models of hypertension: from Goldblatt to genetic engineering. *Cardiovascular Research* **39**, 77-88.

Quigley, A. F., Kapsa, R. M. I., Esmore, D., Hale, G., & Byrne, E. (2000). Mitochondrial respiratory chain activity in idiopathic dilated cardiomyopathy. *Journal of Cardiac Failure* **6**, 47-55.

Recchia, F. A., McConnell, P. I., Bernstein, R. D., Vogel, T. R., Xu, X., & Hintze, T. H. (1998). Reduced nitric oxide production and altered myocardial metabolism during the decompensation of pacing-induced heart failure in the conscious dog. *Circulation Research* **83**, 969-979.

Riccio, M. L., Koller, M. L., & Gilmour, R. F., Jr. (1999). Electrical restitution and spatiotemporal organization during ventricular fibrillation. *Circulation Research* **84**, 955-963.

- Robert, V., Gurlini, P., Tosello, V., Nagai, T., Miyawaki, A., Di Lisa, F., & Pozzan, T. (2001). Beat-to-beat oscillations of mitochondrial $[Ca^{2+}]$ in cardiac cells. *EMBO Journal* **20**, 4998-5007.
- Rocheleau, J. V., Head, W. S., & Piston, D. W. (2004). Quantitative NAD(P)H/flavoprotein autofluorescence imaging reveals metabolic mechanisms of pancreatic islet pyruvate response. *Journal of Biological Chemistry* **279**, 31780-31787.
- Romashko, D. N., Marban, E., & O'Rourke, B. (1998). Subcellular metabolic transients and mitochondrial redox waves in heart cells. *Proceedings of the National Academy of Sciences of the United States of America* **95**, 1618-1623.
- Rouslin, W. & Broge, C. W. (1996). IF1 function in situ in uncoupler-challenged ischemic rabbit, rat, and pigeon hearts. *Journal of Biological Chemistry* **271**, 23638-23641.
- Rubart, M. (2004). Two-photon microscopy of cells and tissue. *Circulation Research* **95**, 1154-1166.
- Sack, M. N., Rader, T. A., Park, S., Bastin, J., McCune, S. A., & Kelly, D. P. (1996). Fatty acid oxidation enzyme gene expression is downregulated in the failing heart. *Circulation* **94**, 2837-2842.
- Sakamoto, T., Limouze, J., Combs, C. A., Straight, A. F., & Sellers, J. R. (2004). Blebbistatin, a myosin II inhibitor, is photoinactivated by blue light. *Biochemistry* **44**, 584-588.
- Scaduto, R. C. & Grotyohann, L. W. (1999). Measurement of mitochondrial membrane potential using fluorescent rhodamine derivatives. *Biophysical Journal* **76**, 469-477.
- Scaduto, R. C. & Grotyohann, L. W. (2000). 2,3-Butanedione monoxime unmasks Ca^{2+} -induced NADH formation and inhibits electron transport in rat hearts. *American Journal of Physiology - Heart and Circulatory Physiology* **279**, H1839-H1848.
- Schmitt, J. M. & Kumar, G. (1998). Optical scattering properties of soft tissue: a discrete particle model. *Applied Optics* **37**, 2788-2797.
- Scholz, R., Thurman, R. G., Williamson, J. R., Chance, B., & Bücher, T. (1969). Flavin and pyridine nucleotide oxidation-reduction changes in perfused rat liver. *Journal of Biological Chemistry* **244**, 2317-2324.

Sedlic, F., Pravdic, D., Hirata, N., Mio, Y., Sepac, A., Camara, A. K., Wakatsuki, T., Bosnjak, Z. J., & Bienengraeber, M. (2010). Monitoring mitochondrial electron fluxes using NAD(P)H-flavoprotein fluorometry reveals complex action of isoflurane on cardiomyocytes. *Biochimica et Biophysica Acta - Bioenergetics* **1797**, 1749-1758.

Sharma, V. K., Ramesh, V., Franzini-Armstrong, C., & Sheu S.S (2000). Transport of Ca^{2+} from sarcoplasmic reticulum to mitochondria in rat ventricular myocytes. *Journal of Bioenergetics and Biomembranes* **32**, 97-104.

Shattock, M. J. & Bers, D. M. (1989). Rat vs. rabbit ventricle: Ca flux and intracellular Na assessed by ion-selective microelectrodes. *American Journal of Physiology - Cell Physiology* **256**, C813-C822.

Sies, H. (1993). Strategies of antioxidant defense. *European Journal of Biochemistry* **215**, 213-219.

Smythe, C. V. (1936). The reaction of iodoacetate and of iodoacetamide with various sulfhydryl groups, with urease, and with yeast preparations. *Journal of Biological Chemistry* **114**, 601-612.

Stanley, W. C., Recchia, F. A., & Lopaschuk, G. D. (2005). Myocardial substrate metabolism in the normal and failing heart. *Physiological Reviews* **85**, 1093-1129.

Stapleton, M. T., Fuchsbaue, C. M., & Allshire, A. P. (1998). BDM drives protein dephosphorylation and inhibits adenine nucleotide exchange in cardiomyocytes. *American Journal of Physiology - Heart and Circulatory Physiology* **275**, H1260-H1266.

Straight, A. F., Cheung, A., Limouze, J., Chen, I., Westwood, N. J., Sellers, J. R., & Mitchison, T. J. (2003). Dissecting temporal and spatial control of cytokinesis with a myosin II inhibitor. *Science* **299**, 1743-1747.

Stryer, L. (1988). Glycolysis. In *Biochemistry* pp. 349-372. W. H. Freeman & Co.

Suleiman, M. S. & Chapman, R. A. (1993). Calcium paradox in newborn and adult guinea-pig hearts - changes in intracellular taurine and the effects of extracellular magnesium. *Experimental Physiology* **78**, 503-516.

Swift, L., Martell, B., Khatri, V., Arutunyan, A., Sarvazyan, N., & Kay, M. (2008). Controlled regional hypoperfusion in Langendorff heart preparations. *Physiological Measurement* **29**, 269-279.

- Szalai, G., Csordas, G., Hantash, B. M., Thomas, A. P., & Hajnoczky, G. (2000). Calcium signal transmission between ryanodine receptors and mitochondria. *Journal of Biological Chemistry* **275**, 15305-15313.
- Tamura, M., Oshino, N., Chance, B., & Silver, I. A. (1978). Optical measurements of intracellular oxygen concentration of rat heart in vitro. *Archives of Biochemistry and Biophysics* **191**, 8-22.
- Taylor, M., Wallhaus, T. R., DeGrado, T. R., Russell, D. C., Stanko, P., Nickles, R. J., & Stone, C. K. (2001). An evaluation of myocardial fatty acid and glucose uptake using PET with [¹⁸F]fluoro-6-thia-heptadecanoic acid and [¹⁸F]FDG in patients with congestive heart failure. *Journal of Nuclear Medicine* **42**, 55-62.
- Teicher, B. A., Menon, K., Northey, D., Liu, J., Kufe, D. W., & Kaddurahdaouk, R. (1995). Cyclocreatine in cancer-chemotherapy. *Cancer Chemotherapy and Pharmacology* **35**, 411-416.
- Ten Hove, M., Chan, S., Lygate, C., Monfared, M., Boehm, E., Hulbert, K., Watkins, H., Clarke, K., & Neubauer, S. (2005). Mechanisms of creatine depletion in chronically failing rat heart. *Journal of Molecular and Cellular Cardiology* **38**, 309-313.
- Territo, P. R., Mootha, V. K., French, S. A., & Balaban, R. S. (2000). Ca²⁺ activation of heart mitochondrial oxidative phosphorylation: role of the F₀/F₁-ATPase. *American Journal of Physiology - Cell Physiology* **278**, C423-C435.
- Tian, R., Christe, M. E., Spindler, M., Hopkins, J. C. A., Halow, J. M., Camacho, S. A., & Ingwall, J. S. (1997). Role of MgADP in the development of diastolic dysfunction in the intact beating rat heart. *Journal of Clinical Investigation* **99**, 745-751.
- Tokoro, T., Ito, H., & Suzuki, T. (1996). Alterations in mitochondrial DNA and enzyme activities in hypertrophied myocardium of stroke-prone SHR. *Clinical and Experimental Hypertension* **18**, 595-606.
- Trollinger, D. R., Cascio, W. E., & Lemasters, J. J. (1997). Selective loading of Rhod 2 into mitochondria shows mitochondrial Ca²⁺ transients during the contractile cycle in adult rabbit cardiac myocytes. *Biochemical and Biophysical Research Communications* **236**, 738-742.
- Turrens, J. F. (2003). Mitochondrial formation of reactive oxygen species. *Journal of Physiology* **552**, 335-344.

van Bilsen, M., Smeets, P. J. H., Gilde, A. J., & van der Vusse, G. J. (2004). Metabolic remodelling of the failing heart: the cardiac burn-out syndrome? *Cardiovascular Research* **61**, 218-226.

van Bilsen, M., van Nieuwenhoven, F. A., & van der Vusse, G. J. (2009). Metabolic remodelling of the failing heart: beneficial or detrimental? *Cardiovascular Research* **81**, 420-428.

Vogel, R., Wiesinger, H., Hamprecht, B., & Dringen, R. (1999). The regeneration of reduced glutathione in rat forebrain mitochondria identifies metabolic pathways providing the NADPH required. *Neuroscience Letters* **275**, 97-100.

Wainio, W. W. & Greenlees, J. (1960). Complexes of cytochrome c oxidase with cyanide and carbon monoxide. *Archives of Biochemistry and Biophysics* **90**, 18-21.

Wallimann, T., Wyss, M., Brdiczka, D., Nicolay, K., & Eppenberger, H. M. (1992). Intracellular compartmentation, structure and function of creatine-kinase isoenzymes in tissues with high and fluctuating energy demands - the phosphocreatine circuit for cellular-energy homeostasis. *Biochemical Journal* **281**, 21-40.

Weitzman, P. D. J., Jenkins, T., Else, A. J., & Holt, R. A. (1986). Occurrence of two distinct succinate thiokinases in animal tissues. *FEBS Letters* **199**, 57-60.

White, R. L. & Wittenberg, B. A. (1993). NADH fluorescence of isolated ventricular myocytes: effects of pacing, myoglobin, and oxygen supply. *Biophysical Journal* **65**, 196-204.

White, R. L. & Wittenberg, B. A. (2000). Mitochondrial NAD(P)H, ADP, oxidative phosphorylation, and contraction in isolated heart cells. *American Journal of Physiology - Heart and Circulatory Physiology* **279**, H1849-H1857.

Williamson, D. H., Lund, P., & Krebs, H. A. (1967). Redox state of free nicotinamide-adenine dinucleotide in cytoplasm and mitochondria of rat liver. *Biochemical Journal* **103**, 514-527.

Wilson, B. C. & Jacques, S. L. (1990). Optical reflectance and transmittance of tissues - Principles and applications. *IEEE Journal of Quantum Electronics* **26**, 2186-2199.

Wittenberg, J. B. & Wittenberg, B. A. (2003). Myoglobin function reassessed. *Journal of Experimental Biology* **206**, 2011-2020.

- Xu, C. & Webb, W. W. (1996). Measurement of two-photon excitation cross sections of molecular fluorophores with data from 690 to 1050 nm. *Journal of the Optical Society of America B-Optical Physics* **13**, 481-491.
- Xu, C., Zipfel, W., Shear, J. B., Williams, R. M., & Webb, W. W. (1996). Multiphoton fluorescence excitation: new spectral windows for biological nonlinear microscopy. *Proceedings of the National Academy of Sciences of the United States of America* **93**, 10763-10768.
- Yan, G. X. & Antzelevitch, C. (1996). Cellular basis for the electrocardiographic J wave. *Circulation* **93**, 372-379.
- Yan, G. X., Wu, Y., Liu, T., Wang, J., Marinchak, R. A., & Kowey, P. R. (2001). Phase 2 early afterdepolarization as a trigger of polymorphic ventricular tachycardia in acquired long-QT syndrome : direct evidence from intracellular recordings in the intact left ventricular wall. *Circulation* **103**, 2851-2856.
- Zhou, Z., Matlib, M. A., & Bers, D. M. (1998). Cytosolic and mitochondrial Ca²⁺ signals in patch clamped mammalian ventricular myocytes. *Journal of Physiology* **507**, 379-403.
- Zurbier, C. J., Kruyver, B., Eerbeek, O., Mik, E. G., & Ince, C. (2003). Commonly Used Numbers of Microspheres Affect Cardiac Vascular Resistance. *Journal of Cardiovascular Pharmacology* **41**.